

OPERATIONAL HYDROLOGICAL FORECASTING OF SNOWMELT
RUNOFF BY REMOTE SENSING AND GEOGRAPHIC INFORMATION
SYSTEMS INTEGRATION

A THESIS SUBMITTED TO
THE GRADUATE SCHOOL OF NATURAL AND APPLIED SCIENCES
OF
MIDDLE EAST TECHNICAL UNIVERSITY

BY

AHMET EMRE TEKELİ

IN PARTIAL FULFILLMENT OF THE REQUIREMENTS
FOR
THE DEGREE OF DOCTOR OF PHILOSOPHY
IN
CIVIL ENGINEERING

MAY 2005

Approval of the Graduate School of Natural and Applied Sciences

Prof. Dr. Canan ÖZGEN
Director

I certify that this thesis satisfies all the requirements as a thesis for the degree of Doctor of Philosophy.

Prof. Dr. Erdal ÇOKÇA
Head of Department

This is to certify that we have read this thesis and that in our opinion it is fully adequate, in scope and quality, as a thesis for the degree of Doctor of Philosophy.

Prof. Dr. A. Ünal ŞORMAN
Supervisor

Examining Committee Members

Prof. Dr. İbrahim Gürer	(Gazi Univ., CE)	_____
Prof. Dr. A. Ünal Şorman	(METU, CE)	_____
Prof. Dr. Veysel Eroğlu	(ITU, ENVE)	_____
Assoc. Prof. Dr. Nuri Merzi	(METU, CE)	_____
Asst. Dr. Zuhale Akyürek	(METU, GGIT)	_____

I hereby declare that all information in this document has been obtained and presented in accordance with academic rules and ethical conduct. I also declare that, as required by these rules and conduct, I have fully cited and referenced all material and results that are not original to this work.

Name, Last Name : Ahmet Emre TEKELI

Signature :

ABSTRACT

OPERATIONAL HYDROLOGICAL FORECASTING OF SNOWMELT RUNOFF BY REMOTE SENSING AND GEOGRAPHIC INFORMATION SYSTEMS INTEGRATION

TEKELİ, Ahmet Emre

Ph. D., Department of Civil Engineering

Supervisor: Prof. Dr. A. Ünal ŞORMAN

May 2005, 226 pages

Snow indicates the potential stored water volume that is an important source of water supply, which has been the most valuable and indispensable natural resource throughout the history of the world. Euphrates and Tigris, having the biggest dams of Turkey, are the two largest trans-boundary rivers that originate in Turkey and pass throughout the water deficit nations Syria, Iran, Iraq and Saudi Arabia bringing life as well as water all their way. Snowmelt runoff originating from the mountains of Eastern Turkey accounts for 60 to 70 % of total annual discharge observed in Euphrates and Tigris. For an optimum operation of the dams, maximizing energy production, mitigation of floods and satisfying water rights, hydrological models which can both simulate and forecast the river discharges of Euphrates and Tigris are needed.

In this study a hydrological model, snowmelt runoff model (SRM), is used in conjunction with remote sensing and geographic information systems to forecast the river discharges in the headwaters of Euphrates River, Upper Euphrates Basin.

NOAA and MODIS satellite images were used to derive the snow covered area (SCA) information required by SRM. Linear reduction methodologies based on accumulated air temperature, with constant or varying gradient, were developed to get the continuous daily SCA values from the discrete daily satellite images.

Temperature and precipitation forecasts were gathered from two different numerical weather prediction models, namely European Center for Medium Range Weather Forecasts (ECMWF) and Mesoscale Model Version 5 (MM5) from Turkish State Meteorological Services. These data sets provided t+24 hour forecasts of both temperature and precipitation.

Temperature, precipitation and SCA information are fed into SRM. Discharge forecasts obtained from the model outputs are compared with the observed values. The overall performance of the model was seen as promising. Possible reasons of the mismatches between the forecasted and observed values are searched. Experiences gained throughout the study are summarized and recommendations on further forecast studies are mentioned.

Keywords: Snowmelt runoff model (SRM), forecasting, Upper Euphrates River, MODIS, NOAA

ÖZ

UZAKTAN ALGILAMA VE COĞRAFİ BİLGİ SİSTEMLERİNİN HİDROLOJİK MODEL TAHMİNLERİNDE İŞLEVSEL KULLANIMI

TEKELİ, Ahmet Emre

Doktora, İnşaat Mühendisliği Bölümü
Tez Yöneticisi: Prof. Dr. A. Ünal ŞORMAN

Mayıs 2005, 226 sayfa

Kar, insanlık tarihi boyunca en değerli ve vazgeçilemez doğal bir kaynak olan suyun önemli bir kaynağı olup, potansiyel olarak depolanmış su rezervleridir. Fırat ve Dicle, Türkiye’de doğan ve ülkenin en büyük barajlarına sahip olup, Suriye, İran, Irak ve Sudi Arabistan gibi su ihtiyacı fazla olan ülkelerden geçen en büyük iki sınır aşan sularımızdır. Dağlık Doğu Anadolu bölgemizden ilkbahar ve yaz aylarında kar erimesinden gelen akımlar Fırat ve Dicle nehirlerimizin yıllık toplam akım hacminin yüzde 60 ile 70 ini oluşturmaktadır. Barajların optimum işletilmesi, enerji üretimini maksimum hale getirilmesi, taşkın engelleme çalışmaları ve su haklarının sağlıklı bir şekilde sağlanabilmesi için, Fırat ve Dicle nehirlerindeki akımları hem simule hem de ön tahmin edebilen hidrolojik modellere ihtiyaç duyulmaktadır.

Bu çalışmada hidrolojik bir model olan ve kar erimesinden kaynaklanan akımı gerek simule gerekse ön tahmin edebilen kar erimesi akış modeli (SRM) modeli, uzaktan algılama ve coğrafi bilgi sistemleri ile, Fırat nehrinin ana kaynaklarından biri olan Yukarı Fırat Havzası’ndaki akımın ön tahmin çalışmalarında beraber kullanılmıştır.

NOAA ve MODIS uydu görüntüleri SRM modelinin istediđi karla kaplı alan (KKA) bilgisini elde etmek için kullanılmıştır. Münferid günlerdeki uydu görüntülerinden elde edilen bu bilginin havzadaki kar erime periyodunu içeren süre boyunca günlük bir halde sağlamak için kümülatif hava sıcaklığına bađlı sabit yada deđişen eğimli linear metodlar geliştirilmiştir.

Hava sıcaklık ve yağış tahminleri, farklı iki sayısal hava tahmin modeli olan Avrupa Orta Vadeli Hava Tahmini (ECMWF) ve Orta Ölçek Model Sürüm 5 (MM5) den elde edilmiştir. Bu modellerden alınan veri setleri t+24 saat içindeki hava sıcaklık ve yağış tahminlerini içermektedir.

Hava sıcaklık, yağış ve KKA bilgileri SRM modeline veri olarak girilmiştir. Modelin verdiđi akım tahmin deđerleri gözlemlenmiş olan akım ölçümleri ile karşılaştırılmıştır. Model sonuçları genel itibari ile umut vericidir. Tahmin edilmiş ve gözlemlenmiş akım deđerleri arasındaki uyumsuzluđun olası sebepleri araştırılmıştır. Çalışma boyunca elde edilen deneyimler özetlenmiş ve daha sonraki çalışmalara ışık tutacak öneriler belirtilmiştir.

Anahtar Kelimeler: Kar erimesi akış modeli (SRM), öntahmin, Yukarı Fırat Nehri, MODIS, NOAA

Aileme ...

ACKNOWLEDGMENTS

My great thanks are to Prof. Dr. A. Ünal Şorman whom I see as a man full of enthusiasm to learn, to search and to teach. It was more than honoring to be part in the projects taken under his supervision. His contributions were every where, extending from the meetings lasting for hours in the meeting room of Water Resources Laboratory to the open fields at the site, in the high lands of Eastern Anatolia. His advices and criticism made this and many other studies a frontier in Turkey.

Many thanks are also extended to Asst. Prof. Dr Zuhale Akyürek. The contributions made throughout the thesis and publications can not be over simplified. Her valuable comments and relaxing sentences have always given power to the cope with the hard, tiring and painful days of dissertation and, I believe will still give in the remaining days.

Thanks are also given to Assoc. Dr. Nuri Merzi, for his encouragements, stress releasing attitudes and positive thinking which were giving moral and anticipation.

I would like to thank Prof. İbrahim Gürer for his valuable comments and corrections related with the thesis. My thanks should also be extended to Prof. Dr. Veysel Eroğlu who tried it hard to find time to evaluate the thesis and come to the jury.

My deepest thanks are extended to Arda and Aynur, two main members of the snow hydrology group. They have been more than a friend, sometimes judging you without pitiless sometimes digging trenches with you shoulder to shoulder

under the sun over 2300m. Long office hours, and the endless seeming nights of the thesis, projects and the hard passing juries were more than a fun with their smiling. I wish them a happy, successful and a healthy life in their remaining time for which they agreed to share in common.

I have to admit the contribution of Musa Yılmaz, research assistant of water resources laboratory for his technical suggestions and Tülin Ecevit, who is both the secretary and psychological therapist of the laboratory.

Many thanks are extended to Dr. Tahir Kemal Erdem, Murat Tepegöz and Hüsnü Demir for their technical guidance in many areas of the thesis covering a wide range from data transfer via ftp to the arrangements during the jury. Sharing time with them both in office issues and in spare has been more than relaxing and made the thesis a possibility. Mustafa Kaya, the MM5 decoder, should be mentioned specially for his codes that changed meaningless figures into valuable precipitation and temperature values. Durmuş Bayram merits special thanks for his helps during the process of printing out, photocopying and bounding processes.

The support of General Directorate of State Meteorological Organization, General and VIIIth Regional Directorate of State Hydraulic Works are greatly appreciated. Nurullah Sezen, the first field man, merits many thanks for his guidance and experience sharing with us, which made the dreams come into reality. Meral Çukurçayır and Serkan Eminoğlu helped too much to supply the satellite data on time without any problem, for which they deserve special thanks. Alper Güser and Ersin Küçükkaraca provided the numerical weather forecasts on time and helped too much to receive data without much delay. I thank them very much for

Dear personnel of water resources laboratory also merit many thanks for bearing up namely, Nermin, Tülay, Ömer, Emre and Gençer.

Many of others, some of whom are Yasin, Ekrem and Nedim, helped me to finish the thesis successfully. I want from the ones that I forgot, to forgive me while I was writing these sentences.

I also would like to thank Remote Sensing Division of General Directorate of State Meteorological Organization for allowing me to concentrate on the thesis.

Before giving an end, I am grateful to each member of Tekeli, Yazıcıođlu, Akbulut, Aydın and Bayram family for their support and belief in me. It was their moral support that made the things go all right at the back side without which the success could not have been achieved.

TABLE OF CONTENTS

PLAGIARISM.....	iii
ABSTRACT.....	iv
ÖZ.....	vi
DEDICATION.....	viii
ACKNOWLEDGEMENTS.....	ix
TABLE OF CONTENTS.....	xii
LIST OF TABLES.....	xvii
LIST OF FIGURES.....	xx
LIST OF SYMBOLS.....	xvi
CHAPTER	
1. INTRODUCTION.....	1
1.1 Problem Definition.....	1
1.2 Purpose of the Study.....	4
2. BASIN DESCRIPTION AND DATABASE.....	7
2.1 Introduction.....	7
2.2 Upper Euphrates River Basin.....	8
2.3 Automated Snow and Meteorological Stations.....	13
2.4 Initial Automated Meteorological and Snow Station Setup at Güzelyayla.....	15
2.4.1 Location, Geography and Climate.....	15
2.4.2 Instrumentation.....	16
2.4.3 Data Collection and Data Transfer.....	25

2.5	Instrumentation at Other Observation Sites.....	26
2.5.1	Ovacık Station.....	27
2.5.1.1	Instrumentation.....	28
2.5.1.2	Data Collection and Data Transfer.....	32
2.5.2	Çat Station.....	32
2.5.2.1	Instrumentation.....	32
2.5.2.2	Data Collection and Data Transfer.....	35
2.5.3	Hacımahmud Station.....	36
2.5.3.1	Instrumentation.....	36
2.5.3.2	Data Collection and Data Transfer.....	37
2.5.4	Sakaltutan Station.....	38
2.5.4.1	Instrumentation.....	38
2.5.4.2	Data Collection and Data Transfer.....	39
2.6	Database.....	39
2.6.1	Data Retrieval.....	40
2.6.2	Data Processing.....	41
2.6.3	Data Bank Formation.....	44
3.	REMOTE SENSING METHODS USED IN SNOW HYDROLOGY...	45
3.1	Introduction.....	45
3.2	Spectral Characteristics of Snow.....	46
3.2.1	Gamma Rays.....	47
3.2.2	Visible and Near Infrared.....	47
3.2.3	Thermal Infrared.....	51
3.2.4	Microwave.....	51
3.3	History of Remote Sensing of Snow.....	53
3.4	Choice of Remote Sensing Sensor.....	54
3.4.1	Spatial Resolution.....	57
3.4.2	Temporal Resolution.....	58
3.4.3	Cloud Intrusion Problem.....	58
3.5	Medium Resolution Optical Imagery.....	59
3.5.1	Review of Medium Resolution Optical Imagery Methods.	59

3.5.1.1	Processing Steps of Medium Resolution Optical Images	60
3.5.2	Snow Cover Monitoring for NOAA-AVHRR.....	67
3.5.2.1	Real Time Data Access.....	67
3.5.2.2	Data Download.....	68
3.5.2.3	Band Reduction.....	68
3.5.2.4	Geocoding.....	68
3.5.2.5	Snow Classification.....	69
3.5.2.6	Export to GIS.....	71
3.5.3	Moderate Resolution Imaging Spectroradiometer (MODIS).....	71
3.5.3.1	MODIS File Format.....	75
3.5.3.2	MODIS Snow Products.....	77
3.5.3.3	MODIS Snow Detection Algorithm.....	82
3.5.3.4	MODIS Data Processing Scheme for Snowmelt Runoff Model.....	86
4.	SNOWMELT RUNOFF MODELING.....	90
4.1	Introduction.....	90
4.2	Hydrological Modeling.....	91
4.3	Essentials of Snowmelt Modeling.....	93
4.3.1	Components of Snowmelt Modeling.....	94
4.3.1.1	Extrapolation of Meteorological Data.....	97
4.3.1.2	Point Melt Rate Calculations.....	98
4.3.1.3	Integration of Melt Water Over the Snow Covered Areas.....	100
4.3.1.4	Runoff Routing.....	102
4.3.2	Quality Assessment of Model Accuracy.....	102
4.4	Snowmelt Runoff Model.....	103
4.4.1	Background.....	104
4.4.2	Model Inputs.....	106
4.4.2.1	Meteorological Variables.....	107

4.4.2.2	Snow Cover Depletion Curves.....	108
4.4.2.3	Model Parameters.....	109
5.	NUMERICAL WEATHER PREDICTION MODELS.....	119
5.1	A Short History of Numerical Weather Prediction.....	120
5.2	ECMWF.....	121
5.2.1	ECMWF Forecasts.....	122
5.2.2	Making Forecast in ECMWF.....	123
5.3	Mesoscale Model (MM5).....	124
5.3.1	Components of MM5.....	125
5.3.2	Horizontal and Vertical Grids of MM5.....	131
5.3.3	Map Projections.....	133
5.3.4	Data Required to Run the Modeling System.....	134
5.3.5	Lateral Boundary Conditions.....	134
6.	NEAR REAL TIME SNOWMELT RUNOFF FORECASTING STUDIES.....	136
6.1	Introduction.....	136
6.2	Near Real Time Runoff Forecasting in Upper Euphrates Basin – An Overview	137
6.3	Forecast Processing Chain.....	137
6.4	Data Used in Near Real Time Forecasting.....	143
6.4.1	Meteorological Data.....	143
6.4.2	Hydrological Data.....	144
6.4.3	Snow Cover Data.....	144
6.4.3.1	NOAA 17 Images.....	144
6.4.3.2	MODIS Daily Snow Cover Maps (MOD10A1)...	146
6.4.3.3	MODIS 8 Daily Snow Cover Maps (MOD10A1)	147
6.4.4	Calculation of Snow Depletion Curves.....	150
6.5	Verification of Meteorological Variables.....	165
6.5.1	Temperature Comparison.....	165
6.5.2	Precipitation Comparison.....	170
6.6	Forecasting Discharges Using SRM Runs.....	171

6.6.1	Re-Runs for Verification of Model Parameters.....	176
6.6.2	Near Real Time Forecasting Studies.....	179
6.7	Summary and Discussion of Results.....	194
6.7.1	Near Real Time Forecasting.....	194
6.7.2	Problems Faced During Project.....	197
7.	CONCLUSIONS AND FUTURE WORK.....	199
	REFERENCES.....	204
	APPENDICES.....	215
A.	COMPARISON OF LONG TERM TEMPERATURE AND PRECIPITATION VALUES.....	215
	CURRICULUM VITAE.....	225

LIST OF TABLES

TABLES

Table 2.1	Elevation zones of Karasu Basin.....	9
Table 2.2	Long term discharges observed at EIE 2119.....	14
Table 2.3	Instrumentation at Güzelyayla research site.....	17
Table 2.4	Database of Güzelyayla station with respect to years.....	25
Table 2.5	Location and elevation of automated snow and meteorological stations within Upper Euphrates River Basin.....	27
Table 2.6	Instrumentation in Ovacık station.....	29
Table 2.7	Database of Ovacık station with respect to years.....	31
Table 2.8	Instrumentation in Çat station.....	33
Table 2.9	Database of Çat station with respect to years.....	35
Table 2.10	Instrumentation in Hacımahmud station.....	36
Table 2.11	Database of Hacımahmud station with respect to years.....	38
Table 2.12	Instrumentation in Sakaltutan station.....	38
Table 2.13	Database of Sakaltutan station with respect to years.....	39
Table 2.14	Data collection interval, data transfer system and the connectivity to stations in Karasu Basin.....	40
Table 3.1	Snow properties affecting its reflectance.....	52
Table 3.2	Relation between snow properties and spectral bands.....	53
Table 3.3	Characteristics of satellites for snow cover mapping.....	56
Table 3.4	Rationing procedure.....	70
Table 3.5	Technical properties of MODIS.....	71
Table 3.6	List of main MODIS products.....	76
Table 3.7	Summary of MODIS snow data products.....	78

Table 3.8	Explanation of level numbers in MODIS data products.....	79
Table 3.9	MODIS data product inputs to MOD10_L2.....	80
Table 4.1	SRM model variables.....	107
Table 4.2	SRM model parameters.....	110
Table 4.3	Proposed degree day factors.....	112
Table 5.1	Operational products that are available from ECMWF dissemination.....	124
Table 6.1	Timing of daily forecast data.....	142
Table 6.2	Timing of meteorological observations downloaded from site..	142
Table 6.3	Timing of snow cover maps.....	142
Table 6.4	Listing of NOAA 17 images used during forecasting.....	145
Table 6.5	MOD10A1 image availability for winter of 2005.....	146
Table 6.6	MOD10A2 image availability for winter of 2005.....	148
Table 6.7	Comparison of the DEM used by MM5 and the actual topography.....	168
Table 6.8	Calculation of temperature lapse rate values ($^{\circ}\text{C}/100\text{m}$) for MM5.....	169
Table 6.9	Runoff coefficient values.....	175
Table 6.10	Comparison of model runs with different c_r and c_s values.....	179
Table 6.11	Case numbers as a function of SCA and figure numbers of related output hydrographs.....	180
Table 6.12	Summary of initial forecasts for MM5 data.....	183
Table 6.13	Case numbers as a function of SCA and figure numbers of related output hydrographs for temperature correction.....	184
Table 6.14	R^2 comparison of updated model runs.....	188
Table 6.15	Volume difference comparison of updated model runs.....	188
Table 6.16	Observed and forecasted precipitation ratios for Güzelyayla and Ovacık stations.....	189
Table 6.17	Case numbers as a function of SCA and figure numbers of related output hydrographs for precipitation correction.....	190

Table 6.18	R^2 comparison of updated precipitation model runs.....	193
Table 6.19	Volume difference comparison of updated precipitation model runs.....	193
Table 6.20	Summary of R^2 values for forecasting model runs.....	195
Table 6.21	Summary of D_v values for forecasting model runs.....	195

LIST OF FIGURES

FIGURES

Figure 2.1	Location of Upper Euphrates River Basin.....	8
Figure 2.2	Hypsometric curve for the whole Karasu Basin.....	9
Figure 2.3	Hypsometric curve for Zone A of Karasu Basin.....	10
Figure 2.4	Hypsometric curve for Zone B of Karasu Basin.....	10
Figure 2.5	Hypsometric curve for Zone C of Karasu Basin.....	11
Figure 2.6	Hypsometric curve for Zone D of Karasu Basin.....	11
Figure 2.7	Hypsometric curve for Zone E of Karasu Basin.....	12
Figure 2.8	Overview of Güzelyayla station.....	16
Figure 2.9	Schematic drawing of the Güzelyayla snow pillow.....	18
Figure 2.10	Installed snow pillow at Güzelyayla station.....	19
Figure 2.11	Schematic drawing of the snowmelt lysimeter at Güzelyayla station.....	20
Figure 2.12	Installed snowmelt lysimeter at Güzelyayla station.....	21
Figure 2.13	Distribution of automated snow and meteorological stations within the Upper Euphrates River Basin (Karasu).....	27
Figure 2.14	General view of Ovacık station.....	30
Figure 2.15	Snowmelt lysimeter installed at Ovacık station.....	30
Figure 2.16	General view of Çat meteorological and snow station.....	34
Figure 2.17	General view of Hacımahmud station.....	37
Figure 2.18	Flow chart of data processing.....	41
Figure 2.19	Sample ASCII format of the Güzelyayla station.....	42
Figure 2.20	Sample excel format of Güzelyayla station.....	43

Figure 2.21	Graphs of snow depth observations obtained from the automated stations within the basin.....	43
Figure 2.22	The folder structure of the station's data bank.....	44
Figure 3.1	Electromagnetic spectrum and intervals.....	46
Figure 3.2	Spectral reflectance curve of snow.....	48
Figure 3.3	Variation of reflectivity for fresh snow, firn, glacier ice and dirty glacier ice.....	49
Figure 3.4	Grain size effect on the reflectivity of snow.....	50
Figure 3.5	Spatial and temporal resolution of various satellite sensors...	55
Figure 3.6	Flow line for snow cover monitoring system for NOAA-AVHRR.....	67
Figure 3.7	A true color MODIS image of Eastern TURKEY on 20/01/2004.....	74
Figure 3.8	Flow chart for processing MODIS snow cover maps.....	87
Figure 3.9	MODIS tiles that are used for the study.....	88
Figure 4.1	Hydrological modeling in a broad sense.....	94
Figure 4.2	Components of snowmelt runoff modeling.....	96
Figure 4.3	Components of SRM.....	105
Figure 4.4	Lag time effect on discharge calculations.....	116
Figure 4.5	Recession flow plot Q_n vs Q_{n+1}	117
Figure 5.1	MM5 modeling system data flow chart using Little_R/Rawsin.....	126
Figure 5.2	MM5 modeling system data flow chart using 3DVAR.....	127
Figure 5.3	Interpolation from regular latitude - longitude to selected mesoscale domain by Terrain.....	128
Figure 5.4	Vertical sigma coordinate levels used in MM5.....	132
Figure 5.5	Horizontal grid system of MM5.....	133
Figure 6.1	Processing chain for discharge forecasts.....	138
Figure 6.2	ECMWF Grib data format processing chain.....	139
Figure 6.3	MM5 Rip data format processing chain.....	140

Figure 6.4	Snow covered area percentages obtained from NOAA 17 for 2004 water year (April 1~ July 1).....	145
Figure 6.5	Snow covered area percentages obtained from MOD10A1 images for 2004 water year.....	147
Figure 6.6	Snow covered area percentages obtained from MOD10A2 images for Zone C of 2004 water year.....	149
Figure 6.7	Snow covered area percentages obtained from MOD10A2 images for Zone D of 2004 water year.....	149
Figure 6.8	Snow covered area percentages obtained from MOD10A2 images for Zone E of 2004 water year.....	150
Figure 6.9	The conventional depletion curves obtained from NOAA satellite images.....	151
Figure 6.10	The conventional depletion curves obtained from MODIS satellite daily snow cover images.....	151
Figure 6.11	The conventional depletion curves obtained from MODIS satellite 8-day snow cover composites for Zone B.....	153
Figure 6.12	The conventional depletion curves obtained from MODIS satellite 8-day snow cover composites for Zone C.....	154
Figure 6.13	The conventional depletion curves obtained from MODIS satellite 8-day snow cover composites for Zone D.....	154
Figure 6.14	The conventional depletion curves obtained from MODIS satellite 8-day snow cover composites for Zone E.....	155
Figure 6.15	Snow cover depletion curves obtained from NOAA, MOD10A1 and MOD10A2 for Zone B.....	156
Figure 6.16	Snow cover depletion curves obtained from NOAA, MOD10A1 and MOD10A2 for Zone C.....	157
Figure 6.17	Snow cover depletion curves obtained from NOAA, MOD10A1 and MOD10A2 for Zone D.....	158
Figure 6.18	Snow cover depletion curves obtained from NOAA, MOD10A1 and MOD10A2 for Zone E.....	159
Figure 6.19	The modified temporal interpolation of snow covered area...	160

Figure 6.20	The modified temporal interpolation of snow covered area for Zone B.....	161
Figure 6.21	The modified temporal interpolation of snow covered area for Zone C.....	162
Figure 6.22	The modified temporal interpolation of snow covered area for Zone D.....	163
Figure 6.23	The modified temporal interpolation of snow covered area for Zone E.....	164
Figure 6.24	Comparison of forecasted and measured temperature values for Zone C during April 2004.....	166
Figure 6.25	Comparison of forecasted and measured temperature values for Zone C during May 2004.....	166
Figure 6.26	Comparison of forecasted and measured temperature values for Zone C during June 2004.....	167
Figure 6.27	Comparison of forecasted and measured temperature values for Zone D during April-June 2004.....	167
Figure 6.28	Comparison of forecasted, measured and recalculated temperature values for Zone D during April to June 2004.....	169
Figure 6.29	Comparison of forecasted and recalculated temperature values for Zone E during April to June 2004.....	170
Figure 6.30	Comparison of forecasted and measured precipitation values for Zone B during April to June 2004.....	170
Figure 6.31	Comparison of forecasted and measured precipitation values for Zone C during April to June 2004.....	171
Figure 6.32	Comparison of 1997 and 1998 water years.....	172
Figure 6.33	Flowchart of model parameter selection.....	173
Figure 6.34	Re-runs for 1998 water year with 2004 parameters.....	176
Figure 6.35	Re-runs for 1998 water year with 2004 parameters and runoff coefficients (c_s , c_r) from 1998.....	177
Figure 6.36	Re-runs for 1997 water year with 2004 parameters.....	178

Figure 6.37	Re-runs for 1997 water year with 2004 parameters and runoff coefficients from 1997.....	178
Figure 6.38	Comparison of forecasted and measured discharges for Case 1 for MM5 data.....	181
Figure 6.39	Comparison of forecasted and measured discharges for Case 2 for MM5 data.....	181
Figure 6.40	Comparison of forecasted and measured discharges for Case 3 for MM5 data.....	182
Figure 6.41	Comparison of forecasted and measured discharges for Case 4 for MM5 data.....	182
Figure 6.42	Comparison of forecasted and measured discharges for Case 5 for MM5 data.....	183
Figure 6.43	Comparison of forecasted and measured discharges for various SCA information for MM5 data.....	184
Figure 6.44	Comparison of forecasted and measured discharges for Case1 for temperature correction.....	185
Figure 6.45	Comparison of forecasted and measured discharges for Case 2 for temperature correction.....	185
Figure 6.46	Comparison of forecasted and measured discharges for Case 3 for temperature correction.....	186
Figure 6.47	Comparison of forecasted and measured discharges for Case 4 for temperature correction.....	186
Figure 6.48	Comparison of forecasted and measured discharges for Case 5 for temperature correction.....	187
Figure 6.49	Comparison of forecasted and measured discharges for various SCA information for temperature correction.....	187
Figure 6.50	Comparison of forecasted and measured discharges for Case 1 for precipitation correction.....	190
Figure 6.51	Comparison of forecasted and measured discharges for Case 2 for precipitation correction.....	191

Figure 6.52	Comparison of forecasted and measured discharges for Case 3 for precipitation correction.....	191
Figure 6.53	Comparison of forecasted and measured discharges for Case 4 for precipitation correction.....	191
Figure 6.54	Comparison of forecasted and measured discharges for Case 5 for precipitation correction.....	192
Figure 6.55	Comparison of forecasted and measured discharges for various SCA information for precipitation correction.....	193
Figure A.1	Comparison of Temperature Values for Zone A.....	215
Figure A.2	Comparison of Temperature Values for Zone B.....	216
Figure A.3	Comparison of Temperature Values for Zone C.....	217
Figure A.4	Comparison of Temperature Values for Zone D.....	218
Figure A.5	Comparison of Temperature Values for Zone E.....	219
Figure A.6	Comparison of Precipitation Values for Zone A.....	220
Figure A.7	Comparison of Precipitation Values for Zone B.....	221
Figure A.8	Comparison of Precipitation Values for Zone C.....	222
Figure A.9	Comparison of Precipitation Values for Zone D.....	223
Figure A.10	Comparison of Precipitation Values for Zone E.....	224

LIST OF SYMBOLS

SYMBOL

ASP	:	Automated Snow Pillow
AMS	:	Automated Meteorological Station
AVHRR	:	Advanced Very High Resolution Radiometer
BUFR	:	Buffer
CDC	:	Conventional Depletion Curve
CMG	:	Climate Modeling Grid
D_v	:	Deviation of runoff volumes
DEM	:	Digital Elevation Model
DMI	:	State Meteorological Organization
DMSP	:	Defense Meteorological Satellite Program
DSI	:	State Hydraulic Works
ECMWF	:	European Center for Medium Range Weather Forecasts
EDG	:	EOS Data Gateway
EOS	:	Earth Observing System
ETA	:	Numerical Weather Prediction Model run at National Centers for Environmental Prediction
GCP	:	Ground Control Point
GIS	:	Geographic Information Systems
GRIB	:	Grid in Binary
HCMM	:	Heat Capacity Mapping Mission
HBV	:	Hydrological Model of Sweden's Meteorological and Hydrological Institute
HDF	:	Hierarchical Data Format

Hydalp	:	Hydrology of Alpine and High Latitude Basins
L	:	Time Lag
M	:	Snowmelt rate
MDC	:	Modified Depletion Curve
MM5	:	Mesoscale Model Version 5
MODIS	:	Medium Resolution Imaging Spectroradiometer
MSG	:	Meteosat Second Generation
NCAR	:	National Center for Atmospheric Research
NDSI	:	Normalized Difference Snow Index
NDVI	:	Normalized Difference Vegetation Index
NOAA	:	National Oceanic and Atmosphere Administration
NSIDC	:	National Snow and Ice Data Center
NWP	:	Numerical Weather Prediction
NWS	:	National Weather Service
OLS	:	Operational Line Scan System
Q	:	Average daily discharge
R^2	:	Nash-Sutcliffe coefficient
RCA	:	Rainfall Contributing Area
RIP	:	Read Interpolate Plot
RS	:	Remote Sensing
RMS	:	Root Mean Square
S	:	Ratio of Snow Covered area to the total area
SCA	:	Snow Covered Area
SDC	:	Snow Depletion Curve
SDS	:	Scientific Data Set
SMMR	:	Scanning Multi Channel Microwave Radiometer
SRM	:	Snowmelt Runoff Model
SWE	:	Snow Water Equivalent
T	:	Number of Degree Days
T_a	:	Average Daily Temperature
T_b	:	Base Temperature

T_{crit}	:	Critical Temperature
VISSR	:	Visible/Infrared Spin Scan Radiometer
WMO	:	World Meteorological Organization
ρ_s	:	Density of Snow
ρ_w	:	Density of Water
γ	:	Temperature Lapse Rate

CHAPTER I

INTRODUCTION

1.1 Problem Definition

Water, the most precious natural source, is gaining more and more importance due to the increasing demands in domestic, industrial and agricultural uses as a result of the increasing population, climate change and reduced water quality due to pollution.

Precipitation in the form of either rainfall or snowfall is the major source of fresh water. Mountains are the major springs of fresh water by the high amount of rainfall and snowfall they receive. Even though, there is not very much difference in between them as being fresh water source, importance of snow is much more pronounced in mountainous regions where the seasonal accumulation is followed by lengthy melting periods lasting for months.

Snow gains a bit more importance due to the fact that snow induced runoff, which is triggered by melting snow, usually begins in spring, a period after which high demands of water will arise. A good planning scheme of the melting snow can meet the increasing demand of agriculture, municipal water supply, energy production, enable the flood mitigation and provide navigation besides recreational facilities.

Methods of estimation and planning of the melting snow are being searched as the importance of snow became apparent. Methods ranging from purely statistical methods which neglect the physics of snowmelt process to the complicated energy budget equations are being used. Temperature index and energy budget equations are the most commonly used approaches. The discrepancies in model formulations related with the snowmelt have been the difficulties in obtaining input data, existence of little historical measurements and the accuracy of the performed measurements. Till recent times, snow data has been obtained by manual snow courses performed, which are labor intensive and expensive. With the advances in sensor technology, equipments that are durable to extreme weather and harsh winter conditions are provided. Such equipments enable the construction of automatic data acquisition systems that make snow and meteorology related data collection and data transfer from remote site even in real time basis. These continuously and real time collected data form the basis for snow related studies. The reducing prices following the mass production in sensor technology, makes the construction of such automated stations a possibility. Even though successful applications of such systems exist, due to the calibration and updating of the stations, the manual snow surveys are still needed. More over, data gathered from these automated data acquisition systems are site specific and there remains the problem of representativeness of these point values of the whole basin.

Remote sensing (RS) and geographic information systems (GIS) are two new technologies that are being used increasingly in snow hydrology. They can be used for analyses of the measured snow and meteorological data, performing necessary up and/or down scaling processes, preparation of input variables to the hydrological models, determination of parameters required by these models and presenting the outputs of the model runs.

Spatial and temporal heterogeneity of snow is a well-known problem. Estimation of snowmelt from this heterogeneous medium by conventional

methods is very difficult. Remote sensing offers the advantage of obtaining snow data like snow covered area and snow water equivalent for snowmelt runoff prediction in real time which is an important factor for a dynamic phenomenon like snow.

GIS became an inevitable tool in hydrology and gaining importance with the capabilities it offers in hydrological modeling. It enables the collection, storage and analysis of large data volumes. Topographic properties like elevation, slope and aspect of the basin can be combined with the performed snow measurements and their interrelations can be found. Such analysis can be helpful in upscaling of the point measurements of hydrologic and meteorological parameters. The auxiliary data such as land cover and land use can be integrated to GIS to calculate the model parameters required by the hydrological models. GIS can also be used to prepare the input files of the hydrological models. Especially for forecasting studies, the data obtained from Numerical Weather Prediction models (NWP) can be imported into GIS to determine the meteorological variables that the basin will be subject to in the following date(s).

Hydrologic modeling approaches are tools of transforming the incoming water into the basin to the discharge observed at the outlet. The discharge formulation can vary from black box approaches to physically based models having different degrees of spatial variation. The formulations may change according to the type of the precipitation (i.e. rainfall or snowfall), the way that flow ways are determined, losses are handled and the basin is considered (i.e. either lump or distributed). Independent of the formulation, the accurate timing and volume estimation of the calculated discharge are the key information for the efficient water use.

It is believed that a suitable integration between RS, GIS and an appropriate hydrological model would provide accurate estimates for efficient water management, energy production and flood mitigation.

1.2 Purpose of the Study

Snowmelt runoff induced by melting snow is extremely important in the mountainous eastern part of Turkey. Although the precipitation observed in these high elevation ranges are not very much, these mountainous regions have very strong effects on feeding of the rivers. Euphrates River, being such, originates among the highest regions of Turkey, Eastern Anatolia and passes through arid and semi arid regions and makes its way along Syria, Iran, Iraq and Saudi Arabia. Largest dams of Turkey, namely Keban, Karakaya and Atatürk are located on this river. The aridity of the region, existence of large dams and the water requirements of the downstream nations necessitate accurate and optimum operation of these dams. The case of which is highly dependent upon the forecasting of the melting of snow which covers the ground nearly in the half of the year and constitutes nearly 70% of the total annual flow (Kaya, 1999; Tekeli, 2000).

Since the performed snow studies are not in a sufficient quality for a detailed near real time snowmelt runoff forecasting study, a number of missions needed to be completed. Some of the missions performed during this study cover a wide range starting from selection of sensors, ordering of selected sensors, construction of automated snow and meteorological stations, on line data transfer from the remote stations to the main office in Ankara, searching the methods for satellite data analysis, formation of a transfer protocol for meteorological data retrieval, decoding of numerical weather prediction models, deriving the basin wide precipitation and temperature values and integration of the meteorological variables into the snowmelt runoff model (SRM). These studies which are used for pre-operational runoff forecasts in this present work will be used to form a basis for the real time forecasting of the snowmelt runoff coming to headwaters of Euphrates River.

The topics mentioned in the following chapters can be summarized as;

In chapter 2, the test basin and the snow-meteorological stations that were constructed during project study is mentioned in detail. Some of the issues that can be considered as frontiers in Turkey can be summarized as following. Installation of first hypalon snow pillows in Turkey, collection of meteorological data such as air temperature, air pressure, air humidity, incoming and outgoing solar radiation, net radiation, net long wave radiation, wind speed & direction, precipitation rate, snow data such as snow depth, snow water equivalent and snow albedo. Automatically transfer of the above variables by one of the satellite phone, GSM or hard wire lines in real time can be counted among the successes of the thesis. The chapter also mentions about the first real time snowmelt lysimeter that is designed and installed in Turkey. The snow melt timing and rate gathered from this instrument is used as main information for the other snow related studies (Tekeli et al., 2005a). Chapter ends with mentioning the preliminary works for a snow database formation.

In chapter 3 the remote sensing properties of snow and the two optical satellites namely National Oceanic and Atmospheric Administration (NOAA) and Moderate Resolution Imaging Spectroradiometer (MODIS) are mentioned in a concise manner (Tekeli et al., 2005b). Earth observation data was mainly used for deriving snow covered area. The snow albedo information gathered from MODIS satellite is also downloaded and compared with albedo measurements performed at the snow stations. From the NOAA series, the Advanced Very High Resolution Radiometer (AVHRR) satellite 17 is used. A multi criteria threshold scheme was prepared for determination of snow covered area (SCA). The initial derived SCA maps are compared with those obtained from MODIS. Thus, an intercomparison of snow cover products from various sensors is carried out. Due to cloud obscure the optical satellite images are degraded. Thus a method is needed to determine the SCA values for the cloudy dates (Tekeli et al., 2005c).

In chapter 4, snowmelt runoff model (SRM) which is the basis for hydrological modeling in this thesis is presented after a summary of the snow hydrology.

In chapter 5, a short history of numerical weather prediction (NWP) models is provided. The two well known NWP models, European Center for Medium Range Weather Forecasts (ECMWF) and Mesoscale Model Version 5 (MM5) used in the thesis study are summarized. Sub programs and the specific data formats of each data set are also mentioned.

In chapter 6, hydrological forecasting studies performed at Upper Euphrates River Basin are mentioned. The way the NWP model data handled and the model runs are summarized. The comparison of NWP with the observed data from the meteorological stations and the necessary adjustments made for model input file preparation are also presented. The comparison of Digital Elevation Model (DEM) and the land use layers used by the NWP are also compared with the data sets at hand. Discussion of results is provided at the end of the chapter.

In chapter 7, some information related with future work and the possible areas for development are mentioned. Conclusions and recommendations derived from this doctorate study are also included in the chapter.

CHAPTER II

BASIN DESCRIPTION AND DATABASE

2.1 Introduction

In this chapter some common means of obtaining meteorological and snow data i.e. the way to measure snow related properties, quantities and the way to handle the gathered data will be discussed. Although these techniques are being used for long times in developed nations, most of these common methods are new to developing nations. Some of the automated instrumentations were used for the first time in Turkey. This caused some ambiguities and anxiety. But most of the time the designs performed better than expected and provided the data as expected in a sufficient accuracy and quality both during the test stages and in the operation life time.

Following sections will provide a short summary of the basin studied during the research and will give detailed information about the automated snow and meteorological stations and the instrumentations that were designed, manufactured and operated in these stations during the work carried out in research period.

2.2 Upper Euphrates River Basin

Euphrates and Tigris rivers are the two major rivers both for Turkey and Middle East Countries. Of these two rivers, Euphrates originates from the mountainous, rough topography of Eastern Anatolia. For this mountainous topography of Eastern Anatolia, snow is the main supply of the Euphrates River. Among the several branches of Euphrates River, Upper Euphrates River Basin, which is also known as Karasu Basin, receive high amount of its annual discharge mainly from snowmelt runoff.

In this study, the near real time application of snowmelt runoff model (SRM) for 2004 water year is performed for Karasu Basin. The basin boundaries can be given by longitudes from $38^{\circ} 58'013''$ E to $41^{\circ} 38'28''$ E and latitudes $39^{\circ} 23'18''$ N to $40^{\circ} 24'26''$ N. Figure 2.1 shows the basin location in map of Turkey.

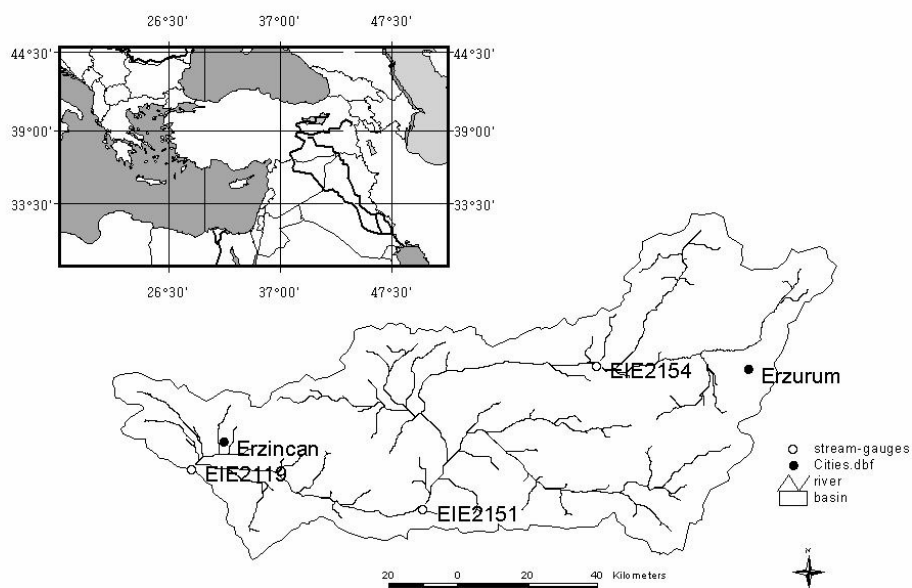


Figure 2.1 Location of Upper Euphrates River Basin

Karasu Basin, with an area of 10215.7 km^2 is mountainous and rugged with elevation ranging from 1125 to 3487m. For SRM runs the basin is sub

divided in to five elevation zones. Table 2.1 presents the sub zones of the Karasu basin. Figure 2.2 ~ Figure 2.7 shows the hypsometric curves of the zones and the whole Karasu Basin.

Table 2.1 Elevation zones of Karasu Basin

Zone	Elevation Range (m)	Area (km²)	Area (%)	Hypsometric Mean Elevation (m)	Mean Slope (%)
<i>A</i>	1125-1500	1123.2	11	1352	6.1
<i>B</i>	1500-1900	3268.5	32	1751	11.5
<i>C</i>	1900-2300	3459.3	34	2097	18.1
<i>D</i>	2300-2900	2196.8	21	2482	21.3
<i>E</i>	2900-3487	167.9	2	2989	26.3
<i>Whole Basin</i>	1125-3487	10215.7	100	1977	15.5

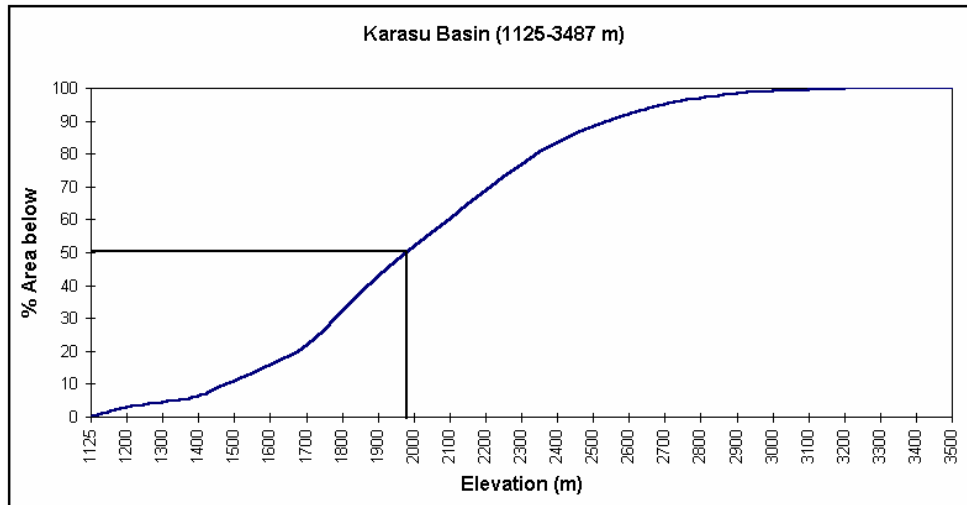


Figure 2.2 Hypsometric curve for the whole Karasu Basin

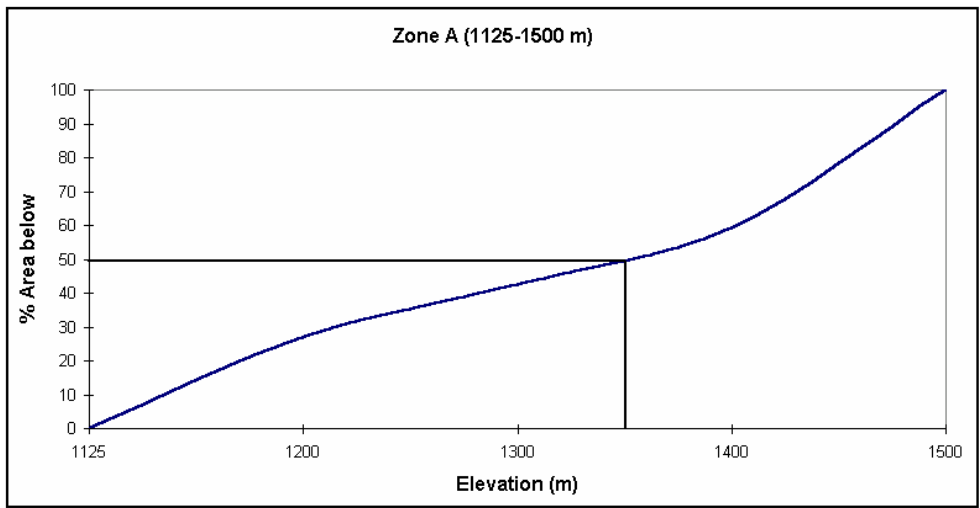


Figure 2.3 Hypsometric curve for Zone A of Karasu Basin

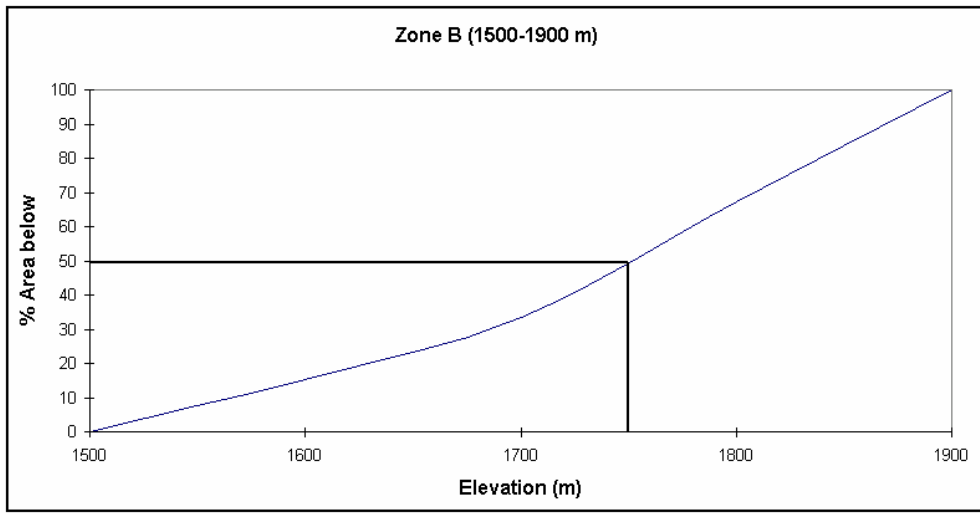


Figure 2.4 Hypsometric curve for Zone B of Karasu Basin

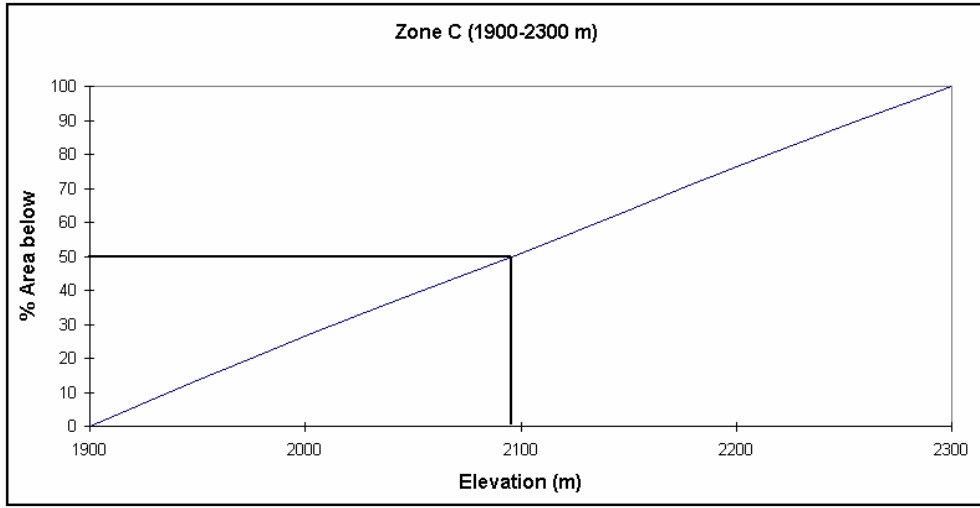


Figure 2.5 Hypsometric curve for Zone C of Karasu Basin

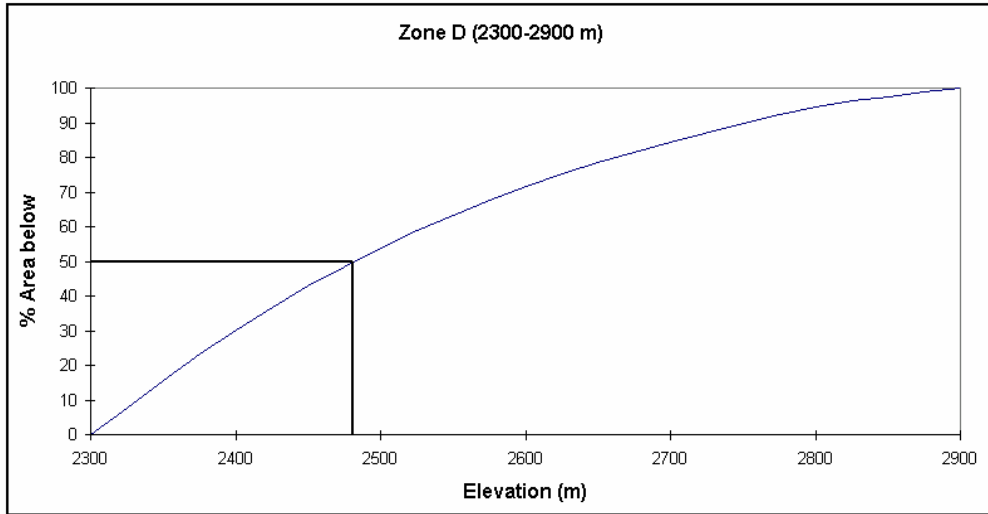


Figure 2.6 Hypsometric curve for Zone D of Karasu Basin

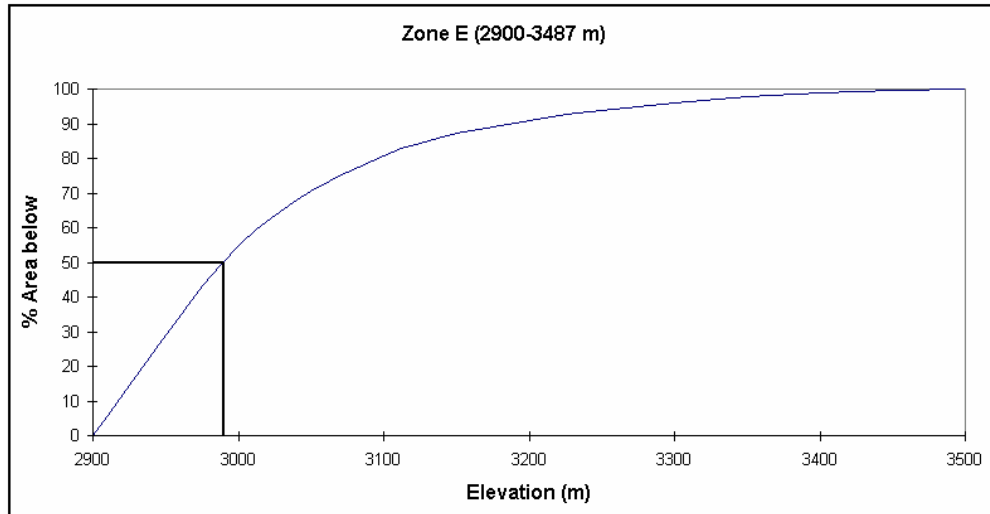


Figure 2.7 Hypsometric curve for Zone E of Karasu Basin

Land cover in Karasu Basin is mainly grass, shrub and bare land. Erzurum city, Erzincan city and Tercan plain with a total area of 1310 km² are the main agricultural plains of the basin (Kaya, 1999).

With drainage areas of 2120 km² and 372 km² the Tercan and Kuzgun are the major dams in the basin.

Runoff from the basin is recorded by several gauging stations one of which is (EIE 2119) at the basin outlet at 39° 41' N, 39° 23'36''E. Electrical Power Resources Survey & Development Administration (EIE) is operating it since 1954. In the downstream of the basin there exist large dams of Turkey, namely Keban, Karakaya and Atatürk, all, which are designed for hydropower production, irrigation and water supply.

Based on the long-term analysis of EIE 2119 station records, it is seen that 60~70 % of the total annual runoff comes between 15 March-15 July, which matches with the main snow melting period of the region.

Table 2.2 represents the long term observed discharges in EIE 2119 gauging station. The high percentage of snowmelt runoff indicates the necessity of accurate snowmelt runoff estimation both in rate, volume and timing.

2.3 Automated Snow and Meteorological Stations

Hydrological models, either designed for snow processes or rainfall-runoff relationships, need areal average precipitation and temperature values as the main input variables. Most of the time these are obtained from point values at the meteorological stations. The accuracy and the representative character of these point measurements are vital considerations.

What makes the things more complicated is the rough topography. Especially in mountainous regions these point values may show large differences. Unfortunately, in Turkey, the highest meteorological station is located at Erzurum with an elevation of 1758m. Thus, for an accurate estimation and/or measuring of precipitation and temperature values in Upper Euphrates Basin, establishment of automated meteorological stations at higher elevations is needed.

Furthermore, from hydrological point of view, snow water equivalent (SWE), which is actually the multiplication of snow density and snow depth, is an important characteristic of snow. This important variable is measured by state organizations twice a month at different dates. In this 15-day period most of the snow may diminish in some elevations of the basin. Thus the time interval between the measurements around the Upper Euphrates Basin should be decreased.

But, accessing the remote sites may be both problematic and dangerous in wintertime. Thus, for continuous observation of SWE in the area of study, automated snow stations are needed.

Table 2.2 Long term discharges observed at EIE 2119

Water Year	Total volume of water (10 ⁶ m ³)	Volume of water (15 March-15 July) (10 ⁶ m ³)	% of Total volume
1954	36402.2	26564.1	73.0
1956	29380.9	21586.5	73.5
1957	30014.7	20467.8	68.2
1958	22910.7	15318.0	66.9
1959	25051.1	17971.1	71.7
1960	31057.1	22082.8	71.1
1961	14393.5	8051.9	55.9
1962	19499.0	13280.0	68.1
1963	43774.7	33460.2	76.4
1964	28980.1	20425.2	70.5
1965	26796.7	19064.7	71.1
1966	34596.5	22481.5	65.0
1967	36461.7	26378.5	72.3
1968	54525.8	41014.4	75.2
1969	42826.2	30501.2	71.2
1970	24826.6	14620.0	58.9
1971	24230.9	16185.0	66.8
1972	22524.9	15213.4	67.5
1973	21080.4	13985.0	66.3
1974	24566.7	16991.2	69.2
1975	25485.0	18596.6	73.0
1976	34838.0	26896.4	77.2
1977	28407.5	19363.1	68.2
1978	32814.5	23460.1	71.5
1979	31229.6	22020.2	70.5
1980	40071.5	28506.7	71.1
1981	30143.0	20242.4	67.2
1982	32958.5	23522.7	71.4
1983	18231.9	11300.3	62.0
1984	28378.3	18007.3	63.5
1985	21391.5	13862.4	64.8
1986	22828.4	14980.9	65.6
1987	42123.2	31760.9	75.4
1995	34331.3	24645.4	71.8
1996	32236.7	18991.9	58.9
1997	31319.2	20101.9	64.2
1998	34003.5	24082.7	70.85
Average	30126.8	20972.8	68.8

During this research period, first real time operating automated meteorological stations and automated snow stations were constructed at Güzelyayla station. As a successful operation is obtained at Güzelyayla station - the related coordinates and information of the station will be given briefly in the following section- the formerly constructed snow stations are updated and provided to work in real time mode.

Following sections will mention about the automated meteorological and snow station Güzelyayla and others that are either constructed or updated during this study.

2.4 Initial Automated Meteorological and Snow Station Setup at Güzelyayla

Güzelyayla, automated snow pillow (ASP) and automated meteorological station (AMS), is the first real time data collecting, storing and transferring station of its kind. Since this station is the first of its kind, the instruments installed and monitored at this station will be mentioned in a more detailed manner and then other observation sites will be described.

2.4.1 Location, Geography and Climate

Güzelyayla station, a research site within the ASP-AMS monitoring system of the Upper Euphrates River Basin, was built in October 2001. It is located in Güzelyayla district about 30 km North East of the Erzurum city. The station is located at 40°12'01'' N, 41°28'22'' E and at an elevation of 2065m. The vegetation cover in site is mainly grass. The topography at the station is gentle and the aspect is horizontal. The site is near to the basin boundary. Winters are usually cold and dry. Snow normally covers the ground from late October to mid of April. The maximum observed snow depth was 600 mm with a snow water equivalent of 175 mm for winter period of 2002-2003. Maximum snow water occurs in late March.

2.4.2 Instrumentation

Güzelyayla observation site is equipped with instrumentation necessary for monitoring several hydrological and meteorological parameters needed for energy-based snow melt modeling. The instruments in Güzelyayla available for conducting snowmelt studies can be seen in Figure 2.8 and they are listed in Table 2.3.

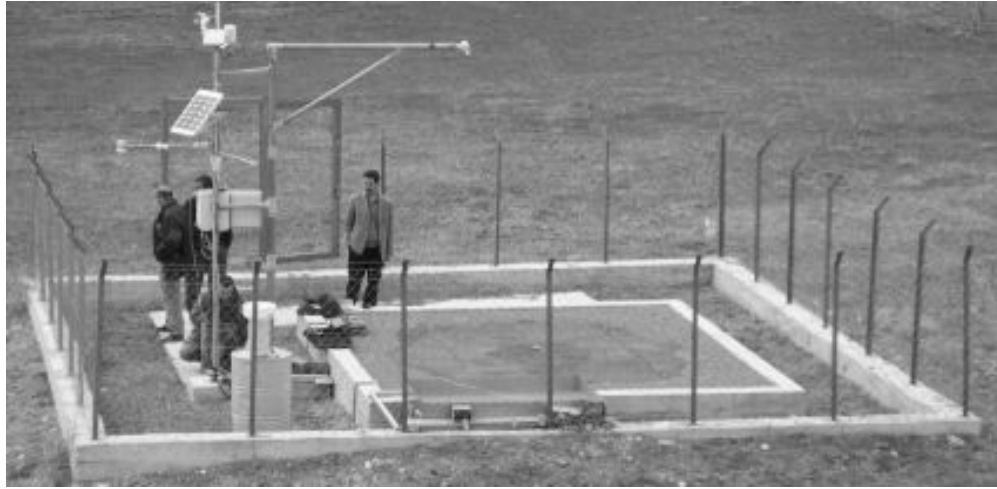


Figure 2.8 Overview of Güzelyayla station

Table 2.3 Instrumentation at Güzelyayla research site

Meteorological /Snow Parameter & Devices	Instrument	Observation Interval	Installation (month/year)
Snow Water Equivalent	Hypalon Snow Pillow	Continuous	10/2001
Snow Depth	Judd Communications Depth Sensor	Continuous	10/2001
Air Temperature	HMP 45 C Temperature and Relative Humidity Probe	Continuous	10/2001
Relative Humidity			
Wind Speed & Direction	Metone 034A-L Wind Set	Continuous	10/2001
Air Pressure	Vaisala, PTB101B	Continuous	10/2001
Global Radiation	CM3, Kipp & Zonen	Continuous	10/2001
Net Radiation	NR Lite, Kipp & Zonen	Continuous	9/2001
Precipitation	Met One-385L	Continuous	9/2002
Albedometer	2- CM3, Kipp & Zonen	Continuous	9/2002
Snowmelt Runoff	Snowmelt Lysimeter	Continuous	9/2002
Soil Temperature		Continuous	10/2003
Data Logger	CR10 X (Campbell Scientific)		10/2001
Satellite Telephone	Inmarsat Mini-M		10/2001 6/2003*
Telephone Modem	Turk Telekom		6/2003
Power Supply	20 W Solar Panel		10/2001

* Date of dismantle

Sensors observe all of the above listed parameters continuously. The measurements are performed at every 30 seconds by the sensors and logged to the data logger as two hourly averages.

Snow Water Equivalent

Snow water equivalent (SWE) is the amount of liquid water that will result by melting of a given amount of snow. Since the liquid water that will be released

for runoff is highly dependent to SWE value, it is the utmost important snow related parameter in hydrology. Snow water equivalent is usually indexed by measuring the snow mass at one or more points with stationary, hydraulically operated, “snow pillow” balances or by taking snow cores and weighing them with portable scales (Steppuhn, 1981). A number of observations at one site is performed and the average of the measurements are used.

A hypalon snow pillow, enabling real time data transfer is constructed in Güzelyayla station for the first time in Turkey in October 2001. The snow pillow continuously measures the water equivalent of the snow cover. A schematic drawing of the snow pillow and the installed pillow in site can be seen in Figure 2.9 and Figure 2.10 respectively.

The snow pillow is a 3-meter diameter hypalon, flat pillow filled with a total of around 600 liters liquid mixture of water, antifreeze and alcohol. The snow pillow is in level with the surrounding ground (See Figure 2.10). Through a copper-connecting pipe, the snow pillow is connected to a pressure sensor. The pressure sensor measures the liquid pressure in the pillow, which reflects the weight of the overlying snow cover. The pressure transducer used is custom made, Sensotec 060-C851-02-02. It can measure between 0 to 25 mBar with accuracy of $\pm 0.1 \%$. The details of the snow pillow design can be obtained from Tekeli (2002a).

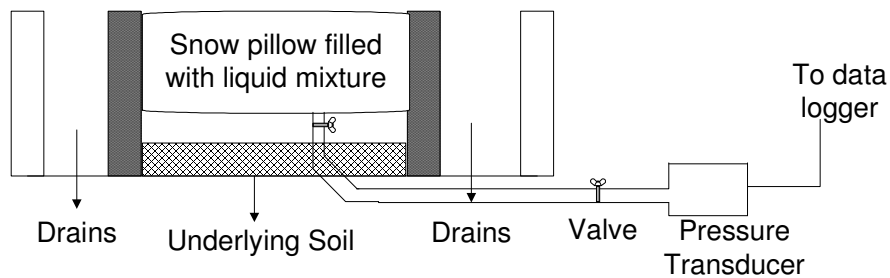


Figure 2.9 Schematic drawing of the Güzelyayla snow pillow

Since, bridging effects within the snow cover can affect the accuracy in the measurements, the ground-based measurements of SWE are used in conjunction with the snow pillow measurements.



Figure 2.10 Installed snow pillow at Güzelyayla station

With the removal of the snow from the snow pillow the pressure measurements of the snow pillow are expected to be zero. But due to the settlement of the adjacent soil near to the pillow, this may not be the actual case. Thus, before the formation of new snow cover, adjusting the reading of the snow pillow to zero is a necessity.

Snowmelt Lysimeter

Snowmelt runoff is measured by snowmelt lysimeter at the Güzelyayla station. The first operational snowmelt lysimeter was installed at Güzelyayla station in October 2002. Tekeli (2002b) gives detailed description of the installed snowmelt lysimeter. Figure 2.11 shows the schema of the first operational snowmelt lysimeter installed in Turkey.

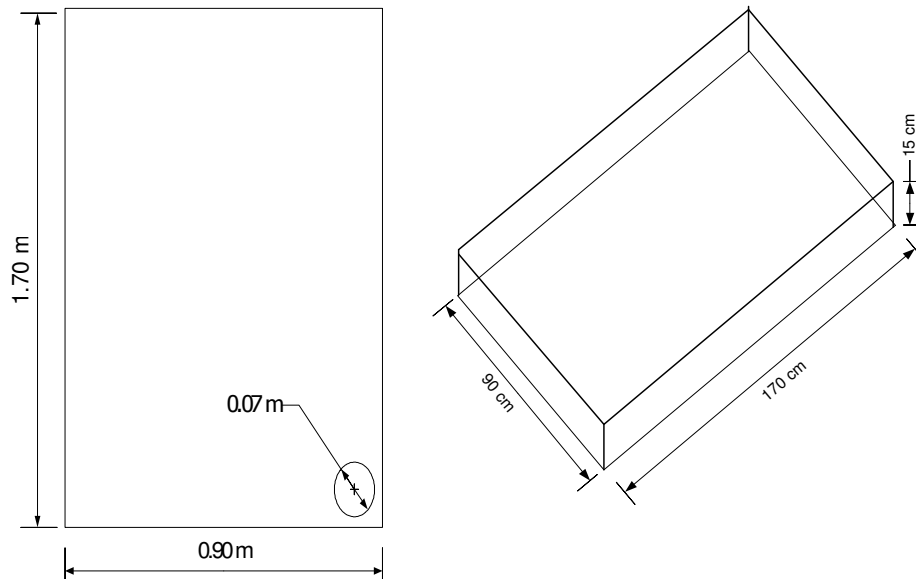


Figure 2.11 Schematic drawing of the snowmelt lysimeter at Güzelyayla station

Collector tray is made from 2 mm thick 200 cm x 120 cm rectangular galvanized sheet. Previous studies in literature proposed a rim of 15 cm. After leaving 15 cm for the rims, the dimensions of the collector tray are reduced to 90 cm x 170 cm with a net area of 1.53 m². Collected melt water drains through an opening of 7 cm in diameter to a tipping bucket type rain gauge. Installed lysimeter at site can be seen in Figure 2.12. The performance evaluation of the Güzelyayla snowmelt lysimeter can be found in Tekeli et al. (2003c, 2004 and 2005a)



Figure 2.12 Installed snowmelt lysimeter at Güzelyayla station

Snow Depth

Judd Ultra Sonic Depth Sensor monitors snow depth continuously. Sensor can measure in the range of 0.5-10 m with an accuracy of $\pm 1\text{cm}$ or 0.4% of the distance to target. However, the sensor can measure up to 3 m snow depth at Güzelyayla station due to installation conditions. A code is written to the data logger to overcome the faulty readings that may arise due to the bouncing back of the sonic waves from the falling snow.

Precipitation

Precipitation is measured continuously by Met One 385-L tipping bucket type rain gauge since October 2002. The gauge has an orifice area of 200 cm². Although there is a heater in the tipping bucket, it was not operated due to the high power consumption. The sensor has an accuracy of 0.1 mm.

Air Temperature

Air temperature is automatically recorded by Campbell Scientific HMP 45C air temperature and humidity probe. The probe has a Platinum Resistance Temperature detector fitted inside a radiation screen. The working range of the sensor is given between – 40°C to + 60°C with an accuracy of ±0.5°C varying with temperature.

Relative Humidity

Relative humidity is measured by Campbell Scientific HMP 45C air temperature and humidity probe. The probe uses Vaisala Humicap 180 capacitive relative humidity sensor. The sensor is fitted in a shield to protect it from rain and solar radiation. Working range of the instrument is given from 0 % to 100 % with an accuracy of ±2 % (0 to 90 % Relative Humidity) or ±3% (90 to 100 % Relative Humidity).

Wind Speed and Direction

Met One, 034A-L wind set, measures wind speed and direction. The set uses an anemometer with 3 cups to measure the wind speed. The measuring range is from 0 m/s to 49 m/s. For wind speeds less than 10.1 m/s the accuracy is ±0.12 m/s, whereas the accuracy is given as ±1.1% of readings for wind speeds greater

than 10.1m/s. The direction angle can measure between 0~360° with an accuracy of $\pm 4^\circ$.

Air Pressure

Air pressure is recorded continuously by Vaisala PTB101B analog barometer instrument. The sensor is inside the shelter of the data logger to keep away from the rain and solar radiation. The operating range of the sensor is between 600-1600 mbar with an accuracy of ± 0.5 to ± 3 mbar varying with operating temperature.

Global Radiation (Short wave Radiation)

Short wave radiation is measured by Kipp & Zonen, CM3 pyranometer. The pyranometer mainly uses thermopile sensor. CM3 is sensitive to the wavelengths 0.305 to 2.8 μm with a sensitivity of 10 ~35 W/m^2 and accuracy of $\pm 10\%$ in daily sums. The pyranometer measures the sum of diffuse and direct beam short wave radiation. The sensor construction is such that it measures the solar energy that is received from the whole hemisphere (180° field of view).

Net Radiation

Net radiation is the summation of the net short wave and net long wave radiation thus usually called as net (total) radiation. It is measured by Kipp&Zonen NR-Lite sensor. It is based on a thermopile detector. It has a working range in the spectral range of 0.2 ~100 μm with a nominal sensitivity 10 $\mu\text{V}/\text{W}/\text{m}^2$ and stability is less than $\pm 2\%$ per year. The operating range is from – 2000 to 2000 W/m^2 . The expected directional error 0-60° at 1000 W/m^2 is less than 30 W/m^2 .

Albedometer

This is the first time that the albedo of snow is measured and transferred in real time in Turkey. The instrument is composed of two 2- CM3, Kipp & Zonen sensors, an Albedometer fixture CAF1 is used to combine the two pyranometers. One of the sensors face up to the sky and one face down to the ground surface, both parallel to ground surface. The one looking to the sky measures the incoming solar radiation, where else the one facing down measures the reflected solar radiation. Details of the installation can be found in Tekeli (2002b)

Soil Temperature

First measurements of the soil temperatures were initiated in Güzelyayla in October 2003. The sensor was placed 15-20 cm bellow the ground surface. The design and installation of the sensor can be seen in Şorman (2004) in detailed manner. This was among the pioneers in the snow studies in Turkey. However, the expected performance could not be obtained from the sensor. Thus, upgrading of the sensor is under consideration.

Data Logger

All the sensors mentioned in the above paragraphs are connected to a data logger. For Güzelyayla station CR10X data logger produced by Campbell Scientific is used. CR10X has Hitachi 6303 processor, with a data storage capacity of 128 kbytes standard SRAM. Approximately 60,000 data values are stored at most. As new data is received, they are overwritten on the data with the earliest record date. CR10X has an operating range of -25°C to $+50^{\circ}\text{C}$, these values can also be extended.

2.4.3 Data Collection and Data Transfer

Campbell Scientific CR10X data logger records data collected at Güzelyayla station in every two hours, taking the average of the sensor measurements performed at every 30 seconds in two hour duration. Based on two hourly values, daily averages are also computed. Daily maximum and minimum values of each parameter and the observation time of these maximum and minimum values are also logged.

The database of the Güzelyayla station with respect to water years is shown in Table 2.4.

Table 2.4 Database of Güzelyayla station with respect to years

Parameter	2001	2002	2003	2004
Snow Water Eq.				
Snow Depth				
Air Temperature				
Relative Humidity				
Wind Speed & Direction				
Air Pressure				
Global Radiation				
Net Radiation				
Precipitation				
Albedometer				
Snowmelt Runoff				
Soil Temperature				

||||| : Data present

□ : Missing due to uninstalation

|||||: Data available except from 19 December 2001 to 1 February 2002; due to power problem (break of charger unit)

 : Data available except from 21-24 September 2002; due to data logger program update

 : Available by April 2004

The data from the field at Güzelyayla station was initially transferred by Inmarsat Mini-M Satellite phone to the main office in Ankara. But the high communication rates necessitated the change of the data transfer system. Normal telephone modem was installed in July 2002 (Tekeli, 2003b). The new communication system enabled cheaper data transfer costs. In addition to automatically collected data, regular manual snow depth and snow water equivalent measurements performed by 8th District of State Hydraulic Works (DSI) near to Güzelyayla station enabled comparison of the snow depth and snow water equivalent values obtained from the continuous recording snow pillow.

2.5 Instrumentation at Other Observation Sites

Meteorological and hydrological parameters show great variability in mountainous regions. To adequately represent these variations, meteorological stations in the other representative points within the basin is a necessity. Thus, during this study, three previously established stations during the collaborated research done by Middle East Technical University (METU) and DSI between 1997-2000, namely Hacımahmud, Ovacık and Çat were revised. Some necessary equipment changes and upgrades were performed. The general distribution of the stations within the basin can be seen in Figure 2.13. Table 2.5 summarizes the location, elevation and other relevant data of each station. The following sections (2.5.1~2.5.4) will discuss each automated meteorological and snow stations separately.

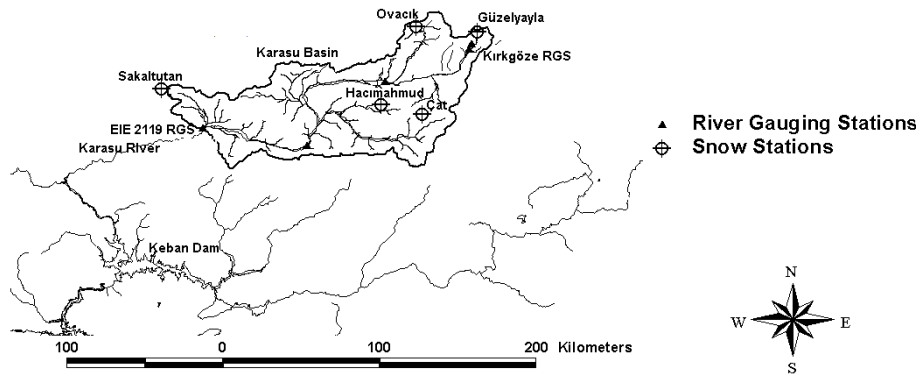


Figure 2.13 Distribution of automated snow and meteorological stations within the Upper Euphrates River Basin (Karasu)

Table 2.5 Location and elevation of automated snow and meteorological stations within Upper Euphrates River Basin

Name of Station	Coordinates (Geographic WGS84*)		Elevation (m)	Within Zone	Date of Construction.	Date of Renewal
	Lat.	Long.				
Hacımahmud	39° 48' 21'' N	40° 43' 45'' E	1965	C	1999	2002
Güzelyayla	40° 12' 01'' N	41° 28' 22'' E	2065	C	2001	2003
Ovacık	40° 14' 48'' N	41° 00' 03'' E	2130	C	1999	2003
Sakaltutan	39° 52' 24'' N	39° 07' 54'' E	2150	C	1999	----
Cat	39° 44' 37'' N	41° 00' 34'' E	2340	D	1999	2003

* World Geodetic System 1984

2.5.1 Ovacık Station

Ovacık meteorological and snow station was located at 40° 14' 48'' N 41° 00' 03'' E at an elevation of 2130m. The station was initially established by NATO SfP project in 1999 (Şorman et al., 2002) and updated during the ongoing research. The climate is much more severe than Güzelyayla Station. Increased

elevation may be a reason both for the climate change and the deeper snowpack formation with respect to Güzelyayla.

2.5.1.1 Instrumentation

At Ovacık station, data collection and its storage are all performed automatically. Similar to Güzelyayla station, sensors make measurements at every 30 seconds, logging the average of the measured values in two hourly periods. Besides, the daily average, maximum and minimum recorded values and their respective times are also logged to the data logger. The related instrumentation for snow studies can be seen in Table 2.6. A general view from the station is given in Figure 2.14. The second snowmelt lysimeter designed by the team is installed at Ovacık station in October 2003. The installed lysimeter can be seen in Figure 2.15.

Table 2.6 Instrumentation in Ovacık Station

Meteorological /Snow Parameter	Instrument	Observation Interval	Installation (month/year)
Snow Water Equivalent	Metal Snow Pillows	Continuous	1999
	Hypalon Snow Pillow	Continuous	9/2002
Snow Depth	Judd Communications Depth Sensor	Continuous	1999
Air Temperature	HMP 45 C Temperature and Relative Humidity Probe	Continuous	1999
Relative Humidity			
Wind Speed Direction	Young 05103 RM	Continuous	1999
Wind Direction	Young 05103 RM	Dismantled (10/2003)	
Air Pressure	Vaisala, PTB101B	Dismantled (10/2003)	
Global Radiation	CM3, Kipp & Zonen	Continuous	9/2002
Incoming and out going thermal radiation	CG2, Kipp & Zonen	Continuous	10/2003
Precipitation	Met One-385L	Continuous	1999
Albedometer	2- CM3, Kipp & Zonen	Continuous	10/2003
Snowmelt Runoff	Snowmelt Lysimeter	Continuous	10/2003
Data Logger	CR10 X (Campbell Scientific)		1999
Satellite Telephone	Inmarsat Mini-M		1999
Telephone Modem	Turk Telekom		10/2003



Figure 2.14 General view of Ovacık station



Figure 2.15 Snowmelt lysimeter installed at Ovacık station

Ovacık station was built in 1999. The metal snow pillows which were placed as the station was constructed were replaced with Hypalon snow pillow in September 2002. Global radiation sensor was upgraded in September 2002. In October 2003, an albedometer, a net long wave radiation sensor and a snowmelt lysimeter were installed. However, air pressure and wind direction sensor had to be dismantled from the data logger due to insufficient data logger input capacity. Table 2.7 shows the database of Ovacık station with respect to water years.

Table 2.7 Database of Ovacık station with respect to years

Parameter	2001	2002	2003	2004
Snow Water Eq.	▨	▨	▨	▨
Snow Depth	▨	▨	▨	▨
Air Temperature	▨	▨	▨	▨
Relative Humidity	▨	▨	▨	▨
Wind Speed	▨	▨	▨	▨
Wind Direction	▨	▨	▨	▨
Air Pressure	▨	▨	▨	▨
Global Radiation	▨	▨	▨	▨
Precipitation	▨	▨	▨	▨
Net Longwave Radiation	▨	▨	▨	▨
Albedometer	▨	▨	▨	▨
Snowmelt Runoff	▨	▨	▨	▨

▨ : Data present

▨ : Missing due to uninstallation

▨ : Data available except 26/12/2002 to 30/12/2002 ; due to power problem (break of charger unit)

▨ : Data available except from 1/1/2003 to 6/1/2003; due to power problem:

▨ : Available after October 2003

▨ : Dismantled as October 2003

 : Data available except from 8/11/2003 to 11/11/2003; due to power problem

 : Data available except from 13/3/2004 to 16/3/2004; due to power problem

2.5.1.2 Data Collection and Data Transfer

Before October 2003, the communication with data logger from remote access was performed with Inmarsat Mini-M satellite phone. The system was changed to normal telephone modem in October 2003. This change enabled cheaper data transfer from the site to the main office at METU in Ankara.

The consistency of downloaded data were checked and then uploaded to the database. Harsh weather conditions resulted some data losses especially in winter time. But in the overall the Ovacık station worked quite satisfactorily.

2.5.2 Çat Station

With an elevation of 2340 m, Çat station is the highest located real time data transferring meteorological and snow station in Turkey. The station is located at 39° 44' 37'' N 41° 00' 34'' E. As the Ovacık station, Çat was also established as a part of NATO SfP project (Şorman et al., 2002) and updated by the sponsored State Planning Organization Project which is ongoing at the moment. The site is much more windy with respect to other stations and instruments are more exposed to severe winter conditions. The snow covers ground from November to early May. The depth of snow may reach two meters. The climate is mountainous with air temperatures below freezing in winter period.

2.5.2.1 Instrumentation

As the station was established daily averages of the measured values were collected. Beginning from October 2003 data collection and storage were all performed automatically in a fashion that sensors make measurements at every 30

seconds, logging the average of the measured values in two hourly periods similar to Güzelyayla and Ovacık stations. Besides, the daily average, maximum and minimum recorded values were also logged to the data logger. The related instrumentation for snow studies can be seen in Table 2.8. A general view from the station is provided in Figure 2.16.

Table 2.8 Instrumentation in Çat Station

Meteorological /Snow Parameter	Instrument	Observation Interval	Installation (month/year)
Snow Water Equivalent	Metal Snow Pillows	Continuous	1999
	Hypalon Snow Pillow	Continuous	10/2003
Snow Depth	Judd Communications Depth Sensor	Continuous	1999
Air Temperature	HMP 45 C Temperature and Relative Humidity Probe	Continuous	10/2003
Relative Humidity			
Wind Speed & Direction	Metone 034A-L Wind Set	Continuous	10/2003
Air Pressure	Vaisala, PTB101B	Continuous	10/2003
Global Radiation	Davis 7823	Continuous	9/2002
	CM3, Kipp & Zonen	Continuous	10/2003
Net Radiation	NR Lite, Kipp & Zonen	Continuous	10/2003
Data Logger	CR10 X (Campbell Scientific)		1999
Satellite Telephone	Inmarsat Mini-M		1999



Figure 2.16 General view of Çat meteorological and snow station

Çat station was installed and initiated to operate automatically via Inmarsat Mini-M satellite in 1999. The initially provided metal snow pillows were replaced with Hypalon snow pillow in October 2003. Moreover, a temperature and humidity sensor in addition to wind speed and direction sensor, air pressure and global radiation sensors were also installed. Table 2.9 shows the database of Çat station with respect to water years.

Table 2.9 Database of Çat station with respect to water years

Parameter	2001	2002	2003	2004
Snow Water Eq.				
Snow Depth				
Air Temperature				
Relative Humidity				
Wind Speed & Direction				
Air Pressure				
Global Radiation				
Net Radiation				

- : Data present
- : Missing due to uninstallation
- : Missing date 15/1/2003
- : Available after 6/2/2003
- : Available after 10/2003
- : Data available except from 20/10/2003 to 27/10/2003

2.5.2.2 Data Collection and Data Transfer

There occurred serious technical and electronic changes since Çat station started to operate in 1999. However, the communication system of the station could not be changed from satellite phone to either GSM or normal telephone modem. The high elevation and the location of the station within the mountains prevented the usage of the above mentioned data transfer systems. Thus unfortunately, communication with the station is provided by Inmarsat Mini-M satellite phone, which is rather expensive with respect to budget constraints. The other means of data transfer are under research. Data collection and storage interval was set similar to Güzelyayla and Ovacık stations in October 2003.

2.5.3 Hacımahmud Station

Hacımahmud station was established within the NATO SfP Project in 1999. The station is located at 40° 43' 45'' E and 39° 48' 21'' N and at an elevation of 1965m. Since this station is at the lowest elevation, the climate is much more warmer than the remaining other stations. SWE and snow depth values and the time period that the ground surface is covered with snow are much less than the other stations.

2.5.3.1 Instrumentation

Hacımahmud station records data on daily averages since it was built. Besides the daily averages, daily maximum, minimum values and their time of observation are also logged. Instrumentation within the station can be seen in Table 2.10.

Figure 2.17 shows the general view of the station and the installed sensors.

Table 2.10 Instrumentation in Hacımahmud station

Meteorological /Snow Parameter	Instrument	Observation Interval	Installation (month/year)
Snow Water Equivalent	Metal Snow Pillows	Continuous	1999
Snow Depth	Judd Communications Depth Sensor	Continuous	1999
Air Temperature	HMP 45 C Temperature and Relative Humidity Probe	Continuous	1999
Relative Humidity			
Wind Speed & Direction	Young 05103 RM	Continuous	1999
Air Pressure	Vaisala, PTB101B	Continuous	1999
Global Radiation	Li-Cor 200x	Continuous	1999
Data Logger	CR10 X (Campbell Scientific)		1999
Satellite Telephone	Inmarsat Mini-M		1999-2002*
GSM Modem	Siemens		2001

* Date of dismantle

Although, most of the other stations are changed from metal snow pillows to hypalon ones, financial constraints did not allow the team members to upgrade metal snow pillow of Hacımahmud.



Figure 2.17 General view of Hacımahmud station

2.5.3.2 Data Collection and Data Transfer

Communication with Hacımahmud station was achieved with Inmarsat Mini-M satellite phone for some time. However in 2001, the communication system was changed to GSM system. This enabled faster and cheaper data transfer from site to main office in Ankara. With the reduced cost advantage of the GSM system, high power consumption prevented every time connection to the station. Thus, data logger turned on the GSM system between 10:00 to 12:00 and 15:00 to 17:00 enabling the communication. Table 2.11 presents the database of Hacımahmud station.

Table 2.11 Database of Hacımahmud station with respect to years

Parameter	2001	2002	2003	2004
Snow Water Eq.				
Snow Depth				
Air Temperature				
Relative				
Wind Speed & Direction				
Air Pressure				
Global Radiation				

 : Data present

2.5.4 Sakaltutan Station

Sakaltutan station is located in the most downstream portion towards the north western boundary of the basin. It is located at 39° 07' 54'' E and 39° 52' 24'' N and at an elevation of 2150m. This station is also one of the stations those were constructed within the NATO Sfp Project in 1999.

2.5.4.1 Instrumentation

Sakaltutan station records data on daily averages since it was built. Besides the daily averages, daily maximum, minimum values and their time of observation are also logged. Instrumentation within the station can be seen in Table 2.12.

Table 2.12 Instrumentation in Sakaltutan station

Meteorological /Snow Parameter	Instrument	Observation Interval	Installation (month/year)
Snow Water Equivalent	Metal Snow Pillows	Continuous	1999
Snow Depth	Judd Communications Depth Sensor	Continuous	1999

Due to the budget constraints and due to the location of the Sakaltutan station no upgrades were performed.

2.5.4.2 Data Collection and Data Transfer

Communication with Sakaltutan station is achieved with Inmarsat Mini-M satellite phone. Table 2.13 represents the database of the station.

Table 2.13 Database of Sakaltutan station with respect to years

Parameter	2001	2002	2003	2004
Snow Water Eq.				
Snow Depth				

 : Data present

2.6 Database

Accurate and representative data collection is a crucial point in snow hydrology related studies. Where else the data management is another vital issue in operational snow studies. A good data management would allow data share among different organizations in an efficient manner, reducing the data duplication, eliminating erroneous data production and preventing the data loss. Thus, data collection, handling and the flow of information are the key issues in a successful application of operational and near real time forecasting studies.

The data management concept can be subdivided into three main steps as; data retrieval, data processing and the data bank formation. Following sections will explain some of the performed studies related with each step through out the thesis study.

2.6.1 Data Retrieval

Data can be downloaded either by remote access or on site. In both cases, a computer is needed to supply the connection with the data logger. The serial port of the computer with a RS232 connector cable can perform connection any time on site.

For remote connection, either an ordinary telephone line is enough or a GSM line with data transfer capability is required. Table 2.14 summarizes the data collection interval, data transfer system and the connectivity to stations in Karasu Basin by October 2003 in remote access mode.

Table 2.14 Data collection interval, data transfer system and the connectivity to stations in Karasu Basin.

Station Name	Elevation (m)	Data collection interval	Data transfer system	Communication
Hacımahmud	1965	Daily average	GSM	10:00-12:00 15:00-17:00
Güzelyayla	2065	2 hourly averages & daily averages	Turk Telekom	24 hours
Ovacık	2130	2 hourly averages & daily averages	Turk Telekom	24 hours
Sakaltutan	2150	Daily average	Inmarsat Mini-M	24 hours
Çat	2340	2 hourly averages & daily averages	Inmarsat Mini-M	24 hours

Through out the study, the data from the site were downloaded partly by METU Water Resources Laboratory's staff by remote access or by 8th District of State Hydraulic Works personnel from site.

2.6.2 Data Processing

Figure 2.18 summarizes the data processing schema followed during the research period.

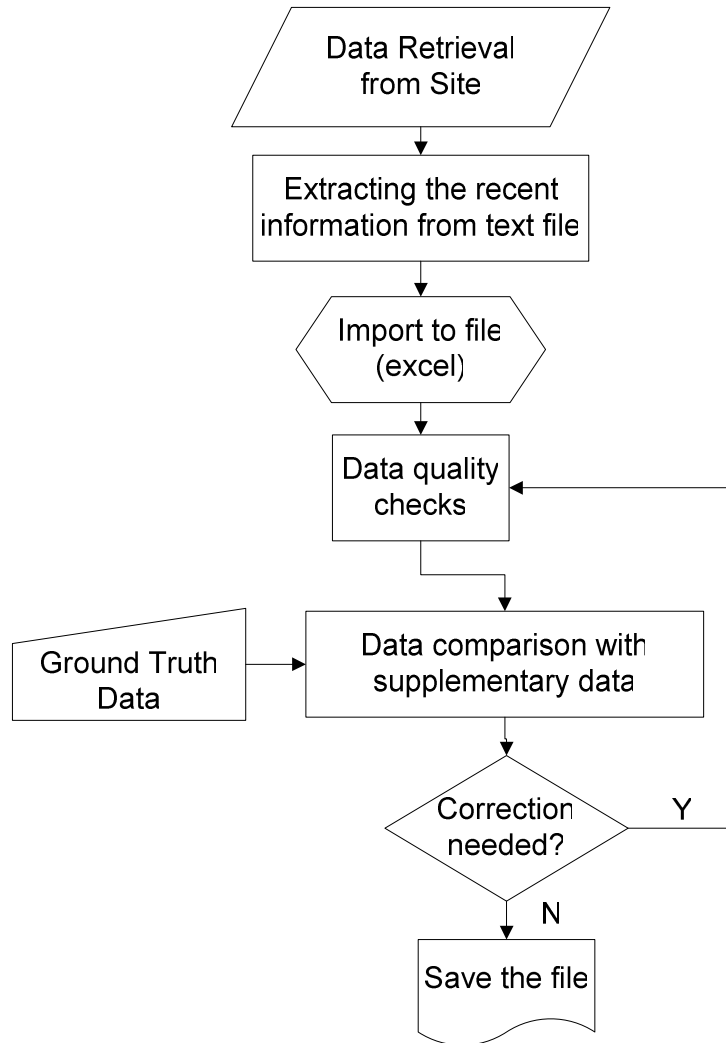


Figure 2.18 Flow chart of data processing

Even though, time and manpower required to pre-process the data for providing model inputs should be minimized in an operational study, this could not be achieved. One of the reasons is the fact that most of the supplementary data comes either in hard copy format or the formats of the digital data changes too much. It is believed that further studies would enable the automatic data flow.

Processes indicated in Figure 2.18 are applied for each station in site. Downloaded data from the site comes in ASCII text format.

Figure 2.19 shows a part of the downloaded data received from Güzelyayla station. The file includes the two hourly and the daily averages in the same file with different id numbers. Two hourly values have 100 as id and the daily average values have 110 as id. For each id data comes in predefined order. The order and the heading of each data with the same id are programmed in data logger before hand.

```

100,2004,144,200,7.95,.365,1.161,4.581,79.9,1.568,356.6,0,-65.77,6999,795.71,0,0,-317.48,358.91,11.182
100,2004,144,400,8.27,.486,4.6,4.138,79.2,1.116,7.92,0,-63.32,6999,795.32,0,0,-317.35,359.22,10.416
100,2004,144,600,8.83,.103,-.158,4.345,78.9,1.848,348.6,34.53,-40.99,6999,795.03,0,0,-317.74,359.76,9.5165
100,2004,144,800,8.56,-.913,-.077,8.6,68.04,3.046,40.2,366.1,172.6,.197,794.89,0,0,-318.75,359.5,8.2238
100,2004,144,1000,6.963,-1.644,-.668,12.15,52.62,1.435,136.8,741.458,.169,795.02,0,0,-319.48,357.97,8.2564
100,2004,144,1200,3.813,-1.254,-.651,14.08,45.75,2.164,247.8,965.629,4,.163,794.72,0,0,-319.09,354.96,9.4454
100,2004,144,1400,1.582,-.685,-.461,14.79,40.87,1.751,208.4,613.2,359.5,.17,794.3,0,0,-318.53,352.82,10.771
100,2004,144,1600,2.371,-.416,-2.689,15.97,40.98,3.181,202,804,462.6,.18,793.64,0,0,-318.26,353.58,11.458
100,2004,144,1800,2.516,.002,.575,13.4,51.63,4.519,25.06,264,4.084,.201,793.62,0,0,-317.84,353.72,13.382
100,2004,144,2000,4.042,.32,1.426,10.88,63.61,2.727,52.48,26.4,-35.46,6999,794.39,0,0,-317.52,355.18,14.264
100,2004,144,2200,6.083,.314,2.484,9.3,67.64,3.81,154.1,0,-38.26,6999,795.61,0,0,-317.53,357.13,13.498
100,2004,144,2400,6.709,458,2.187,8.34,76.1,1.12,347.2,0,-51.37,6999,795.55,0,0,-317.38,357.73,12.778
110,2004,144,2400,7.0425,.58545,1.2029,10.05,62.102,2.3571,16.663,317.84,149.25,99999,794.82,0,0,12.944,2.74
74,339,32.345,1153,17.035,1446,87.084,2357,7.5786,1656,17.781,-3.7432,932,1.2108,136,-
317.25,358.05,11.099,2065

```

Figure 2.19 Sample ASCII format of the Güzelyayla station

Related portion from the text file is imported to Excel. The pre-defined parameter headings are inserted, necessary calculations; graphing and quality checks are performed. Figure 2.20 shows some of two hourly averaged Güzelyayla data imported into excel. Figure 2.21 represents graph of the snow depth observations obtained from the stations mentioned in above paragraphs.

Station	Year	Day	Time	A Snow Press	A Snow Depth	A Snow Density	A W Temp
No			hh:mm	(mm) or (kg/m2)	(cm)	(%)	(oC)
100	2003	60	200	132,7	53,69	0,247	-19,56
100	2003	60	400	132,8	53,47	0,248	-20,45
100	2003	60	600	132,9	53,38	0,249	-20,99
100	2003	60	800	133,1	51,88	0,257	-18,53
100	2003	60	1000	133,3	51,63	0,258	-13,33
100	2003	60	1200	133,4	51,6	0,258	-11,61
100	2003	60	1400	133,2	52,19	0,255	-10,7
100	2003	60	1600	133,2	52,84	0,252	-11,56
100	2003	60	1800	133,1	53,34	0,25	-15,39
100	2003	60	2000	132,9	53,42	0,249	-17,21
100	2003	60	2200	133,1	53,32	0,25	-18,32
100	2003	60	2400	132,7	53,19	0,25	-18,51

Figure 2.20 Sample excel format of Güzelyayla station

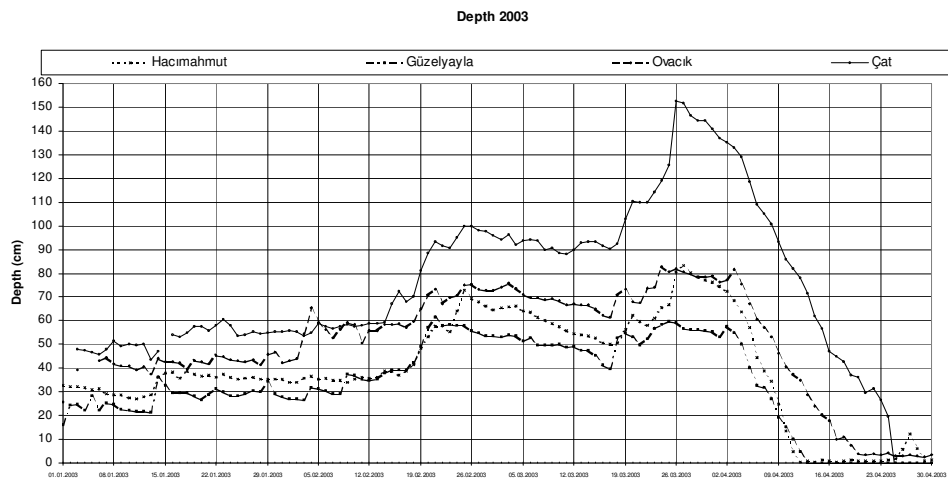


Figure 2.21 Graphs of snow depth observations obtained from the automated stations within the basin

2.6.3 Data Bank Formation

Figure 2.18 is applied to each station and the final data are stored as excel files. The files are named with the name of the month that the data belongs to. The same station's files are kept in the same folder under the respective month. And all of the stations are kept under the same folder named with the year that the data they contain. Figure 2.22 shows the file structure of the data bank.

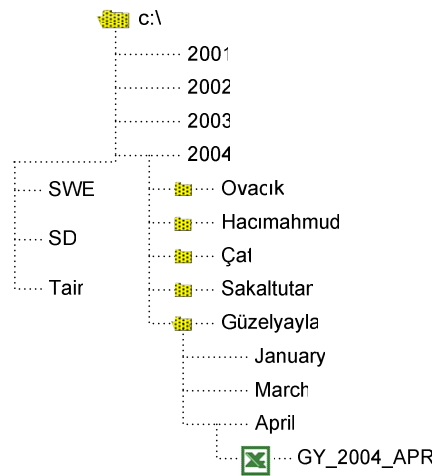


Figure 2.22 The folder structure of the station's data bank

Since variation of some parameters such as snow water equivalent, snow depth, air temperature among the stations is important in calculation of some variables such as temperature lapse rate, the charts and data of the stations are also produced as separate excel files.

CHAPTER III

REMOTE SENSING METHODS USED IN SNOW HYDROLOGY

3.1 Introduction

This chapter mentions about the spaceborn remote sensing methods required for snowmelt runoff monitoring and/or forecasting in mountainous basins of Eastern Turkey. Main objective of this chapter is deriving the spatially distributed snow covered area (SCA) percentage that is required as one of the main input variables of the hydrological snowmelt runoff model (SRM) from earth observation satellites. SRM requires estimates of SCA at least on weekly basis (Rango, 1993).

Runoff volume induced from snowmelt is directly correlated to the snow covered area. It is therefore of advantage to exploit satellite monitoring instead of modeling the snow coverage from precipitation and temperature (Seidel and Martinec, 2004).

At the moment some methods exist for performing the above-mentioned task. But the thing to be done is implementing an operational processing scheme that allows fast, objective and reliable snow cover mapping enabling routine

applications of the methods. The methods developed during the study are tested in Upper Euphrates River Basin.

A success criterion of such studies is the runoff forecasting ability in near-real time. The ultimate goal is to make a forecast within twelve hours after image acquisition. Transfer of remotely sensed image is made over the Internet. Geocoding, information extraction, hydrological modeling and forecasting should be completed within 6 hours.

3.2 Spectral Characteristics of Snow

Rango (1993) mentions the usability of radiation gamma ray to microwave portions of the electromagnetic spectrum for determination of snow properties. Figure 3.1 shows the electromagnetic spectrum and its intervals.

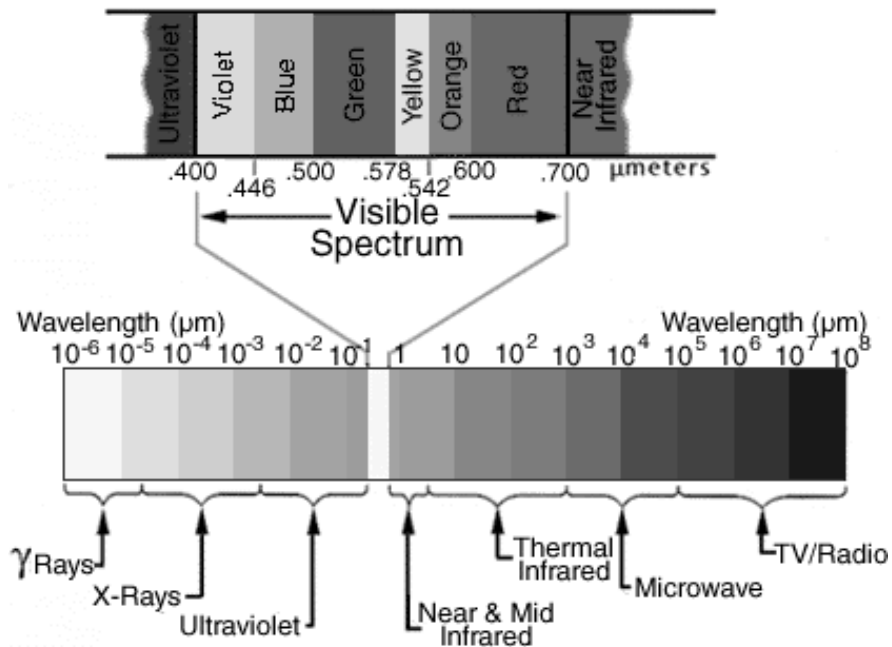


Figure 3.1 Electromagnetic spectrum and intervals
(adapted from Lillesand and Kiefer, 1994)

Using the microwave region of the spectrum has some advantages than the visible and near infrared region. However, visible region has been the most utilized part of the electromagnetic spectrum for operational studies (Rango, 1996). Snow has a unique reflectance behavior; illuminated by the sun; snow is one of the brightest objects in nature in the optical and near infrared range ($\sim 0.410 \mu\text{m}$), but is rather dark in the medium infrared ($\sim 1.5\text{-}2.5 \mu\text{m}$) (Seidel and Martinec, 2004). Unfortunately, shadow makes snow in any case as “dark”. Following sections will summarize the snow properties in each electromagnetic spectrum range.

3.2.1 Gamma Rays

Snow absorbs gamma radiation emitted by radioisotopes in the soil such as potassium, uranium and thorium. The use of gamma radiation to measure snow water equivalent is based on the attenuation of natural terrestrial radiation by the mass of water in the overlying snow cover (Rango et al., 2000). Successful operational applications of gamma measurements for snow water equivalent are reported by NWS operational airborne snow survey program. Atmosphere also rapidly absorbs the gamma radiation. Thus, gamma radiation sensors can only be applied in low flying aircraft. This situation prevents the airborne gamma measurement in rugged topographic areas.

3.2.2 Visible and Near Infrared

High reflectivity of snow in the visible (VIS) and near infrared (NIR) portion of the spectrum is used for discriminating snow from other land features. Freshly fallen snow may have reflectance values as high 90~95 % in the visible region.

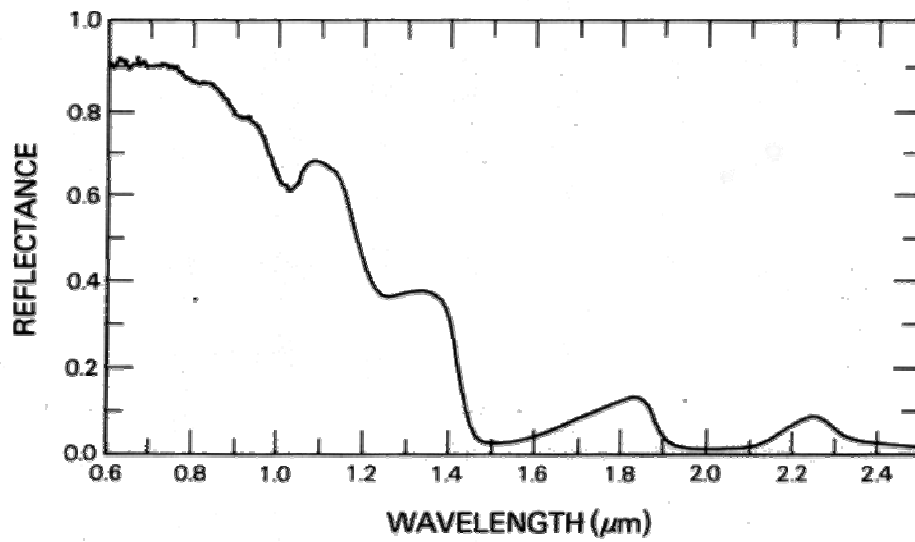


Figure 3.2 Spectral reflectance curve of snow
(Adapted from Hall and Martinec, 1985)

Reduction of snow reflectivity in VIS and NIR region is reported by Hall and Martinec (1985). Figure 3.3 shows the variation of spectral curves for fresh snow, firn, glacier ice and dirty glacier ice.

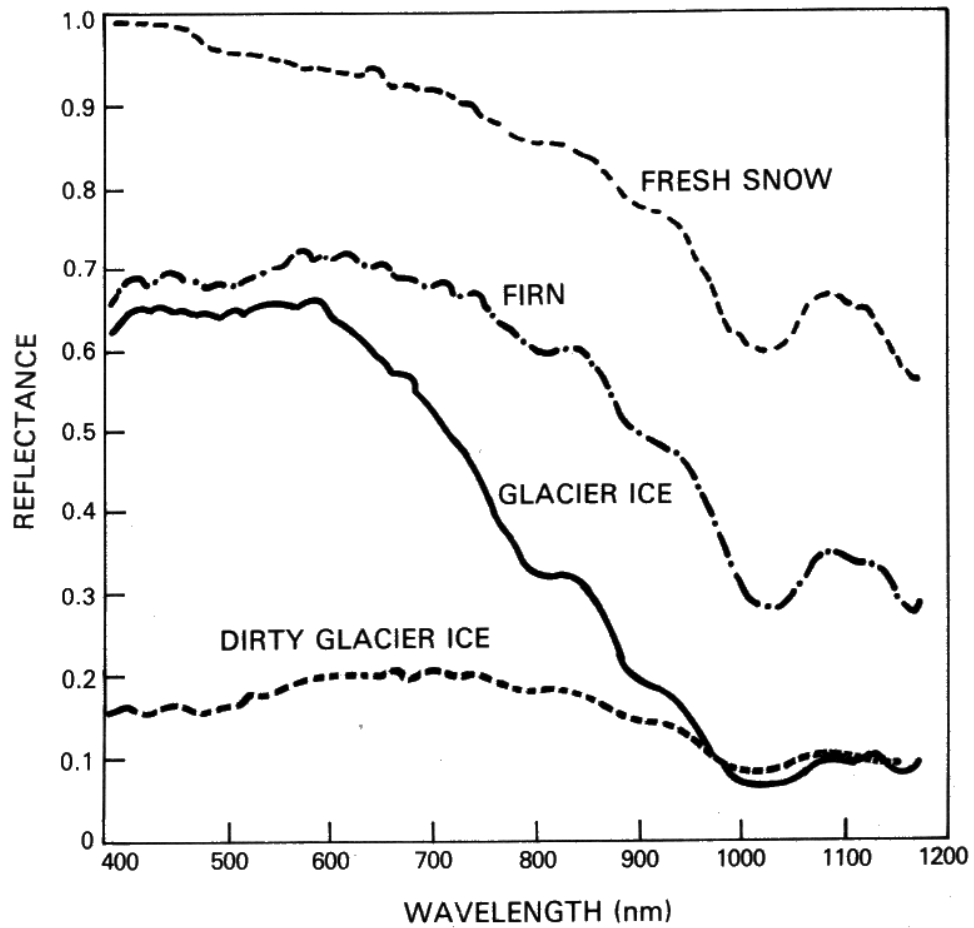


Figure 3.3 Variation of reflectivity for fresh snow, firn, glacier ice and dirty glacier ice (Adapted from Hall and Martinec, 1985)

Increase of grain size as a result of melting and refreezing cycles and the impurity contamination cause the reflectivity reduction of snow with aging (See Figure 3.3). Wavelengths from 0.95 to 1.4 μm best show the grain size change effect. Figure 3.4 represents the grain size effect on the snow reflectivity.

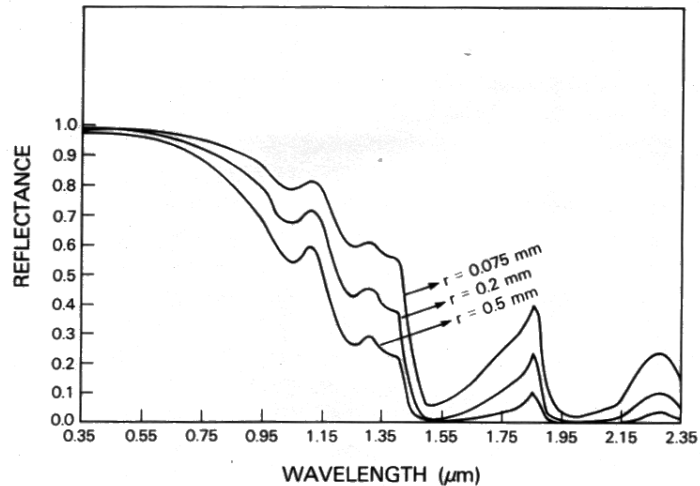


Figure 3.4 Grain size effect on the reflectivity of snow
(Adapted from Hall and Martinec, 1985)

High albedo of snow (even firn may have reflectance as high as 60 %), makes it to be easily detected by EO satellites in the VIS channels. Dozier et al (1981) summarized the effect of different snow characteristics on the reflection in VIS and NIR channels of AVHRR. Schneider et al. (1981) extended the same study to the land use classes.

An important topic in remote sensing of snow, directional reflectance of snow is discussed by bidirectional reflectance density function of snow in Foster et al. (1987). Kuhn (1985) reported a reflective peak at 60° of polar and alpine snow.

An advantage of using visible and near infrared data is the easy interpretation of the image. Many operational snow cover mapping applications are performed using visible and near infrared region of spectrum.

Even though, snow extent can be easily extracted, no information regarding the snow water content can be derived. Clouds, on the other hand may degrade the use of visible and near infrared images in snow related studies.

3.2.3 Thermal Infrared

Thermal infrared channels measure the radiation emitted by the Earth's surface that is dependent on surface temperature. These channels can be used to measure snow surface temperature (Collier et al., 1989). If the snow surface stays at 0°C both day and night, then it is highly likely that the snowpack is isothermal and that melt is occurring and being released at the base of the snowpack (Rango, et al., 2000).

Like visible and near infrared images, clouds limit the usability of thermal infrared images. If there exist cloud, temperature at the top of the cloud would be measured. Moreover, Dozier and Warren (1982) have mentioned about the viewing angle effects on the emission of radiation in thermal wavelengths.

3.2.4 Microwave

Radiation emitted at wavelengths of millimeters to centimeters from the surface is within the range of microwave radiometers. Microwaves not only penetrate snow to a limited amount but also get scattered by snow crystals. As a result of scattering the microwave emission from the snow surface becomes less than the ground emission.

Actually the physical characteristics of the snowpack determine its microwave properties. Properties affecting microwave response from a snowpack include; depth and water equivalent, liquid water content, density, grain size and shape, temperature, stratification as well as snow state and land cover. Since the response of snow varies with its state, regular monitoring may allow the detection of the onset of melt.

Radiation measured at different wavelengths and at different polarizations enables the extraction of information related with snow depth and snow water equivalent. Superiority of microwave with respect to visible imagery is the independency of measurements from weather condition and illumination. Thus nighttime data can also be used.

For large catchments, microwave images have been used for snow cover and depth analysis. However, their low spatial resolutions prevent their usability in mountainous basins (Rango, 1996).

Before giving an end to the spectral characteristics of snow, a summary of the above mentioned issues are summarized in Table 3.1 and Table 3.2. Table 3.1 shows the snow properties that affect its reflectance values. Table 3.2 summarizes the relation between spectral bands and the snow properties.

Table 3.1 Snow properties affecting its reflectance

	Visible Reflectance	Near Infrared Reflectance	Thermal Infrared Emissivity	Microwave Emissivity
Grain size	*	Yes	No	Yes
Zenith Angel	No	Yes	Yes	Yes
Depth	Yes	No	No	Yes
Contaminants	Yes	No	No	No
Liquid water content	No	*	No	Yes
Temperature	No	No	No	Yes
Density	No	No	No	Yes

* Only for thin snowpack or impurities exist

Table 3.2 Relation between snow properties and spectral bands
(adapted from Engman and Gurney, 1991)

Property	Visible/Near Infrared	Thermal Infrared	Microwave
Snow covered area	Yes	Yes	Yes
Depth	If very shallow	Weak	Moderate
Snow water equivalent	If very shallow	Weak	Strong
Stratigraphy	No	Weak	Strong
Albedo	Strong	No	No
Liquid water content	Weak	Weak	Strong
Temperature	No	Strong	Weak
All weather capability	No	No	Yes
Current best resolution of satellites	Tens of meters	Hundreds of meters	Passive: 30-150 km Active: tens of meters

3.3 History of Remote Sensing of Snow

Rango et al. (1977), proved the effective application of remote sensing for prediction of snowmelt runoff.

In 1978, Rott used Landsat MSS and Very High Resolution Radiometer for frequent snow cover mapping in the Alps (Rott, 1978).

Martinec and Rango (1987) used satellite derived snow cover data for hydrological modeling and showed usefulness of this information. In the same

year Wiesnet et al. (1987) outlined the importance of remote sensing methods for snow cover mapping.

Hall and Martinec (1985) summarize the initial snow studies related with snow mapping using earth observation data.

Medium resolution optical imagery has been long used for snow cover monitoring both in nation and individual groups wide. Carroll (1990) and Carroll and Holroyd (1990) mention the national wide usage.

During the last twenty years, many snow cover-mapping campaigns ranging from local to national, continental to global applications using medium resolution optical imagery have been conducted. Frank et al (1988), Harrison and Lucas (1989), Hu et al. (1993), Seidel et al (1994), Baumgartner and Rango (1995) and Rango (1996) are some of the key activities reported with snow cover mapping.

Rango (1996), Hall (1996), Kite and Pietroniro (1996) summarize the use of remote sensing of snow. Seidel and Martinec (2004) gives the current status of remote sensing of snow.

3.4 Choice of Remote Sensing Sensor

Every object emits radiation in all wavelengths. Thus, sensors that operate in the gamma ray wavelengths to the very high frequencies have been employed for remote sensing of snow and ice (Hall and Martinec, 1985). However, it may be more advantageous to use discrete portions of the electromagnetic spectrum for the specific task at hand. Since there may be distinguishing key wavelength portions enabling easy detection of the object under search, as discussed in spectral characteristics of snow subsection.

Figure 3.5 shows the relation between spatial and temporal resolutions of various satellite systems where else, sensors systems that are in the orbit are given in Table 3.3.

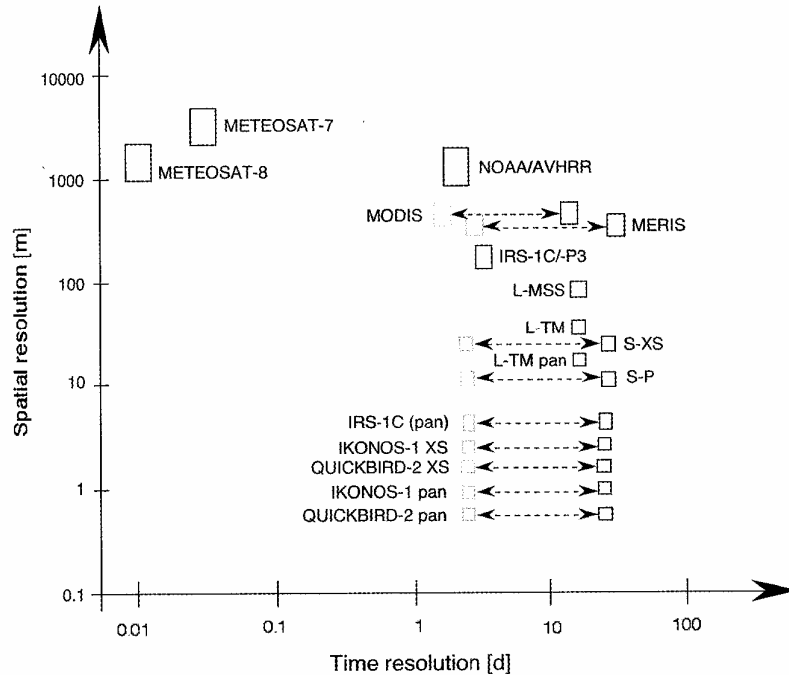


Figure 3.5 Spatial and temporal resolution of various satellite sensors (adapted from Seidel and Martinec, 2004)

Table 3.3 Characteristics of satellites for snow cover mapping (Status: June 2003)
(adapted from Seidel and Martinec, 2004)

Satellite	Sensors	Spectral Bands	Spatial Resolution	Repetition Cycle
Meteosat-7	VIS/IR	3	2.5 x 2.5 km (at nadir)	30 min.
Meteosat-8	VIS/IR	12	1 x 1 km (at nadir)	15 min.
NOAA 16-17	AVHRR	5	1 x 1 km	12~24 h.
TERRA, AQUA	MODIS-XS	36	250,500,1000m	1~18 d
ENVISAT	MERIS	15	300 x 300m	35d
Landsat -4-5	MSS	4	59 x 79 m	16 d
	TM	7	30 x 30 m	
Landsat -7	ETM+	7	30 x 30 m	16 d
	PAN	1	15 x 15 m	
SPOT -2-3-4	XS	3	20 x 20 m	26 d
	PAN	1	10 x 10 m	
SPOT -5	XS	3	10 x10 m	26 d
	PAN	1	5 x 5 m	
IRS-1C	PAN	1	5.8 x 5.8 m	5~24 d
	LISS-3	4	23 x 23 m	
IRS-P3	WIFS	3	188 x 188 m	24 d
IKONOS	XS	4	4 x 4 m	3 d
	PAN	1	1 x 1 m	
QUICKBIRD-2	XS	4	2.44 x 2.88 m	3 d
	PAN	1	0.61 x 0.72 m	

One must judiciously select the proper sensor to use for a particular analysis taking into consideration factors such as: wavelengths, resolution and frequency and timing of ground coverage (Hall and Martinec, 1985).

For operational snow cover monitoring, satellites with high repetition rates are important for the advantage of obtaining a cloud free image. In this sense, Landsat and NOAA satellite images are more available than the aircraft data. Even though, NOAA satellites can be used for small-scale area analysis due to the spatial resolution, many successful applications exist. Landsat can be used for small catchment areas. However, both for NOAA and Landsat, which use the visible and near infrared region of electromagnetic spectrum, clouds are the main problem. Although, thermal imagery cannot penetrate through clouds, they may be used for night passages during which there is the possibility of cloud free images.

A solution to the cloud problem is the microwave data either passive or active. Both can be acquired during night or day. Although, cloud problem is removed, interpretation of the images is much more difficult with respect to optical satellites. The difficulty of the microwave image interpretation arises due to the fact that the images are highly affected from surface and subsurface properties, such as temperature and electrical properties of the material under study.

Main criteria for satellite platform selection are the spatial and the temporal resolution, which will be mentioned in the following sections.

3.4.1 Spatial Resolution

Rango et al (1983) and Hall and Martinec (1985) mention about the relation between the basin size and spatial resolution of sensors. Baumgartner et al. (1987) studied the effective pixel resolution for snow classification in rugged terrain.

Studies performed in literature indicate that the effective use of medium resolution optical imagery satellites whose spatial resolution varies from hundreds of meters to tens of kilometers is dependent on the basin size under study. Use of

NOAA-AVHRR satellite images with a spatial resolution of 1.1 km at nadir is not recommended for basins smaller than 200 km².

3.4.2 Temporal Resolution

Temporal resolution is the duration to be passed between two successive satellites images to obtain the image of the same area. Duration between the two snow cover maps is important in snowmelt runoff simulation and/or forecasting. Rango (1993) recommends the use of one image per week during the snowmelt season. Relation between temporal and spatial resolution of the available sensors are given in Figure 3.5.

As it can be seen from Figure 3.5, for most of the medium resolution optical imageries, the temporal resolution varies from 15 minutes (Meteosat-8/MSG) to a few days (polar orbiters). Although cloud cover degrades the usability of the image of the above-mentioned optical satellites, the increased temporal resolution increases the possibility of obtaining a cloud free image.

3.4.3 Cloud Intrusion Problem

Spectral similarity of snow and cloud is the main problem in optical remote sensing of snow cover. High temporal resolution of the satellite platform may not be sufficient to get a cloud free image even for a month. Spectral similarity hardens the separation of snow and clouds based on the reflected radiation in visible wavelengths. Moreover, the thermal wavelengths may not help much since cloud and snow can have similar temperatures.

Clouds act different than snow in the mid-infrared part of the spectrum. At this portion of electromagnetic spectrum, clouds tend to have high reflectance with respect to low reflectance of snow. NOAA –14 and 15 have band 3 including this wavelength. NOAA-16 and 17 have a separate channel located in this part of electromagnetic spectrum.

Operational snow cover monitoring requires as many sensors in orbit as possible with repetition rates as high as possible in order to take advantage of some cloud free or partially cloud covered scenes (Seidel and Martinec, 2004).

3.5 Medium Resolution Optical Imagery

This section deals with the use of medium resolution optical satellite images for snow cover monitoring. The near infrared portion of the electromagnetic spectrum is included with visible part in this optical terminology.

A review of the methods utilized so far in the literature is given initially. A methodology is presented for near-operational snow cover monitoring for AVHRR images in the following sections.

3.5.1 Review of Medium Resolution Optical Imagery Methods for Snow Cover Monitoring

Till 1960's medium resolution optical imagery have been used in a variety of areas from oceanography to meteorology.

Various medium resolution optical imageries have been utilized during this time to monitor snow cover area including Advanced Very High Resolution Radiometer (AVHRR) on the NOAA polar orbiters, Visible/Infrared Spin Scan Radiometer (VISSR) on Geostationary Operational Environmental Satellite, Heat Capacity Mapping Mission (HCMM), Scanning Multichannel Microwave Radiometer (SMMR) on NIMBUS-7 and Operational Linescan System (OLS) on Defense Meteorological Satellite Program (DMSP) (Foster and Hall,1991).

Medium resolution optical images have been used in various applications due to the following advantages that they provide.

1. High temporal resolution (2 images per day increase the possibility of cloud free image)

2. Possibility of near real time data access
3. Large radiometric range of the sensors enable measuring high radiances over clouds and snow without saturation.

Above the three advantages, the first two make MROI sensors preferred candidates in regular and effective snow covered area monitoring.

With the above-mentioned advantages, there exist two main disadvantages of MROI sensors that are;

1. Their spatial resolution is coarse, limiting their usage for large basins.
2. Since they are not solely designed for snow, the spectral bands are seldom optimally located for snow related studies.

Among the large number of MROI sensors, Carsey (1992) summarizes the snow and ice related use of remote sensing sensors and algorithms in particular with AVHRR, SSM/I and SMMR.

AVHRR is the sensor that has been used for the longest time and there exist a large number of studies related with extraction of snow-covered area from AVHRR images. Baumgartner and Apfl (1997) can be mentioned as a recent example.

Since AVHRR is the main image source in this thesis, following sections will deal in a more detailed manner specifically to AVHRR. Cracknell (1997) provides detailed information related with AVHRR, where else a short overview can be found in Hastings and Emery (1992).

3.5.1.1 Processing Steps of Medium Resolution Optical Images

Processing steps of the medium resolution images for remote sensing of snow can be itemized as

1. Calibration of raw data
2. Atmospheric correction
3. Geocoding
4. Snow classification

3.5.1.1.1 Calibration of raw data

Digital numbers recorded by sensors should be converted to meaningful physical quantities if the data will be used in quantitative manner. The conversion is achieved by pre-launch calibration values. Accurate calibration is a must for the development of data sets that can be used for many years and enable comparison between different sensors.

However the sensors degrade with time and it may become necessary to perform in-flight calibration measurements by monitoring the system and updating the calibration parameters when necessary. The in-flight calibration measurements are made by monitoring the system response to an invariant feature. Deserts were used as an invariant feature for calibration of NOAA 12 satellites (Rao and Chen, 1995).

Reflective channels (VIS and NIR) are located in a region of electromagnetic spectrum through which only solar radiation reflected from Earth's surface reaches the sensor. Che and Price (1992), Kaufman and Holben (1992) and Rao and Chen (1995) are a few studies performed for determination of degradation in these channels. Comparisons are made by measuring constant reference targets. NOAA regularly publishes calibration coefficients.

Reflective (VIS and NIR) channels are calibrated in a different manner than the thermal (emissive) channels.

In-flight calibration data that are available in the header of each scan line of the satellite image is used for the calibration of thermal channels (3,4,5) to radiance and brightness temperature.

Collier et al (1989) mentions that the thermal information measured with AVHRR is of enough quality for snow cover mapping. Where else, Warren (1989) explains the methods to remove the noise in channel 3.

3.5.1.1.2 Atmospheric Correction

Aerosols and water vapor present in atmosphere interfere with the reflected surface radiation and cause alterations of the actual values. Thus, atmospheric effects should be taken into consideration if one tries to obtain exact measurements of surface parameters.

Radiative transfer calculations try to model the influence of the atmospheric processes on the radiation. Lowtran (Kneizys et al., 1988), a computer program is made for this purpose. As these processes are modeled, their influence on the images can be corrected.

Popp (1995) shows an atmospheric correction algorithm for AVHRR images, in which multiple scattering is considered.

Split window technique is another method applied to correct atmospheric effects. This technique uses the fact that; different wavelengths are affected by different scattering processes. Mainly solar and thermal part of the spectrum is used in conjunction in this methodology. Saunders and Kriebel (1988), Mitchell (1989), Paltridge and Mitchell (1990) and Cracknell (1997) are among the ones who used split window technique.

Although there are computer codes and procedures to remove atmospheric effects, these cannot be directly applied to snow classification in mountainous

environment due to the pre-assumption of homogeneous atmospheric conditions and constant atmospheric depth. Elevation variations in a mountain environment can be as high as 2000 m and lead large variation in atmospheric depth. Thus, no atmospheric correction will be applied to VIS and NIR channels.

3.5.1.1.3 Geocoding

Geocoding can be defined as the process registering an image specifically to a cartographic projection with the use of an explicit image model.

There are two main reasons for geocoding

- 1) Transforming the image into a common reference system so that
 - The geographic locations of the pixels and objects in the image can be seen.
 - Correct area and distance measurements can be performed.
 - The image can be exported to GIS for further analysis
 - Possibility of using the image with other data sets (ground data and/or other data sets)
- 2) Correcting the topography induced geometric distortions

Due to the above-mentioned reasons, it is important to geocode all the data to a standard cartographic projection. For this, a set of ground control points (GCP's) is located both in the image and in the reference map. These are used to define a least square polynomial transformation for warping the image into the desired projection. The absolute geocoding accuracy is defined as one pixel for each sensor (Hydalp, 2000)

At the moment, geocoding is achieved manually. For this, linear features such as lakes, valleys and coastlines are the most suitable ones to use as ground control point. Automatic matching system such as the one proposed by Eales (1989) is under study.

3.5.1.1.4 Snow Classification

Detection of snow from the satellite images is important for a number of uses. These vary from providing input to numerical weather prediction forecasts to hydrological applications. Before, mentioning this important issue, cloud problem that may be encountered and the possible ways to overcome will be mentioned.

For NOAA satellites before NOAA 15, the mid infrared channel 3, is important for distinguishing between snow and clouds.

Saunders and Kriebel (1988), Scorer (1989), Gessell (1989) and Derrien et al. (1993) mainly mention about the ways to deal with cloud detection.

Theta, an image classification based on comparison of angles between the multi channel vectors that is proposed by Maxson et al. (1996) and applied by Akyürek and Şorman (2002) has proven its usability in separating clouds from snow.

Frank et al (1988), Harrison and Lucas (1989) and Hu et al (1993) focused on the snow cover detection from AVHRR images.

Another solution is using the cloud free data obtained from satellite images for analysis. This is also the main method applied in this study.

There exist a number of methodologies for snow classification. In the broadest sense they fall into two main categories. These are statistical methods and the thresholding scheme. These two main categories also show variations within themselves.

3.5.1.1.4.1 Statistical Classification Methods

Even though, there are a quite number of statistical methods, they all in common use the multi dimensional data space of the spectral bands of the satellite image. For AVHRR, by the 5 spectral channels of the sensor 5 dimensional data exist.

Statistical methods can also be subdivided as supervised and unsupervised classification. In the former, the analyst is required to guide the classification by identifying areas on the image that are known to belong each category. The identifying areas are called as training areas. Training areas are like an interpretation key, describing the spectral attributes for each feature type of interest (Lillesand and Kiefer, 1994). Collecting representative training data set is important since; each pixel value in the image is compared with interpretation keys and labeled with the name of the category that it most resembles. For snow cover mapping the features of interest are: snow free (aper), transition zone; and snow covered areas (Seidel and Martinec, 2004).

Whereas, in unsupervised classification, minimal involvement of the analyst is required. The image is classified purely by statistical methods, aggregating pixels into natural groupings that are present within the scene. Then the analyst compares the classified data with ground data and the appropriate labeling is performed.

Also there exist hybrid classifications that share the characteristics of both supervised and unsupervised methods. Frank et al (1988) used principle component analysis, supervised classification and maximum likelihood classification approach on bands 2 and 3. Harrison and Lucas (1989) used unsupervised classification using bands 1,3 and 4. Hu et al (1993) used the same channels to distinguish between clouds and snow. They initially used unsupervised ISODATA algorithm to obtain the spectral features of the appropriate classes then classified them using maximum likelihood.

Baumgartner et al (1994a) use a combination of supervised minimum distance classification with Mahalanobis distance classifier on bands 1 and 2.

3.5.1.1.4.2 Thresholding

The concept behind the threshold is to define the boundary conditions for determining whether a pixel in a satellite image is influenced by snow or not. Various such boundary criteria for delineation of snow with NOAA-AVHRR exist. But, thresholding single bands may not alone be sufficient to separate snow from other surface types. With a combination of such criteria, snow covered area can be found. Threshold can be either derived empirically or based on physical considerations. The second one is the most objective one. Theta, proposed by Maxson et al (1996) describes an operational snow mapping system based on interactive thresholding procedure. Theta was also applied by Akyürek et al (1999), Tekeli (2000). Voigt et al (1999) proposed another thresholding scheme for snow cover mapping.

Most of the thresholding methods such as Saunders and Kriebel (1988), Gessel (1989), Allen et al. (1990), Yamanouchi and Kawaguchi (1992), Derrien et al (1993) and Baum and Trepte (1997) deal mainly with cloud detection. Above-mentioned studies mainly use band 3 radiance. Such methods can be simplified for snow monitoring.

Ultimate goal of thresholding technique is to remove the subjectivity that may arise due to intrusion of the analyst both in supervised and unsupervised classifications.

To be used for near real time forecasting of snowmelt runoff, the snow covered area information should be available as soon as the image is received. This requires an automated classification procedure and an automated processing

chain. Thresholding approaches constitute the preliminary steps of an automated snow mapping system.

3.5.2 Snow Cover Monitoring for NOAA-AVHRR

Figure 3.6 shows the flow line for snow cover monitoring system developed for NOAA-AVHRR during the thesis study. Following sections will mention each step of the flowchart in detail.

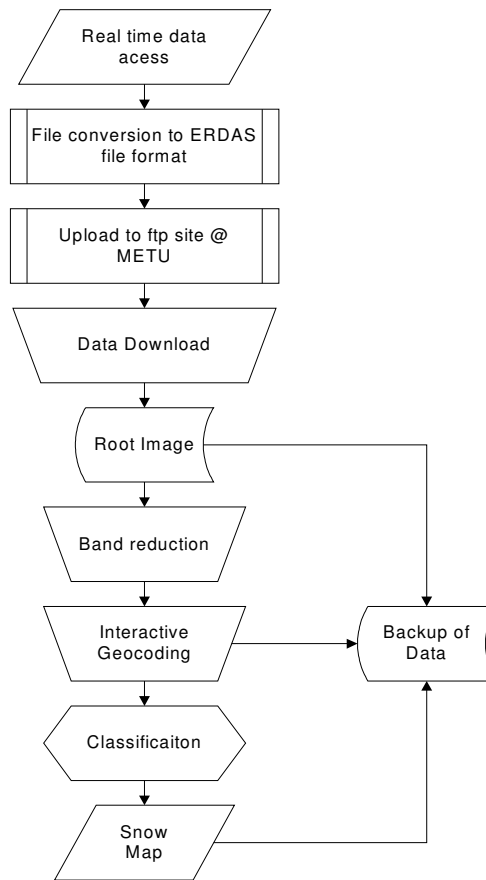


Figure 3.6 Flow line for snow cover monitoring system for NOAA-AVHRR

3.5.2.1 Real Time Data Access

NOAA AVHRR satellite data is obtained from Turkish State Meteorological Services (DMI) starting from March 2004. DMI has its own

AVHRR receiving antenna and downloads the data himself. Data is obtained on real time basis and the received images are used for a number of processes varying from cloud motion detection to numerical weather predictions.

As the data is received by DMI the image is converted into ERDAS file format and uploaded to the ftp site at Middle East Technical University.

3.5.2.2 Data Download

Satellite images uploaded by DMI to METU ftp site, are downloaded to the local machines at the Water Resources Laboratory of Civil Engineering Department of METU. Root images are saved to local disks. Files in the ftp are deleted due to the storage limit after they are saved. The images at the local disks are recorded to CD.

3.5.2.3 Band Reduction

In NOAA 17 satellite band 3 is shifted between day and night and named as 3A and 3B respectively. The software used at DMI handles the 3A as the 6th band and records the data as band 6 while 3B is recorded as band 3 in night flights. In the daytime images the band 3 records zero, similarly band 6 records zero in the night time values since they receive nothing during the indicated time. Thus the bands with zero data should be removed.

In this manner, the image that was originally having 6 bands is reduced to an image with 5 bands. A graphical model written in ERDAS graphical modeler module performs this procedure.

3.5.2.4 Geocoding

To provide compatibility with the other data sets, AVHRR data are referenced to a geometric coordinate system. GCP's are obtained from arcview shape files including lakes, coastlines and dam reservoirs.

8~9 GCP distributed uniformly over the image are selected. A least square method is used to define a first order polynomial transformation. A first order polynomial, being computationally economic can model a rotation, scale and a translation. Selection of a low ordered polynomial prevented the high geometric distortions in areas of no ground control points. Reprojection is carried using nearest neighbor resampling.

Lake Van's boundaries, coastline of North east of Black Sea, Keban, Karakaya and Atatürk Dam reservoirs are used for GCP collection. The root mean square error of geocoding is kept less than 1 pixel.

Finally the images are geocoded to WGS 84 UTM Zone 37 projection.

3.5.2.5 Snow Classification

Numerous algorithms and methodologies have been proposed and developed for snow covered area monitoring from satellite images (Dozier 1989, Rosenthal and Dozier 1996, Simpson et al. 1998, Barret et al. 2001, Romanov and Tarpley 2004). These mainly depend on the differences of the spectral signatures of different land covers within the scene.

However, clouds and snow covered areas have similar spectral reflectance in visible region. Thus, the most tackling problem in snow cover mapping has been the separation of clouds from snow covered areas. Fortunately, shortwave infrared region of spectrum (1~4 μm) enables cloud snow separation. In this range, snow covered surfaces have low reflectivity where else, clouds still have high reflectivity.

Preliminary steps of an operational processing chain of NOAA-AVHRR imagery to provide nearly real time snow cover information for Upper Euphrates River in Eastern Anatolia starting from 2004 April are provided within a couple of

hours after the on line image reception. New AVHRR/3 sensor provided by NOAA 15 and 17 enables improved snow and cloud discrimination with the mid-infrared band (1.58~1.64 μm) by channel 3A.

Pixels of the image are classified using band ratios and temporarily invariable thresholds. The output is the snowy and non-snowy areas. This is also in agreement with “When using NOAA AVHRR for training and classification, only the two categories snow covered and open (snow free) seem meaningful” as indicated by Seidel and Martinec (2004). A kind of hierarchical decision tree is used for snow classification process. First of all, a ratio is calculated based on visible and mid infrared bands. Table 3.4 summarizes the philosophy behind the rationing procedure.

Table 3.4 Rationing procedure

	Visible (VIS)	Short wave (mid) infrared (MIR)	MIR/VIS
Snow	High	Low	Low
Cloud	High	High	High

For NOAA 17 this ratio is determined by equation

$$\text{Ratio} = (\text{VIS}-\text{MIR}) / (\text{VIS}+\text{MIR}) \tag{3.1}$$

Remaining of the classification is performed based on the thresholding of band 1, band 2 and band 3A. Pixels that pass all of the tests are labeled as snow covered. If the pixel cannot satisfy any of the tests it is determined to be non-snowy.

The obtained snow covered area information will provide the input variable of snow cover depletion curves required by snowmelt runoff model. Detailed information of snow cover depletion curves are provided in section 6.4.3.

3.5.2.6 Export to GIS

After the images are classified the outputs are exported into GIS for further analysis. Overlaying of the snow cover images with the basin and/or sub basins is the mostly performed GIS analysis. Moreover, detailed aspect, elevation, slope and land use analysis can also be performed.

3.5.3 Moderate Resolution Imaging Spectroradiometer (MODIS)

With the content of Earth Observation Satellites (EOS) platform, Terra satellite was launched with five other instruments including MODIS on 8/12/1999 for a design life of 6 years. MODIS is an imaging spectroradiometer that employs a cross-track scan mirror, collecting optics and a set of individual elements to provide imagery of the Earth's surface and clouds in 36 discrete, narrow spectral bands from approximately 0.4 to 14 μm (Barnes et al., 1998). The spatial resolution of MODIS ranges from 250 m to 1km and varies with spectral bands as indicated in Table 3.5 with other technical properties. Further information can be obtained from <http://modis.gsfc.nasa.gov>.

Table 3.5 Technical properties of MODIS
(adapted from <http://modis.gsfc.nasa.gov/about/specs.html>)

Orbit:	705 km, 10:30 a.m. descending node (Terra) or 1:30 p.m. ascending node(Aqua), sun-synchronous, near-polar, circular
Scan Rate	20.3 rpm, cross track
Swath Dimensions	2330 km (cross track) by 10 km (a long track at nadir)
Telescope	17.78 cm diam. Off-axis, afocal (collimated), with intermediate field stop

Table 3.5 (Continued)

Size	1.0 x 1.6 x 1.0 m			
Weight	228.7 kg			
Power	162.5 W (single orbit average)			
Data Rate	10.6 Mbps (peak day time), 6.1 Mbps (orbital average)			
Quantization	12 bits			
Spatial Resolution	250 m (bands 1-2) 500 m (bands 3-7) 1000 m (bands 8-36)			
Design Life	6 years			
Primary Use	Band	Bandwidth ¹	Spectral Radiance ²	Required SNR ³
Land/Cloud/Aerosols Boundaries	1	620-670	21.8	128
	2	841-876	24.7	201
Land/Cloud/Aerosols Properties	3	459-479	35.3	243
	4	545-565	29.0	228
	5	1230-1250	5.4	74
	6	1628-1652	7.3	275
	7	2105-2155	1.0	110
Ocean Color Phytoplankton Biogeochemistry	8	405-420	44.9	880
	9	438-448	41.9	838
	10	483-493	32.1	802
	11	526-536	27.9	754
	12	546-556	21.0	750
	13	662-672	9.5	910
	14	673-683	8.7	1087
	15	743-753	10.2	586
	16	862-877	6.2	516

Table 3.5 (Continued)

Atmospheric Water Vapor	17	890-920	10.0	167
	18	931-941	3.6	57
	19	915-965	15.0	250
Surface/Cloud Temperature	20	3.660-3.840	0.45 (300K)	0.05
	21	3.929-3.989	2.38 (335K)	2.00
	22	3.929-3.989	0.67 (300K)	0.07
	23	4.020-4.080	0.79 (300K)	0.07
Atmospheric Temperature	24	4.433-4.498	0.17 (250K)	0.25
	25	4.482-4.549	0.59 (275K)	0.25
Cirrus Clouds Water Vapor	26	1.360-1.390	6.00	150 (SNR)
	27	6.535-6.895	1.16 (240K)	0.25
	28	7.175-7.475	2.18 (250K)	0.25
Cloud Properties	29	8.400-8.700	9.58 (300K)	0.05
Ozone	30	9.580-9.880	3.69 (250K)	0.25
Surface/Cloud Temperature	31	10.780-11.280	9.55 (300K)	0.05
	32	11.770-12.270	8.94 (300K)	0.05
Cloud Top Altitude	33	13.185-13.485	4.52 (260K)	0.25
	34	13.485-13.785	3.76 (250K)	0.25
	35	13.785-14.085	3.11 (240K)	0.25
	36	14.085-14.385	2.08 (220K)	0.35
¹ Bands 1 to 19 are in nm; Bands 20 to 36 are in μm ² Spectral Radiance values are ($\text{W}/\text{m}^2 \cdot \mu\text{m}\cdot\text{sr}$) ³ SNR = Signal-to-noise ratio ⁴ NE(Δ)T = Noise-equivalent temperature difference Note: Performance goal is 30-40% better than required				

Many land surface properties, geophysical products and snow cover products are obtained recently from MODIS data in global coverage. Justice et al. (1998) summarizes the key land surface objectives as to study global land surface change, vegetation properties, surface albedo, surface temperature and snow cover on daily basis. Table 3.6 shows the list of main products. Figure 3.7 represents a jpeg true color image of MODIS showing eastern part of Turkey on date 20/01/2004.

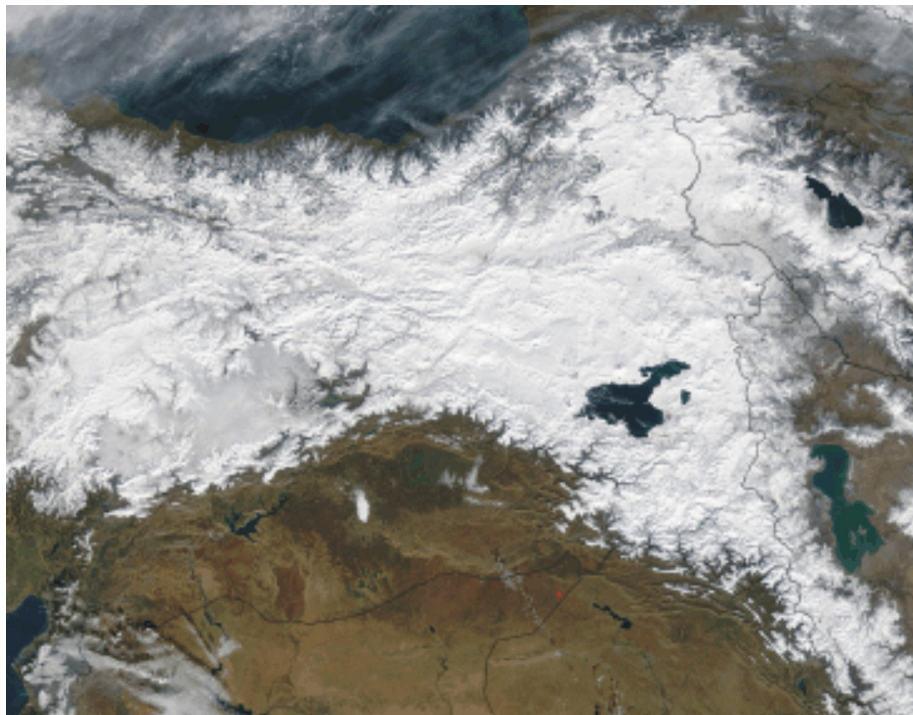


Figure 3.7 A true color MODIS image of Eastern TURKEY on 20/01/2004
(Adapted from <http://visibleearth.nasa.gov>)

Among the many products listed in Table 3.6, the MODIS snow and ice products are distributed freely through the National Snow and Ice Data Center (NSIDC) Distributed Active Archive Center (DAAC), starting from 13 September 2000.

With the daily, global and 500 m spatial resolution offered by MODIS, MODIS snow cover products are prone to improve and/or enhance the currently available operational products (Hall et al., 2002).

Main distinguishing character of MODIS snow data is the fact that the processing chain is automated, i.e. no subjectivity of the analyst is introduced. This enables the production of a consistent data set required for long-term climate studies. Moreover, the quality assurance (QA) information embedded within the data sets is very informative about the snow extent.

3.5.3.1 MODIS File Format

Hierarchical Data Format – Earth Observing System (HDF-EOS), which is developed by National Center for Supercomputing Applications (NCSA), is the standard format for EOS- Data Information System (EOSDIS) products.

The snow product files contain two layers, which are namely, meta data including the attributes and the Scientific Data Sets (SDS) including the data arrays. Use of HDF features to provide point, swath and grid structures which enable geolocation of data is the unique character of HDF-EOS data. These structures (V groups and V data) provide geolocation relationships between data in a SDS and geographic coordinates (latitude and longitude or map projections) to support mapping the data (Riggs et al, 2003).

A separate file including meta data will accompany data products ordered from DAAC. This meta file with an “.met’ extension contains some of the same meta data as in the product file but also has some other information regarding

archiving and user support services as some post production quality assurance (QA) information relevant to the granule ordered (Riggs et al, 2003).

Table 3.6 List of main MODIS products

Level 1A Radiance Counts	MOD 01	Chlorophyll a Pigment Concentration	MOD 21
Level 1B Calibrated, Geolocated Radiances	MOD 02	Photosynthetically Active Radiation (PAR)	MOD 22
Geolocation Data Set	MOD 03	Suspended Solids Concentration in Ocean Water	MOD 23
Aerosol Product	MOD 04	Organic Matter Concentration	MOD 24
Total Precipitable Water (near-IR method)	MOD 05	Coccolith Concentration	MOD 25
Cloud Products (optical thickness, particle radius, etc)	MOD 06	Ocean Water Attenuation Coefficient	MOD 26
Cloud Products (cloud top properties and phase)	MOD 06	Ocean Primary Productivity	MOD 27
Atmospheric Profiles	MOD 07	Sea Surface Temperature	MOD 28
Gridded Atmosphere Products-Level 3	MOD 08	Sea Ice Cover	MOD 29
Atmospherically Corrected Surface Reflectance	MOD 09	Temperature and Moisture Profiles	MOD 30
<u>Snow cover</u>	<u>MOD 10</u>	Phycoerythrin Concentration	MOD 31
Land Surface Temperature and Emissivity	MOD 11	Ocean Processing Framework and Matchup DB	MOD 32
Land Cover/Land Cover Change	MOD 12	Gridded Snowcover	MOD 33
Vegetation Indices	MOD 13	Gridded Vegetation Indices	MOD 34
Thermal Anomalies, Fires, Biomass Burning	MOD 14	Cloud Mask	MOD 35
Leaf Area Index and FPAR	MOD 15	Total Absorption Coefficient	MOD 36
Surface Resistance and Evapotranspiration	MOD 16	Ocean Aerosol Properties	MOD 37
Vegetation Production , Net Primary Productivity	MOD 17	Clear Water Epsilon	MOD 39
Normalized Water Leaving Radiance	MOD 18	Albedo 16-Day Level 3	MOD 43
Pigment Concentration	MOD 19	Vegetaion Cover Conversion and Continuous Fields	MOD 44
Chlorophyll II Fluorescence	MOD 20	Vegetaion Cover Conversion and Continuous Fields	MOD 44

3.5.3.2 MODIS Snow Products

Detection of snow covered area from space has been used since 1960's by National Oceanic and Atmospheric Administration (NOAA). Attention to snow cover area maps was increased with the studies performed by Martinec (1975) and Rango and Martinec (1979).

Both the production and accuracy of the snow maps derived from satellites improved as new satellite platforms became available. However, most of the time these snow cover maps were produced by a remote sensing specialist interactively. Moreover, most of the studies were regional, specific to the area under study. Even though, this was advantageous for operational studies, climate modeling studies which required long term consistent data sets were hindered by the subjectivity of the analyst involved.

Such a bottle neck was overcome with the launch of Terra spacecraft that included MODIS. MODIS enabled the automatic production of snow cover products by the automated algorithm developed at Goddard Space Flight Center in Greenbelt, Maryland. The outputs of the algorithm are transferred to National Snow And Ice Data Center (NSIDC) in Boulder, Colorado, Co, where they are archived and distributed via EOS Data Gateway (EDG) (Hall et al., 2002).

3.5.3.2.1 MODIS Snow Product Sequence

MODIS snow products are provided as a sequence of products beginning with a swath (scene) and progressing, through spatial and temporal transformations to an eight day gridded product (Riggs et al., 2003). MODIS snow products are provided as a series 6 different products throughout this production sequence. A summary of the snow product sequence is provided in Table 3.7.

The long MODIS snow data production begins with the derivation of a 5 min swath segment (granule) at a nominal pixel spatial resolution of 500 m and a nominal swath coverage of 2330 km (across track) by 2030 km (along track) (Hall et al, 2002).

Table 3.7 Summary of MODIS snow data products
(adapted from Riggs et al., 2003)

Earth Science Data Type (ESDT)*	Product Level	Nominal Data Array Dimensions	Spatial Resolution	Temporal Resolution	Map Projection
MOD10_L2	L2	1354 km x 2000 km	500 m	Swath (scene)	None
MOD10L2G	L2G	1200 km x 1200 km	500 m	Day of multiple coincident swaths	Sinusoidal
MOD10A1	L3	1200 km x 1200 km	500 m	day	Sinusoidal
MOD10A2	L3	1200 km x 1200 km	500 m	eight days	Sinusoidal
MOD10C1	L3	360° by 180° (Global)	0.05°x 0.05°	day	Geographic
MOD10C2	L3	360° by 180° (Global)	0.05°x 0.05°	eight days	Geographic

ESDT * : Short name is used for identifying snow data product

All of the snow products, excluding MOD10_L2, are derived from the preceding snow product as input. The level numbers in Table 3.7 indicate the temporal and spatial processing applied to the data. Table 3.8 gives some definitions of the level numbers.

Table 3.8 Explanation of level numbers in MODIS data products

L1B	A swath (scene) of MODIS data geolocated to latitude and longitude centers of 1 km resolution pixels.
L2	A geophysical product with L1B spatial orientation
L2_G	A gridded format of map projection
L2G	Referred as tiles, each covering a 10°x10° area Define a gridded product necessary for level 3 production
L3	A geophysical product in a gridded map projection coming as tiles of a global grid

Following sections will briefly mention about the snow products indicated in Table 3.7. More detailed information can be obtained from Riggs et al., (2003).

MOD10_L2 Snow Product

For the derivation of MOD10_L2 snow product, three main data sets are used. These are (i) MODIS calibrated radiance data products [MOD02HKM and MOD021KM], (ii) Geolocation product [MOD03] and (iii) cloud mask product [MOD35_L2]. Table 3.9 shows these input files and the data used for obtaining them.

The snow analysis is performed in the pixels that satisfy the following criteria (Riggs et al., 2003)

1. have nominal Level 1B radiance
2. are on land or inland water
3. are in day light
4. are unobstructed by clouds
5. have an estimated surface temperature less than 283 °K

The constraints are applied in the ordered list, enabling the snow analysis on the pixels having a day light clear sky view of land surface.

Table 3.9 MODIS data product inputs to MOD10_L2
(adapted from Riggs et al., 2003)

ESDT	Long Name	Data Used
MOD02HKM	MODIS Level 1B Calibrated and Geolocated Radiances	Reflectances for MODIS Band 1 (0.645 μm) Band 2 (0.865 μm) Band 4 (0.555 μm) Band 6 (1.640 μm)
MOD021KM		Band 31 (11.28 μm) Band 32 (12.27 μm)
MOD03	MODIS Geolocation	Land/Water Mask Solar Zenith Angles Sensor Zenith Angles Latitude Longitude
MOD35_L2	MODIS Cloud Mask	Cloud Mask Flag Unobstructed Field of View Flag Various cloud test results Day/Night Flag

MOD10_L2G Snow product

This is an intermediate product which is used as an input to daily snow cover product MOD10A1. MOD10_L2G is obtained by mapping MOD10_L2 swaths that are acquired during a day to grid cells of the Sinusoidal projection. Even though, these are an intermediate product, they are not archived at DAAC and are not available for order.

MOD10A1 Daily snow cover product

This is a Level 3 snow product that is derived from MOD10_L2G outputs. MOD10A1 data set is in gridded sinusoidal projection with coverage of approximately 1200 km by 1200 km containing a single scientific data set of snow

cover and a quality assurance data set. Local and global attributes related with the tile are also provided with the data.

Data set is made by selecting the observations acquired nearest nadir and having the greatest coverage of the grid cell from many observations acquired during a day (Hall et al., 2002). Detailed information related with the MODIS snow detection algorithm is provided in section 3.5.3.3

MOD10A2 – Eight day snow cover product

Exact ground track repeat of Terra platform is eight days. Thus; 8 day composing was selected in MOD10A2 snow products. Eight day periods begin on the first day of the year and extent into the next year (Riggs et al., 2003). MOD10A2 data is composed of two scientific data sets (SDS), in the first the maximum snow cover is mapped and in the second the chronology of observations is kept. Depending on the image availability, MOD10A2 can be produced from 2 to 8 images. The number of image availability is indicated in the chronology of observations.

In this study both MOD10A1 and MOD10A2 snow covered area products are used.

MOD10C1 Daily climate modeling grid snow product

MOD10C1 gives a global view of snow cover at 0.05 degree resolution in geographic projection. For a daily image of climate modeling grid (CMG) data; outputs of MOD10A1 is used in which approximately, 320 tiles of land data is used. Snow cover extent is expressed as a percentage of snow observed in the MOD10A1 cells at 500 m when mapped into a grid cell of CMG at 0.05 degree resolution (Riggs et al., 2003).

MOD10C2 – Eight day climate model grid snow product

MOD10C2 is the final product of MODIS snow data set. This is obtained by merging all MOD10A2 tiles for predetermined 8 day periods. 500 m spatial resolution is converted to $1/20^\circ$ or ≈ 5.6 km resolution, leading an array of 3600 rows by 7200 columns. Snow cover, cloud cover data and quality assurance information are included in the product also (Riggs et al., 2003).

3.5.3.3 MODIS Snow Detection Algorithm

Superiority of MODIS snow data over the available data sets is the fact that snow mapping algorithms;

1. Tested over a variety of surfaces
2. Automatic, with no need to human intervention
3. Global
4. Easy to understand, straight forward
5. Computational frugal

The automated fashion of the algorithm removes the possible errors occurring due to human subjectivity. This elimination of human subjectivity enables the production of stable, consistent data needed for long term climate studies.

The snowmapping algorithm (SNOWMAP) employs a grouped criteria technique using Normalized Difference Snow Index (NDSI) and other spectral threshold tests to identify and classify snow on a pixel-by-pixel basis and map snow cover in dense forests (Hall et. al, 2001). The usefulness of the NDSI is based on the fact that snow and ice are considerably more reflective in the visible than in the short wave infrared part of spectrum, and the reflectance of most clouds remains high in the shortwave infrared, while reflectance of snow is low (Seidel and Martinec, 2004). The other spectral threshold techniques are

developed upon the previously performed rationing techniques that were proven to be successful at both regional and local scales.

MODIS bands covering the visible through infrared parts of the spectrum (Salomonson and Toll, 1991) are used in the MODIS snow and sea ice mapping algorithm (Hall et. al, 2001). MODIS bands 1,2,4,6,31 and 32 are the main inputs to the snow cover algorithm.

3.5.3.3.1 Normalized Difference Snow and Vegetation Indices

Strong visible reflectance and strong absorbing characteristics of snow has been long known (Section 3.2). Normalized difference snow index (NDSI) is a measure of the relative magnitude of the characteristic reflectance difference between the visible and shortwave infra red reflectance of snow (Hall et. al, 2001). The NDSI is useful for the identification of snow and ice and for separating snow/ice and most clouds (Seidel and Martinec, 2004).

NDSI is a similar method of normalized difference vegetation index (NDVI) (Townshend and Tucker, 1984, Tucker 1986) which has been proven to be an effective method for monitoring global vegetation conditions throughout a year. MODIS Band 4 (0.545~0.561 μm) and Band 6 (1.628~1.652 μm) are used in calculation of NDSI. The NDSI is insensitive to a wide range of illumination conditions, is partially normalized for atmospheric effects, and does not depend on reflectance in a single band (Hall et. al, 2001).

Equation 3.2 ,based on MODIS band 4 and band 6, shows the calculation of NDSI.

$$NDSI = \frac{Band4 - Band6}{Band4 + Band6} \quad (3.2)$$

The high reflectance of snow in the visible compared to mid infrared portion of the spectrum yields high NDSI values for snow compared to other surface materials (Seidel and Martinec, 2004). Clouds also tend to have high reflectances in both visible and mid infrared wavelengths so the NDSI also serves as a snow/cloud discriminator (Klein and Stroeve, 2002).

Comparison of NDSI with Landsat TM data; the threshold of NDSI is set as 0.4. Thus; a pixel in a non-densely forested region will be mapped as snow if $NDSI > 0.4$ (Hall et. al, 2002).

Possibility of water having $NDSI \geq 0.4$ necessitates an additional test to separate water from snow. Snow and water may be discriminated by MODIS Band 2 (0.841~0.876 μm) test. If MODIS band 2 is $\geq 11\%$ and $NDSI \geq 0.4$ then that pixel is mapped as snow.

These NDSI thresholds have been verified from a detailed analysis of numerous TM scenes, comparison with supervised classification techniques and comparison of a snow map with a map derived at 10 May 1992 TM scene at the Sierra Nevadas with a snow map derived from Rosenthal and Dozier 1996 (Hall et. al, 2001).

Even though, a pixel passes the above criteria, it will not be mapped as snow if the reflectance in band 4 is less than 10 %. This is required since very low reflectances cause the denominator in the NDSI to be quite small, and only small increases in the visible wavelengths are required to make NDSI value high enough to classify a pixel erroneously as snow (Hall et. al, 2002). Such a criteria prevents pixels with very dark targets being mapped as snow.

Forests are among the dark objects that cause a classification problem in NDSI. For the detection of snow cover in a forest extent, the change in spectra of a forest stand is used. The spectra of a forest stand observed in the visible range

will change as the soil, leaves and bark are covered with snow, a much higher reflective material. A fundamental change that a snow cover causes in the spectral response of a forest, which can be used in a global algorithm, is that the reflectance in the visible will often increase with respect to the near infrared reflectance (Hall et. al, 2002). Normalized difference vegetation index (NDVI) is the index used for detecting this variation. Snow will cause reduction in NDVI of a forest cover.

For determination of NDVI, MODIS bands 1 (0.620~0.670µm) and 2 (0.841~0.876 µm) are used. Equation 3.3 is used for NDVI calculation.

$$NDVI = \frac{NIR - VIS}{NIR + VIS} = \frac{Band2 - Band1}{Band2 + Band1} \quad (3.3)$$

High values of NDVI indicate healthy and a denser vegetation. Combined use of NDVI and NDSI provide a strong signal that can be exploited to classify snow-covered forests (Klein and Stroeve, 2002). . Thus, by using the NDSI and NDVI in combination, it is possible to lower the NDSI threshold in forested areas without compromising the algorithm performance in other land covers (Hall et al., 2001). If the NDVI \approx 0.1, the pixel may be mapped as snow even if the NDSI is lower than 0.4 (Klein et al., 1998).

3.5.3.3.2 Snow Cloud Discrimination With Ocean and Thermal Masks

MODIS snow algorithm (SNOWMAP) is applied to pixels that have a clear view of the surface i.e. the pixel is not set to a “certain cloud”. Clouds are masked using data from the MODIS cloud mask data product MOD35_L2 (Riggs et al., 2003). Investigations and improvements on snow-cloud confusion still continue.

Ocean mask

SNOWMAP is executed on land and inland lake pixels. In this content, the oceans are skipped by the program. Masking oceans and inland water bodies is performed with the 1 km resolution land/water mask contained in MODIS geolocation product (MOD03) (Riggs et al., 2003).

Thermal mask

Spurious snow cover was found in many parts of the world (Hall et al., 2002). Cloud intrusion, aerosol affects, snow/sand confusion on coastlines were reported as the main error sources.

A split window technique using MODIS bands 31 (10.78~11.28 μm) and 32 (11.77~12.27 μm) is performed to estimate surface temperature values. Based on the calculated value, the pixel is not mapped as snow if estimated surface temperature is greater than 277 °K. It is reported as; snow covered areas have not changed much, but results in warm areas have improved dramatically (Hall et al., 2002).

3.5.3.4 MODIS Data Processing Scheme for Snowmelt Runoff Model

As the MODIS data came available, methodologies are needed to process the images and prepare the input data file for snowmelt model studies regularly. During the study, two main snow products, namely, MOD10A1 daily snow cover and MOD10A2 – 8 day snow cover products that are described in section 3.5.3.2.1 are used. The main processing scheme is the same for both of the products. Only the input files are varied as the product type is changed. Figure 3.8 shows the general procedure followed here.

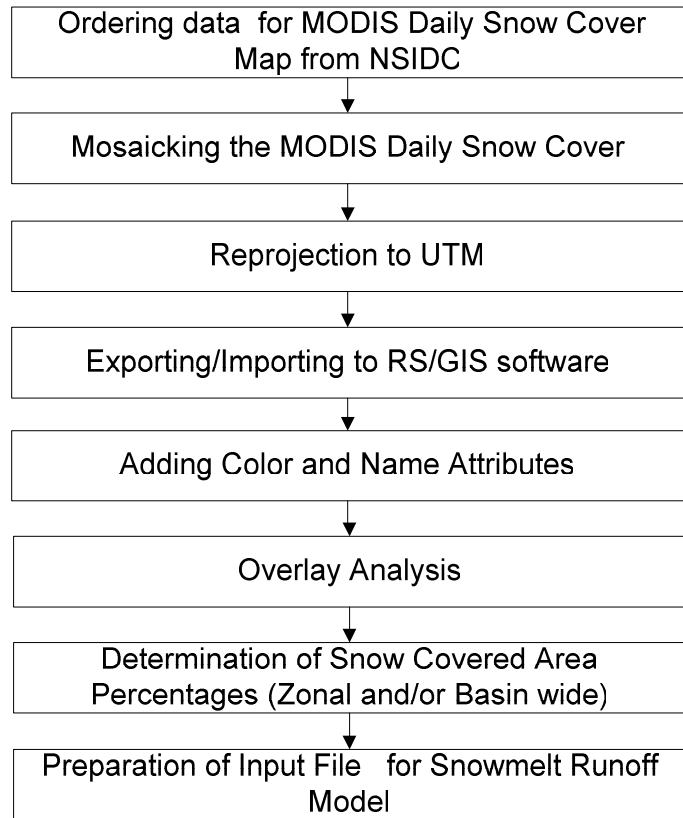


Figure 3.8 Flow chart for processing MODIS snow cover maps

Processing begins with the order of data from National Snow and Ice Data Center (NSDIC). Out of the available versions, version 4 data is used since; this version is supposed to have better cloud screening (Ackerman et al., 1998) and better snow determination in forest area (Klein et al., 1998).

The study area is eastern part of Turkey and since it is contained between two scenes namely, h21v04 and h21v05, two images needed to be tied together. Figure 3.9 shows the location of the scenes related with the study. MODIS Reprojection Tools (MRT,2003) is used to tile images together.

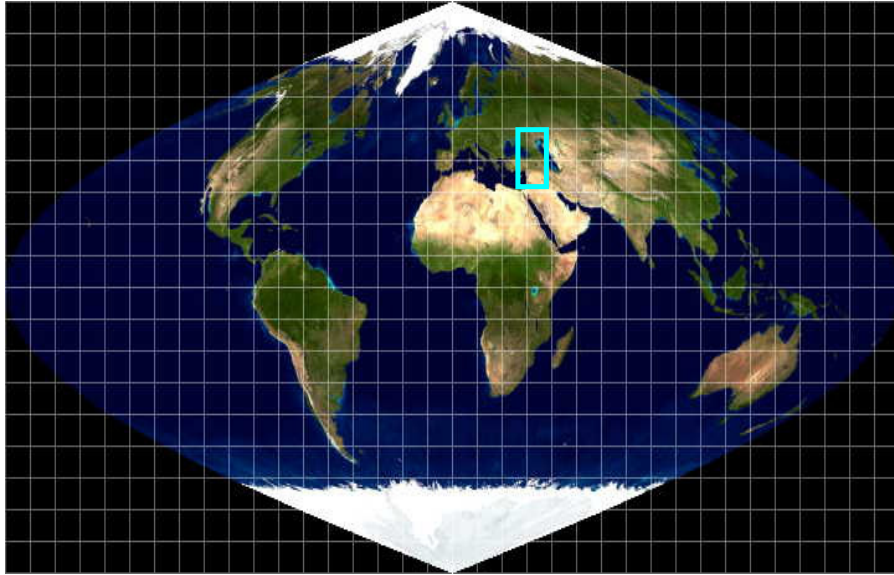


Figure 3.9 MODIS tiles that are used for the study

Tiled images are then reprojected into World Geodetic System 1984 (WGS 84), Universal Transverse Mercator (UTM) Zone 37 with a cell size of 500m.

The tiled HDF-EOS files are then imported to ERDAS Imagine remote sensing software. The data comes in 8 bit continuous format. These are to be converted in to thematic layers and the appropriate colors and name attributes should be attached. For this reason a module was written in Spatial Modeler of ERDAS Imagine. The module is executed to get the thematic snow cover product from the 8 bit continuous MODIS image format. As the snow cover map is converted into thematic form, the name and the color attributes of the data are also attached by the model. The output than can be used in any GIS software for further analysis.

The main GIS analysis is the validation studies of the snow products. Such analyses require the ground truth data which includes the presence of the snow on the ground, depth and density information of the snowpack. The ground data are fed into GIS as point data including relevant information. The ground data point

layer information is compared with the snow covered products and the accuracy assessments are performed. Such a validation study is performed for MOD10A1 daily snow cover maps. The study is presented in Tekeli et al. (2005b).

Overlay analysis with the basin and/or sub-basin layers to determine the depletion curves of the snow covered area is among the other major GIS analysis performed.

CHAPTER IV

SNOWMELT RUNOFF MODELING

4.1 Introduction

There is an increasing need for advanced hydrological modeling to manage the indispensable unique resource, water, starting from optimization for hydropower production to understand the impacts of climate change on the water balance. In this sense, this section describes one of the most widely preferred and used hydrological models for snowmelt runoff simulation and forecasting, namely Snowmelt Runoff Model (SRM) because of its simplicity and the requirement of relatively less number of input data.

SRM requires daily values of temperature, precipitation and snow-covered area (SCA). The daily snow covered area percentages are provided to specify fixed points in the depletion of snow cover. The interpolations between the observed values of snow cover area for simulation studies and extrapolation for forecasts require extensive historical records or algorithms based on statistical or physically based methods besides the remotely sensed image processing techniques to derive the observed values.

SRM used in the thesis is based on temperature index method. In this method, the snowmelt is related to temperature using the degree-day factor (DDF). Although, this methodology is an oversimplification of the full energy balance methodology, the less data requirement makes the model a possible candidate for operational studies especially for the governmental organizations in charge.

It has been well known that integration of data at different spatial and temporal scales is a serious problem in catchment hydrology. Models that determine the melt water require the snow cover as the initial and boundary conditions. Remote sensing (RS) although can provide the required information related with snow cover efficiently, the areal snow water equivalent (SWE) cannot directly be obtained from it. However, by the analysis of historic time series of snow cover obtained by RS and SRM model outputs, SWE can be calculated. The calculated SWE values from the model outputs of SRM can then be compared with ground observations.

The following sub-sections will deal with the respective topics. Motivation of hydrological modeling will be mentioned in section 4.2. Section 4.3 provides the essentials of snowmelt modeling. And finally section 4.4 gives a summary of SRM.

4.2 Hydrological Modeling

The project sponsored partly by NATO SfS and State Planning Organization under which this doctorate study is performed, aimed at operational forecasting of river runoff in Upper Euphrates River (Karasu), which includes high altitude basins with mountains for which the snowmelt is a major component of the total annual discharge. The model is implemented in a series of pre-operational tests, the result of which would direct operational studies.

Similarity is a serious problem in basins with pronounced topography, like the one under study, because of the high spatial variability of hydro-meteorological parameters. By the growing number of satellite platforms and improvements in the data transmission and processing algorithms, remote sensing enables to handle the spatial variations. Since the runoff at the outlet of the watershed is an integration of the whole basin rather than the point measured values, RS is gaining importance in distributed watershed modeling by its spatial variation handling capacity.

The advances in RS and GIS enable new data to scientific community. New data necessitate improvements in hydrological modeling rather than using the conventional methods. New models would provide better hydrological outputs, enabling the understanding of the complex world. Thus, there will be mutual developments between RS, GIS and hydrological modeling, leading improvements in the other ones.

Rango (1996) points out to this by: "... data from different remote sensors and various types of low altitude and ground measurements be combined and integrated to give more areal information content than available from any one data source" and "deterministic models need to prepare to use these real data rather than continue to use snow accumulations derived from point precipitation data which have been commonly shown to have inherent errors associated with precipitation gauge collection deficits and poor coverage with increasing elevations."

The need for model modifications with increasing data availability is stated in Hydalp (2000) as "Existing models are designed for a limited number of types of input and may need to be made more flexible to make optimum use of the range of possible inputs."

4.3 Essentials of Snowmelt Modeling

This section will provide the conceptual and physical basis and the fundamentals of SRM that is used in this research.

A trade off degree between the scientific complexity and practical applicability is the main difference between the hydrological models. The frontiers of snowmelt modelers, such as Vivan (1979), developed regression equations. These data based regression equations may work well under the circumstances similar to in which the model is developed. However, in new situations, the model may not be dependable. On the other extreme, a fully developed model in which all the temporal and spatial variable parameters are handled may demand large data amounts. The calibration of the parameters may be difficult and the end users may find it hard to understand the physical background of model and the modelers may have difficulty to get the physical input parameters.

For a model to be operational and easily applicable to basins other than for which the model is developed the following rule of thumbs should be satisfied.

“The goal was a conceptual model... of reasonable complexity, and with a requirement on input data that could be met in most ... basins” (Bergström, 1991).

“The model shall be based on a sound scientific background ... [but] ... complexity must be justified by model performance ... [and] ... the model must be understandable by users” (Lindström et al., 1997)

In this sense, SRM takes an intermediate between the data driven regression equations and the physically complex models by using a simplified conceptual representation. SRM outputs may have some percent of error because of imperfections and simplifications resulting from model structure. However, the

studies performed all over the world, over 100 basins in 25 countries; prove its usability in hydrological studies (Seidel and Martinec, 2004).

4.3.1 Components of Snowmelt Modeling

Hydrologic modeling approaches are nothing else than a transformation of incoming water (input) into outgoing discharge (output). Outgoing discharge is formulated by means of precipitation, flow way determination, lag times and losses. These formulations may show great variation from black box approaches to physically based models having different degrees of spatial variation. Figure 4.1 shows the hydrological modeling in a broad perspective.

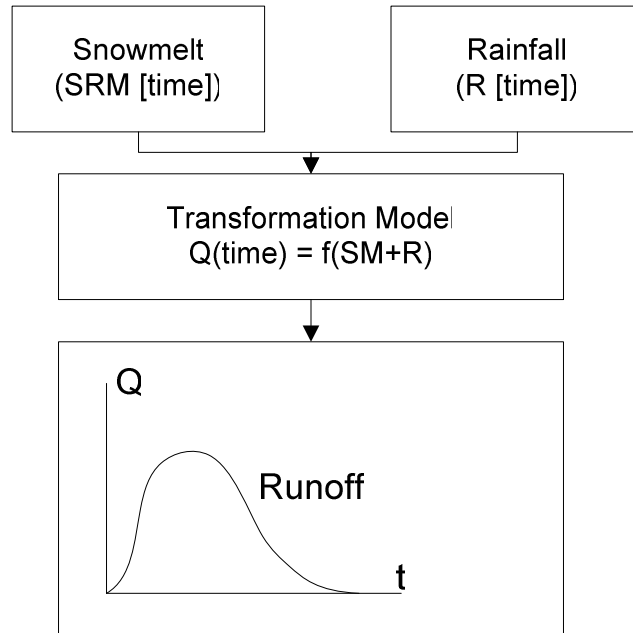


Figure 4.1 Hydrological modeling in a broad sense

Formulations may also be changed according to the type of the precipitation i.e. based on rainfall (liquid) or snowfall (solid). The cause of the variation is the fact that when precipitation occurs as snowfall, the discharge timing is not only a function of precipitation timing. The timing of runoff is also depended on the heat supplied to the snowpack either by temperature or by

radiation. In either forms, rainfall or snowfall, the total runoff volume is still total precipitation minus losses; however, snowfall is stored in snowpack until warmer weather allows the phase change from snow/ice to liquid (i.e. melting).

Snowmelt runoff modeling has four main components;

1. Extrapolation of meteorological data
2. Point melt rate calculations
3. Integration of melt water over the snow covered areas
4. Runoff Routing

Figure 4.2 represents the interrelation between these four components.

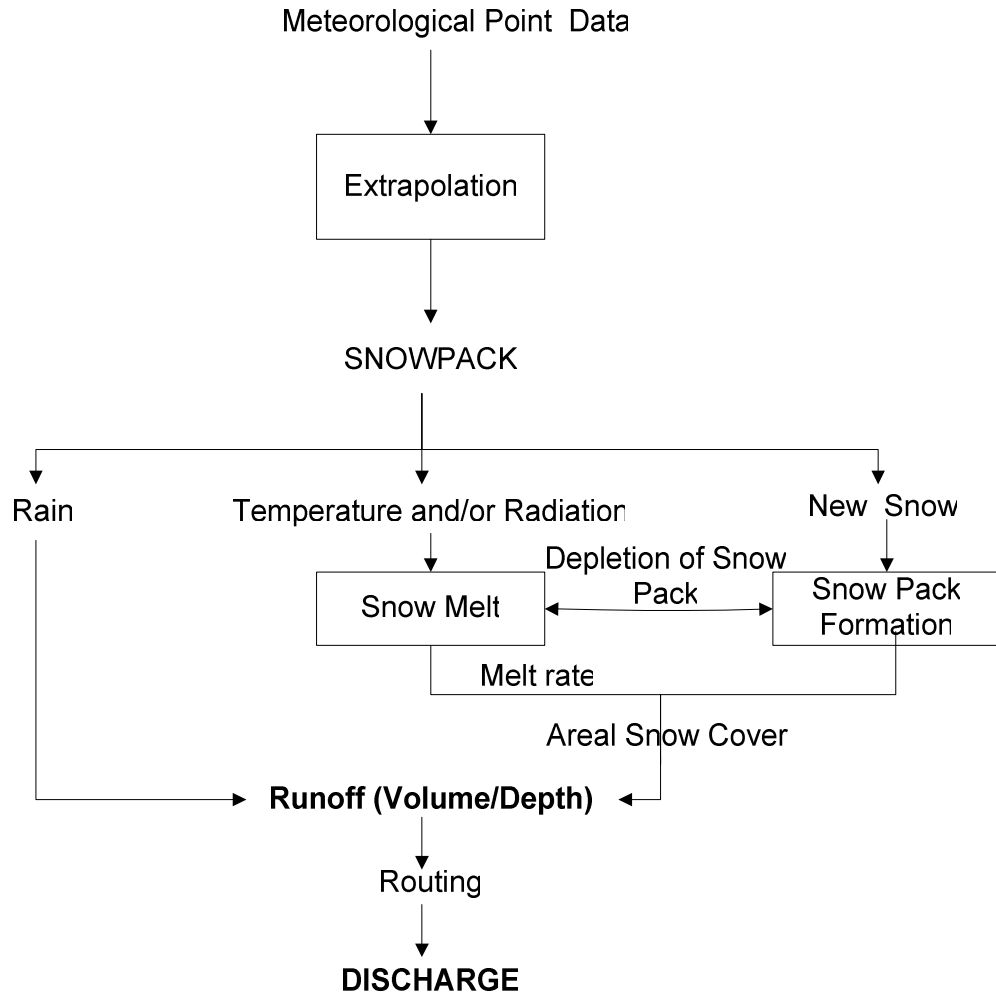


Figure 4.2 Components of snowmelt runoff modeling

For computation of discharge resulting from snowmelt runoff, meteorological point data should be extrapolated to the places at where snow cover exists. These extrapolated meteorological values are used to calculate the point snowmelt rates and point snowmelt volumes. SCA values can either be provided into models as input or the model itself can determine it internally. In either case, the computed point snowmelt rates are integrated over the snow-covered areas to find the total melt water that will be routed towards the basin outlet.

The main components of the snowmelt runoff modeling will be explained in the following subsections.

4.3.1.1 Extrapolation of Meteorological Data

In basins for which the snowmelt runoff constitutes a high portion of the total annual runoff volume, it is very hard and mostly impossible to find meteorological stations in adequate number and good quality with even distribution. The existing stations found, are mostly located in major valleys rather than the more inaccessible high portions of the basin at where most of the snow exist. Thus, most of the time, it is a necessity to use data from a station even though it may be a long distance away and at a much lower elevation from the snowpack.

Air temperature, which is the most important meteorological data, is mainly used for two purposes in the snowmelt models. It is used both as threshold temperature, separating precipitation as rainfall or snow and as critical temperature, used for estimating snowmelt rates. The values that are used as threshold and critical temperatures do not need to be same and both may be other than zero. Since air temperature alters with elevation, and most of the meteorological stations are located at lower elevations than the snowpack formations, a temperature lapse rate must be used to convert the measured air temperature at the lower station to the air temperature at the snowpack location. Although, most runoff models assume a fixed value for the lapse rate, the actual value may be a varying value depending on the present meteorological conditions. Often the temperature lapse rate, threshold and critical temperature values are treated as calibration parameters (Hydalp, 2000) of the model used.

Distribution of precipitation from a point station to the rest of the basin has always been a problem in the hydrology. The methods utilized may give unrealistic and inaccurate results. Besides, the systematic under catch of snow by most rain gauges especially under high wind speeds has long been reported in

literature such as Sevruk (1983). A phenomenon, which makes the things more complicated, is the fact that precipitation amount increases with elevation. When all the above issues are combined, the necessity of using a lapse rate for precipitation becomes more than a must, even though the variability in precipitation would be much more than in temperature. If the melt model used also, simulates the snowpack accumulation as the melting, then accurate estimation of snowfall at higher elevations become compulsory. To overcome this problem some models (such as HBV- a Scandinavian snowmelt model) may apply an internally designed correction factor for under catch of snow (WMO, 1986).

For all hydrological studies extrapolation of data from a limited number of point stations over the basin under study has always been a hot topic. There exists numerous methods starting from simple arithmetic averaging, Thiessen polygons to inverse distance relations. These methods allow the extrapolation in a horizontal plane (2D), disregarding the topography of the area under study. Some methods such as De-trended Kriging (Garen, 2003) may also take the topography into consideration when distributing the meteorological variables. By this manner the third dimension which is the elevation factor is also included during the distribution of the variables.

Before the selection of the methodology that will be used for the distribution of the meteorological variables a preliminary study must be performed since some times, distributing the variables in 2D may give better results than distribution in 3D (Weibel et al., 2002).

4.3.1.2 Point Melt Rate Calculations

The energy flux that a surface absorbs or emits is dependent to the sum of the following items.

- Net all wave radiation (sum of net short (net solar) and long wave (net thermal) radiation)

- Sensible heat transfer to the surface by turbulent exchange from atmosphere
- Latent heat of condensation or evaporation
- Heat added by precipitation (if the temperature of precipitation is different than the surface temperature)
- Heat conducted from ground

Main discrepancy in applying the energy balance methodology (Şensoy, 2005) to predict snowmelt is high variability of the above terms not over time (i.e. at diurnal, synoptic and seasonal scales) but also over the location (i.e. spatial variations). Although, some highly scientifically based equipped automated stations enable the application of the energy based snowmelt models at a point, there still remains the extrapolation of these measurements over the basin. This can be further explained as; “It is rare for such instrumentation to be available at even a single point in a basin, and even then a problem remains in extrapolating the measurements to other parts of the basin” (Hydarp, 2000).

Instead of measuring all of the components required by energy methods, some approximations to them can be made from the available data at hand. There are a number of these “parametric energy balance” methods. In these, the values of some energy components that are hard to find can be based on readily available data. Such as; incident radiation, a function of latitude, time of year, shading effects, cloud cover and snow albedo can be used to compute net short wave radiation. Multiplication of wind speed and air temperature approximates the sensible heat. Product of rainfall rate and temperature quantifies the precipitation heat supply.

But still, remains the problem of extrapolating these readily available data over the other parts of the basin. And additional assumptions should be made about the seasonal variations of these terms.

Studies performed in the literature show that using the air temperature for snowmelt modeling alone works quite well as the most basic approximation. This is due to the fact that temperature is the common factor in all of the energy balance components except the net radiation. Thus, even the other variables such as wind speed are involved; temperature differences are the main driving factor of the variations from day to day in heat supply. Even though the net radiation, the second dominant factor of the energy balance, does not directly depend on the temperature, there is generally a good correlation between them (Hydarp, 2000).

The above-mentioned issues and the fact that the temperature is the meteorological variable that can most safely be extrapolated across the basin makes it an indispensable variable in snow melt models. That is why most of the runoff models use temperature index to predict the melt water production. If the model is run on daily basis, a degree-day factor is used to convert the temperature above a critical value to a depth of melt. A good default and/or calibrated value of degree-day may lead the correct amount of melting. Unfortunately, under or over estimations should be expected due to variations in synoptic conditions.

SRM used in this thesis study used degree day factor method for computation of melt water production.

4.3.1.3 Integration of Melt Water Over the Snow Covered Areas

Depletion of snow cover takes place over a specified period called as melting season. During the melt season which mostly corresponds to spring months and early summer, incident solar radiance and air temperatures increase.

Snow cover does not disappear at the same time everywhere in the basin. Even, a spatially uniform rate of melting may lead a progressive reduction in snow cover over time rather than a sudden disappearance due to heterogeneities in snow depth. Initial snowpack tends to be deeper in higher elevations where the

heat supply for melting tends to be low. This results a much more gradual reduction of snow cover in mountain basins. Consequently, snow stays longer in higher regions of the basin.

Runoff predictions of a model will unavoidably be inaccurate even though the melt rates at each elevation are correct; if those melt rates are applied to a faulty SCA. Inaccurate high values of SCA will lead model to over estimate the runoff, where as low values will cause underestimation.

Two main methodologies are readily available at present to keep actual track of SCA. First one is snowpack modeling that is used by some hydrologic models such as HBV and the second is snow cover observations that are directly utilized by SRM.

In the snowpack modeling, simulation starts at autumn before the melt season of interest. Precipitation and temperature data are extrapolated to each elevation zone to determine the height of freezing level and the amount of snowfall (Şorman, 2004). SWE is used as an indication of growth and decay of snowpack. Snow depth is not used since the density of lying snow can vary with time through wind drift, compaction and freeze-thaw metamorphism. SCA is given by the sum of areas within which SWE is greater than zero. Ground measurements may be used to calibrate/validate these kinds of models.

In snow cover observation method snowpack is not modeled, but observed. These observations of the snow cover are provided as snow covered area percentage input to the model that works mainly in melt season. The required repeated observations of SCA can be obtained from RS. Mapping of the SCA was one of the first practical uses of RS in hydrology in the early 1970's and this formed the basis of SRM.

There should be ways that each approach can benefit from the other one. The interpolation and/or extrapolation of SCA should be done in considering the SWE and its distribution within the basin. Conversely, simulation of SWE over time could clearly benefit from direct observations of SCA that can be used for accuracy calculation of model performance and/or for parameter updates.

4.3.1.4 Runoff Routing

Open channel flow, over land flow, infiltration, percolation and ground water flow are the common pathways of both rainfall and snowmelt as they reach ground surface.

Most models represent the above processes in a simplified conceptual manner in which a small number of stores namely, upper and lower for representing fast and slow flow, are connected in series, parallel or both. The outflow from any store can be a linear or non-linear function of the volume in that store. Besides, the routed amount through the store may not be constant but some increasing function of the soil moisture content. Two stores or even single stores can give good daily predictions for rainfall runoff modeling (Jakeman and Hornberger, 1993). Where else, general purpose hydrological models need an extra store for snowpack.

4.3.2 Quality Assessment of Model Accuracy

Accuracy of the hydrological models is evaluated mainly by comparison of observed and simulated daily discharges. Even though recent studies try to make evaluations based on comparison of observed and modeled values of both SWE and SCA, the utmost used method is the comparison of hydrograph values. For quality assessment, most common method has been the Nash & Sutcliffe goodness of fit statistic (R^2) given by

$$R^2 = 1 - \frac{\sum_{i=1}^n (Q_i - Q_i')^2}{\sum_{i=1}^n (Q_i - \bar{Q})^2} \quad (4.1)$$

where;

Q_i : measured daily discharge

Q_i' : computed daily discharge

\bar{Q} : average measured discharge of the season under study

n : number of daily discharge values

R^2 approaches to one as the root mean square prediction error decreases to zero.

Volume difference; which is the percentage difference between the observed and simulated/forecasted mean or total discharge D_v is also used for accuracy comparison.

$$D_v [\%] = \frac{V - V'}{V} \cdot 100 \quad (4.2)$$

V : measured runoff volume

V' : simulated/forecasted runoff volume

4.4 Snowmelt Runoff Model

Up to here some general concepts of snowmelt modeling is summarized. Starting this section snowmelt runoff model (SRM) used in this study will be introduced.

4.4.1 Background

Jaroslav Martinec has developed the SRM model in 1975 when he was in the Swiss Snow and Avalanche Research Institute at Davos. The model changed and further developed under the collaboration of Al Rango (US ARS), Ralph Roberts (US ARS), Michael Baumgartner (University of Bern) and Klaus Seidel (University of Zurich). There are a number of versions of the model. With version 4.0 (April, 1998) the climate change effect was added and at present Beta version of WinSRM (designed for windows) is available.

On the contrary to general-purpose hydrological models with extra snow subroutines, SRM was initially developed specifically to predict the snowmelt runoff. However, the year around simulation capability of the model was also shown by Martinec et al 1998. SRM or variations of it are applied over 100 basins in 25 countries at altitudes 32-60 °N and 33-54°S with basin sizes varying from <1 to 120 000 km² and documented in about 80 scientific references (Seidel and Martinec, 2004). Nash-Sutcliffe R^2 , statistics (Equation 4.1) and the percentage error in total runoff (Equation 4.2) are the measures of goodness of fit.

SRM is an empirically derived but physically based, deterministic, degree-day hydrologic model used to simulate and/or forecast daily runoff resulting from snowmelt and rainfall in mountainous regions.

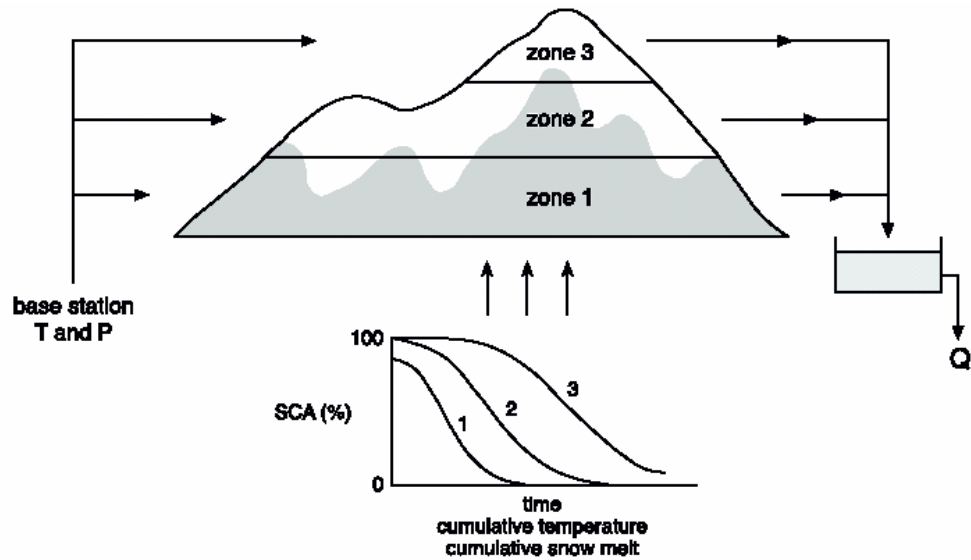


Figure 4.3 Components of SRM (Adapted from Hydalp, 2000)

Figure 4.3 shows the structure of SRM. The key points of the model can be itemized as;

- A daily time step is used.
- Basin is divided into elevation zones.
- Snowmelt runoff in each zone is computed by summation of the predicted/measured air temperature.
- Runoff from rainfall is added to the snowmelt runoff.
- Runoff from all elevation zones are summed together before routing.
- Losses for evaporation and ground water recharge are handled by runoff coefficients of snow and rain
- Recession coefficient is used to compute the recessed amount of discharge
- The total amount of water is routed through a single store.
- New daily runoff is added to previous day's discharge to obtain daily discharge at $(n+1)^{\text{th}}$ day.

The basic equation of SRM can be formulized as;

$$Q_{n+1} = [c_{sn} \cdot a_n (T_n + \Delta T_n) S_n + c_{rn} \cdot P_n] (A \cdot 10000/86400) (1 - k_{n+1}) + Q_n k_{n+1} \quad (4.3)$$

Where;

- n : is the number indicating the day
- Q : discharge from the basin
- T : extrapolated air temperature to the hypsometric elevation of each zone
- P : precipitation falling as rain in the zone
- S : snow covered area in the zone
- A : Area of the zone
- k_{n+1} : recession coefficient
- a_n : degree day factor
- c_{sn} : correction factors for losses for snowmelt
- c_{rn} : correction factors for losses for rainfall

and the term in square brackets in equation 4.3 defines the total daily water produced. Also implicitly a temperature lapse rate is needed to extrapolate the temperature and/or precipitation from a base station. Since SCA is an input to SRM, no method is needed to derive it.

4.4.2 Model Inputs

SRM has three main input variables which are temperature, precipitation and snow covered area. These will be mentioned in the following sections.

Table 4.1 SRM model variables

	Definition Variable		Symbol	Spatial Variability	Mode
1	Daily	Max-Min	T	Basin wide-Zonal	S*/F*
	Temperature	Average			
2	Precipitation		P	Basin wide-Zonal	S/F
3	Snow Covered Area		SCA	Basin wide-Zonal	S/F
* ²	Actual stream flow		Q	Basin wide-Zonal	S/F

* S: Simulation Mode

* F: Forecasting Mode

*² Not actually an input variable (used for calculation of model accuracy)

4.4.2.1 Meteorological Variables

SRM can use temperature and precipitation time series either from a single station or from separate sites to represent each elevation zone. If a single station, which can either be a base or a synthetic, is used temperature is extrapolated to the hypsometric mean elevation of each zone by a lapse rate. The lapse rate value can be changed depending to the synoptic conditions (seasonally or on particular dates). SRM predicts the snowmelt rate in each zone from the temperature in the zone, with no melt if temperature is less than 0°C.

To determine the type of precipitation, i.e. either snowfall or rainfall, in each zone, critical temperature that may not be zero is used. The snowfall falling on the non-snowy area of the zone is treated as a temporary snowpack that will contribute to runoff as soon as sufficient degree-days occur. Rainfall falling on the snowpack would result runoff if the snow is already ripened. The user defines the approximate timing of the snowpack to be ripened. Melting effect of rain on a cold snowpack is neglected. Rainfall falling on the non-snowy area would result runoff directly.

4.4.2.2 Snow Cover Depletion Curves

Time series of snow-covered area (SCA) are required as daily input into equation 4.3 as boundary conditions. Time series of SCA are termed as either snow depletion curves (SDC) or conventional depletion curves (CDC).

SDC or CDC was initially determined by ground observations and areal photographs in the early applications of SRM. But the succeeding studies have utilized satellite remote sensing as the main information source of snowpack depletion.

Disappearing snow cover patterns are similar year after year (Martinec, 1980). But differences in the amount of winter snow accumulation and variations in melting conditions may result differences in CDC from year to year. A hard and snowy winter may cause early SCA to be higher. But it is proven that same initial SCA may give different amounts of stored snow (Martinec, 1980). Increase in the initial SWE causes reduction in rate of declining SCA even at the same temperature input. Thus, a family of CDCs might be expected to exist for a particular basin and zone, all similar in shape but the timing varying according to initial SWE in the year under study (Hydalp, 2000).

For modeling year under study, required CDCs can be obtained by one of the followings

- from direct observations of CDCs by frequent satellite data
- knowledge of basin average SWE from ground observations
- selection of most suitable CDC from the family of curves derived from previous model studies.

In the absence of the near real time frequent earth observation and lack of accurate basin wide SWE, the last approach is the most suitable one (Rango and Martinec, 1982). Based on one or two satellite images, acquired in the early melt

season, a family of CDCs can be selected. The rate of SCA decline from initial value is related to the initial SWE content. The decline rate of SCA increases as initial SWE decreases.

However, further studies revealed that the rapidity of SCA decline is related to the temperature conditions besides the initial SWE content. Modified depletion curves (MDC) came into existence at this point. MDCs are plots of SCA percentage versus cumulative degree-days, instead of number of days in CDCs. Even MDCs include the initial SWE content and cumulative degree days to enable the comparison between years; they showed great variability from year to year (Seidel and Martinec, 2004, Martinec et al., 1998).

In 1985, Martinec plotted the SCA against the cumulative snowmelt depths rather than the cumulative degree-days. This method considers the possible degree-day variations throughout the season. This last MDC type is the default option in the recent version of SRM (WinSRM, 2005).

Since, SRM requires daily SCA percentages, it may be necessary to extrapolate and/or interpolate the SCA trend over time. MDC based past years is the best way. But in the absence of such information, curve fittings; either linear (Rott and Nagler, 1995) or quadratic interpolation (Swamy and Brivio, 1997) can be used. A methodology based on the cumulative air temperatures was developed to help the extrapolation and/or interpolation of SCA during the thesis study (Tekeli et al, 2005c).

4.4.2.3 Model Parameters

Model parameters required by SRM can be summarized in Table 4.2. These parameters define the climate, snow cover dynamics and stream flow regime. Some explanations can be found in the following sections. Further details can be obtained from the one of the available SRM manuals.

Table 4.2 SRM model parameters

	Definition of Parameter	Symbol	Spatial Variability	
1	Degree day factor	a	Basin wide-Zonal	
2	Runoff coefficient factor for	snow	c_s	Basin wide-Zonal
		rain	c_r	
3	Recession coefficient	k	Basin wide-Zonal	
4	Temperature Lapse rate	γ	Basin wide-Zonal	
5	Critical Temperature	T_{crit}	Basin wide-Zonal	
6	Rainfall contributing area	RCA	Basin wide-Zonal	
7	Lag time	L	Basin wide-Zonal	

For the present study, metric version of the program is used. Thus, the parameters are presented in metric units.

4.4.2.3.1 Degree-day

Although, sometimes criticized because of its simplicity, degree-day method maintains its foremost position in snowmelt runoff modeling (Martinec and Rango,1986).

Degree-day factor can be determined by comparing degree-day values (temperature values above a certain base temperature) with the daily decrease of snow water equivalent. The variation of SWE can be obtained from snow pillows records (Chapter 2), snow lysimeter data (Chapter 2) or from radioactive snow gages.

In the absence of such records, an empirical equation given by (Martinec, 1960) is proposed for determination of the degree day values.

$$a = 1.1 * \rho_s / \rho_w \quad (4.4)$$

where;

a : the degree-day factor (cm/°C/d)

ρ_s : density of snow

ρ_w : density of water

The degree-day factor, a, is used to convert the number of degree days T (°C d) into daily snowmelt depths M (cm) by;

$$M = a * T \quad (4.5)$$

Studies have shown that; degree-day values show variation from day to day and are not a fixed value. On the contrary, it is expected to be a kind of time series.

The daily variations are understandable to a degree that; the method does not take account into the other components of the energy balance. Such as; solar radiation, wind speed and the latent heat of condensation. However; when the daily values are averaged for a few days, the degree-day factor becomes more consistent and can represent the melting conditions.

As the snow ages, the density increases in conjunction with increase in snow water content and decrease in albedo. All of the above favor melting. Thus, increase in degree-day factor is expected as snow ages. Table 4.3 shows the proposed degree-day factor values by WMO (1964) depending on the land use and time of the year.

Table 4.3 Proposed degree-day factors (Adopted from WMO 1964)

Month	Moderate Forest Cover	Partial Forest Cover	No Forest
April	0.2	0.3	0.4
May	0.3	0.4	0.6
June	0.4	0.6	0.7

From Table 4.3, the increase of degree-day factor through out the melting season can easily be observed. The factors causing an increase in the degree-day factor can be itemized as;

1. Increase in snow ripeness
2. Increase in insulation
3. Increase in percent of sheltered snow covered area
4. Depletion of snow cover
5. Increase in the mean elevation of the snow covered area (Levick L. R., 1998)

It is seen that degree-day factor method will maintain its popularity since temperature is tentatively, a good measure of energy flux, in addition to easy to measure and forecast (Martinec and Rango, 1986).

4.4.2.3.2 Critical Temperature

Critical temperature is used to determine the type of precipitation i.e. either rainfall and contribute to runoff immediately ($T > T_{crit}$) or snowfall and lead to accumulation of snowpack and a delayed runoff ($T < T_{crit}$). In this manner, new snowfalls are kept in storage until warm days allow the melting.

Varying values of T_{crit} from +3 °C in April to 0.75 °C in July is reported (WinSRM, 2005). A similar trend with a narrower range +1.5 °C to 0 °C is reported by US Army Corps of Engineers (1956).

Sharp rainfall runoff peaks may be missed by SRM due to the determination of temperature values being less than the T_{crit} . In such a case, the T_{crit} and temperature lapse rate values should be revised and logically adjusted using engineering judgment and model experience. However, this still may not provide a solution since, the daily average temperature values are fed to SRM. Distinguishing between rain and snowfall through out a day may be difficult. Moreover, precipitation can occur during the warmer or colder hours of the daily temperature cycle.

4.4.2.3.3 Temperature Lapse Rate

Temperature lapse rate is used to define a temperature gradient across the watershed, which will be used in extrapolating temperature values from a given station.

SRM accepts a single, basin wide temperature lapse rate or zonal temperature lapse rates. As the zonal values of the temperature lapse rate may change, the value in the same zone may also change with time. Higher temperature lapse rates for winter and lower values for the summer months are expected (Hydalp, 2000).

The depletion of snow cover may represent requirement of the value change of the lapse rate. If high temperatures result from extrapolation by a certain lapse rate but no change in snow areal extent is observed, then probably no appreciable snowmelt is taking place (WinSRM, 2005) and the lapse rate should be modified accordingly.

4.4.2.3.4 Runoff Coefficients

Differences between the basin runoff and the available precipitation (either snowfall or rainfall) are explained by the runoff coefficients. If there were not any

catch deficit affecting snowfall recording and no inadequate precipitation data from the mountainous regions, the long term averages of the ratios of the measured precipitation to the measured runoff would give a good starting point; unfortunately this is not the case.

Runoff coefficients account for the volume of water, which does not leave the basin, taking into account the site characteristics, such as soil type, soil depth, elevation, slope, aspect, vegetation type and vegetation density (Levick, 1998).

SRM uses two runoff coefficients c_s and c_r that are related to snow melting and rainfall respectively. The two values are expected to be different from each other due to their characteristics. C_s and c_r can be formulated by

$$c_s = \frac{\text{Volume of snowmelt contributing to runoff}}{\text{Total volume of snowmelt}} \quad (4.6)$$

$$c_r = \frac{\text{Volume of rain contributing to runoff}}{\text{Total volume of rain}} \quad (4.7)$$

Monthly variations in runoff coefficients can be explained by an analysis of the seasonal changes in vegetation and climate (Levick, 1998, Kaya 1999, Tekeli 2000). Frozen soil early in the melt period has lower infiltration and storage capacities. Spring will thaw the soil and snow melt will soak in the soil, leading a drop in the runoff coefficients. As soil becomes saturated, the values will increase again.

4.4.2.3.5 Time Lag

This parameter indicates the time delay between the daily rise in temperature and runoff production. Thus, it is used for time wise matching of the observed and calculated peaks in the simulation mode. For the forecasting mode,

it gives the expected peak times of the flood hydrograph, providing more efficient reservoir operations and enabling flood mitigation.

The hydrographs of past years and the daily fluctuating character of the snowmelt enable the predetermination of the time lag value. Value can be modified by comparing the timing of simulated hydrograph peaks with the observed hydrograph peaks.

For a time lag of 6 hours, 50 % of input computed for temperature and precipitation on the nth day (I_n) plus 50 % if I_{n+1} results n+1 day's runoff after being processed by the SRM computer program (WinSRM, 2005) by;

$$L= 6 \text{ hours } Q_{n+1}= 0.5 \times I_n + 0.5 \times I_{n+1} \quad (4.8)$$

Similarly

$$L= 12 \text{ hours } Q_{n+1}= 0.75 \times I_n + 0.25 \times I_{n+1} \quad (4.9)$$

$$L= 18 \text{ hours } Q_{n+1}= I_n \quad (4.10)$$

Figure 4.4 shows the time lag effect on the calculation of discharges.

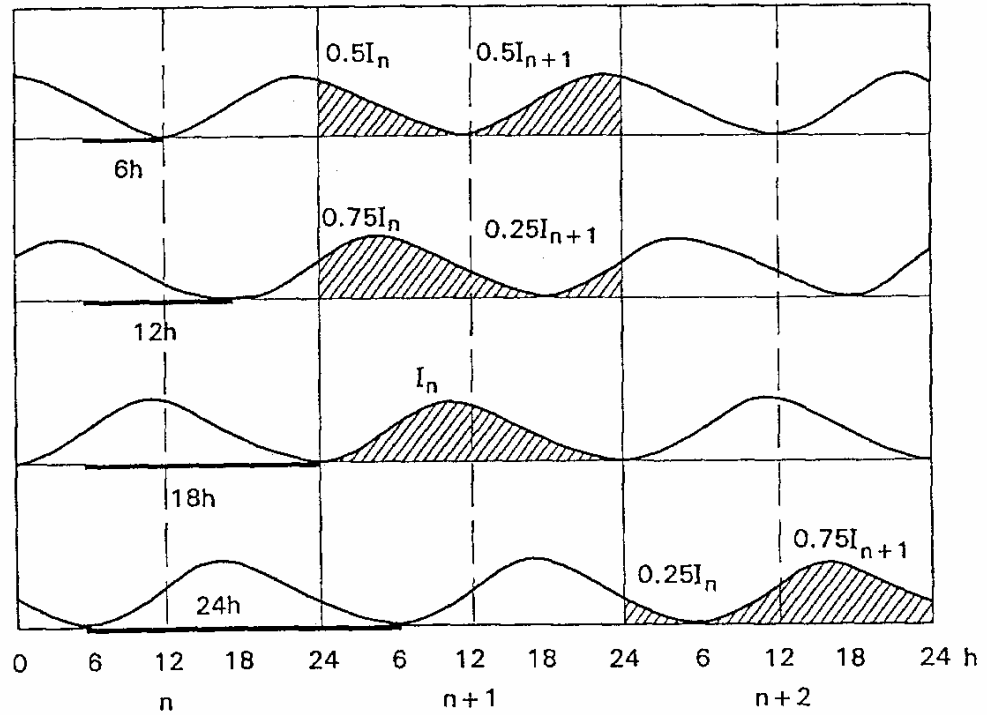


Figure 4.4 Lag time effect on discharge calculations
(Adapted from Martinec and Rango, 1986)

4.4.2.3.6 Recession Coefficient

Since $(1-k)$ defines the portion of the daily melt water production (Equation 4.3), which immediately appears in the runoff, accurate determination of recession coefficient is a necessity for SRM. For the determination of the value of this parameter, analysis of historic discharge data may be a starting point.

The value of k may be computed by;

$$k_{n+1} = x (Q_n)^y \quad (4.11)$$

where x and y can be determined by using stream flow data and equation 4.11. Q_n are plotted against Q_{n+1} on log-log scale. A median line can be drawn

between 1:1 line and the envelope line. Two points can be read and used in solving

$$\begin{aligned} \log k_2 &= \log x - y \log Q_1 \\ \log k_3 &= \log x - y \log Q_2 \end{aligned} \quad (4.12)$$

where k_2 and k_3 are the slopes of tangents at points 1 and 2.

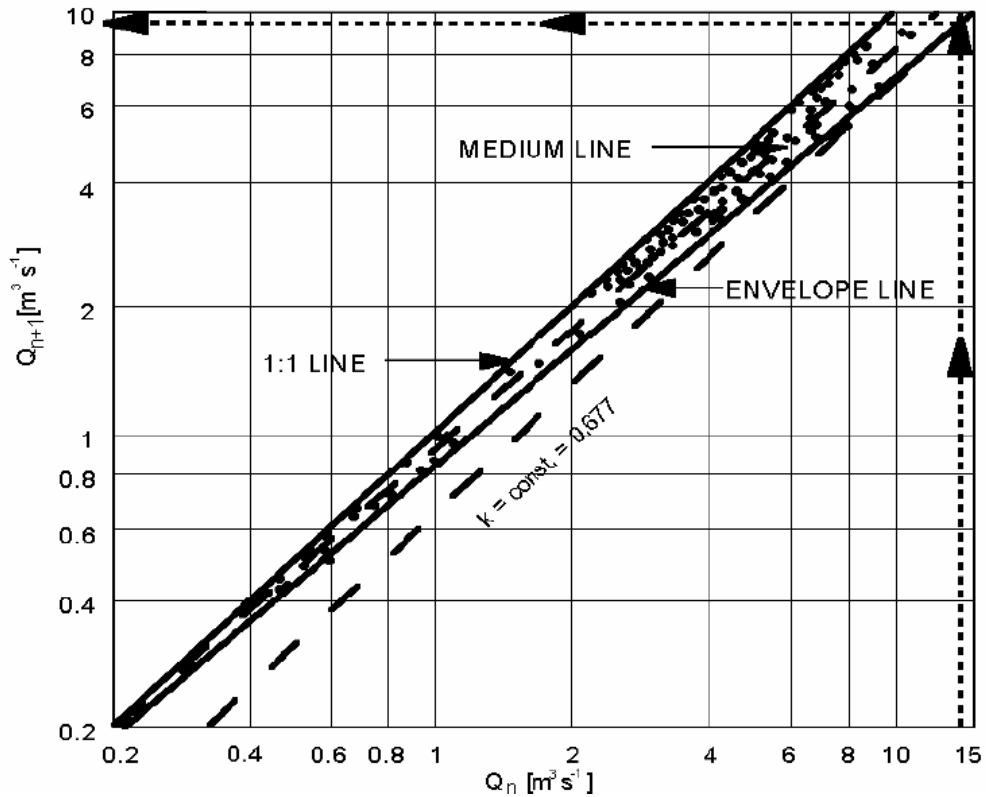


Figure 4.5 Recession flow plot Q_n vs Q_{n+1}
(Adapted from Martinec and Rango, 1986)

With positive values of y , the recession from a high discharge is relatively steeper than from a low discharge, which is a commonly observed situation (Seidel and Martinec, 2004).

4.4.2.3.7 Rainfall Contributing Area

SRM determines the type of precipitation and related amount according to the provided temperature and precipitation data. If the precipitation is determined to be in rainfall form, different approaches can be followed. As the approach chosen changes, the effect of the precipitation on the hydrograph changes. The selection of the approach is dependent on the existing snow condition.

If the snow is dry and deep, the snow largely retains the rainfall. At this situation, the rainfall directly affecting the runoff values are reduced by the ratio of non-snow covered area to the total area of the respective zone.

As snow softens and ripens, it becomes ready to release the same amount of water as entering to the snowpack. In this case, rainfall falling on the whole area directly affects the hydrograph.

The user determines the date of change of the snow condition during the model runs.

CHAPTER V

NUMERICAL WEATHER PREDICTION MODELS

Hydrological rainfall-runoff models require meteorological input data in addition to model parameters for computation of watershed runoff values. These required meteorological values show variation both in time and space. A common source of spatially and temporally varying meteorological data is the outputs of numerical weather prediction models.

Numerical weather prediction models can provide input to hydrological models by the short and/or long term weather forecasts. Numerical weather prediction is the name given to the technique used to forecast the weather by computer from its present, measured state up to several days ahead (ECMWF, 2004). Hydrologic forecast analyses are highly dependent on the forecasted meteorological data. As the accuracy of the meteorological forecast data increases, the better results of the hydrologic analysis can be derived. Such accurate hydrologic analyses enable better hydropower production, optimization of water supply and flood control. Thus, future weather situations are the key interest of hydrological and meteorological model forecasters.

Turkish State Meteorological Service (DMI) implements a number of numerical weather models. The operational estimates and forecasts of weather conditions of Turkey are available from the European Center for Medium Range

Weather Forecasts (ECMWF) and Mesoscale Model Version 5 (MM5) model runs performed by DMI.

This chapter will give a brief history of the numerical weather prediction (NWP) which is followed by brief description for each of the NWP models used in the thesis and the procedures to follow for deriving the related meteorological variable for input to hydrologic models especially for real time forecasting studies.

5.1 A Short History of Numerical Weather Prediction

Around 1904, the Norwegian hydrodynamist V. Bjerknes claimed that the weather can be quantitatively predicted by applying the complete set of thermodynamic and hydrodynamic equations to the correct initial atmospheric conditions. Even though he was not able to make any quantitative prediction, he initiated such studies.

The construction of a hemispherical network of upper air stations and the development of early computers after the Second World War were the two major developments for accomplishing the claim of Bjerknes.

Jule Charney succeeded to forecast the large scale flow in atmospheric motions in 1940s, despite the minor inaccuracies.

In 1950s, the first NWP experiments using the Charney's barometric equation of the atmospheric motion were conducted. Even the most simple equations could be used due to the present computer facility handicap, the results were surprisingly successful. The general 500 hPa flow pattern over North America was forecasted 24 hours in advance with greater skill than the previous subjective methods (ECMWF, 2004).

This success in the NWP motivated the developed nations and two different approaches aroused. Countries having limited computer facility preferred to use barotropic models, in which the vertical motions were neglected. On the other hand, countries like US and Britain used baroclinic models enabling the forecasts of vertical motion.

These baroclinic models were start point for today's modern standard models used in making numerical weather forecasts by operational forecast centers. The studies related with NWP are developing since that time exponentially.

5.2 ECMWF

Forecasting of weather requires solution to the complex scientific and technical problems. As the time interval to forecast increases, the problem gets much more complicated. European countries agreed to combine their scientific and technical resources in the aspect of weather forecasting and decided to establish the European Center for Medium Range Weather Forecasts as soon as they realized the economic and social benefits that could be obtained from more accurate medium range forecasts with the initial establishment in 1975. At the moment, Belgium, Denmark, Germany, Spain, France, Greece, Ireland, Italy, Luxembourg, the Netherlands, Norway, Austria, Portugal, Switzerland, Finland, Sweden, Turkey, United Kingdom are the member states.

ECMWF is a consequence of hundred years development in dynamic and synoptic meteorology, fifty years of which are related with the development of the numerical weather prediction (NWP) methods. The objectives ECMWF having a long history can be summarized as follows;

- Development of numerical methods for medium range weather forecasting

- The preparation of medium range weather forecasts for the distribution to the meteorological services of the member states
- Scientific and technical research directed to the improvement of these forecasts
- Collection and storage of appropriate meteorological data (ECMWF, 2004).

The first operational forecasts were produced on August 1, 1979. Every day ECMWF makes a forecast to 10 days ahead and shares the numerical products with the meteorological offices of the Member States by a dedicated telecommunications network. Member states can use these products to prepare medium-range forecasts for end users. Turkey, being one of the member states till May 1, 1976, can reach the ECMWF data.

5.2.1 ECMWF Forecasts

ECMWF predicts the atmosphere conditions in the medium range up to ten days ahead. In this time, the future state of the atmosphere at any point can be influenced by any phenomena at very distant geographic locations (ECMWF, 2004). Thus, in applications of medium range forecasting, the analysis are not confined to limited areas of the globe, on the contrary, a global atmosphere from earth's surface up to a certain height should be considered. The details of the analysis that will be performed depend on the available computer power.

The horizontal resolution of the analysis available at the moment by the ECMWF is equivalent to 40 km evenly geographically spaced grid points around the globe. This grid network is repeated up to 60 levels in vertical atmosphere. This vertical and horizontal mesh results the forecasts of the wind, temperature and the humidity at 20 911 680 points through the atmosphere (ECMWF, 2004). Even though, small scale effects such as heating of soil by sun, the turbulence of the air near ground can not be represented properly by the present technology, such a mesh, enables the production of realistic forecast of the near surface

weather parameters, such as local winds, and the air temperature at the level of the measurement stations. The possibility of distinguishing the French Massif Central from the Alps, and the Po Valley in the Northern Italy is a proof of the models representation capability (ECMWF, 2004).

The forecast are provided under the three main sections by ECMWF. These are medium range, monthly and seasonal forecasts.

5.2.2 Making Forecast in ECMWF

As every numerical model, initial or starting conditions are required for ECMWF model forecast studies. Initial conditions for the ECMWF global model are prepared by making synthesis of the observed values of atmospheric fields taken over a 24-hour period and the short range forecasts provided by the global model itself (ECMWF, 2004). The synthesis is a way of integrating the observed values into the model. The big bottleneck in this synthesis task is the sparse and irregularly distributed high quality data over the globe. The preparation of the initial conditions is a demanding task that can require a computer power as much as needed for a ten day forecast.

Model variables for forecast computations are temperature, wind and specific humidity. Other atmospheric parameters are derived from these main variables. The operational products provided by the ECMWF dissemination are listed in Table 5.1. These products are computed at 3 hourly intervals from t+3 to t+72 hours and at every 6 hour intervals from t+72 to t+240 hours.

Table 5.1 Operational products that are available from ECMWF dissemination

Upper air parameters
Mean sea level pressure
2 meter temperature
2 meter dew point
10 meter wind
10 meter wind gust
total precipitation
total cloud cover

The 2 meter temperature, dew point, 10 meter wind and wind gust are computed from approximately 30 meters above the ground, which is the lowest model level, and the surface values. In the calculations, surface state such as the albedo and the roughness is taken into consideration (ECMWF, 2004). These parameters are available in the latitude longitude grid form. The data is stored in standard formats namely GRIB (Grid in Binary) for meteorological fields and BUFR (Buffer) for meteorological observations.

ECMWF sends the output numeric products to the meteorological offices of the member states. Member states use these products for preparation of medium range forecasts for end users.

With the signed protocol, Middle East Technical University, Water Resources Laboratory also has access to the data through DMI.

5.3 Mesoscale Model (MM5)

Anthes & Warner at Penn State University documented the first developed Mesoscale Modeling (MM) in the early 70's. The National Center for Atmospheric Research (NCAR) and Penn State University are developing the program since that time. The fifth generation MM5 is the latest version at the

moment including many new developments. MM5 is mainly developed for simulating and/or predicting mesoscale and/or regional scale atmospheric circulation either by hydrostatic or by non-hydro static conditions in terrain flowing sigma coordinate. The model is being developed by contributions from the users at universities or governmental offices. The major improvements achieved through out the usage include the followings;

- Multiple nest capability
- Non hydrostatic dynamic analysis
- Four dimensional data assimilation possibility
- More physical background involvement
- A broader range of computing platforms.

5.3.1 Components of MM5

Actually MM5 is a modeling system, in which the core model (MM5) is run in conjunction with several auxiliary programs. Figure 5.1 shows the flowchart of the program and the data flow when the first guess fields are provided by radiosonde and surface observations. If three dimensional variational analyses are to be performed then Figure 5.2 is the chart of data flow. Following sections will briefly mention about the sub programs included in the MM5 and their functions.

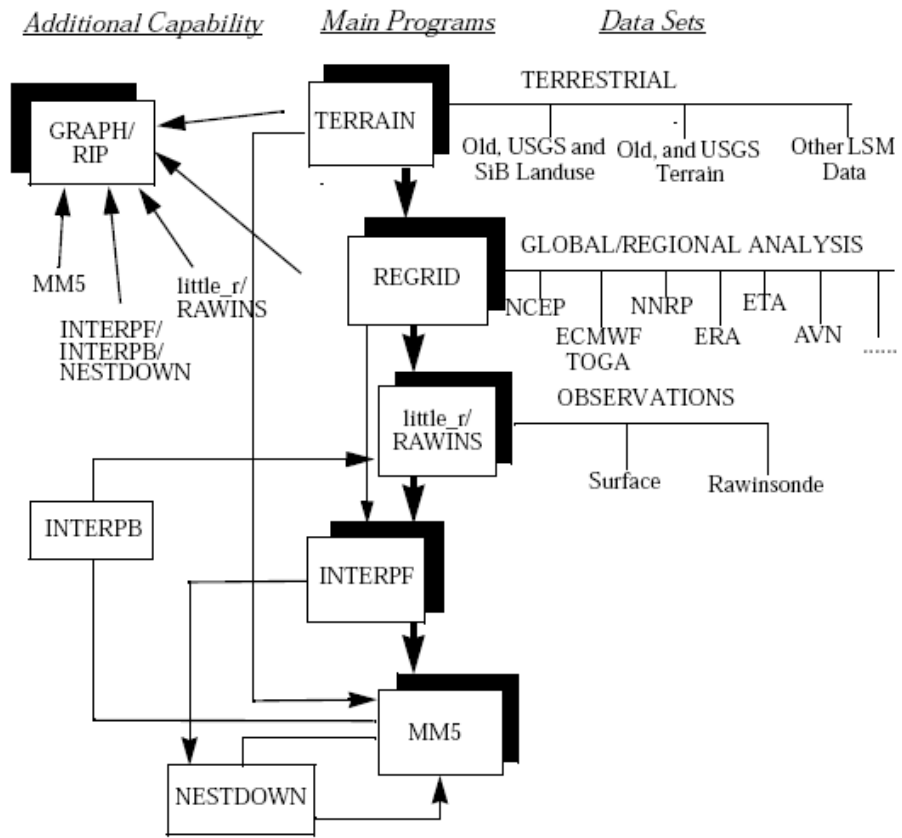


Figure 5.1 MM5 modeling system data flow chart using Little_R/Rawsin
 (Adapted from <http://www.mmm.ucar.edu/mm5/documents>)

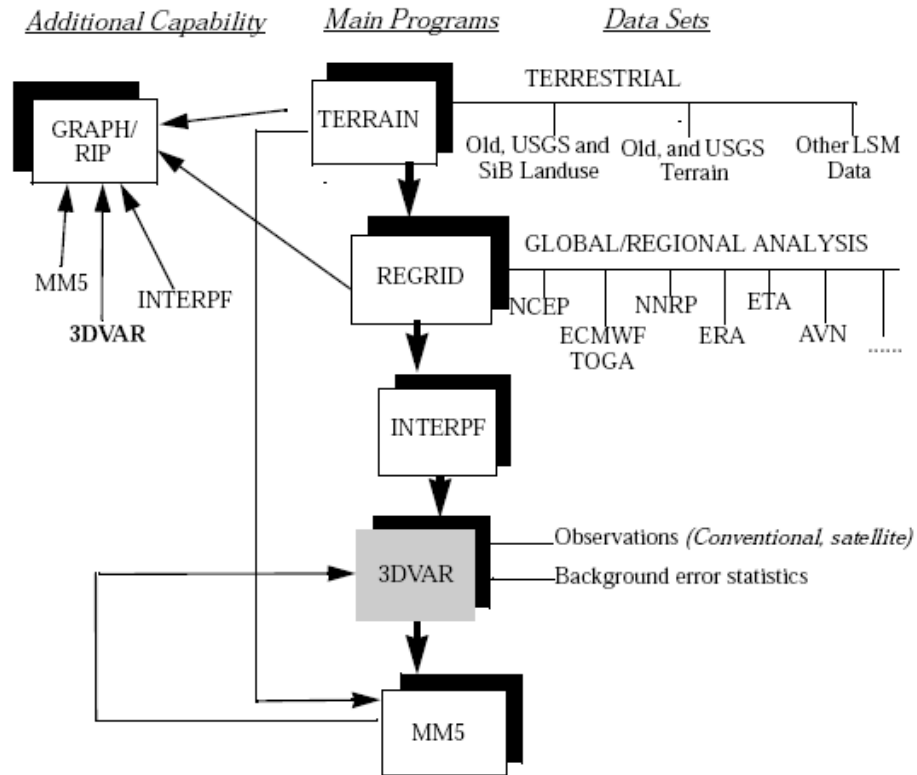


Figure 5.2 MM5 modeling system data flow chart using 3DVAR
 (Adapted from <http://www.mmm.ucar.edu/mm5/documents>)

Terrain

This is the first program to run in MM5 modeling system (Figure 5.1 and Figure 5.2). Terrain horizontally interpolates (analyzes) the regular latitude - longitude terrain elevation and vegetation (land use) onto the selected mesoscale domain (Figure 5.3).

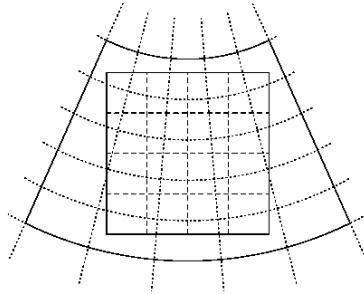


Figure 5.3 Interpolation from regular latitude - longitude to selected mesoscale domain by Terrain (Adapted from <http://www.mmm.ucar.edu/mm5/documents>)

There are two main tasks of the program Terrain

1. Set up mesoscale domains : Both coarse and fine grids
2. Production of terrestrial data fields for all of the mesoscale domains, which will be used by REGRID

Regrid

This is the second program in MM5 modeling system (Figure 5.1 and Figure 5.2). It uses the outputs of Terrain as input and prepares the input files for Rawins/Little_R and Interpf. The main objective of Regrid is reading archived meteorological analyses and forecasts (ECMWF, ETA) on pressure levels (mb) and interpolation of those analyses from some native grid and map projection to the horizontal grid and map projection as defined by Terrain. Regrid handles pressure level and surface analyses and performs two dimensional interpolations on these levels.

Rawins/ Little r:

Interpolation performed in Regrid, may not provide much mesoscale detail. Program Rawins/Little_r, enables the enhancement of these interpolated values with the observations from the standard network of surface and rawinsonde stations. These observations include temperature, humidity and wind as direct observations. Remote sensing techniques also enable indirect observations. Uses

of indirect observations are gaining more importance for researchers and operational modelers as they become available.

Outputs are used to provide fields for initial and boundary conditions (via program Interpf).

Interpf

Interpf deals with data transformation required to go from the analysis program to the mesoscale model. Interpf can take Regrid, Rawins/Little_r or Interpb outputs as input. These are used for making a model initial, lateral boundary condition and a lower boundary condition. During this procedure Interpf performs vertical interpolation, diagnostic computation and data reformatting.

Graph

Graph enables drawing the plots of meteorological variable outputs from each of the modeling system component. Data from Terrain, Regrid, Rawins/Little_r, Interpf, MM5, Nestdown, Lowbdy, and Interpb can be used by Graph.

Rip

RIP, standing for Read/Interpolate/Plot, is a Fortran Program that uses NCAR (National Center for Atmospheric Research) Graphic routines for the purpose of visualizing output from gridded meteorological data sets, mainly from mesoscale numerical models.

Even though, it was originally designed to handle the sigma-coordinate-level output from PSU/NCAR Mesoscale Model (MM4/MM5), in April 2003 it

was generalized to process data sets with any vertical coordinate. Moreover, it can be used to visualize model input or analyses on model grids.

Model is under progress since 1991, primarily by Mark Stoelinga at both NCAR and the University of Washington. This is the program used by the DMI at the moment for visualizing the MM5 model outputs.

MM5

This is the numerical weather prediction part of the modeling system. It performs time integration and produces model outputs. MM5 can be used both for theoretical and real-time studies, including predictive simulation and four dimensional data assimilation to monsoons, hurricanes and cyclones. (MM5 tutorial, 2005).

MM5 starts by the horizontal interpolation of terrestrial and isobaric data from a latitude-longitude grid mesh to a mesoscale rectangular domain. The variable high resolution domain can be in one of the three following (i) Mercator, (ii) Lambert Conformal or (iii) Polar Stereographic projection systems. This interpolation is performed by Terrain and Regrid components.

The poor mesoscale detail of the interpolated data can be enhanced by Rawins/ Little_r. For this process, observations from the standard network of surface and rawinsonde stations are used. During the enhancement either a successive-scan Cressman technique or multiquadic scheme can be followed (MM5 tutorial, 2005).

As the horizontal interpolation is performed, the vertical interpolation from pressure levels to s-coordinate of the MM5 model is handled by program Interpf.

After the MM5 run, the data from s-levels back to the pressure levels are interpolated by Interpb. On the other hand, Nestdown can be used to interpolate model level data to a finer grid for preparation of a new model integration.

Model outputs both on pressure (mb) and σ levels (given by equation 5.1) can be viewed by graphic programs RIP or Graph.

5.3.2 Horizontal and Vertical Grids of MM5 Model

MM5 has two main grid configurations, first of which is the horizontal and the second is the vertical. Modeling system gets and analyzes its data on pressure levels. However, these values should be interpolated to the model's vertical coordinate before used by the model. Vertical coordinate used by MM5 is terrain following, meaning that the lower grid levels follow terrain, while upper surface is flat. Figure 5.4 shows the sigma coordinate levels. Intermediate levels progressively flatten as the pressure decreases towards the chosen top pressure. A dimensionless quantity σ is used to define the model levels.

$$\sigma = (p - p_t) / (p_s - p_t) \quad (5.1)$$

where

- p : the pressure
- p_t : specified constant top pressure
- p_s : surface pressure

For the determination of the vertical coordinate, hydrostatic model uses the actual pressure, where else, nonhydrostatic model uses a reference state pressure. Each model level is defined by a value of σ being zero at the top and one at the surface. Details about the models and coordinates can be obtained from the web page of The National Center for Atmospheric Research (NCAR) available from "<http://www.ncar.ucar.edu>".

The vertical resolution of the model is defined by the values varying from zero to one which may not be evenly spaced (Figure 5.4). Commonly the resolution in the boundary layer is much finer than Figure 5.4, and the number of levels may vary from ten to forty, although there is no limit in practice (MM5 tutorial, 2005). Dashed lines show half sigma levels and solid lines indicate full sigma levels. K in Figure 5.4 denotes the sigma level number.

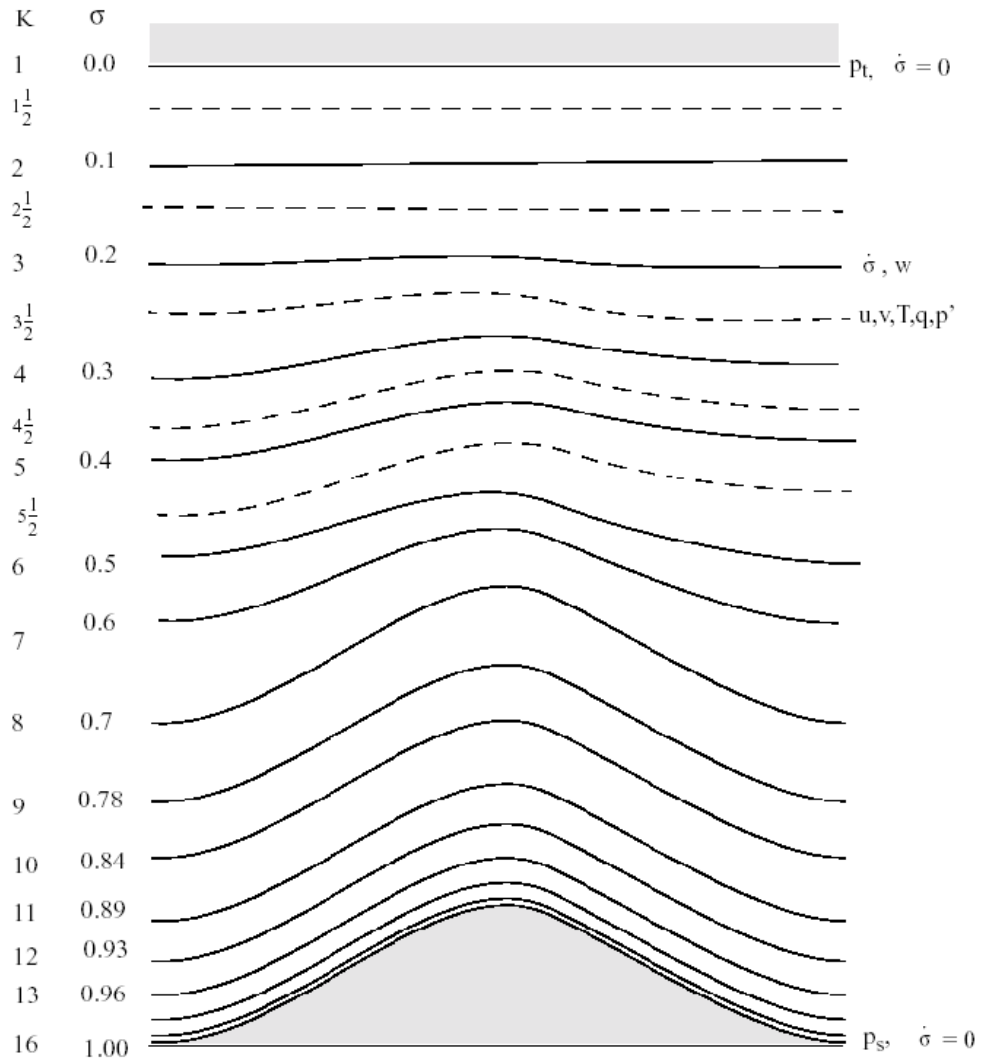


Figure 5.4 Vertical sigma coordinate levels used in MM5
(Adapted from <http://www.mmm.ucar.edu/mm5/documents>)

The horizontal grid system of MM5 can be seen in Figure 5.5. Scalars (Temperature {T}) are shown at the center of grid square (x in Figure 5.5) and the eastward (u) and northward (v) velocity components are located at the corners (in Figure 5.5). The center points of the grid squares are referred as cross points, and the corner points are dot points.

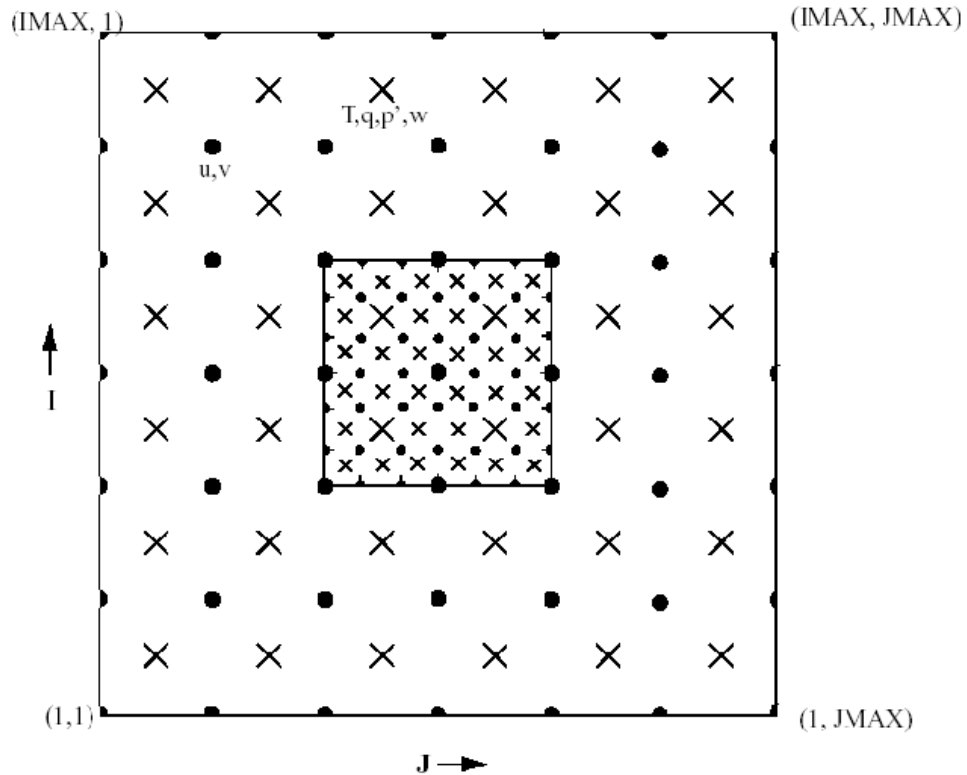


Figure 5.5 Horizontal grid system of MM5. Dots and crosses are shown by (·) and (x)

(Adapted from <http://www.mmm.ucar.edu/mm5/documents>)

5.3.3 Map Projections

MM5 modeling system offers a choice of several map projections. These are (i) Polar stereographic, (ii) Lambert Conformal and (iii) Mercator. The first one is recommended for high latitudes; second one for mid latitudes and the last one for low latitudes.

5.3.4 Data Required to Run the Modeling System

For a successful run of MM5, the following data sets are required.

- Topography data
- Land use data
- Gridded atmospheric data having at least: sea-level pressure, wind, temperature, relative humidity and geopotential height at the following pressure levels, surface, 1000, 850, 700, 500, 400, 300, 250, 200, 150, 100 mb.
- Soundings and surface observations data

Topography, land use and vegetation data with global coverage in varying resolutions are available from NCAR. The scale to use is a function of computer facility. The related data sets used by DMI at the moment are analyzed during the study and findings are mentioned in Chapter 6. All the programs in the MM5 modeling system can be downloaded from <http://www.mmm.ucar.edu/mm5>.

The modeling system is able to run on various computer platforms such as Cray, SGI, IBM, Alpha, Sun, HP and PCs running Unix.

5.3.5 Lateral Boundary Conditions

Regional numerical weather prediction models require lateral boundary conditions data. In MM5, all four boundaries have specified horizontal winds, temperature, pressure and moisture fields and can have specified microphysical fields (such as cloud) if these are available (MM5 tutorial, 2005). Thus, before any model run, boundary values have to be set in addition to the initial values.

The boundary values can come any of the following three places:

- Analyses at the future times
- Previous coarser mesh simulation
- Another model's forecast

For real time forecasts, the boundary values will come from another model's forecast most of them which depend on a global model forecast. DMI uses ECMWF data as boundary conditions to MM5.

CHAPTER VI

NEAR REAL TIME SNOWMELT RUNOFF FORECASTING STUDIES

6.1 Introduction

This chapter discusses the near real time hydrological snowmelt runoff forecasting studies. Remote sensing data from NOAA-AVHRR and Moderate Resolution Imaging Spectroradiometer (MODIS) satellites, meteorological data from numerical weather prediction models ECMWF and Mesoscale Modeling Version 5 (MM5) and the ground-based measurements are used as inputs. The main objective of the study is performing an operational use of snowmelt runoff forecasting using hydrological models with remote sensing data and numerical weather forecasts as input (forcing state) variables. The output of which will enable the optimum operation of water resources systems.

The near real time forecasts studies are performed during the main melting period of 2004. In this period, snowmelt runoff model (SRM) is used as the hydrological model for snowmelt runoff forecasting, NOAA-AVHRR and MODIS provided the information on the snow-covered areas required by SRM. Ground based measurements provided from automated meteorological and snow stations mentioned in Chapter 2 gave information about the in situ values of the

snow and meteorological conditions. Two numerical weather prediction models are used in combination with these in situ values.

This chapter summarizes the real time data transfer system, remote sensing data processing scheme, the results and the quality assessment of the near real time runoff forecasts.

6.2 Near Real Time Runoff Forecasting in Upper Euphrates Basin – An Overview

Near real time hydrological forecasting is conducted from April 1, 2004 to July 1, 2004. In the following pages, forecast results are presented for various cases such as; i) the precipitation and temperature values are directly taken from numerical weather prediction (nwp) models, ii) the temperature values of nwp are corrected, iii) precipitation values of nwp are corrected.

Even the forecasted discharge values, which are obtained from SRM, should be compared with the measured discharge values in near real time; unfortunately the malfunction of the discharge sensor did not enable such a comparison. Thus, the forecast values could be compared with the observed values after the end of model runs.

6.3 Forecast Processing Chain

The processing chain is composed of a series of programs written for Unix and Windows environment. Fortran and Perl codes are mainly used under Unix environment. Where else, custom-made Visual Basic scripts are compiled in Windows media.

Since the data are received from various platforms, a complete master code controlling all of the processes could not be performed yet. However, such a master code is considered as a future progress.

Main steps of the present version of forecasting procedure are outlined in Figure 6.1. T1, T2 and T3 indicate the tasks having sub-tasks to be performed. T1 and T3 are explained in Figure 3.6, Figure 3.8 and Figure 2.18 respectively. Boxes filled in gray indicate the task that was planned. But the operational problems faced during the melting period did not allow this planned task to be performed; nevertheless these tasks will be put into reality as soon as technical difficulties are overcome.

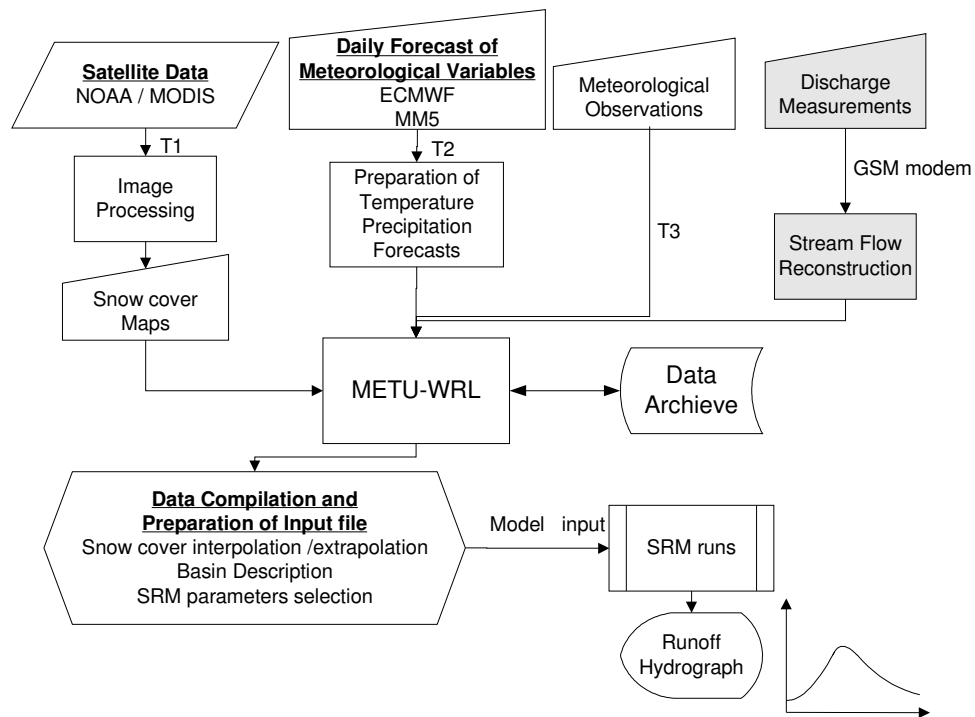


Figure 6.1 Processing chain for discharge forecasts

Daily Forecast ECMWF forecasts are downloaded to Turkish State Metrological Services (DMI) in Ankara. These are used as boundary conditions for Turkey in execution of ECMWF and MM5 runs. The outputs of ECMWF and MM5 runs are uploaded to METU server via shell scripts at around 04:00 AM every day.

Data from DMI come in various formats. ECMWF data are available in GRIB format, where else MM5 data are provided in RIP format. Since the data come in different formats, different strategies are developed to decode each data set. Following the decoding process, both data sets are imported into GIS environment. In GIS environment, the necessary projection information is added to each data and the required GIS analyses are performed. Thus, T2 in Figure 6.1 is divided into two different procedures. Figure 6.2 shows the way to handle the ECMWF Grib data. Detailed explanation related with ECMWF data analysis can be seen from progress report 3 (Tekeli, 2003) and Chapter 5.

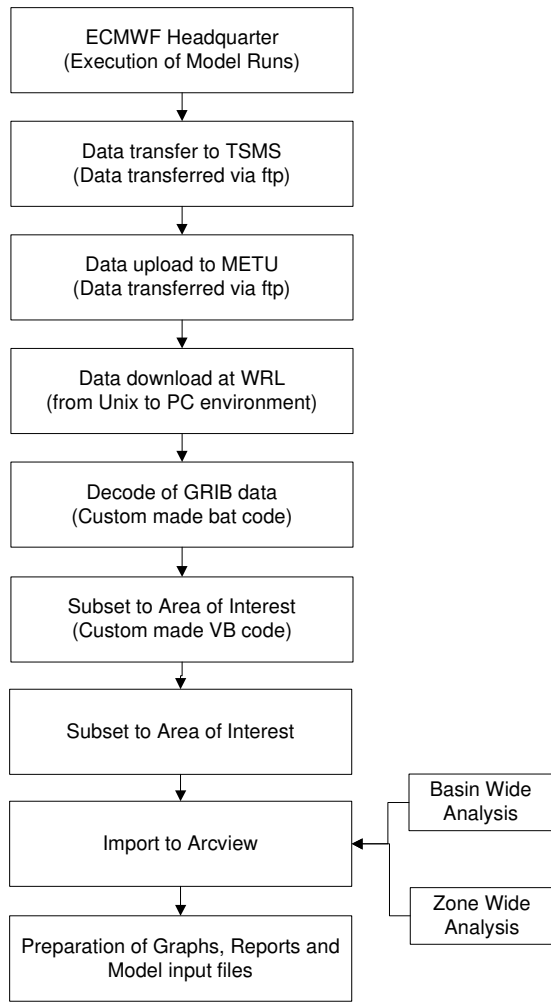


Figure 6.2 ECMWF Grib data format processing chain

MM5 data uses the ECMWF (40x40 km) model outputs as boundary conditions and provides the forecasted meteorological variables up to t+48 hours in 9x9 km grid size. Since the MM5 outputs are provided in RIP format their decoding is performed heavily in Unix environment. Figure 6.3 shows the processing chain of MM5 Rip data.

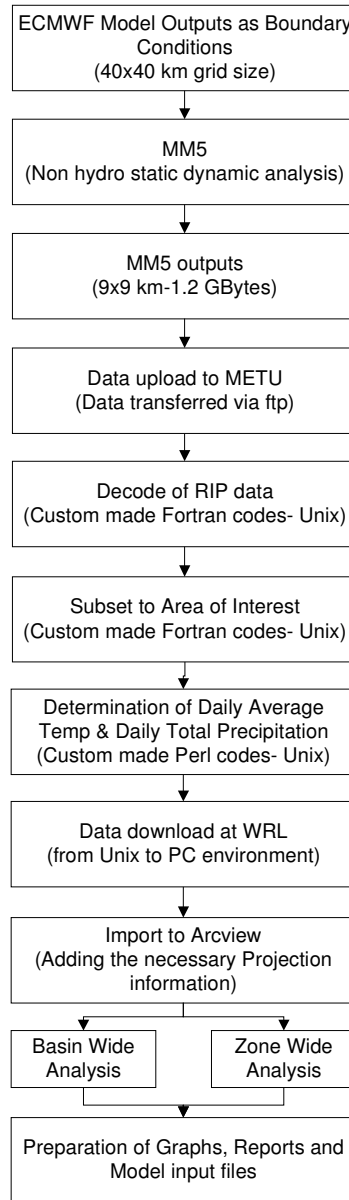


Figure 6.3 MM5 Rip data format processing chain

Meteorological Observation Ground based meteorological data are provided weekly. These are processed as indicated by T3 in Figure 6.1, the details of which are given in Figure 2.18. The ground data are compared with weather forecast values for validation purposes.

Discharge Measurements This module involved the retrieval of river stage from the site. However, operational problems faced during the melt period of 2004 did not allow the desired accurate data transfer in near real time. New sensors for retrieval of river stage values are installed by the project team in site by October 2004.

Snow Covered Area Determination NOAA-17 AVHRR and MODIS images are used for the present study. NOAA-17 images are downloaded by DMI receiving antenna. After certain format conversions the data are uploaded to the METU-WRL account by ftp. MODIS images are downloaded from NSIDC. The processing of images to derive the snow-covered areas are indicated by T1 in Figure 6.1. Details of the processing can be found in Figure 3.6, Figure 3.8 and in Progress Report 3 (Tekeli, 2003).

Data Compilation Since the data arrive from different sources and in various formats, the preparation of input files for SRM are performed manually. Nevertheless, the ways to automate the input file preparation are under search.

SRM runs WinSRM, the windows version of SRM is the model used for forecasting of snowmelt runoff hydrograph. Various runs are performed as the data became available.

Timing of Near Real Time Forecasting

Timing of each data set is indicated in the tables of the related subsections.

Daily Forecast Data

Table 6.1 Timing of daily forecast data

Data Type	Availability	Via	Timing
ECMWF	Daily	ftp	~ 04:00 am
MM5	Daily	ftp	~ 04:00 am

Meteorological Observation

Table 6.2 Timing of meteorological observations downloaded from site

Station Name	Availability	Via	Timing
Hacımahmud	Daily Average	GSM	10:00-12:00 am 03:00-05:00 pm
Güzelyayla	2 hourly averages & daily averages	Türk Telekom	24 hours
Ovacık	2 hourly averages & Daily averages	Türk Telekom	24 hours
Sakaltutan	Daily averages	Inmarsat Mini-M	24 hours
Çat	2 hourly averages & Daily averages	Inmarsat Mini-M	24 hours

Snow Cover Map

Table 6.3 Timing of snow cover maps

Satellite Name	Availability	Via	Timing
NOAA-17 AVHRR	Daily	ftp	~02:00 pm
MODIS	Daily* (*3-6 day delay)	NSIDC	Valid for 3 days after order

Model Runs

Model is executed as the snow-covered area of that day is provided

Quality Analyses

The accuracy of model forecasts is evaluated using the coefficient of determination, R^2 , and volume difference, D_v , given by the outputs of the model runs. The computed discharges are compared with the observed discharges recorded at the basin outlet as METU WRL receives the discharge data from the site on real time basis.

6.4 Data Used in Near Real Time Forecasting

Main data set used is composed of three major sets. These are meteorological, hydrological and snow cover data. Each of these is explained in the following sections. The methods to derive snow depletion curves are explained following the snow cover data section.

6.4.1 Meteorological Data

The meteorological forecast data are composed of daily temperature and precipitation forecasts obtained from numerical weather prediction models, European Center for Medium Range Weather Forecasting (ECMWF) and Mesoscale Model Version 5 (MM5).

Basin under study can be overlaid by 12 partly ECMWF or by 125 MM5 forecast grids. The temperature obtained from ECMWF data is the forecasted temperature for 14:00 local time. The precipitation data obtained from ECMWF is the forecasted daily total precipitation.

Temperature data gathered from MM5 includes the forecasted temperature values for the 07:00, 14:00 and 21:00 local time. From these values, the daily forecasted average temperatures are calculated. To determine the daily forecasted precipitation, the forecasted values of MM5 for convective and non-convective precipitation values for the related day are summed together (Stoelinga, 2004).

6.4.2 Hydrological Data

Real time discharge measurements planned in Upper Euphrates river at 2101 Kırkgöze station, was used for the first time. The system might have collected data at 15 minutes interval if it could have worked. The malfunction of the system is overcome by placing a new pressure sensor and data is automatically transferred via GSM system with October 2004.

6.4.3 Snow Cover Data

The ability to map the areal depletion of snow correctly is important for operational decision making (e.g. reservoir management); for correct specification of boundary conditions in numerical weather prediction models and for modeling atmospheric, hydrological and ecological processes (Simic et al, 2004). This requires daily processing of satellite images on an operational basis since snow has a dynamic behavior. To provide snow cover data, NOAA 17/ AVHRR, MODIS daily and 8 daily composite products are used in this study. Following sections will mention about each satellite system and its data set.

6.4.3.1 NOAA 17 Images

To follow up the highly dynamic snow covered area information, NOAA satellite images are downloaded and processed starting from April 1st to June 30th, 2004.

However, the major flaw in the optical satellites, cloud, prevents the usability of every image. Thus, even all the images in the duration of the

snowmelt season are analyzed not all of them could be used. Table 6.4 shows the NOAA 17 images that were found suitable for snow covered area mapping.

Table 6.4 Listing of NOAA 17 imagery used during forecasting

Image no	Image Date	Image no	Image Date
1	1 April 2004	5	21 May 2004
2	10 April 2004	6	22 May 2004
3	12 April 2004	7	12 June 2004
4	26 April 2004	8	13 June 2004

Based on the above mentioned satellite images the derived snow covered area percentages are plotted for each zone (A~ E) as in Figure 6.4. The hypsometric curves for the whole Karasu and its sub basins can be seen in Chapter 2.

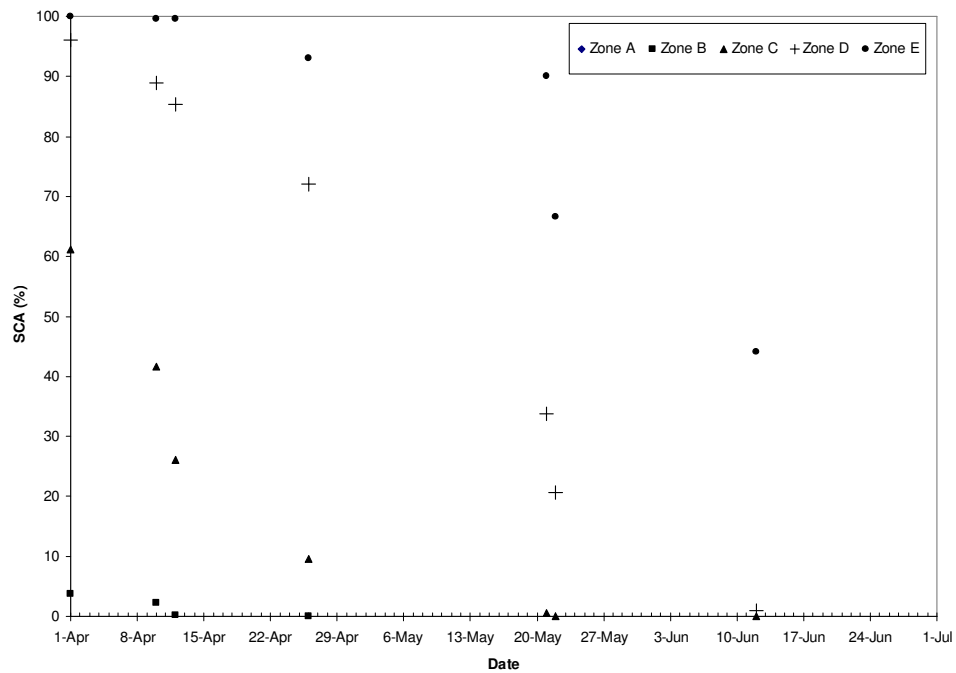


Figure 6.4 Snow covered area percentages obtained from NOAA 17 for 2004 water year (April 1~ July 1)

6.4.3.2 MODIS Daily Snow Cover Maps (MOD10A1)

SRM requires the daily snow covered area information as well as the daily precipitation and temperature values. Thus, MODIS daily snow cover maps, MOD10A1, with a spatial resolution of 500m provided by National Snow and Ice Data Center (NSIDC, 2004) constitute the second snow maps used in this study.

All the images belonging to the snowmelt period of 2004, from 1 April 2004 to 30 June 2004, were downloaded and processed from <http://nsidc.org>. However, the cloud problem also degraded the use of some images. MOD10A1 data was acquired in thematic format. Thus, the spatial queries performed enabled to determine the availability of images for each zone. The image availability for the zones of the basin for snowmelt of 2004 on the basis of cloud cover percentage is indicated by X in Table 6.5.

Table 6.5 MOD10A1 image availability for winter of 2004

Image No	Date	Zone A	Zone B	Zone C	Zone D	Zone E
1	1 April 2004	X			X	X
2	10 April 2004	X	X	X	X	
3	12 April 2004	X		X	X	
4	26 April 2004		X			X
5	22 May 2004		X			
6	11 June 2004				X	
7	12 June 2004			X	X	X
8	13 June 2004				X	X
9	14 June 2004				X	X
10	25 June 2004					X
11	30 June 2004				X	X

X Image available

Based on the available images, snow cover depletion can be drawn as a function of time which is shown as in Figure 6.5.

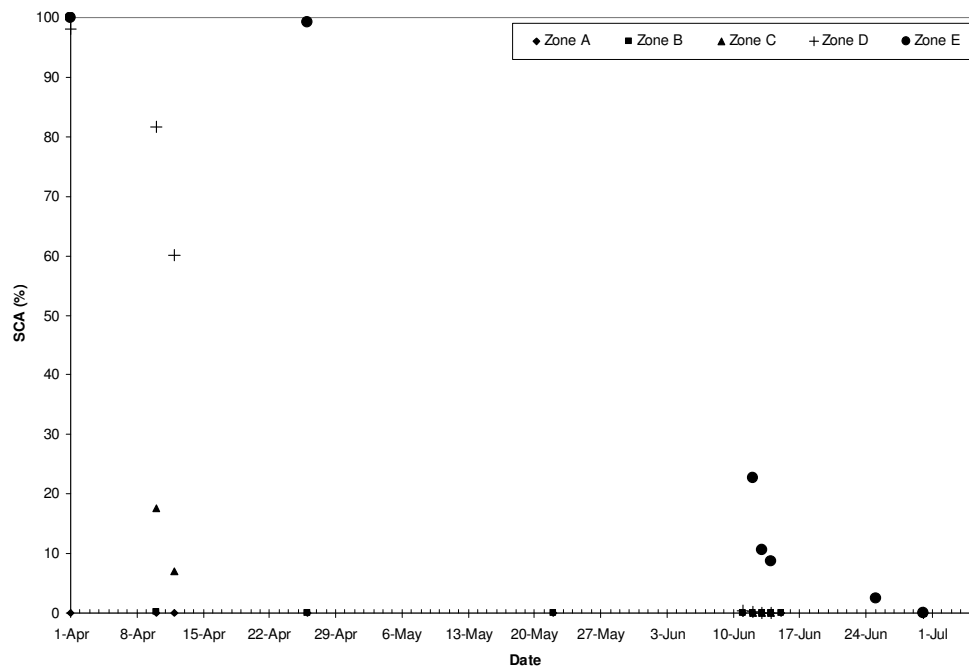


Figure 6.5 Snow covered area percentages obtained from MOD10A1 images for 2004 water year

6.4.3.3 MODIS 8 Daily Snow Cover Maps (MOD10A2)

In snow cover analysis, it is found that maximum snow cover is a more useful parameter than minimum or average snow cover (Hall et al., 2002). Thus, an 8 day composite showing maximum snow cover is produced based on the 8 days of the daily 500m resolution product. Such a compositing technique is believed to be the best method to minimize the cloud cover (Hall et al., 2002) and give better estimates of SCA.

MOD10A2 products with 12 scenes, covering the 2004 snowmelt period were downloaded and processed to get the snow covered area information. The downloaded image listing can be seen in Table 6.6.

Table 6.6 MOD10A2 image availability for winter of 2004

Image No	Date*	Image No	Date*
1	2004_089	7	2004_137
2	2004_097	8	2004_145
3	2004_105	9	2004_153
4	2004_113	10	2004_161
5	2004_121	11	2004_169
6	2004_129	12	2004_177

* Date indicates the start of the 8 day composite time period

Figure 6.6, Figure 6.7 and Figure 6.8 show the snow covered area percentages for the middle zones C and D and the upper zone E with areal percentages of 18.1, 21.3 and 26.3 of the whole basin under study. Even though, better S-shaped representation of snow depletion curves can be sensed from the images, still the problem of cloud contamination can be observed from the below figures.

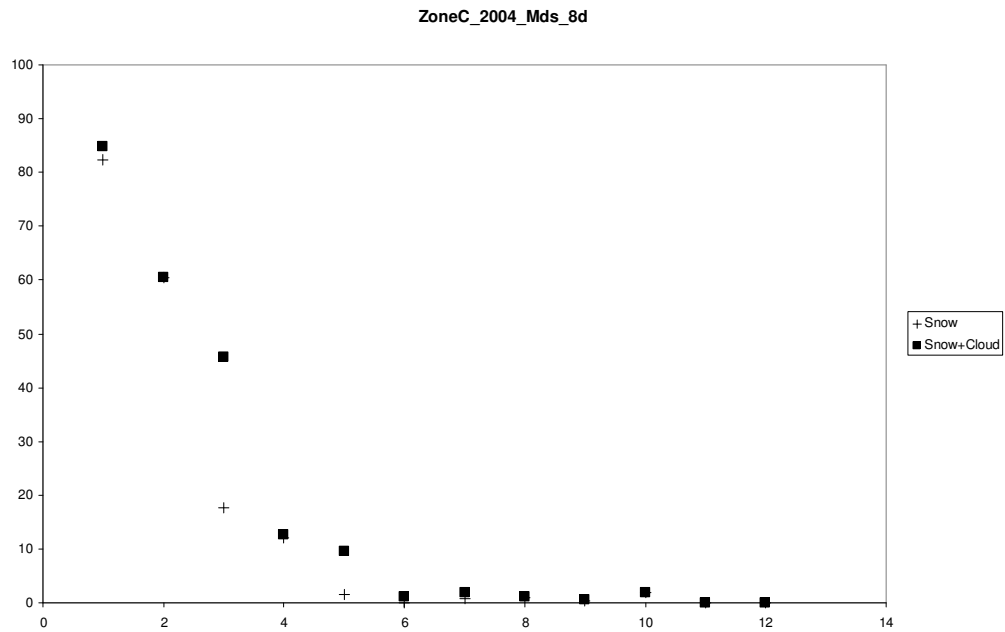


Figure 6.6 Snow covered area percentages obtained from MOD10A2 images for Zone C of 2004 water year

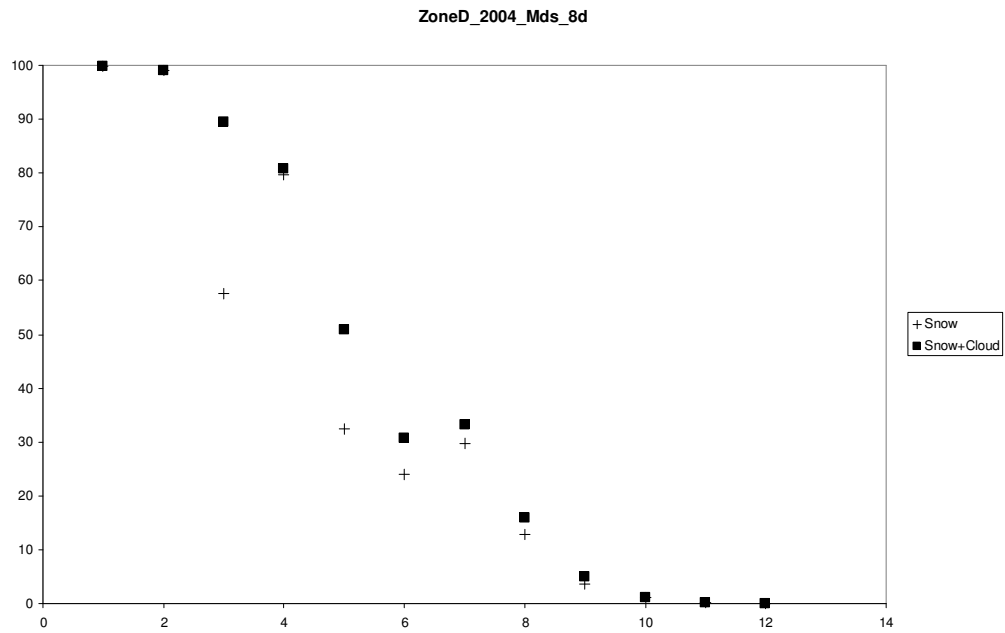


Figure 6.7 Snow covered area percentages obtained from MOD10A2 images for Zone D of 2004 water year

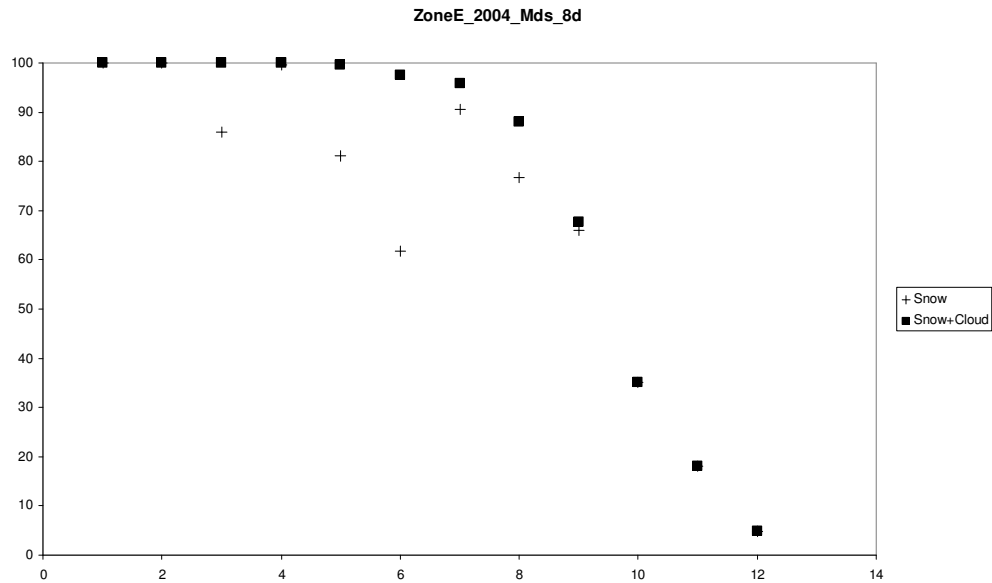


Figure 6.8 Snow covered area percentages obtained from MOD10A2 images for Zone E of 2004 water year

6.4.4 Calculation of Snow Depletion Curves

Snowmelt Runoff Model requires the daily input values of the snow covered area. Thus, a methodology is needed to derive the continuous depletion curves from the discrete satellite observations. Various methodologies are mentioned in the present literature to obtain this continuous depletion with minimum number of satellite images. Most common ones can be summarized as 1) linear interpolation of the snow maps with respect to time, 2) a parametric relation between the change of the snow water content and the snow covered area, 3) linear depletion of SCA with accumulated melt depth (Hydalp, 2000).

For the present case, a methodology that is similar to the third option which will be discussed later in this section, linear depletion of SCA with accumulated melt depth, is used. However, to provide some more flexibility and to enable easy computations, the change in the SCA is directly related to the accumulated temperature.

Figure 6.9 and Figure 6.10 show the conventional snow cover depletion curves which are derived from NOAA 17 and MODIS daily snow cover maps. Due to different spatial resolutions, NOAA 17 and MODIS derived snow cover depletion curves are drawn on separate charts.

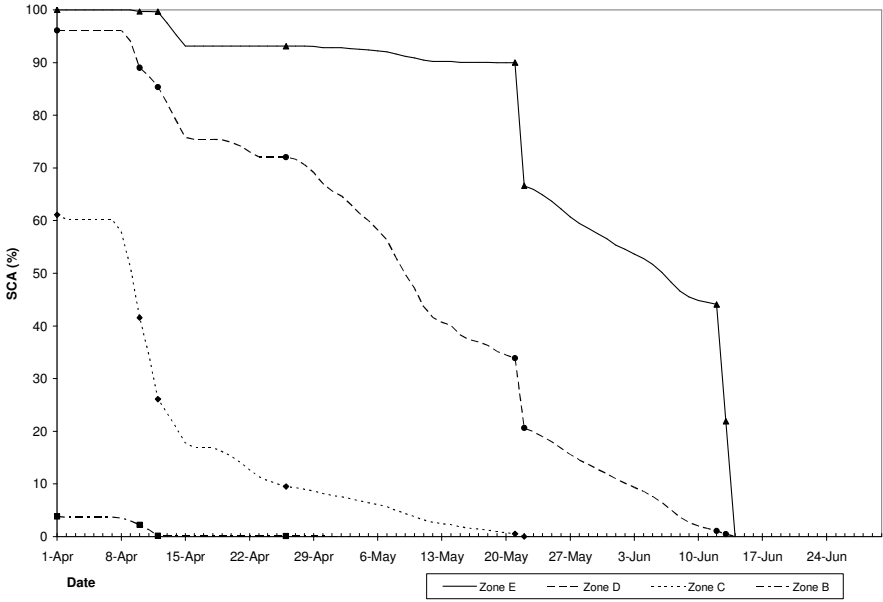


Figure 6.9 The conventional depletion curves obtained from NOAA satellite images

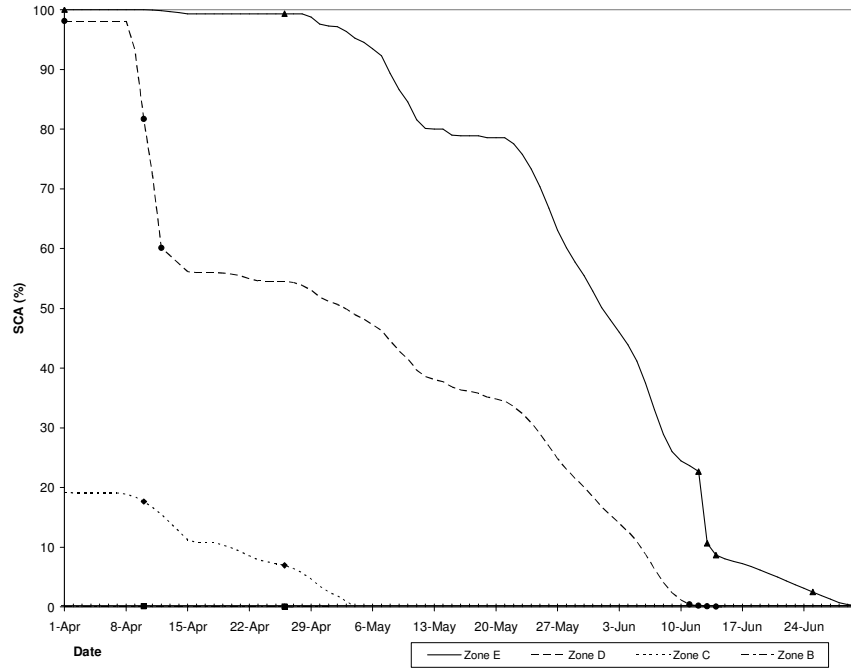


Figure 6.10 The conventional depletion curves obtained from MODIS satellite daily snow cover images

As expected the 8-day snow cover maps obtained from MODIS satellite (MOD10A2) showed more stable snow on the ground. However, the cloud contamination still existed. Since the snow cover was more stable, the snow cover would be provided by two cases. First case will be called as the lower bound (LB); this will be indicated by the points that have smaller values indicating pixels that were identified as snow by the Snowmap algorithm (Figure 6.6, Figure 6.7 and Figure 6.8). The second case will be called as the upper bound (UB); and this will be formed by the points that have higher values indicating the summation of cloud and snow determined pixels (Figure 6.6, Figure 6.7 and Figure 6.8). Since, SRM requires a continuous decrease of the snow covered area values, the increases in the snow covered area values which are actually late spring snowfalls and that are not a part of the seasonal snowpack are neglected.

For Zone B, the upper and lower bound is fairly similar. Thus, only one curve is provided. Figure 6.11 shows the calculated snow depletion curve for Zone B for 2004.

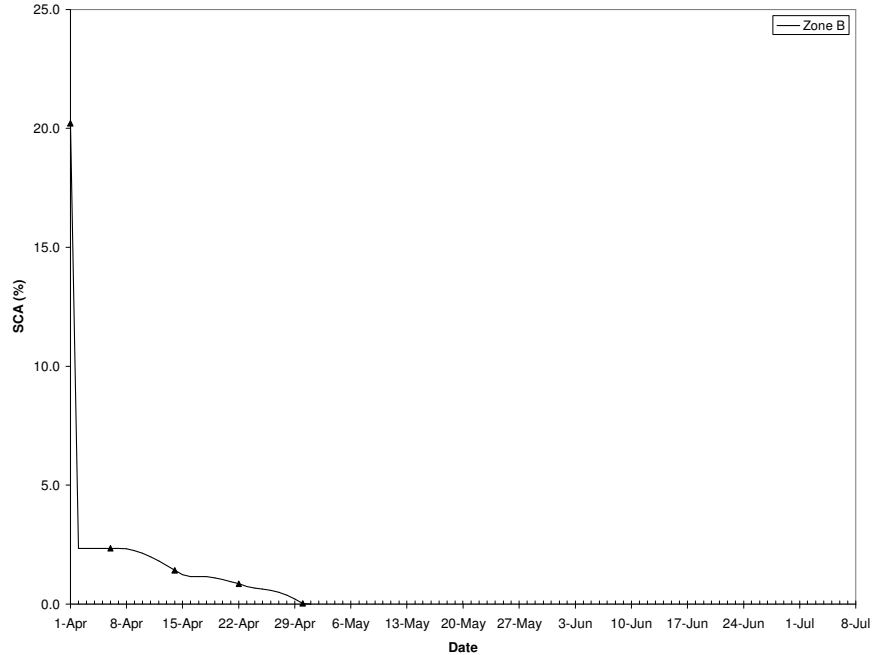


Figure 6.11 The conventional depletion curves obtained from MODIS satellite 8-day snow cover composites for Zone B

As zones representing the higher elevations (zones C, D and E) are analyzed, the upper and lower bounds of the snow depletion curves showed some variation. Figure 6.12, Figure 6.13 and Figure 6.14 represent the snow depletions in Zones C, D and E respectively with the upper and lower bounds for 2004.

Before giving a final decision on the snow covered area, the snow covered information for each zone are drawn on separate charts. Such plots are given in Figure 6.15 through Figure 6.18.

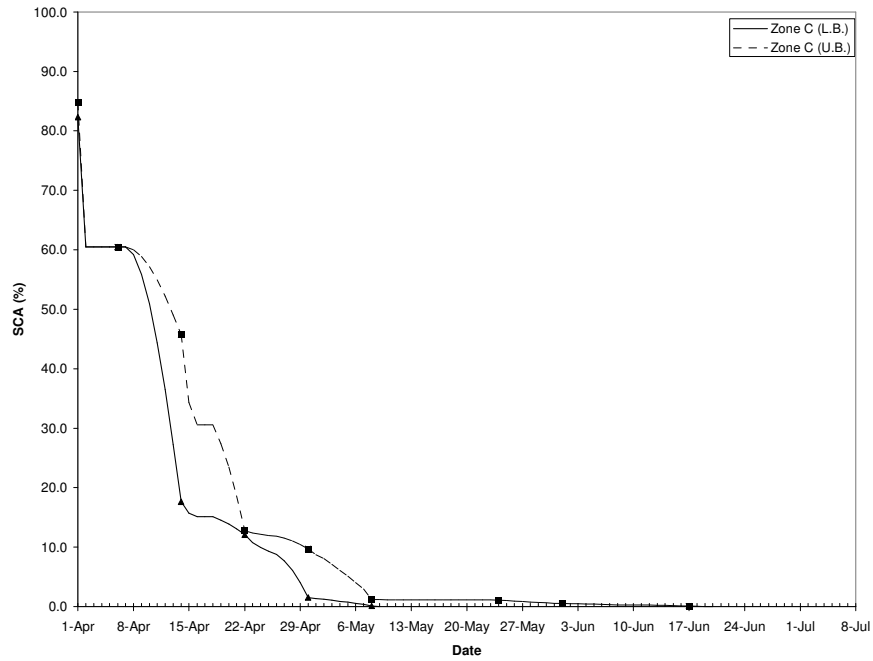


Figure 6.12 The conventional depletion curves obtained from MODIS satellite 8-day snow cover composites for Zone C

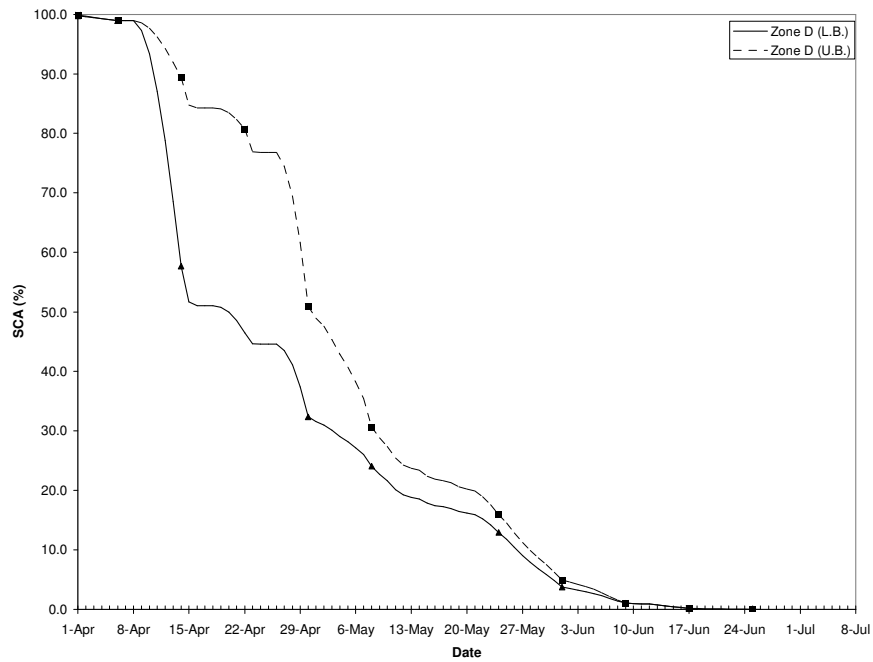


Figure 6.13 The conventional depletion curves obtained from MODIS satellite 8-day snow cover composites for Zone D

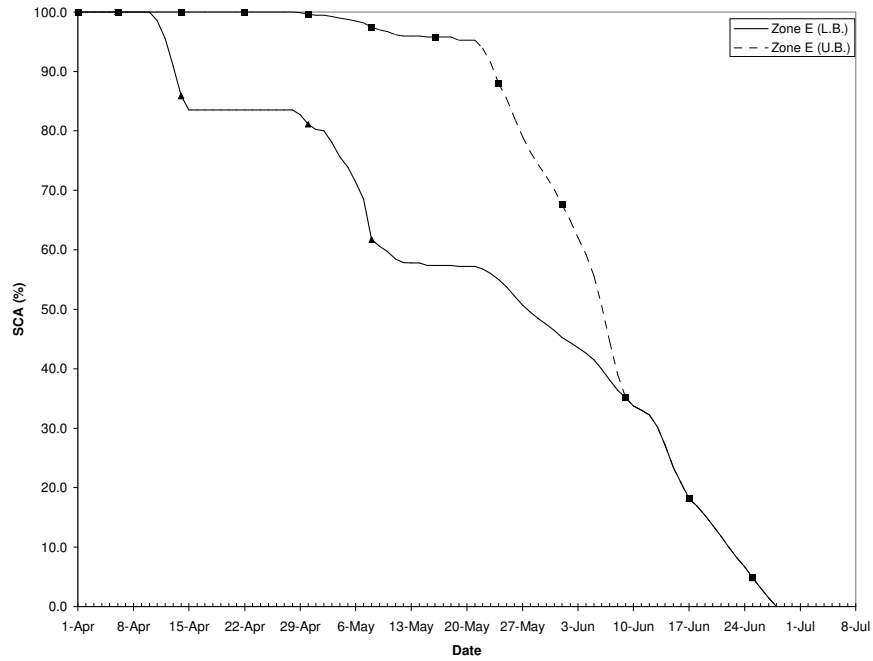


Figure 6.14 The conventional depletion curves obtained from MODIS satellite 8-day snow cover composites for Zone E

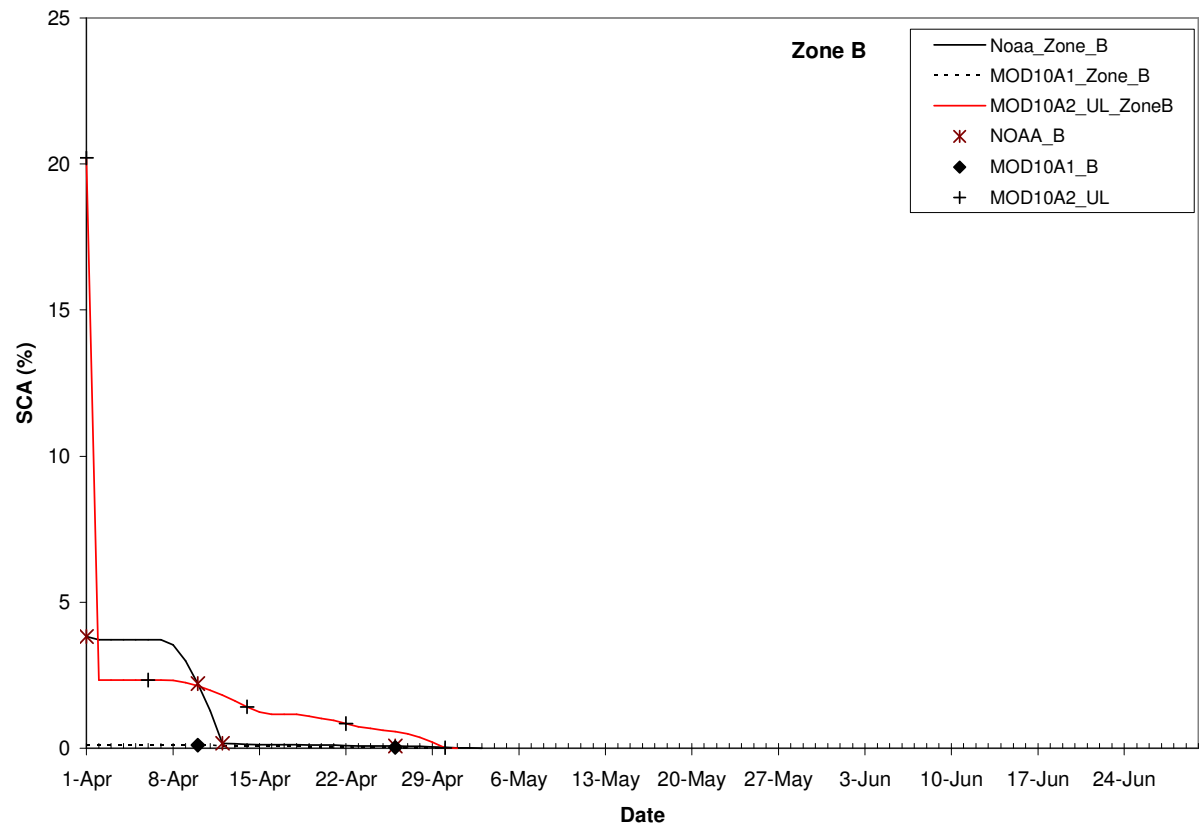


Figure 6.15 Snow cover depletion curves obtained from NOAA, MOD10A1 and MOD10A2 for Zone B

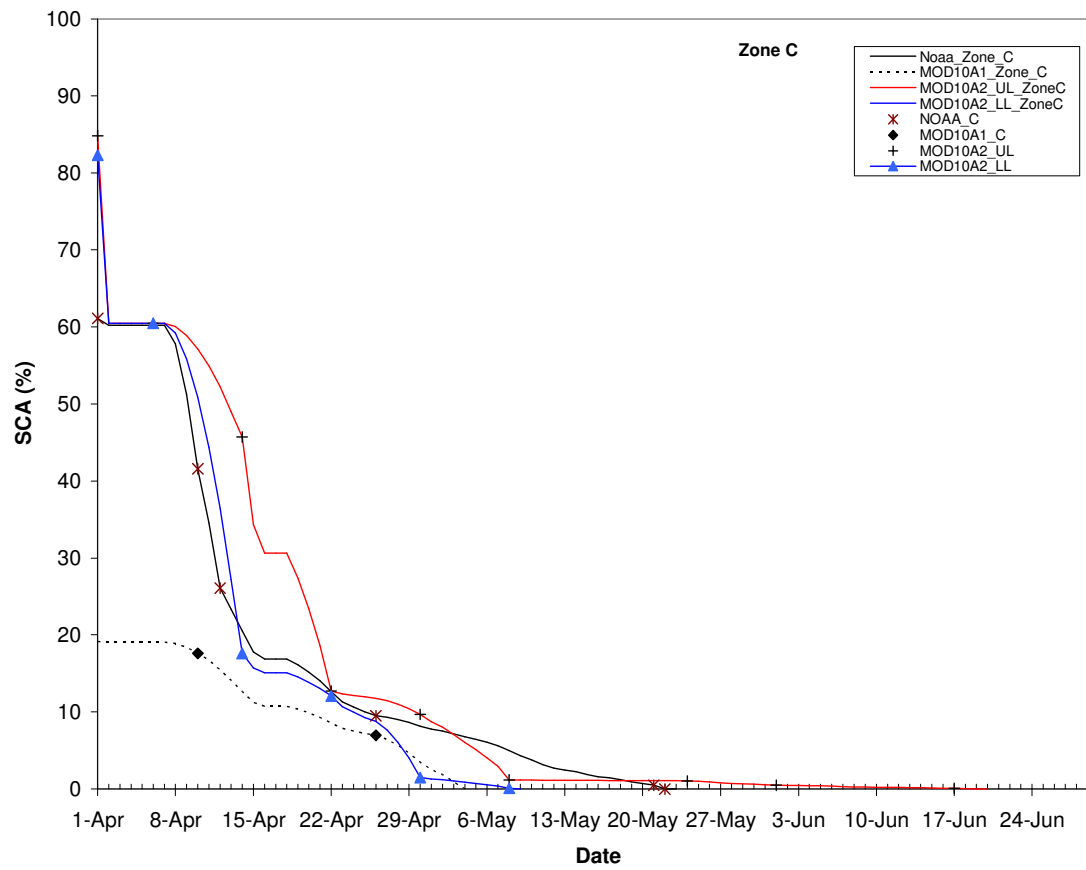


Figure 6.16 Snow cover depletion curves obtained from NOAA, MOD10A1 and MOD10A2 for Zone C

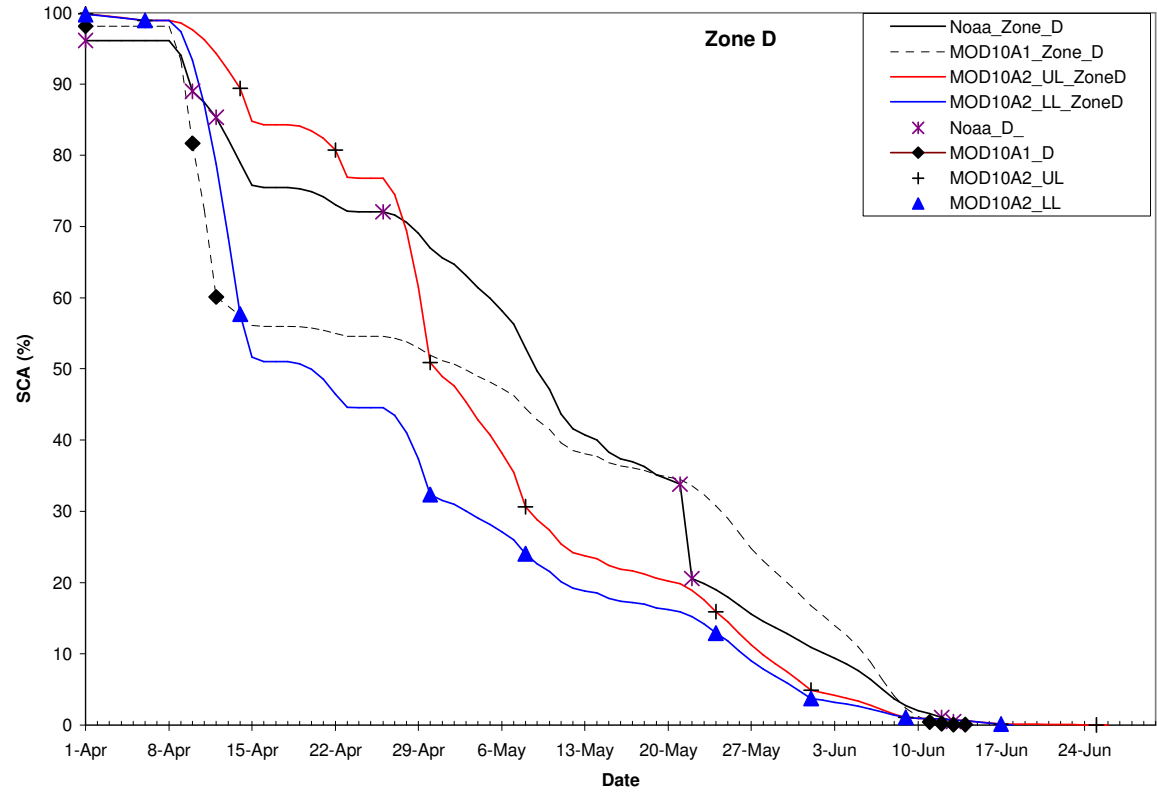


Figure 6.17 Snow cover depletion curves obtained from NOAA, MOD10A1 and MOD10A2 for Zone D

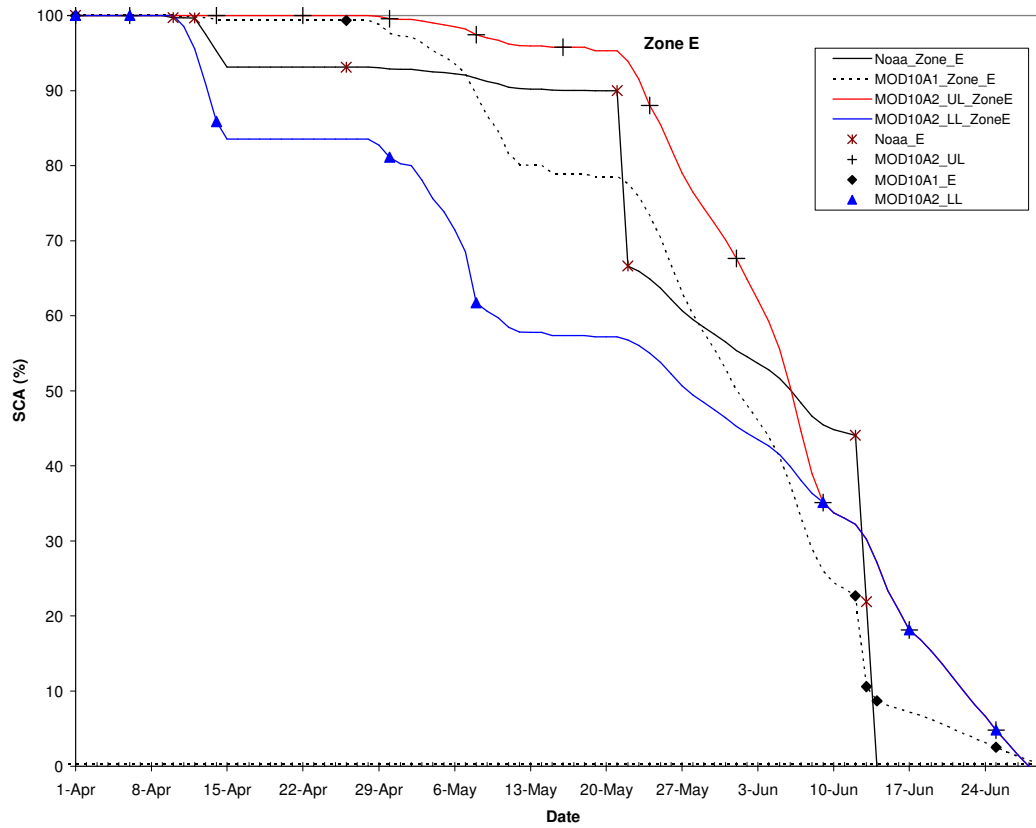


Figure 6.18 Snow cover depletion curves obtained from NOAA, MOD10A1 and MOD10A2 for Zone E

It was expected that the individual observations obtained from NOAA and MOD10A1 might have fallen in between the lines of upper and lower bounds of MOD10A2. However this was not the case. On the contrary, the daily individual observations of MOD10A1, were slightly less than the 8 day composites of MOD10A2. This case was in agreement with Zhou et al. 2005.

Even the MOD10A1 values were less than the MOD10A2 values, the interpolated values were some what greater. This might have arisen due the linear interpolation method used. The initial method used assumed the constant gradient reductions of the snow cover. However, the increasing gradients (slower reduction) of the snow cover with accumulated temperatures as indicated in Hydalp (2000), has been indicated to give better results then the simple linearship and is simpler than computation of the logarithmic relation (Tekeli et al., 2005c). Details of the methodology can be obtained from Kleindienst et al. 1999. A schema of the modified version of this methodology is presented in Figure 6.19. The updated snow cover depletions can be seen in Figure 6.20 through Figure 6.23.

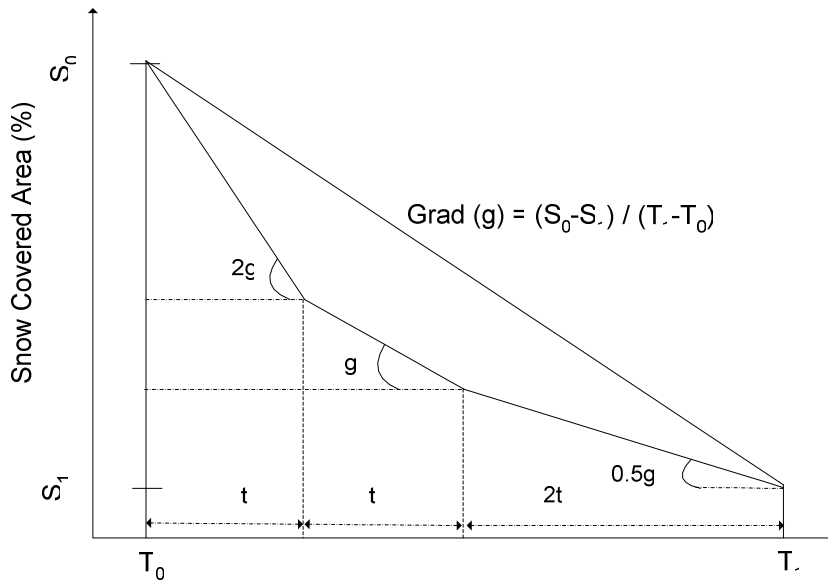


Figure 6.19 The modified temporal interpolation of snow covered area

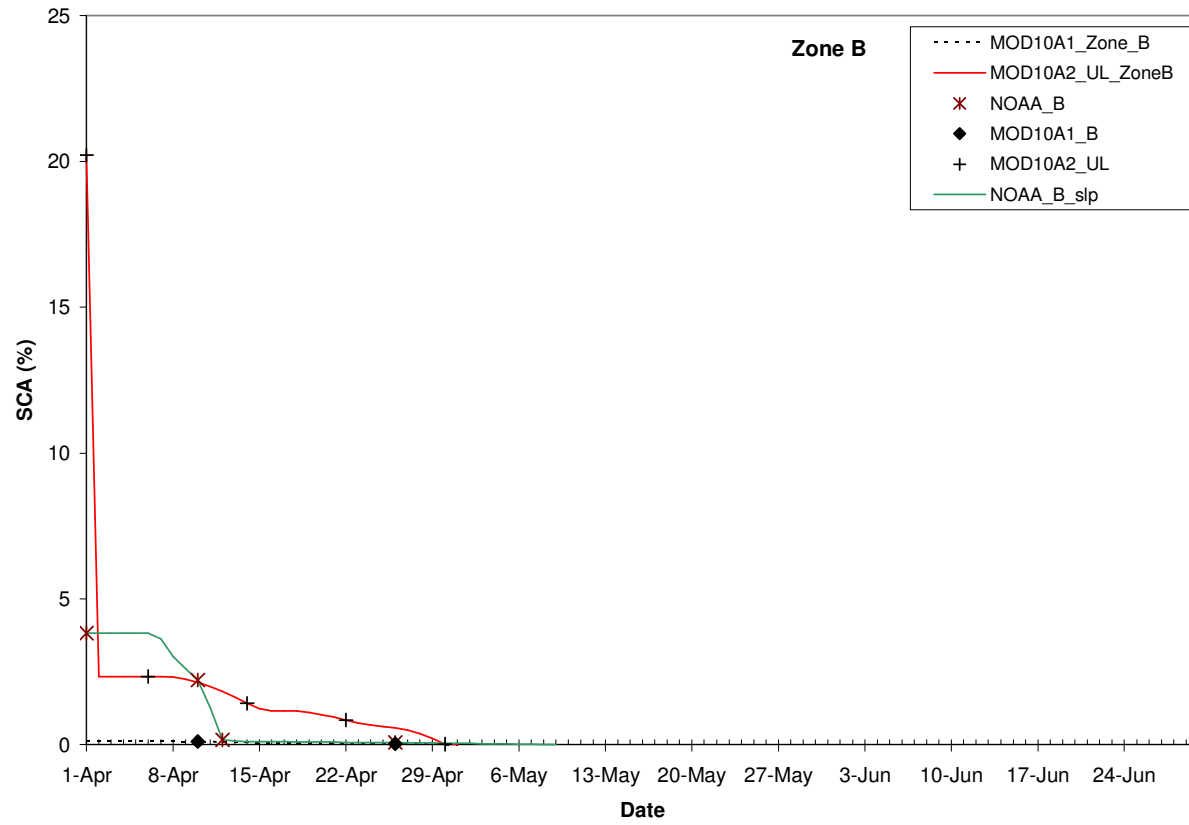


Figure 6.20 The modified temporal interpolation of snow covered area for Zone B

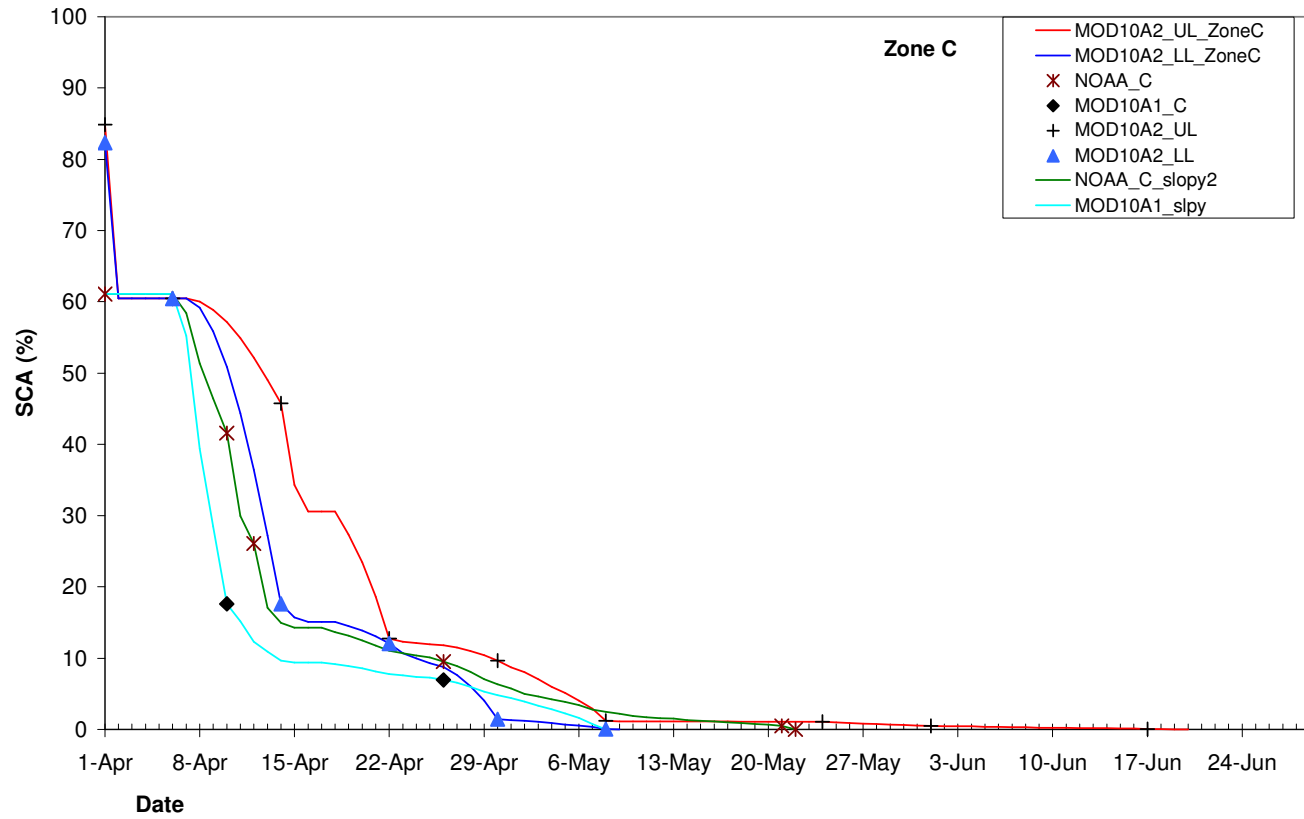


Figure 6.21 The modified temporal interpolation of snow covered area for Zone C

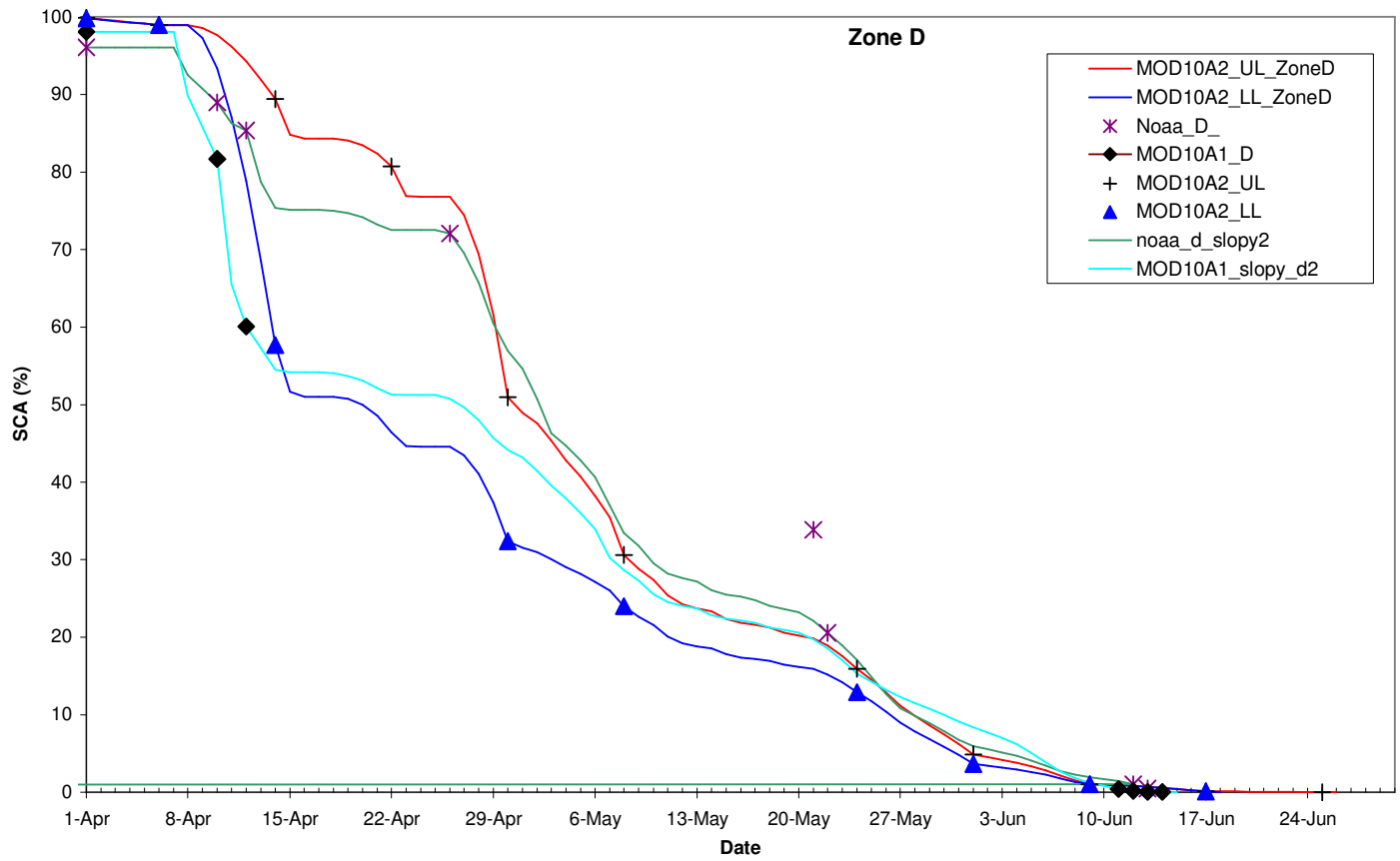


Figure 6.22 The modified temporal interpolation of snow covered area for Zone D

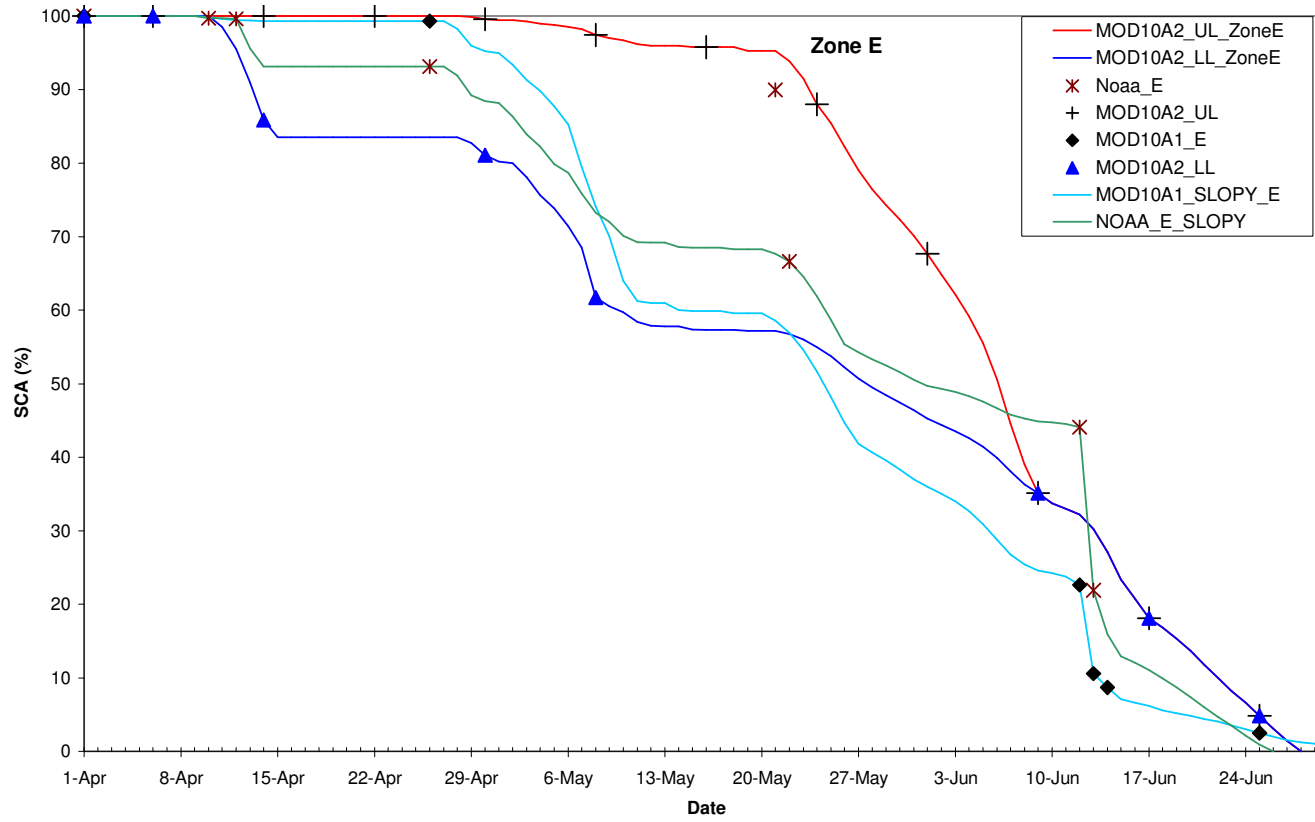


Figure 6.23 The modified temporal interpolation of snow covered area for Zone E

6.5 Verification of the Meteorological Variables

The ground based measurements provides the quality control of the forecast data. Even though the ground based measurements are not directly used, they provide a verification of the forecast values of temperature and precipitation in the model runs. Such verification enabled to correct the model inputs. Data used for verification was daily temperature and precipitation values obtained from the automated snow and meteorological stations mentioned in Chapter 2.

Forecasted data obtained from the numeric weather prediction models are compared with the observed values obtained from these stations in the following sections.

6.5.1 Temperature Comparison

To estimate the quality of the meteorological forecasts, a comparison test was performed. In the test, the measured values of the temperatures gathered from the automated meteorological and snow stations are compared with the forecasted values of MM5 and the results are presented in Figure 6.24 through Figure 6.26 for Zone C during April to June 2004 and in Figure 6.27 for Zone D during April to June 2004.

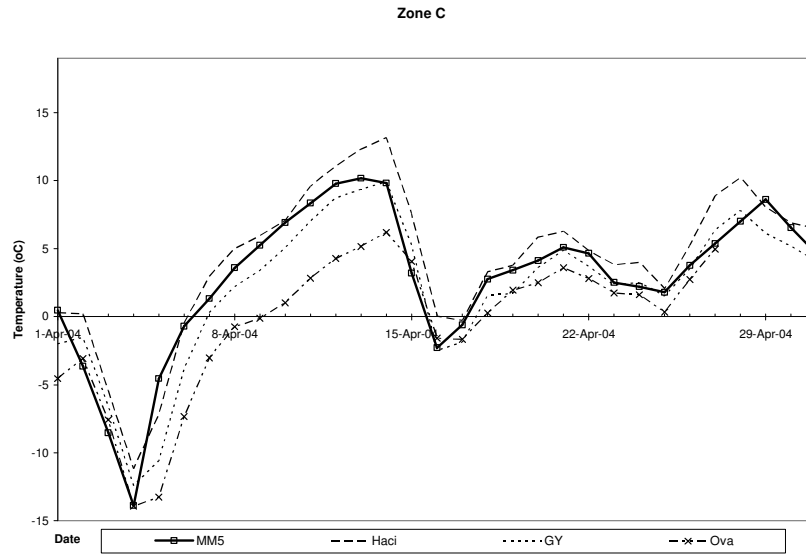


Figure 6.24 Comparison of forecasted and measured temperature values for Zone C during April 2004

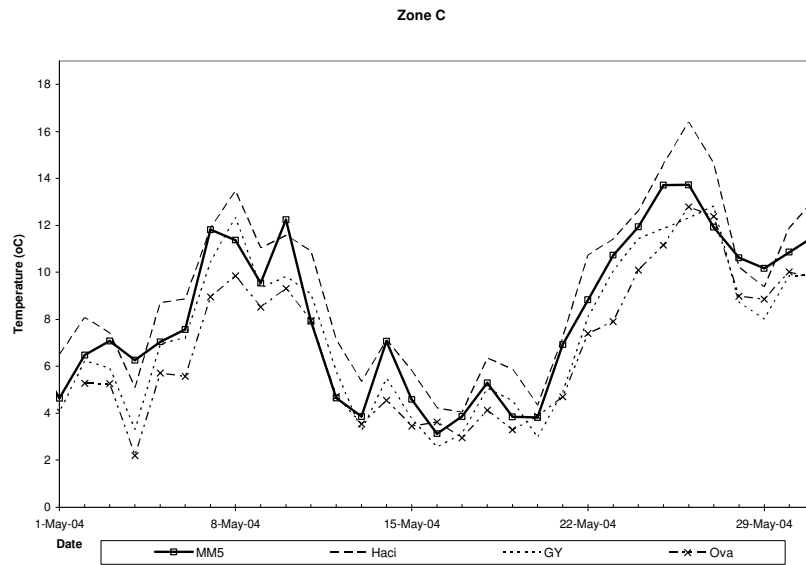


Figure 6.25 Comparison of forecasted and measured temperature values for Zone C during May 2004

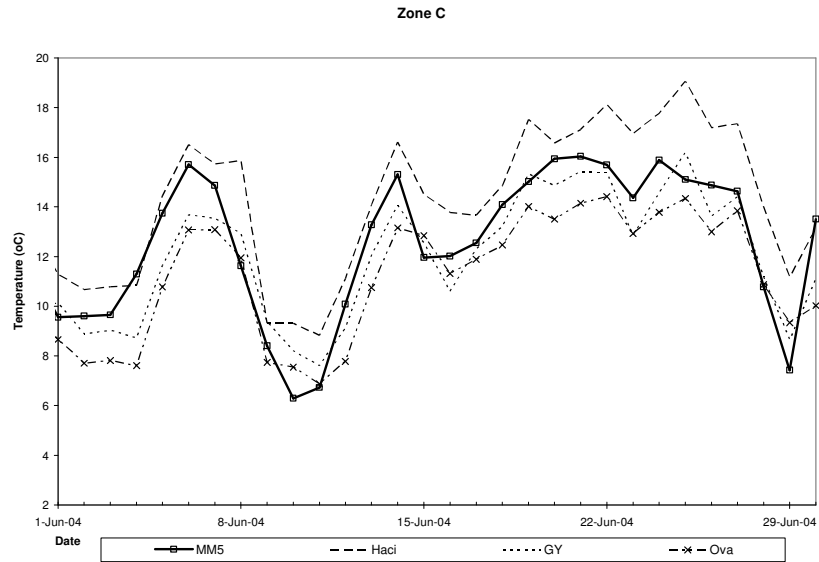


Figure 6.26 Comparison of forecasted and measured temperature values for Zone C during June 2004

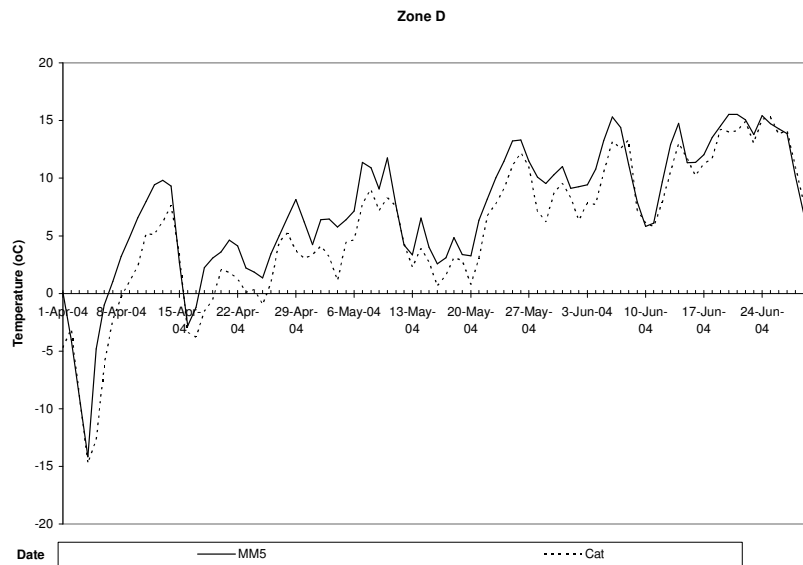


Figure 6.27 Comparison of forecasted and measured temperature values for Zone D during April-June 2004

Before judging the quality of the forecasts, the Digital Elevation Model (DEM) used for MM5 forecasts should also be compared with the actual basin

topography. For this purpose, the DEM used in MM5 data is decoded and the zonal elevations were determined. Mean elevations at each zone derived from actual 1:250 000 topographical maps and DEM used for MM5 are given Table 6.7.

Table 6.7 Comparison of the DEM used by MM5 and the actual topography

	MM5 (m)	Average Altitude from Actual topography (m)
Zone A	1678	1352
Zone B	1884	1751
Zone C	2092	2097
Zone D	2261	2482
Zone E	2413	2989

Based on Table 6.7 and Figure 6.24 ~Figure 6.26, it can be stated that the forecasts of MM5 for Zone C is quite reasonable. The values show variation in between the observations at Hacimahmud, Güzelyayla and Ovacık stations.

However, from Table 6.7 and Figure 6.27 it can be concluded that the temperature forecast values for Zones D and E are rather higher than the values observed on ground. Thus it is thought that these values should be determined by lapse rate method based on the MM5 forecasts in Zone C. To determine the temperature lapse rate values, simulation studied performed for 1997 and 1998 water years are used. Table 6.8 represents the calculated and used lapse rate values for MM5.

Table 6.8 Calculation of temperature lapse rate values (°C/100 m) for MM5

Time Interval		Calculated Lapse Rates		Lapse Rates Used	
		C to D	C to E	C to D	C to E
1-15 April	1997	1.25	1.22	1.11	1.08
	1998	0.96	0.93		
16-30 April	1997	1.0	0.98	1.05	1.03
	1998	1.1	1.07		
1-15 May	1997	0.94	0.92	1.03	1.0
	1998	1.12	1.07		
16-31 May	1997	0.79	0.76	0.92	0.92
	1998	1.08	1.07		
1-15 June	1997	0.81	0.80	0.79	0.79
	1998	0.80	0.77		
16-30 June	1997	1.02	0.99	1.02	0.99
	1998				

Based on the average lapse rate values, the new temperature charts for Zone D and E can be seen in Figure 6.28 and Figure 6.29.

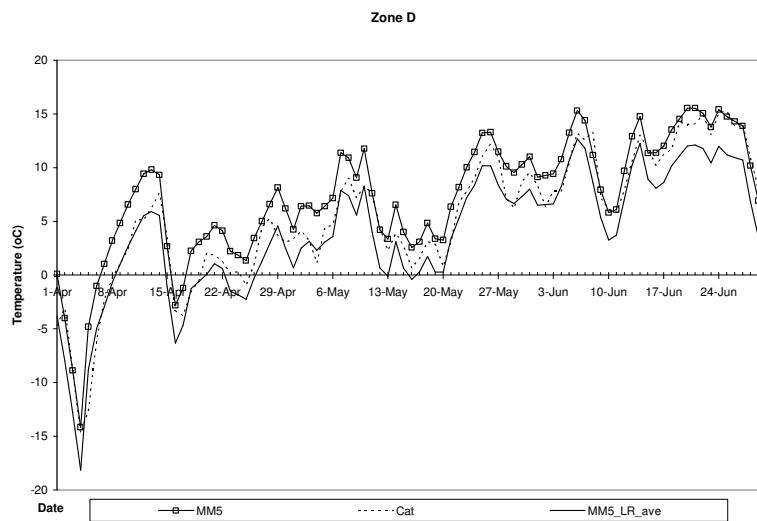


Figure 6.28 Comparison of forecasted, measured and recalculated temperature values for Zone D during April to June 2004

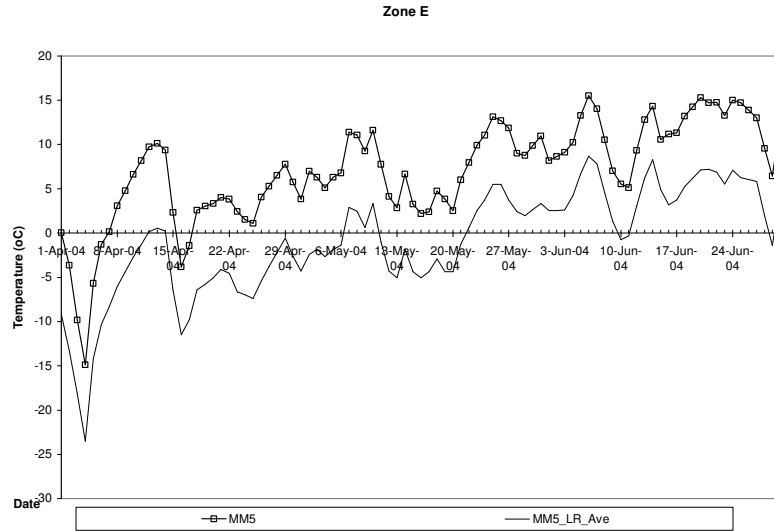


Figure 6.29 Comparison of forecasted and recalculated temperature values for Zone E during April to June 2004

6.5.2 Precipitation Comparison

The forecasted precipitation values using MM5 are compared with the ground truth data gathered from the automated snow and meteorological stations. The graphs of the forecasted and measured precipitation values can be seen in Figure 6.30 and Figure 6.31.

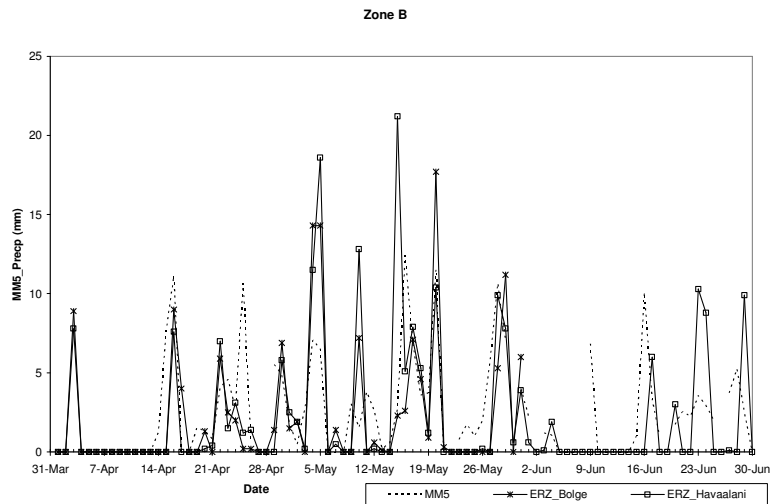


Figure 6.30 Comparison of forecasted and measured precipitation values for Zone B during April to June 2004

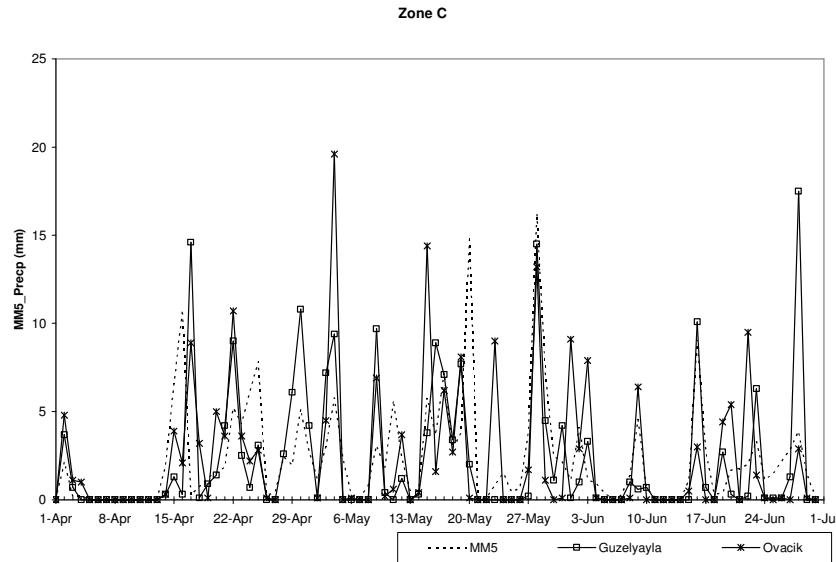


Figure 6.31 Comparison of forecasted and measured precipitation values for Zone C during April to June 2004

Based on the visual comparisons, it was concluded that the precipitation forecasts obtained were quite in agreement with the data gathered from site both with respect to timing and amount. Thus, no corrections on the precipitation values were seen necessary.

6.6 Forecasting of Discharges Using SRM Runs

The descriptions of the model parameters and the calibrations using the runoff rate are provided in Kaya (1999) and Tekeli (2000) for simulation of water years 1997 and 1998 respectively. Since the basin parameters were studied as lump i.e. in basin wide for 1997 and in zonal basis for 1998, there is no one to one comparison. However, the general trend is similar for both of the years except the increases of degree-day factors and the variations of the runoff coefficients. The changes are due to the earlier start of the 1998 melt season. This situation is in agreement with the findings in Hydalp (2000). The early start of 1998 melt season can be seen in Figure 6.32.

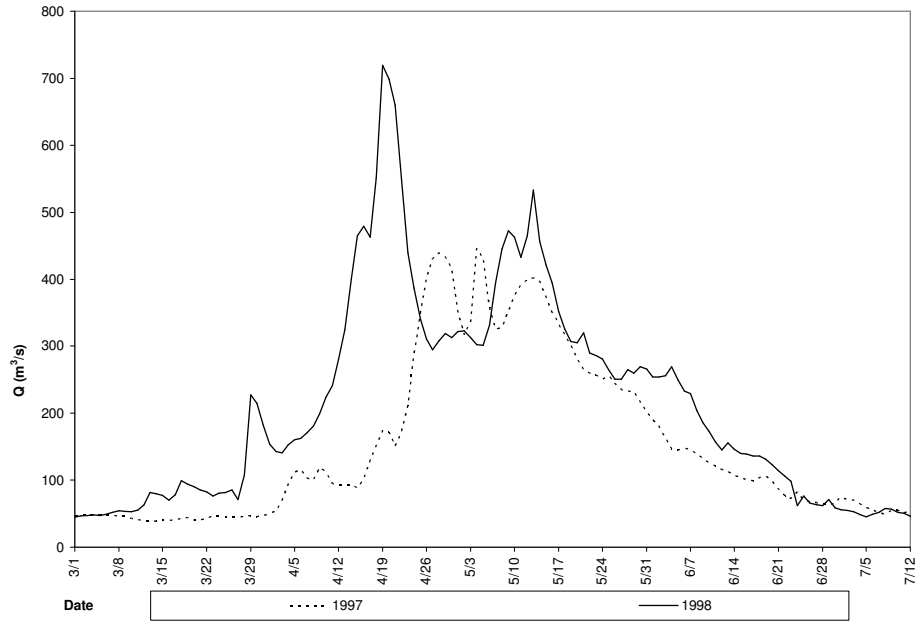


Figure 6.32 Comparison of 1997 and 1998 water years

Based on simulation studies, it was seen that values of some parameters could be determined from experience or by the available data without calibration. It was also realized that some parameters have fixed values that do not vary from year to year. However, some of them still may need calibration with the observed flow such as the runoff coefficients both for snow and rain. Figure 6.33 summarizes the procedure to follow for selection of model parameters.

Based on the outline given in Figure 6.33 the model parameters for the forecasting period are selected during verification studies as described in the following sections. Initial model runs were carried out based on those selected values.

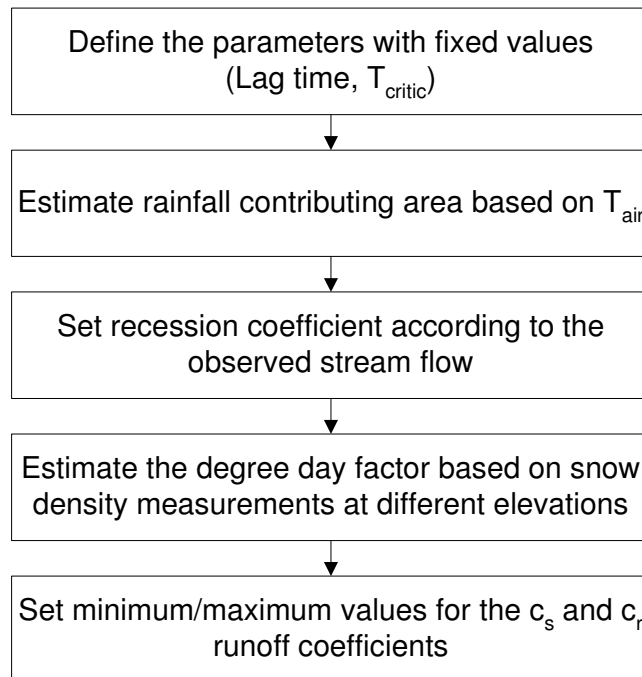


Figure 6.33 Flowchart of model parameter selection

Time Lag (L)

Time lag which is used for synchronization of the computed and measured discharge rates is set to 14 hours for the forecast studies based on previous simulation runs.

Critical Temperature (T_{critic})

Critical temperature which is used to determine the type of precipitation, i.e. either snowfall or rainfall, is set to 0.01°C for the whole period based on the previous studies conducted. This parameter is used to determine whether precipitation immediately contributes to runoff ($T > T_{critic}$) or it is kept in storage until warmer days melt it ($T < T_{critic}$ and snowfall).

Rainfall Contributing Area (RCA)

RCA is used to determine if the whole basin/zone or only the snow free portion contributes to runoff. Effect of rainfall contributing area increases as the amount of rainfall in the total hydrograph increases. It is assumed that cold snow would hold the liquid precipitation and only the rain falling to non snow region would contribute to runoff, thus reducing the rainfall depth by the ratio of the snow free area to the total zonal area.

Previous studies revealed that for zones A, B, C this value is set 1 by April 1st, meaning that rain falling to these zones contributes to runoff with the start of April. However, some variations are found for zones D and E. Kaya (1999) found that these zones contribute to runoff with May, where else Tekeli (2000) determined that they contribute to runoff by April 1 and April 15 respectively. It is believed that RCA timing shift is a function of the meteorological and snowpack conditions of the particular year at hand. Selecting the date of change is explained in section 4.4.2.3.7. Even though, it is not an exact method, but a rule of thumb was found that the RCA is related to air temperature. And the timing that rainfall contributes to runoff is approximately the first day in which air temperature is greater than or equal to 0°C.

Recession Coefficient (k)

Recession coefficient, k , is used to determine the daily melt water production that immediately appears in the runoff by $(1-k)$. The value of k is computed by Equation 4.8. The long term analyses show that 0.9910 can be used for x , where else, 0.029 is suitable for value of y . Some revisions may be needed based on the water year characteristics as mentioned in Hydalp (2000) and Seidel and Martinec (2004).

Degree Day Factor

The best way of determining the degree day factor is to measure air temperature and snow water equivalent at different parts of the basin, simultaneously. Then the degree day factor is computed by the ratio of the change in SWE with respect to the accumulated temperature. Such a procedure was not possible for studies related with 1997 and 1998 water years. For these years, the degree day values were computed by use of the snow density measurements and the method proposed by Martinec et al. (1998). It is expected that the degree day factor should decrease with increasing elevation, though a relation between snow density and elevation can not be derived.

Previous studies (Kaya, 1999; Tekeli, 2000) showed that the degree day factors can be taken as basin wide with 0.35 between 1-15 April, 0.40 between 16 April-1 June and 0.44 after June 1st. The consistency of degree day factor in basin wide was mentioned in Bagchi (1983) and the increase of the value with respect to time is presented in Martinec et al. (1986) and Katwijk et al. (1993).

Runoff Coefficients

Runoff coefficients are used to take care of the differences between the available water volume and the runoff observed at the basin outlet. Runoff coefficients are highly dependent on the actual available water amount and the initial water content. Thus, this value may exhibit variation from year to year due to the varying conditions. The average values determined from the previous studies (Kaya, 1999; Tekeli, 2000) can be summarized as in the below table.

Table 6.9 Runoff coefficient values

	1-15 April	16-30 April	1-15 May	16-31 May	1-30 June
c_s	0.41	0.36	0.36	0.36	0.29
c_r	0.43	0.66	0.54	0.33	0.28

6.6.1 Re-Runs for Verification of Model Parameters

Before performing the forecast studies, the validity of the model parameters should be justified. This is achieved by making simulation runs for 1997 and 1998 based on the parameter set that will be used in forecasting studies. For 1998 the performed re-runs can be seen in Figure 6.34.

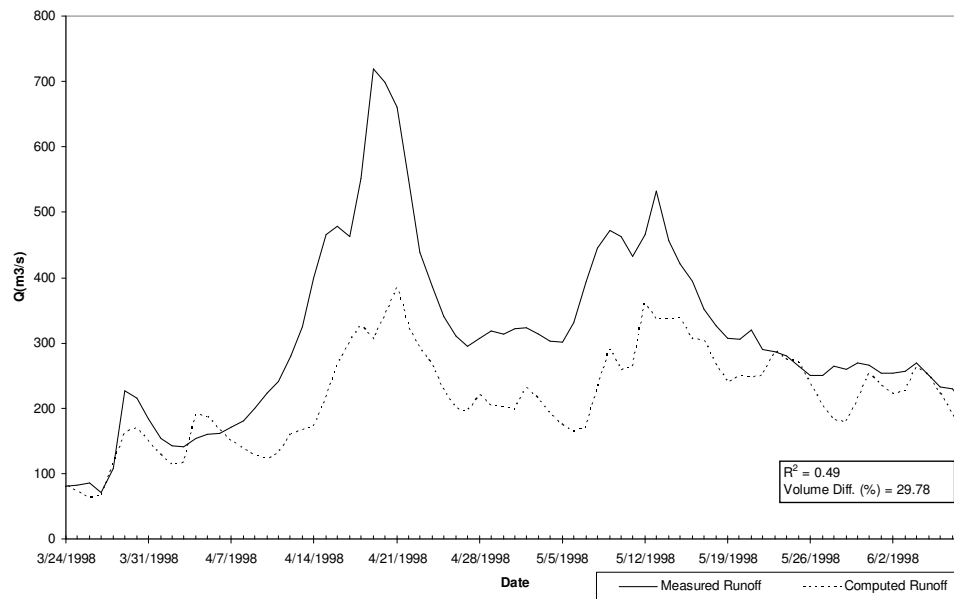


Figure 6.34 Re-runs for 1998 water year with 2004 parameters

Rango (2005) mentioned that “the runoff coefficient appears to be the primary adjustment candidates if a runoff simulation is not at once successful”. Thus, from the 2004 parameters, the runoff coefficients were removed and 1998 runoff coefficient values were used in order to perform new runs. The obtained hydrograph at the end of new run is presented in Figure 6.35.

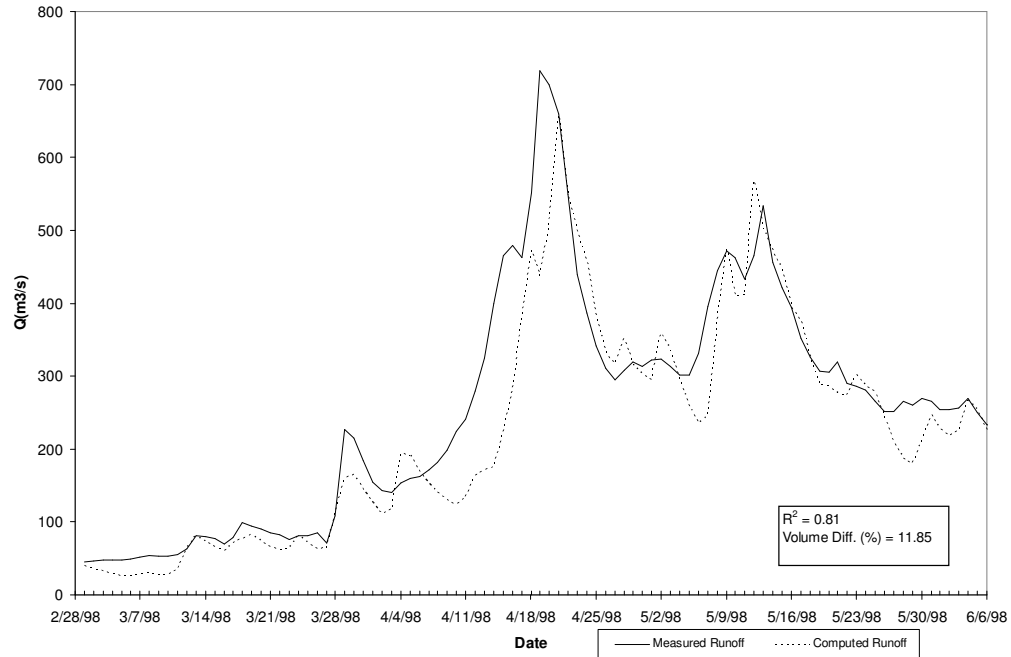


Figure 6.35 Re-runs for 1998 water year with 2004 parameters and runoff coefficients (c_s , c_r) from 1998

Thus values proposed for 2004 runs yielded promising results with the variation of runoff coefficients. Coefficient of determination (R^2) and deviation of volumes (D_v) are obtained as 0.81 and 11.85% respectively.

Similar re-runs were performed for 1997 water year also. Initial results can be seen in Figure 6.36. Even though, under estimation of flows were seen in the computed values of the model for 1998 water year, in 1997 over estimation was recorded. Figure 6.36 represents the computed discharges for 1997 with 2004 parameters. The model gave better results as the runoff coefficients were updated by 1997 values. Figure 6.37 shows the model results with the updated runoff coefficient values.

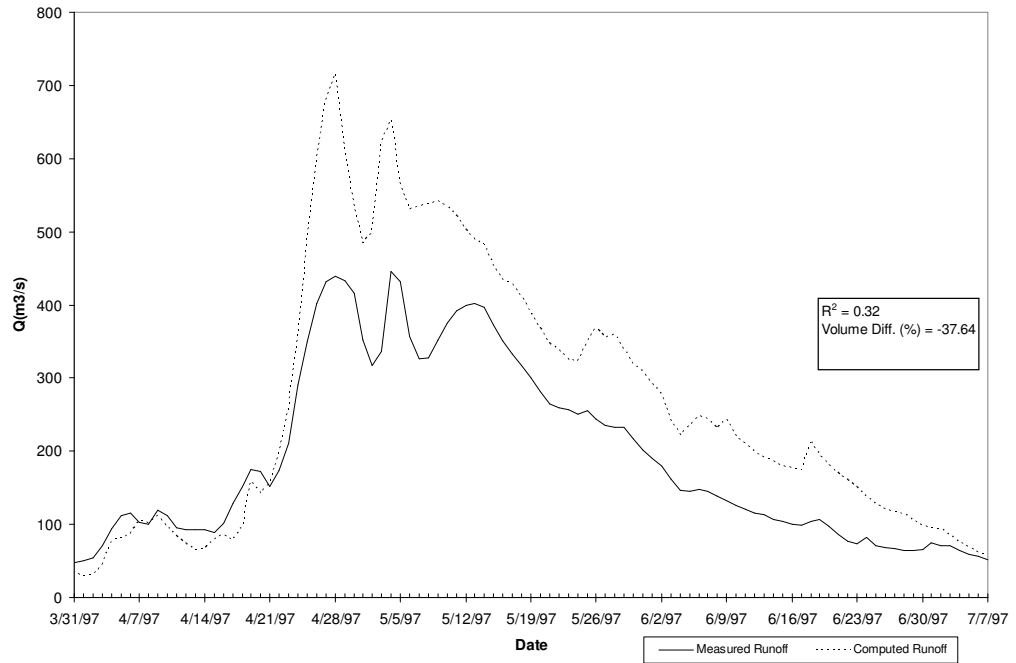


Figure 6.36 Re-runs for 1997 water year with 2004 parameters

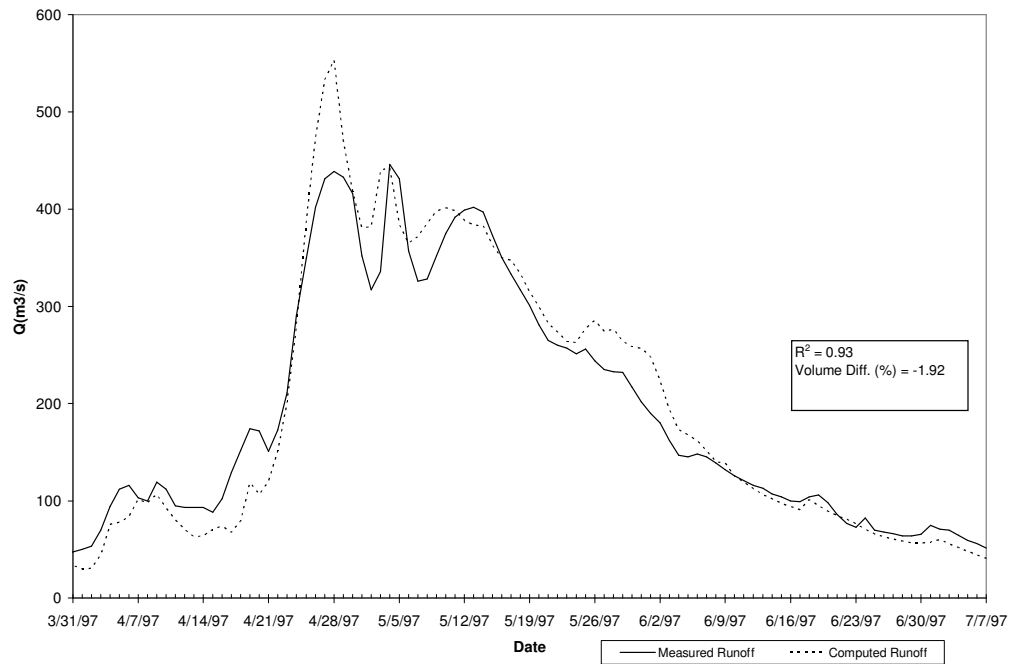


Figure 6.37 Re-runs for 1997 water year with 2004 parameters and runoff coefficients from 1997

A short summary of the performed runs is presented in Table 6.10

Table 6.10 Comparison of model runs with different c_r and c_s values

Water Year	c_r - c_s values	R^2	D_v	Figure No
1998	2004	0.49	29.78	6.34
	1998	0.81	11.85	6.35
1997	2004	0.32	-37.64	6.36
	1997	0.93	-1.92	6.37

Based on the above discussion it can be said that the model parameters derived for 2004 were yielding quite satisfactory results. Results were improving more as the runoff coefficients were updated by the values obtained for the specific water year under study.

6.6.2 Near Real Time Forecasting Studies

As the accuracy of the model parameters were seen satisfactory in the previous section, 2004 forecasting studies were carried out.

Forecasting studies will be performed under 5 cases. Each of these 5 cases will use the same set of parameters and variables except the snow covered area values.

The snow covered area values will modify as the satellite platform, the data set used and the way the data handled are changed. Runs performed with SCA information derived from NOAA satellite is called as NOAA. Where else, the SCA information derived from MODIS daily snow covered area algorithm is called with the name of the data source as MOD10A1.

The third and fourth cases arise from the MODIS 8 daily composite snow cover maps (MOD10A2). In these runs, the upper bound and lower bound concept

of SCA mentioned in section 6.4.4 is used. The runs upper bound (UB) and lower bound (LB) come from MOD10A2 data sets.

The fifth and the final case is the no SCA case and indicated as NO SCA. Table 6.11 summarizes the cases and the shows the figure numbers of the related output hydrographs during which precipitation and temperature data are obtained from MM5 data.

Table 6.11 Case numbers as a function of SCA and figure numbers of related output hydrographs

Case No	SCA Source	Figure Number of the output hydrograph
1	NOAA	6.38
2	MOD10A1	6.39
3	MOD10A2 (UB)	6.40
4	MOD10A2 (LB)	6.41
5	NO SCA	6.42

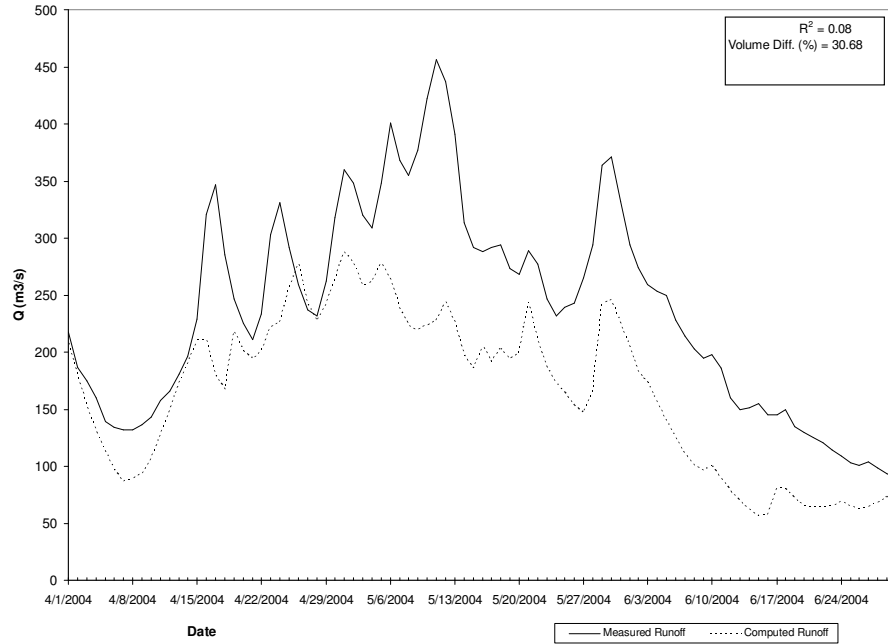


Figure 6.38 Comparison of forecasted and measured discharges for Case 1 for MM5 data

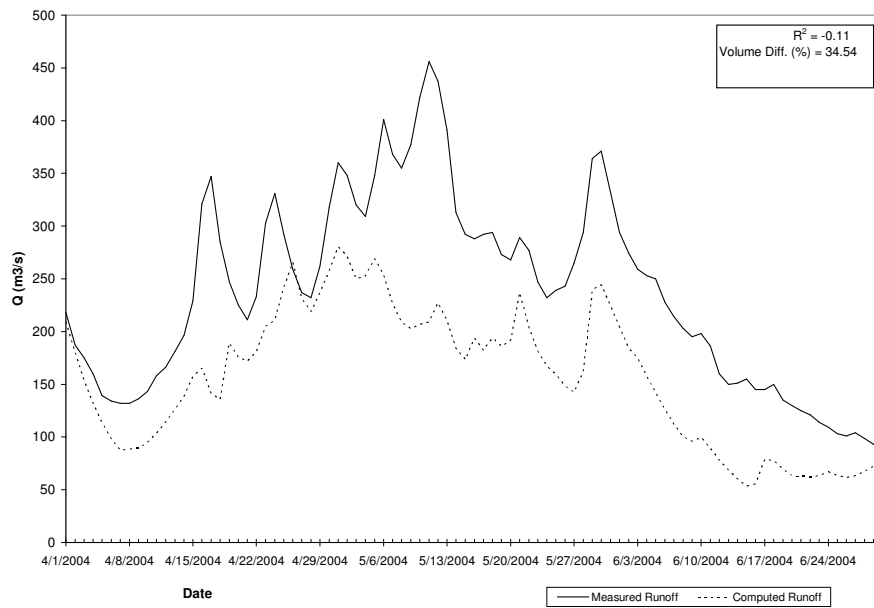


Figure 6.39 Comparison of forecasted and measured discharges for Case 2 for MM5 data

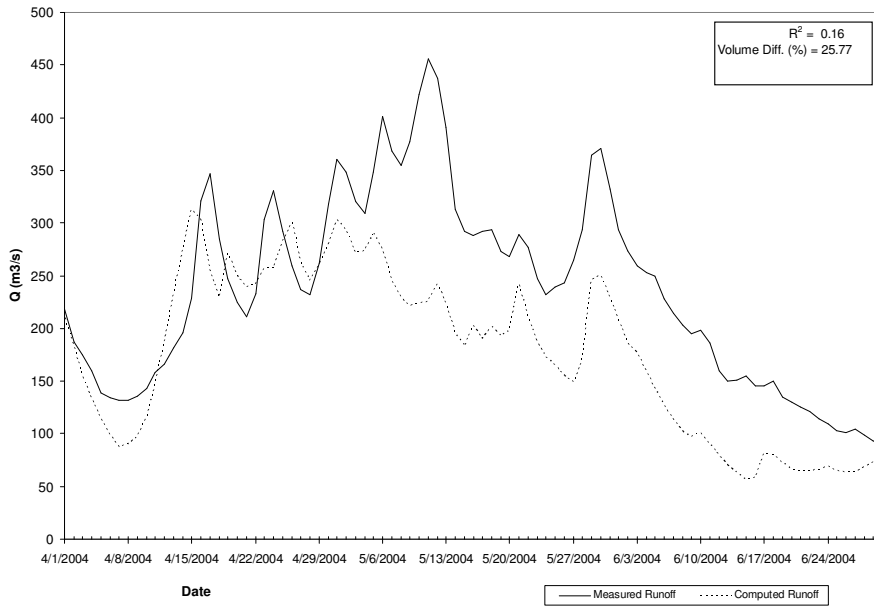


Figure 6.40 Comparison of forecasted and measured discharges for Case 3 for
MM5 data

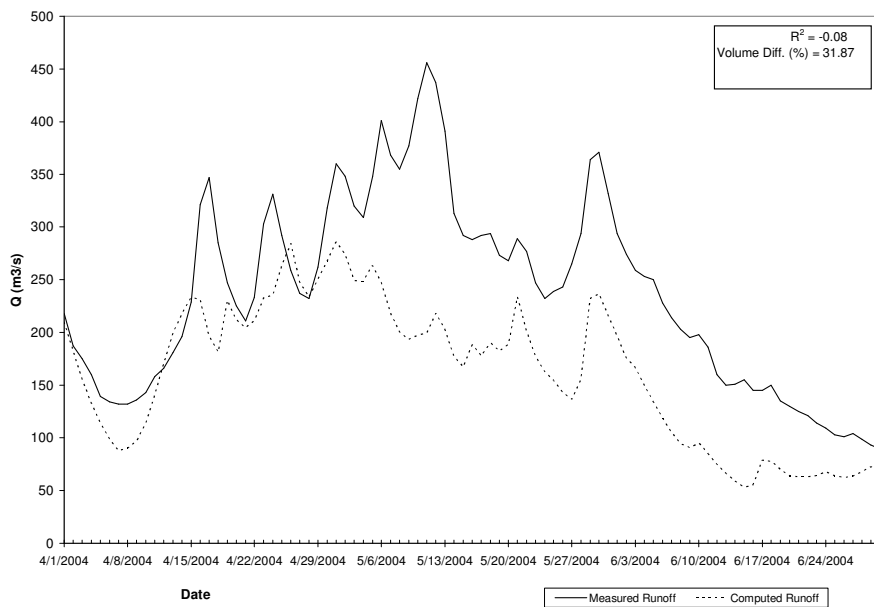


Figure 6.41 Comparison of forecasted and measured discharges for Case 4 for
MM5 data

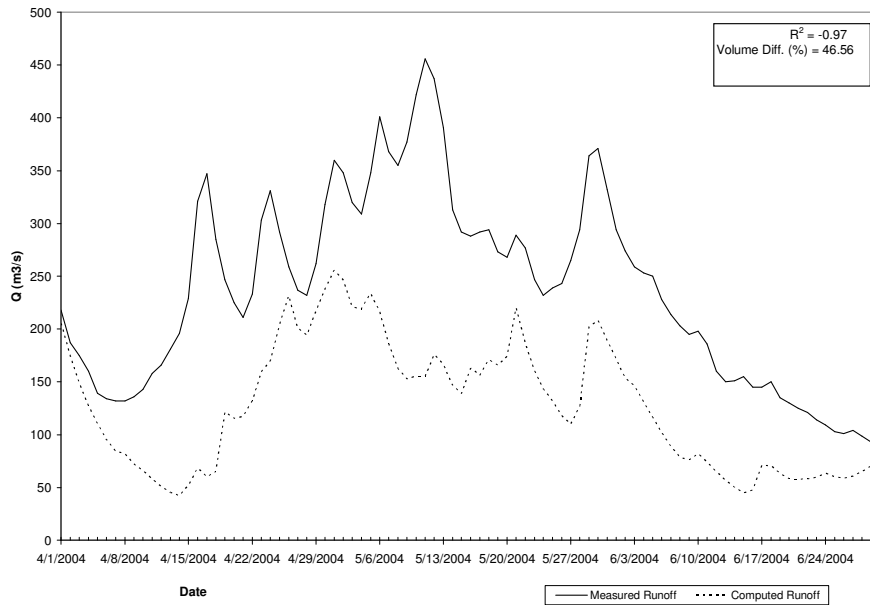


Figure 6.42 Comparison of forecasted and measured discharges for Case 5 for MM5 data

Table 6.12 summarizes the early findings of the forecast studies using various satellite platforms with common statistical measures R^2 and D_v .

Table 6.12 Summary of initial forecasts for MM5 data

	SCA				
	UL	NOAA	LL	MOD10A1	NO SCA
R^2	0.16	0.08	-0.08	-0.11	-0.97
D_v (%)	25.77	30.68	31.87	34.54	40.56

The negativity of the model performance (R^2) indicates that the model performed worse than no model. The negativity of R^2 increases as the SCA values reduce as one goes from upper SCA to no SCA.

The percent volume deviations increase from upper SCA to no SCA. Figure 6.43 represents the forecasted and measured discharges for various SCA

information. From Figure 6.43 it can be seen that all runs underestimate the discharges after May 2004 which is also a main melting season. This might have arisen due to the temperature values (Rango, 2005). Thus, the original temperature values, obtained from MM5 data are fed into runs. Keeping all the model parameters the same, the model runs were executed again by replacing the temperature values for zones D and E with the values as they are received from MM5. Outputs of new model runs can be seen in Figure 6.44 through Figure 6.49.

Table 6.13 Case numbers as a function of SCA and figure numbers of related output hydrographs for temperature correction

Case No	SCA Source	Figure Number of the output hydrograph
1	NOAA	6.44
2	MOD10A1	6.45
3	MOD10A2 (UB)	6.46
4	MOD10A2 (LB)	6.47
5	NO SCA	6.48

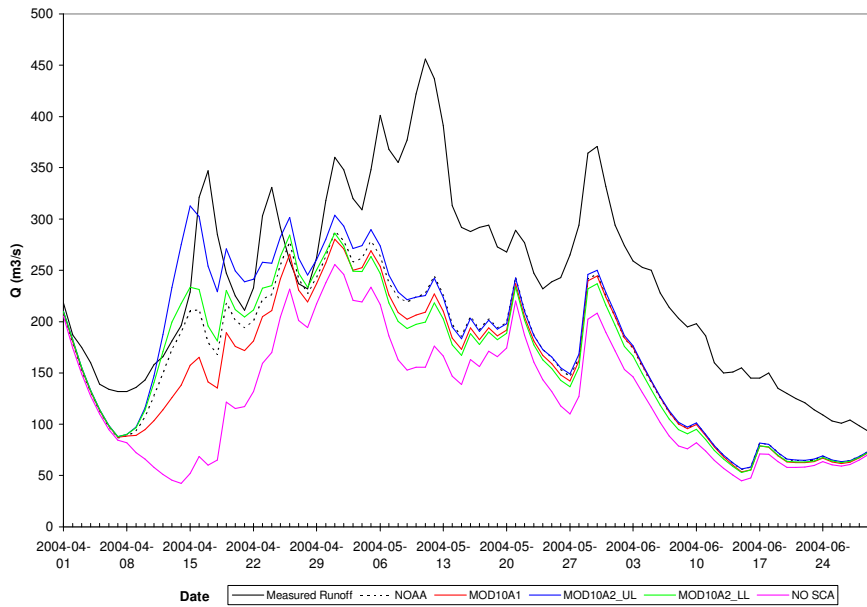


Figure 6.43 Comparison of forecasted and measured discharges for various SCA information for MM5 data

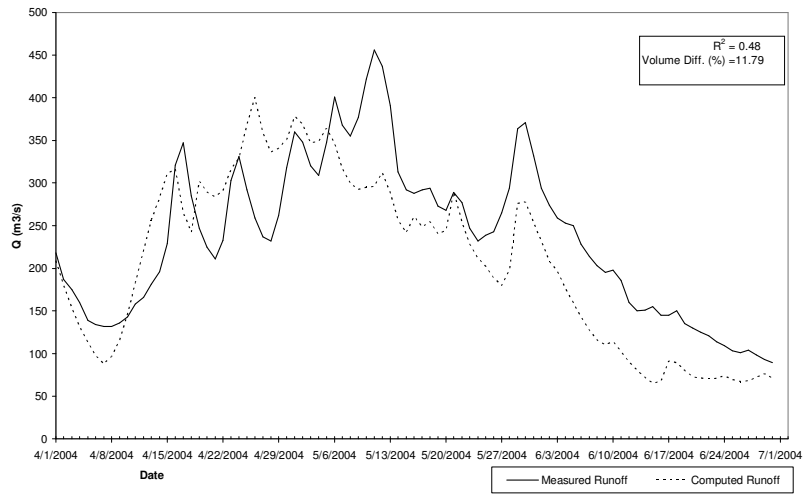


Figure 6.44 Comparison of forecasted and measured discharges for Case 1 for temperature correction

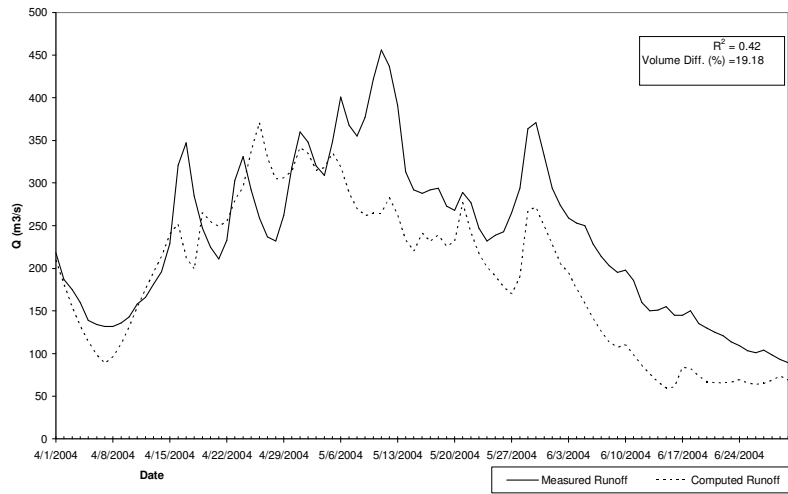


Figure 6.45 Comparison of forecasted and measured discharges for Case 2 for temperature correction

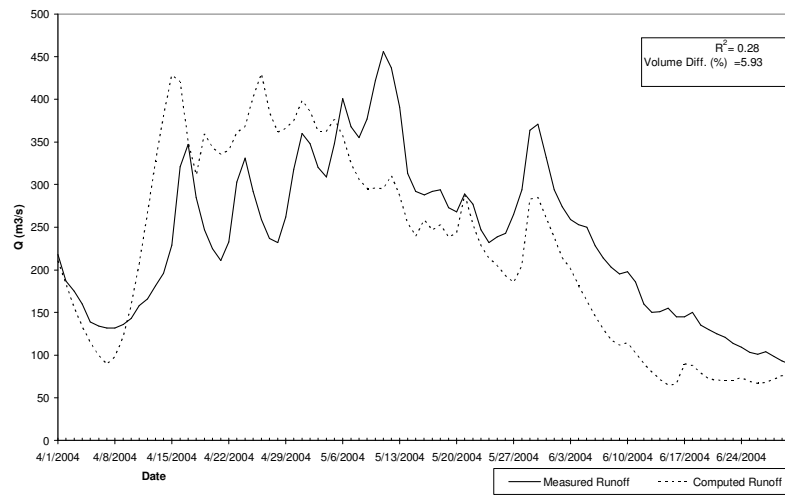


Figure 6.46 Comparison of forecasted and measured discharges for Case 3 for temperature correction

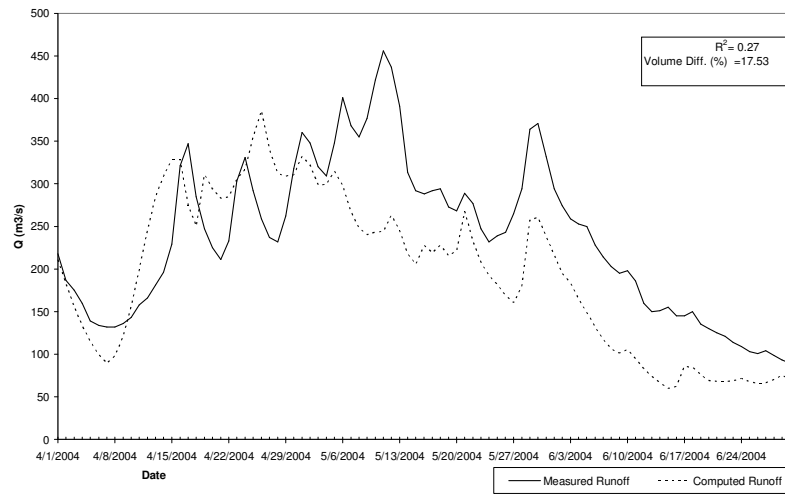


Figure 6.47 Comparison of forecasted and measured discharges for Case 4 for temperature correction

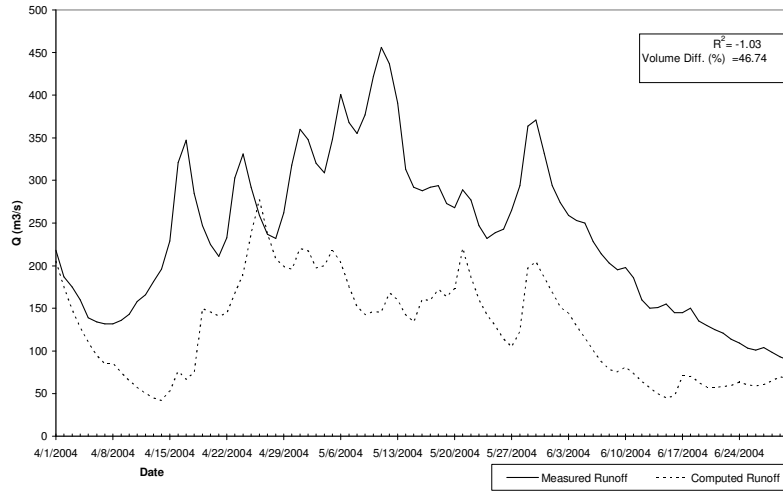


Figure 6.48 Comparison of forecasted and measured discharges for Case 5 for temperature correction

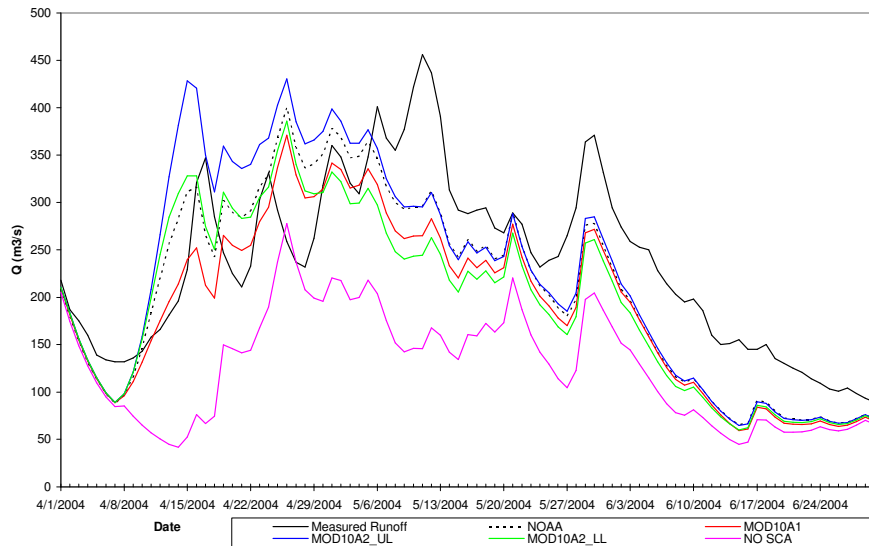


Figure 6.49 Comparison of forecasted and measured discharges for various SCA information for temperature correction

New model runs generally yielded better R^2 values and smaller volume differences. Comparison of the R^2 and volume difference values can be seen in

Table 6.14 and Table 6.15 respectively. In these tables (MM5) indicates the model runs in which the model is executed with the MM5 temperature values for the zones D and E, where else, (LR) indicates the model runs that were executed with the temperatures values computed by lapse rate for zones D and E from zone C.

Table 6.14 R² Comparison of updated model runs

	SCA				
	NOAA	MOD10A1	UL	LL	NO SCA
R ² (MM5)	0.48	0.42	0.28	0.27	-1.03
R ² (LR)	0.08	-0.11	0.16	-0.08	-0.97

Table 6.15 Volume difference comparison of updated model runs

	SCA				
	UL	NOAA	LL	MOD10A1	NO SCA
Dv (MM5)	5.93	11.79	17.53	19.18	46.74
Dv (LR)	25.77	30.68	31.87	34.54	46.56

It can be seen that both R² and volume difference values got better as the temperature values are changed. However, the best fit with the observed discharge sequence of the model runs are not the same for Table 6.14 and Table 6.15.

Even though, the model runs got better values, as the temperature values were changed, the results were not that much of promising. To understand the possible reasons of this event, the temperature and precipitation values for each zone for 1997, 1998 and 2004 values are plotted. The plots of each zone can be seen in Appendix A.

From the figures in Appendix A, an under prediction of the precipitation was sensed. Thus, the MM5 forecasted precipitation values are compared with the

ground truth observations at Güzelyayla and Ovacık automated snow and meteorological stations.

The ratios of the precipitation values between the observed and forecasted values are provided in Case 1 of Table 6.16. When the ratios bigger than 10 are excluded the Case 2 of Table 6.16 is obtained.

Table 6.16 Observed and forecasted precipitation ratios for Güzelyayla and Ovacık stations

Time Interval	Güzelyayla /MM5 forecast		Ovacık/MM5 forecast	
	Case 1	Case 2 (Ratio >10)	Case 1	Case 2 (Ratio >10)
1-15 April	0.18	0.18	0.26	0.26
16-30 April	3.38	2.26	5.44	2.33
1-15 May	0.98	0.98	66.16	1.72
16-31 May	1.31	1.31	1.66	1.66
1-15 June	1.33	1.33	33.59	2.66
16-30 June	1.17	1.17	0.86	0.86

During 1-15 April the average temperature were 0.95 °C and -2.00°C for Güzelyayla and Ovacık stations. Such cold weathers might have caused the freezing of the tipping bucket type precipitation gauges. Thus, the ratios derived during this time might not give indicative results. The remaining ratios yield an average of 1.41 and 1.85 for Güzelyayla and Ovacık and an average of 1.63. This ratio would be used for correction of precipitation falling to Zone C. New runs with the corrected precipitation values for Zone C can be seen in Figure 6.50 ~ Figure 6.54. Table 6.17 summarizes the SCA inputs and the figure numbers for the precipitation corrected runs

Table 6.17 Case numbers as a function of SCA and figure numbers of related output hydrographs for precipitation correction

Case No	SCA Source	Figure Number of the output hydrograph
1	NOAA	6.50
2	MOD10A1	6.51
3	MOD10A2 (UB)	6.52
4	MOD10A2 (LB)	6.53
5	NO SCA	6.54

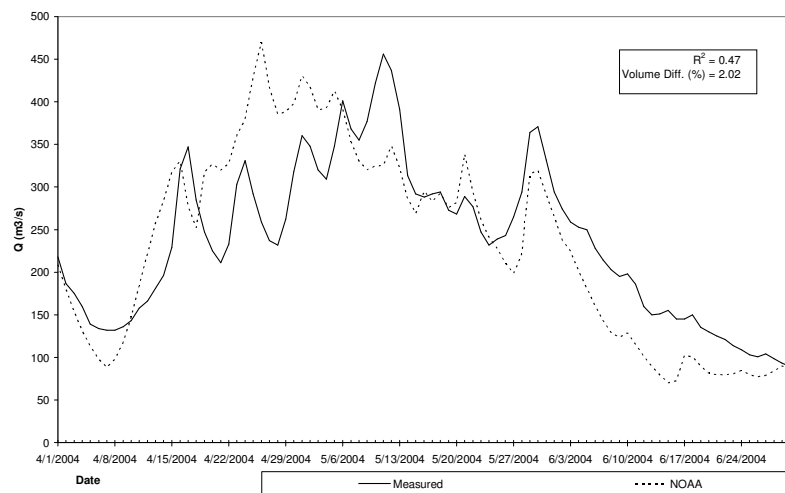


Figure 6.50 Comparison of forecasted and measured discharges for Case 1 for precipitation correction

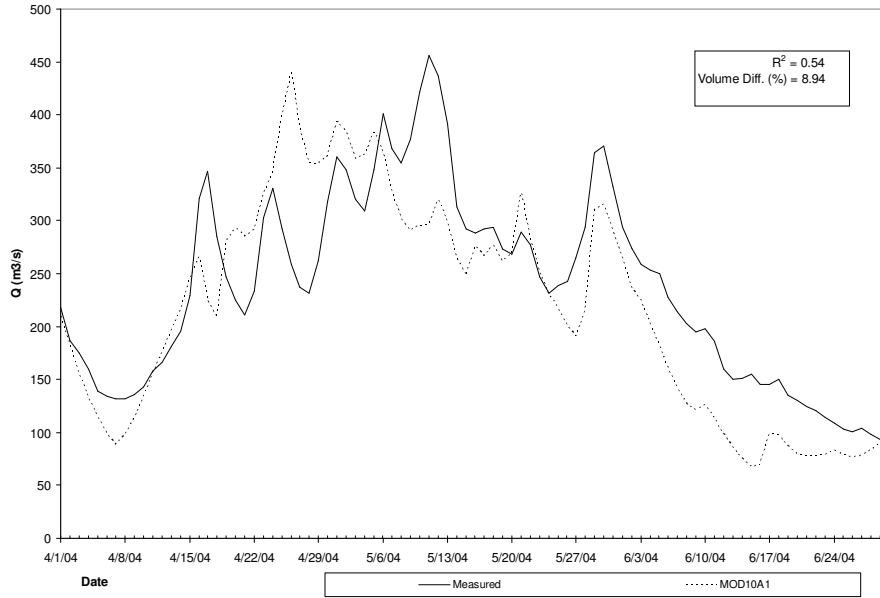


Figure 6.51 Comparison of forecasted and measured discharges for Case 2 for precipitation correction

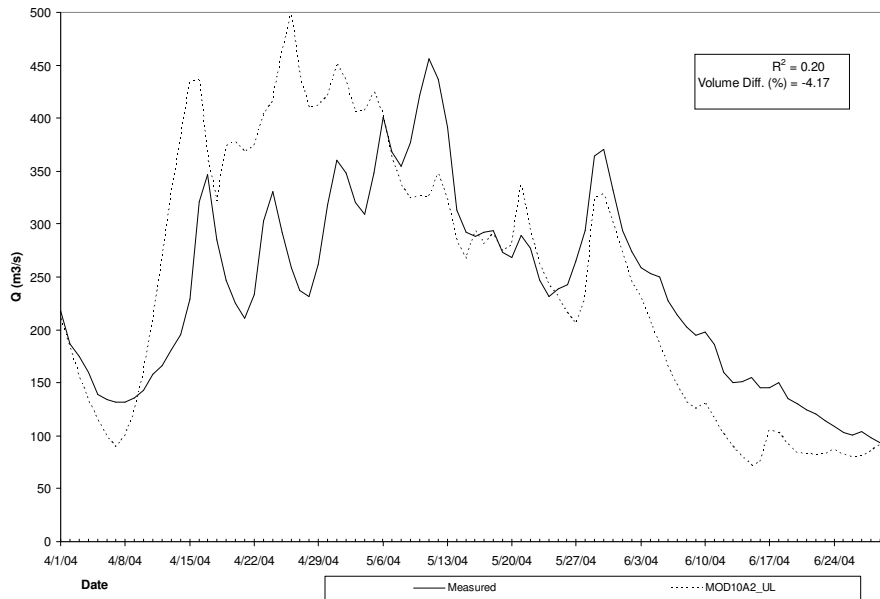


Figure 6.52 Comparison of forecasted and measured discharges for Case 3 for precipitation correction

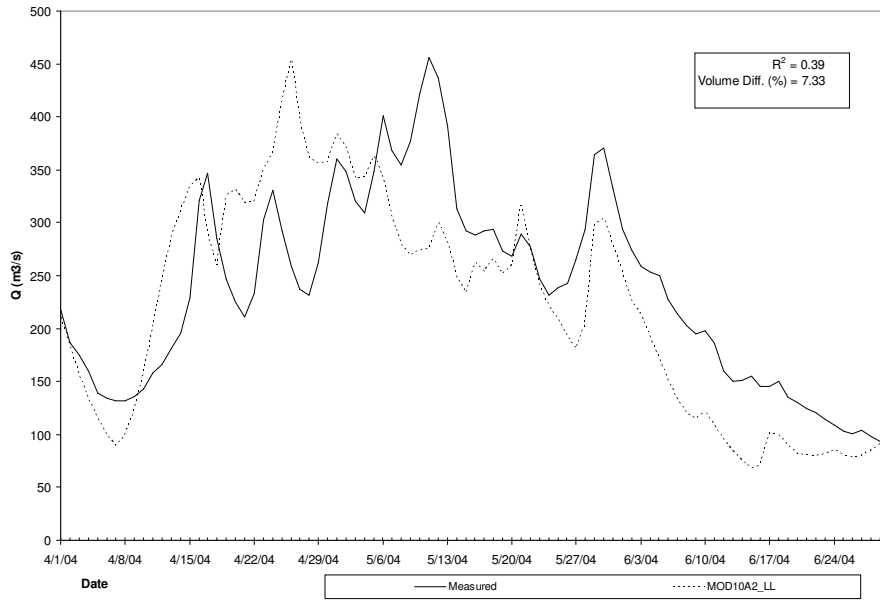


Figure 6.53 Comparison of forecasted and measured discharges for Case 4 for precipitation correction

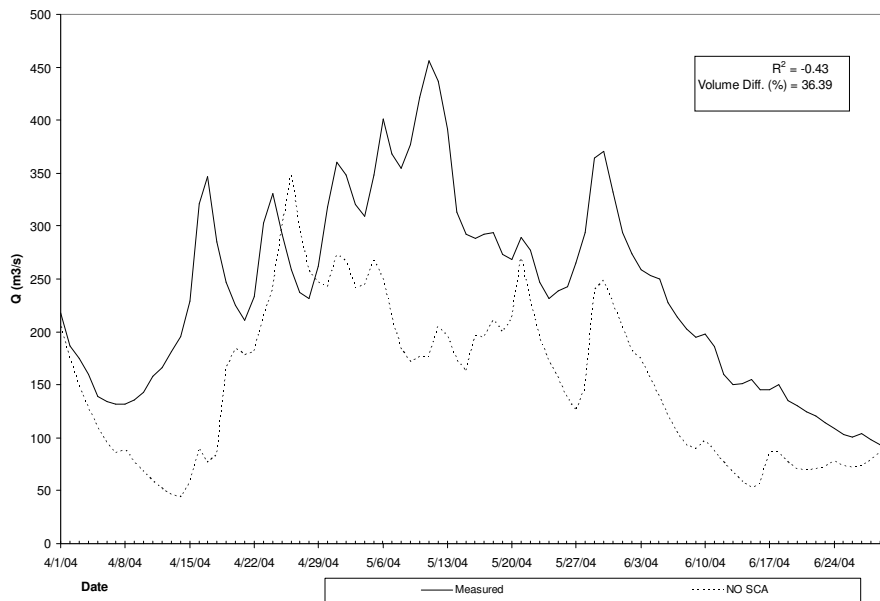


Figure 6.54 Comparison of forecasted and measured discharges for Case 5 for precipitation correction

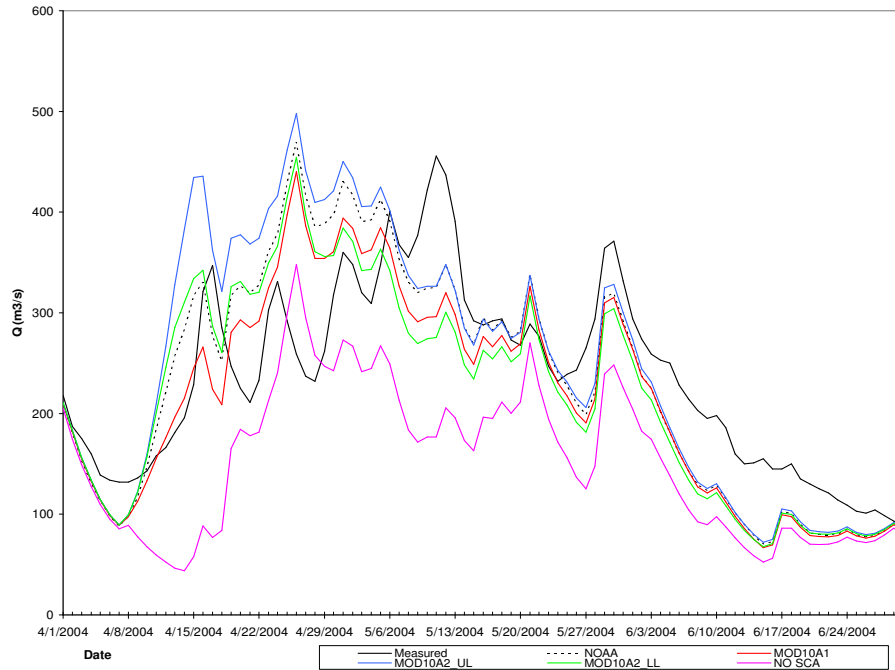


Figure 6.55 Comparison of forecasted and measured discharges for various SCA information for precipitation correction

The summary of the model runs with updated precipitation values can be seen in Table 6.18 and Table 6.19.

Table 6.18 R^2 Comparison of updated precipitation model runs

	SCA				
	MOD10A1	NOAA	LL	UL	NO SCA
R^2	0.54	0.47	0.39	0.20	-0.43

Table 6.19 Volume difference comparison of updated precipitation model runs

	SCA				
	NOAA	UL	LL	MOD10A1	NO SCA
D_v	2.02	-4.17	7.33	8.94	36.39

From the above tables it can be deduced runs with SCA information obtained from MOD10A1 gives the best R^2 which is followed by NOAA, LL, UL and NO SCA afterwards.

From the point of percent deviations, NOAA gives the best estimate followed by UL, LL, MOD10A1 and NO SCA. Among the SCA types, UL is the only one that gives an overestimation of the volume.

6.7 Summary and Discussion of Results

This section will provide a summary of the forecasting studies and the problems encountered during the project lifetime.

6.7.1 Near Real Time Forecasting

Near real time runoff forecasting has been carried out by integration of snowmelt runoff model with numerical weather prediction models for the first trial in Turkey. A solid base for the coupling of a hydrological model with numerical weather prediction application is presented for the rough topography in the eastern region of Turkey where limited data exist. Daily runoff forecasts with $t+24$ hour lead-time have been produced for Karasu Basin from April to July 2004.

During the studies specific model parameters for the basin are searched and determined. Some rule of thumbs for the selection of the model parameters such as rainfall contributing area, were developed. The validity of the selected model parameters were proved with re-runs of model simulations for 1997 and 1998.

Summary of the forecasting model runs performed in this chapter is provided in Table 6.20 and in Table 6.21. In these tables, LR Temp indicates that

the temperature values for Zone D and E are extrapolated from Zone C by the temperature lapse rate. MM5 Temp shows that the Zone D and E temperature are taken as they are from the MM5 model outputs. Finally, Precipitation correction (Precp. Cor.) denotes the runs in which the precipitation for Zone C is corrected by a ratio of 1.63.

Table 6.20 Summary of R^2 values for forecasting model runs

	SCA				
	NOAA	MOD10A1	LB	UB	No SCA
LR Temp.	0.08	-0.11	-0.08	0.16	-0.97
MM5 Temp.	0.48	0.42	0.27	0.28	-1.03
Precp. Cor.	0.47	0.54	0.39	0.20	-0.43

Table 6.21 Summary of D_v values for forecasting model runs

	SCA				
	NOAA	MOD10A1	LB	UB	No SCA
LR Temp.	30.68	34.54	31.87	25.77	46.56
MM5 Temp.	11.79	19.18	17.53	5.93	46.74
Precp. Cor.	2.02	8.94	7.33	-4.17	36.39

From tables it can be seen that UB gave the best R^2 and D_v for LR Temp case.

As the temperatures were changed, NOAA and MOD10A1 gave better R^2 values. However, UB was still the one with the smallest volume difference.

Precipitation correction did not make any improvement in the model efficiencies for NOAA and MOD10A1. However, this caused an increase for LB and a reduction for UB.

It is believed that for the LR Temp case, the smaller temperature values of zones D and E were compensated by the higher SCA percentage, resulting better model efficiency and smaller volume differences.

In the precipitation corrected runs, model gave smaller volume differences in all cases. UB was the only one giving over estimation of the total runoff volume.

As it is presented in Table 6.20 and Table 6.21, major errors in forecast runoff were mainly related to the quality of the forecasted meteorological input data. The wrong interpretation of the meteorological forecasts lead to the assumption of lower precipitation resulting under estimation of flow. A correction to the forecasted precipitation before model input to the model resulted better runoff hydrographs. Thus, it is seen that the quality of the runoff forecasts not only depends on the model but also on the quality of the meteorological forecast input data. The underestimation of runoff values generally in mid May and June also indicates the underestimation of precipitation. Under prediction of precipitation forecasts obtained from numerical weather prediction models were also reported by Collischonn et al. (2005).

Table 6.20 also shows that, remote sensing imagery had much less significant effects on forecast quality than the meteorological input data. In Table 6.20 the model performance (R^2) increases more as one goes in column wise 0.08 to 0.48, -0.11 to 0.54, -0.08 to 0.39, 0.10 to 0.20 rather than row wise -0.11 to 0.16, 0.27 to 0.48, 0.20 to 0.47. Even though, the imagery effect is not clearly seen, images of UB gave smaller volume differences most of the time. The only exception was NOAA. This indicates that if sufficient quality of input data is provided, the model can estimate the seasonal snowmelt runoff volume as well as UB. More over, the higher R^2 values denote that the daily produced water amounts are better predicted.

It is believed that if an updating of the forecasted meteorological and runoff data were available at shorter time intervals and as soon as possible, the runoff forecasts would have been much better. Nevertheless, the results obtained from such an initial study are promising.

6.7.2 Problems Faced During Project

During the operational phase of the project, several technical problems are encountered. These will be mentioned in the followings item by item. The problems encountered will be expressed so that necessary precautions can be taken in a much quicker manner in the proceeding studies.

- Break down of the satellite antenna in Cat station caused delays in the data transfer from this station. The problem was overcome by a field trip and by welding of the antenna. It was seen that of the cable should be inserted to the antenna as straight as possible and the entrance should be strengthened by some external measures. However, the external measures taken must not prevent the dismantle of the antenna.
- The break down of the charger in Ovacık station caused the power failure of the data logger yielding some data loss. Replacing the charger with a new one solved the problem.
- Some problems in data transfer with hard wire telephone lines were encountered. The threshold voltage value of the system for protection against the lightning prevented the data transfer. Thus, the lightning protection had to be removed.
- The earthquake that took place on March 2004 broke up the telephone connection with Ovacık station.
- Different data format of the meteorological forecasts resulted extra decoding work.

- Due to the war in Iraq the Inmarsat satellite communications were cut. This prevented data transfer from the site.
- If possible site visits to the stations should be performed in late summer before the snowfall. In these field trips instruments checks should be made and it must be for sure that they work properly before a harsh winter period.
- The sensors should be removed from site and sent back to manufacturer for recalibration to over come the degrading accuracy and sensitivity.

CHAPTER VII

CONCLUSIONS AND FUTURE WORK

Based on the experience gained during this study, following conclusions and future work proposals can be given. It is believed that the below listed subjects can be some guidelines for the proceeding studies in near future.

- A pre condition for continuation of success in near real time forecasting runoff modeling on snow is the continuity of similar studies with upgrading of existing meteorological stations, especially in a consistent manner with financial support.
- Determination of basin specific model parameters requires long-term data sets and conducted model studies for each basin. Thus, basin specific studies should be continued in the same consistent manner till the model parameters can be well defined within the physical limits. These studies should cover the cases with extreme years also, such as extensive flooding and drought periods.
- Performed studies reveal the importance of runoff coefficients both for rain and snow. Since these are also model parameters, long-term studies should be conducted to provide temporal and spatial variation of representative values. Also, a way to relate these parameters to precipitation and discharge of the specific year under study would give a sound physical basis for selection of the respective values.

- Some rules of thumbs for the selection of model parameters are developed. Such as the selecting the date of rainfall contributing area (RCA) is tied to the daily mean air temperature. The validity of this approach should be verified by future studies.
- Snow covered area (SCA) for each sub catchment values are obtained from discrete snow cover satellite observations in time. A module which can compute the required daily SCA values based on these discrete points can prevent the user to make calculation errors and provide a faster data input opportunity.
- Using areal average air temperature for calculation of the depletion curves from the discrete satellite images may not work for some cases. SCA may reduce with negative temperatures also. This case actually proves that air temperature is not the only meteorological parameter that influences the variation in SCA. Thus, better algorithms to represent SCA depletion are needed. A possible solution may be the inclusion of radiation and turbulent flux terms.
- NOAA-AVHRR (1.1x1.1 km) and MODIS (0.5x0.5 km) images provided the SCA information in this study. Both instruments provided good results, however as all common in the optical imagery; the cloud concept degrades the image usability of both sensors. Even the 8 daily composite snow cover maps obtained from MODIS imagery had some cloud problem. Thus, inclusion of passive or active microwave imagery which both has all weather penetrating capability would be inevitable for all weather SCA monitoring studies. However, processing of the microwave imagery requires complex algorithms and determination of various threshold values. These thresholds should be tested and validated for the area under study.
- It was seen that even the composite snow cover maps were giving better volume estimates; they were not good at representing daily variations of runoff rates (Table 6.20 and Table 6.21). Thus, the purpose of the reservoir management should dictate the selection of satellite imagery type. If the

total volume has a priority over the daily runoff values, composite snow cover maps should be selected. If the daily runoff values are the primary concern, then the daily snow cover maps would be more useful.

- SCA determination algorithms mainly use thresholds to separate snow from clouds. However, these threshold values are mainly obtained from the site measurements conducted at where the sensor is produced. Thus, the validity of these thresholds requires detailed researches and is subject to question. Verification of these thresholds for the area under study with its specific topographic configuration would be performed by the site visits that include both temporal and spatial variation.
- Streamflow and snow covered area are found to be closely related. (Zhou et al., 2005). However, as also indicated in Hydalp (2000), a model based approach would be more beneficial for flood mitigation and reservoir operation. Since the response of a basin to SCA is a complex phenomenon including many spatially and temporally varying factors some of which are soil moisture, air and snow temperature, precipitation (both rain and snow), wind patterns (direction and velocity)... many which may be hard to represent by simple statistical methods.
- Present version of SRM (WinSRM 1.09) divides the basin into sub basins only with respect to elevation called as zones. Even though, satisfactory results are achieved, it is believed that dividing the basin with respect to slope and aspect and ultimately with respect to similar hydrological response units concept, within the SRM boundaries, would improve the results.(Nagler, 2005)
- SRM requires the daily snow covered area information in near real time or preferably advanced in time in forecasting mode. This may be very hard to obtain due to frequent cloud cover in optical imagery. The complexity of the algorithms for microwave imagery may also reduce the forecast time period. A possible improvement would be developing SRM so that there should be no need to SCA. Personnel contact has been made with the SRM developers on this issue.

- SRM calculates the natural flow. It does not consider the effects of the man-made structures and flow regulations. Thus, the Tercan Dam, located on the contributing river to Karasu, might have degraded the forecasting results also. Even though there are some new developments in SRM as to consider these effects it may take some time to appear for practical use.
- Modified depletion curve (MDC), as described in a more detailed manner in manual, concept of SRM should be thoroughly understood. MDCs that are obtained by the simulation runs performed with the observed meteorological variables would give idea about the basin wide snow water equivalent (SWE). These values should be related with the SWE observations that are performed by the manual snow surveys at the snow course scale and with the data obtained from the automated snow stations such as snow pillows at a point and surrounding area.
- It is seen that runoff forecast quality not only depends on the model accuracy. But also on the quality of the forecasted meteorological variables that are required by the model. In this study the effect of temperature and precipitation on model performance is summarized in Table 6.20 and Table 6.21. Providing as accurate as possible input variables in to the model can be achieved by comparing the forecast values with the ground observations. However, here, the concept of scale gets involved. Scale effect can be in any of the three forms that are process, model and measurement. Care must be given in the verification of the forecasted values, since the point of ground observation may not be representative of the remaining pixels, sub basin or the basin as a whole.
- Forecasting studies performed in this study used the t+24 hour lead time. The accuracy of precipitation forecast reduces as the lead time increase. Thus, to obtain better precipitation values, the long term forecast values should be updated with the recent values, which is the topic of nowcasting. It is believed that the accuracy of the forecasted discharges would increase as the precipitation forecast gets better by the values that will be obtained from nowcasting that has lead times less than a day.

- For MM5 data followings can be pointed;
 1. Forecasts can be improved by inclusion of data assimilation procedures.
 2. Topographic and land use maps can be changed with the layers that better represent the actual configuration.
 3. Convective parameterizations are considered as one of the most important model parameters in model simulations with a ground scale of 10 km. Thus, one should make a selection between whether forecasting all of the storm events within a year with the best overall accuracy or capturing the most intensive storm events. The selection would affect the choice of the related parameters.
- Studies related with numerical weather prediction models should be continued. New models and the best configuration of the related parameters should be investigated. In this context, Weather Research and Forecasting (WRF) model which is the next generation of mesoscale numerical prediction models should be searched. The suitability of this model to the prevailing conditions of Turkey should be examined.
- Model parameters selected for forecasting studies were verified by the re-runs of the simulations for the water years 1997 and 1998 (Table 6.10, Figure 6.34~ Figure 6.37). It was seen that as the runoff coefficients of the related water year is used, satisfactory results are obtained. For the selection of these runoff coefficients, El Nino and La Nina effect of the preceding year on the streamflows should also be investigated.

REFERENCES

1. Ackerman S. A., Strabala K. I., Menzel P. W., Frey R. A., Moller C. C., Gumley L. E., *Discriminating clear sky from clouds with MODIS*, Journal of Geophysical Research, 103 (D24), 32141-32157, 1998.
2. Akyürek Z., Şorman Ü., Usul N., Tekeli A. E., *Doğu Anadolu bölgesinde kar kaplı alanların NOAA/AVHRR görüntülerinden belirlenmesi*, 6th Esri & Erdas Users Conference, Ankara, 10-11 June 1999.
3. Akyürek, Z., Şorman Ü., *Monitoring snow-covered areas using NOAA-AVHRR data in eastern part of Turkey*, Hydrological Sciences Journal, 47(2), 2002.
4. Allen R. C., Jr., Durkee, P. A., Wash, C. H., *Snow/cloud discrimination with multispectral satellite measurements*, Journal of Applied Meteorology, Vol. 29, pp. 994-1004, 1990.
5. Bagchi A. K., *Areal value of degree-day factor*, Hydrological Sciences Journal, Vol. 28 , No. 4, pp. 499-511, 1983.
6. Barnes W. L., Pagano T. S., Salomonson V. V., *Prelaunch characteristics of the Moderate resolution imaging spectroradiometer (MODIS) on EOS – AM 1*, IEEE Transactions on Geoscience and Remote Sensing, 36 (4), 1088-1100, 1998.
7. Barret A. P., Leavesley G. H., Viger R. L., *A comparison of satellite derived and modeled snow covered area for a mountain drainage basin*, Remote Sensing and Hydrology (2000), IAHS publication No 267, 2001.
8. Baum B. A., Trepte Q., *The CERES daytime cloud detection algorithm for the tropical rainfall-measuring mission: The grouped threshold method*, <http://www.larc.nasa.gov/~baum/snow/snow.html>, 1997.
9. Baumgartner M. F., Seidel, K Martinec, J., *Toward snowmelt runoff forecast based on multi sensor remote sensing information*, IEEE Transactions on Geoscience and Remote Sensing, Vol. GE-25, No. 6, 1987.
10. Baumgartner M. F., Apfl G., Holzer T., *Monitoring Alpine snow cover variations using NOAA-AVHRR data*, IEEE IGARSS, pp.2087-2089, 1994a.

11. Baumgartner M. F., Rango A., *A microcomputer-based Alpine Snow-Cover Analysis System (ASCAS)*, Photogrammetric Engineering & Remote Sensing, Vol. 61, No. 12, pp. 1475-1486, 1995.
12. Baumgartner M. F., Apfl G. M., *Remote sensing, geographic information systems and snowmelt runoff model- an integrated approach*, IAHS Publications, No. 242, pp.73-82, 1997.
13. Bergström S., *Principles and confidence in hydrological modeling*, Nordic Hydrology, Vol 22, pp 123-136, 1991.
14. Carroll T. R., *Operational Airborne and Satellite snow cover products of the National Hydrologic Remote Sensing Center*, Proceedings of the Forty seventh annual eastern snow conference, pp.87-98, 1990.
15. Carroll T. R., Holroyd E. W., *Operational Remote sensing of snow cover in the US and Canada*, Proceedings of International Symposium HY and IR divisions ASCE, pp. 286-291, San Diego, 1990.
16. Carsey F., *Remote sensing of ice and snow: review and status*, International Journal of Remote Sensing, Vol. 13, No. 1, pp. 5-11, 1992.
17. Chang A. T. C., Foster J. L., Hall D. K., *Nimbus-7 SMMR derived global snow cover parameters*, Annals of glaciology, No.9, pp.39-44, 1987.
18. Che N., Price J. C., *Survey of radiometric calibration results and methods for visible and near infrared channels of NOAA-7-9-11AVHRRs*, Remote Sensing of the Environment, Vol.41, pp.19-27, 1992.
19. Collier P., Runacres A. M. E., McClatchey J., *Mapping very low surface temperatures in the Scottish High lands using NOAA-AVHRR data*, International Journal of Remote Sensing, Vol. 10, No. 9, pp. 1519-1529, 1989.
20. Collischonn W., Hass R., Andreolli I., Tucci C. E. M., *Forecasting River Uruguay flow using rainfall forecasts from a regional weather prediction model*, Journal of Hydrology, 305, pp. 87-98, 2005.
21. Cracknell A. P., *The Advanced Very High Resolution Radiometer*, 1997.
22. Derrien M., Farki B., Harang L., LeGléau H., Noyalet A., Pochic D., Sairouni A., *Automated cloud detection applied to NOAA-11/AVHRR imagery*, Remote Sensing of the Environment, Vol. 46, pp. 246-267, 1993.
23. Dozier J., Scheider S. R., McGinnins D. F., *Effect of grain size and snowpack water equivalence on visible and near infrared satellite*

- observations of snow*, Water Resources Research, Vol. 17, No. 4, pp. 1213-1221, 1981.
24. Dozier J., Warren S. G., *Effect of viewing angle on infrared brightness temperature of snow*, Water Resources Research, Vol.18, No. 5, pp 1424-1434, 1982.
 25. Dozier J., *Spectral signatures of alpine snow cover from Landsat Thematic Mapper data*, Remote Sensing of Environment, Vol. 28, pp. 9-22, 1989.
 26. Eales P., *Automatic linear feature matching for satellite image navigation*, Proceedings of the 4th AVHRR data users meeting, 1989.
 27. ECMWF, available at <http://www.ecmwf.int> (Last accessed 20/11/2004), 2004.
 28. Engman E. T., Gurney, R. J., *Remote Sensing in Hydrology*, Chapman & Hall, New York, 1991.
 29. Frank C., Itten I. K., Staez K., *Improvement in NOAA-AVHRR snow cover determination for runoff prediction*, IEEE IGARSS, pp.433-435, 1988.
 30. Foster J. L., Hall D. K., Chang T. L., *Remote sensing of snow*, Transactions American Geophysical Union, Vol. 68, No.32, 1987.
 31. Foster J. L., Hall D. K., *Observation of snow and ice features during the polar winter using moonlight as source of illumination*, Remote Sensing of Environment, No. 37, pp. 77-88, 1991.
 32. Garen D.C., *Personnel contact*, 2003.
 33. Gessell G., *An algorithm for snow and ice detection using AVHRR data. An extension to the APOLLO software package*, International Journal of Remote Sensing, Vol. 10, pp. 897-905, 1989.
 34. Hall D. K. and Martinec J., *Remote Sensing of Ice and Snow*, Chapman and Hall, London, 1985.
 35. Hall D. K., *Remote sensing applications to hydrology: Imaging radar*, Hydrological Sciences Journal, Vol. 41, No. 4, pp. 609-624, 1996.
 36. Hall D. K., Riggs G. A., Salomonson V. V. , Barton J. S., Casey K., Chien J. Y. L. DiGirolamo N. E., Klein A. G., Powell H. W., Tait B. A., *Algorithm theoretical basis document (ATBD) for MODIS snow and sea ice mapping algorithm*, (available from <http://modis-snow-ice.gsfc.nasa.gov/atbd.html>; last accessed 21/10/2004), 2001.

37. Hall D. K., Riggs G. A., Salomonson V. V. , DiGirolamo N. E., Bayr K. J., *MODIS Snow cover products*, Remote Sensing of Environment, 83, 181-194, 2002.
38. Harrison A. R., Lucas, R. M., *Multi-spectral classification using NOAA/AVHRR imagery*, International Journal of Remote Sensing, Vol. 10, pp. 907-916, 1989.
39. Hastings D. A., Emery W. J., *The advanced very high resolution radiometer (AVHRR): a brief reference guide*, Photogrammetric Engineering and Remote Sensing, 1992.
40. Hu Xu, Bailey J. O., Barret E. C., Kelly E. J., *Monitoring snow area and depth with integration of remote sensing and GIS*, International Journal of Remote Sensing, Vol. 14, No. 17, pp. 3529-3268, 1993.
41. Hydalp, *Hydrology of Alpine and High Latitude Basins Final Report*, Institut fur Meteorologie und Geophysik, Universitat Innsbruck, 2000.
42. Jakeman A. J., Hornberger, *How much complexity is warranted in a rainfall runoff model?*, Water Resources Research, 29,2637-2649,1993.
43. Justice C., Vermote E., Townshed J. R. G.,Defries R., Roy D. P., Hall D. K., Salomonson V. V., Privette J, Riggs G., Strahler A., Lucht W., Myneni R., Knjazihhin Y., Running S., Nemani R., Wan Z., Huete A., Van Leewen W., Wolfe R, *The Moderate Resolution Imaging Spectroradiometer (MODIS): Land remote sensing for global change research*, IEEE Transections on Geoscience and Remote Sensing, 36 (4), pp 1228-1249, 1998.
44. Katwijk V. F., Rango, A., Childress, A. E., *Effect of simulated climate change on snowmelt runoff modeling in selected basins*, Water Resources Bulletin, Vol. 29, No. 5, 1993.
45. Kaufmann Y. J., Holben B. N., *Calibration of the AVHRR visible and near IR bands by atmospheric scattering, ocean glint and desert reflection*, International Journal of Remote Sensing, Vol.14, No.1, pp.21-52, 1992.
46. Kaya I., *Application of Snowmelt Runoff Model Using Remote Sensing and Geographic Information Systems*, Master of Science Thesis, Water Resources Laboratory, Civil Engineering Department, Graduate School of Natural and Applied Sciences, Middle East Technical University, 1999.
47. Kite G. W., Pietroniro A., *Remote sensing applications in hydrological modeling*, Hydrological Sciences Journal, Vol. 41, No. 4, pp. 563-591, 1996.

48. Klein A. G., Hall D. K., Riggs G. A., *Improving snow cover mapping in forests through use of a canopy reflectance model*, Hydrological Processes, 12, 1723-1744, 1998.
49. Klein A. G., Stroeve J., *Development and validation of a snow albedo algorithm for the MODIS instrument*, Annals of Glaciology, 34, 45-52, 2002.
50. Kleindienst H., Pfister M., Baumgartner M. F., *Preoperational snowmelt forecasting based on an integration of ground measurements, meteorological forecasts and satellite data*, IAHS Publications. No 25, pp 81-84, 1999.
51. Kuhn M., *Bidirectional reflectance of polar and alpine snow*, Annals of glaciology, Vol. 6, pp 164-167, 1985.
52. Levick L. R., *Prediction of Rainfall and snowmelt produced runoff: linking a hydrologic model with remote sensing and GIS*, Master of Science Thesis, School Of Renewable Resources, The University of Arizona, 1998.
53. Lillesand T. M., Kiefer, R. W., *Remote sensing and Image Interpretation*, John Wiley & Sons, 1994.
54. Lindström G., Johansson B., Persson M., Gardelin M., Bergström S., *Development and test of the distributed HBV-96 model*, Journal of Hydrology, 201, pp 272-288, 1997.
55. Kneizys F. X., Anderson G. P., Shettle E. P., Abreu :L. W., Chetwynd J. H., *Users Guide to LOWTRAN 7*, Air Force Geophysics Lab. Hanscom AFB TR-88-0177, ERP, #1010, 1988.
56. Martinec J., *The degree-day factor for snowmelt runoff forecasting*, in "Surface Waters", Proceedings of the General Assembly of Helsinki, International Association of Scientific Hydrology, Gentbrugge, Belgium, pp. 468-477, 1960.
57. Martinec J., *Snowmelt-Runoff Model for stream flow forecasts*, Nordic Hydrology, Vol. 6, pp. 145-154, 1975.
58. Martinec J., *Limitations in hydrological interpretations of the snow coverage*, Nordic Hydrology, 11, pp 209-220, 1980.
59. Martinec J., *Snowmelt runoff models for operational forecasts*, Nordic Hydrology, 16, pp 129-136, 1985.
60. Martinec J., Rango, A., *Parameter values for Snowmelt Runoff Modelling*, Journal of Hydrology, Vol. 84, pp 197-219, 1986.

61. Martinec J., Rango A., *Interpretation and utilization of areal snow cover data from satellites*, Annals of Glaciology, Vol. 19 , pp. 166-169, 1987.
62. Martinec J., Rango, A., Roberts, R., *The Snowmelt Runoff Model (SRM) User's Manual*, Geographica Bernensia, P29, Dept. Of Geography, Univeristy of Berne, Berne, Switzerland, 1998.
63. Maxson R.W., Allen, M.W., and Szeliga, T.L., *theta - Image classification by comparison of angles created between multi-channel vectors and an empirically selected reference vector*, North American Airborne and Satellite Snow Data CD-ROM, Chanhassen, Minnesota: National Weather Service, 1996.
64. Mitchell R. M., *Atmospheric correction of vegetation indices using split pass AVHRR imagery*, Proceedings of the 4th AVHRR data users meeting, pp. 153-156, Eumetsat, Darmsdat, 1989.
65. MM5 tutorial, (available from <http://www.mmm.ucar.edu/mm5/mm5v3/tutuorial/teachyourself.html>), 2005.
66. MODIS Reprojection Tools, (available at <http://lpdaac.usgs.gov/landdaac/tools/modis/index.html>, 2003, last accessed 25/10/2004).
67. Nagler T., Personnel contact, 2005.
68. NSIDC (available at <http://www.nsidc.org>, last accessed 14/03/2005), 2004.
69. Paltridge G. W., Mitthell R. M., *Atmospheric and viewing angle correction of vegetation indices and grass land fuel moisture content derives from NOAA-AVHRR*, Remote Sensing of Environment, Vol. 31, pp. 121-135, 1990.
70. Popp T., *Correcting atmospheric masking to retrieve spectral albedo of land surfaces from satellite measurements*, International Journal of Remote Sensing, Vol. 16, No. 8, pp. 3483-3508, 1995.
71. Rango J., Salomonson V. V., Foster J. L., *Seasonal stream flow estimation in the Himalayan region employing meteorological satellite snow cover observations*, Water Resources Research, Vol. 13, No. 1, pp. 109-112, 1977.
72. Rango A., Martinec, J., *Application of Snowmelt Runoff Model using Landsat data*, Nordic Hydrology, Vol. 10, pp. 225-238, 1979.

73. Rango A., Martinec J., *Snow accumulation derived from modified depletion curves of snow coverage*, International Association of Hydrological Sciences Publications, 138,83-90, 1982.
74. Rango A., Martinec J., Foster J. Marks D., *Resolution in operational remote sensing of snow cover*, IAHS publications, No. 145, pp. 371-381, 1983.
75. Rango A., *Snow Hydrology processes and remote sensing*, Hydrological Processes, Vol. 7, pp. 121-138, 1993.
76. Rango A., *Spaceborne remote sensing for snow hydrology applications*, Hydrological Sciences Journal, Vol. 41, pp. 477-494, 1996.
77. Rango A., Walker A. E., Goodison B. E., *Snow and Ice*, in Remote Sensing in Hydrology and Water Management, Eds. Schultz G. A., Engman E. T, pp. 239-261, 2000.
78. Rango A., Personnel communication, 2005.
79. Rao C. R. ,Chen J., *Inter satellite calibration linkages for the visible and near infrared regions of the AVHRR on the NOAA -7-9-11 Spacecraft*, International Journal of Remote Sensing, Vol. 16, No.11, pp. 1931-1942, 1995.
80. Riggs G. A., Barton J. S., Casey K. A., Hall D. K., Salomonson V. V., *MODIS snow products user guide for collection 4 data products*, (<http://>), 2003.
81. Romanov P., Tarpley D., *Estimation of snow depth over open prairie environments using GEOS imager observations*, Hydrological Processes, 18, 1073-1087, 2004.
82. Rosenthal W., Dozier J., *Automated mapping of montane snow cover at subpixel resolution from the Landsat Thematic Mapper*, Water Resources Research, 32, pp 115-130, 1996.
83. Rott H., *Zur Schneekartierung in alpinen Einzugsbeieten aus Satellitenbildern*, Zeitschrift fur Gletscherkunde und Glaziologie, Vol 14, No 1, pp 81-93, 1978.
84. Rott H., Nagler T., *Simultaneous implementation of a synthetic aperture radar and a high resolution optical imager (Phase B)*, Final report, Vol 2, Appendix A, Snowmelt runoff investigation of contemporality, GEC-Marconi publication MTR 95/33C, 1995.

85. Salomonson V. V., Toll D. L., *The Moderate resolution imaging spectrometer-radar (MODIS-N) facility instrument*, Advances in Space Research, 11, pp 231-236, 1991.
86. Saunders R. W., Kriebel K. T., *An improved method for detecting clear sky and cloudy radiance from AVHRR data*, International Journal of Remote Sensing, Vol. 9, No. 1, pp.123-150, 1988.
87. Schneider S. R., McGinns D. F., Gatlin J. A., *Use of NOAA/AVHRR visible and near infrared data for remote sensing*, NOAA Technical Reports, NESS 84, 1981.
88. Schultz G. A., Engman E. T., *Remote Sensing in hydrology and water management*, Springer, 2000.
89. Scorer R. S., *Cloud reflectance variations in channel-3*, International Journal of Remote Sensing, Vol.10, No. 4&5, pp. 675-686, 1989.
90. Seidel K., Brühsh W., Steinmeier C., *Experiences from real time runoff forecasts by snow cover remote sensing*, IEEE IGARSS, 1994.
91. Seidel K. and Martinec J., *Remote Sensing in Snow Hydrology*, Praxis Publishing, 2004.
92. Sevruk , *Correction of measured precipitation in the Alps using the water equivalent of new snow*, Nordic Hydrology, 14,49-58, 1983.
93. Simic A., Fernandes R., Brown R., Romanov P., Pawrk W., *Validation of VEGETATION, MODIS and GOES+SSM/I snow cover products over Canada based on surface snow depth observations*, Hydrological Processes, 18, pp 1089-1140, 2004.
94. Simpson J. J., Stitt, J. R., Sienko, M., *Improved estimates of the areal extent of snow cover from AVHRR data*, Journal of Hydrology, Vol. 204, pp. 1-23, 1998.
95. Stoelinga M. T., *Personnel contact*, 2004.
96. Steppuhn H., *Snow and Agriculture*, in Handbook of Snow: Principles, Processes, Management & Use, eds. Gray D. M., Male D. H., pp 60-65, 1981.
97. Swamy A. N., Brivio P. A., *Modeling runoff using optical satellite remote sensing data in a high mountain alpine catchment of Italy*, Hydrological Processes, 11,1475-1491,1997.

98. Şensoy A., *Physically based point snowmelt modeling and its distribution in Upper Euphrates Basin*, Ph. D Thesis, Water Resources Laboratory, Civil Engineering Department, Graduate School of Natural and Applied Sciences, Middle East Technical University, 2005
99. Şorman A. A., Tekeli A. E., Şorman A. Ü., *Application of Snowmelt Runoff Models by RS/GIS Techniques Over the Central Asia and Türkiye*, XXII Nordic Hydrological Conference, Volume 1, pp. 163-172, 4-7 August 2002.
100. Şorman A. A., *Modeling the dynamic process of seasonal snow cover in the Upper Euphrates Basin- Progress Report 3*, Water Resources Laboratory, Civil Engineering Department, Middle East Technical University, 2004.
101. Tekeli A. E., *Integration of remote sensing and geographic information systems on snow hydrology modeling*, Ms. Thesis, Water Resources Laboratory, Civil Engineering Department, Graduate School of Natural and Applied Sciences, Middle East Technical University, 2000.
102. Tekeli A. E., *Operational hydrological forecasting of snowmelt runoff model by RS-GIS Integration- Progress Report 1*, Water Resources Laboratory, Civil Engineering Department, Middle East Technical University, 2002a.
103. Tekeli A. E., *Operational hydrological forecasting of snowmelt runoff model by RS-GIS Integration- Progress Report 2*, Water Resources Laboratory, Civil Engineering Department, Middle East Technical University, 2002b.
104. Tekeli A. E., *Operational hydrological forecasting of snowmelt runoff model by RS-GIS Integration- Progress Report 3*, Water Resources Laboratory, Civil Engineering Department, Middle East Technical University, 2003.
105. Tekeli A. E., *Operational hydrological forecasting of snowmelt runoff model by RS-GIS Integration- Progress Report 4*, Water Resources Laboratory, Civil Engineering Department, Middle East Technical University, 2003b.
106. Tekeli A. E., Şorman A. A., Şensoy A., Şorman A. Ü., *Design, Installation of a Snowmelt Lysimeter and Analysis for an Energy Balance Model Studies in Turkey*, 60th Eastern Snow Conference, Sherbrooke, Canada, 2003c.
107. Tekeli A. E., Şorman A. A., Şensoy A., Şorman A. Ü., *Kar Lizimetresinin Tasarımı, İmalatı, İletimi ve On Bulgular*, IV. Ulusal Hidroloji Kongresi, 21-25 Haziran, İstanbul, Turkey, 2004.
108. Tekeli A. E., Şorman A. A., Şensoy A., Şorman A. Ü., Bonta J., Schaefer G., *Snowmelt lysimeters for real time snowmelt studies in Turkey*, Turkish Journal of Engineering and Environmental Sciences, Vol 29, No1 ,pp 29-40, 2005a.

109. Tekeli A. E., Akyürek Z., Şorman A. A., Şensoy A., Şorman A. Ü., Using MODIS snow cover maps in modeling snowmelt runoff process in the eastern part of Turkiye, *Remote Sensing of Environment*, (accepted for publication), 2005b.
110. Tekeli A. E., Akyürek Z., Şorman A. A., Şensoy A., Şorman A. Ü., Modeling the temporal variation in snow covered area derived from satellite images for simulating/forecasting of snowmelt runoff in Turkey, *Hydrological Sciences Journal*, (accepted for publication), 2005c.
111. Tucker C. J., *Maximum normalized difference vegetation index images for sub-Saharan Africa for 1983-1985*, *International Journal of Remote Sensing*, 7, pp 1383-1394, 1986.
112. Townshend J. R. G., Tucker C. J., *Objective assessment of Advanced Very High Resolution Radiometer data for land cover mapping*, *International Journal of Remote Sensing*, 5, 497-504, 1984.
113. US Army Corps of Engineers , *Snow Hydrology* , North Pacific Division, Corps Of Engineers, US Army, Portland, Oregon, 1956.
114. Vivian H., *La prevision des debits en bassins montagneux*, *Bulletin of Association of Geographics Francais*, No 459, 1979.
115. Voigt S., Koch M., Baumgartner M. F., *A multi channel threshold technique for NOAA AVHRR data to monitor the extent of snow cover in the Swiss Alps.*, in Tranter M., Armstrong R., Brun E., Jones G., Sharp M., Williams M. (ed): *Interactions between the cryosphere, climate and greenhouse gases*, IAHS publications. No. 256, pp35-43, 1999.
116. Warren D., *AVHRR Channel 3 noise and methods for its removal*, *International Journal of Remote Sensing*, Vol.10, No. 4&5, pp. 645-651, 1989.
117. Weibel D., Wunderle S., Kleindienst H., *A distributed model to simulate the snow cover in Switzerland combining GIS and RS*, 3rd Earsel Proceedings, Prague, 2002.
118. Wiesnet D. R., Ropelevski C. F., Kukla G. J., Robinson D. A., *A discussion of the accuracy of NOAA satellite derived global seasonal snow cover measurements*. IAHS publications Vol. 166, pp. 291-304, 1987.
119. WinSRM, *Windows Snowmelt Runoff Model Users Manual, Version 1.09*, available at <http://hydrolab.arsusda.gov/cgi-bin/srmhome>, 2005.

120. World Meteorological Organization (WMO), *Guide for hydrometeorological practices (Chapter 5)*, WMO, Geneva, Switzerland, p. 24, 1964.
121. World Meteorological Organization (WMO), *Intercomparison of models of snowmelt runoff*, Operational Hydrology Report 23, WMO Publication 646, Geneva, 1986.
122. Yamanouchi T., Kawaguchi S., *Cloud distribution in the Antarctic from AVHRR data and radiation measurements at the surface*, International Journal of Remote Sensing, Vol. 13, No.1, pp.111-127, 1992.
123. Zhou X., Xie H., Hendrickx J. M. H., *Statistical evaluation of remotely sensed snow-cover products with constraints from streamflow and SNOTEL measurements*, Remote Sensing of Environment, 94. pp 214-231, 2005.

APPENDIX A

COMPARISON OF LONG TERM TEMPERATURE AND PRECIPITATION VALUES

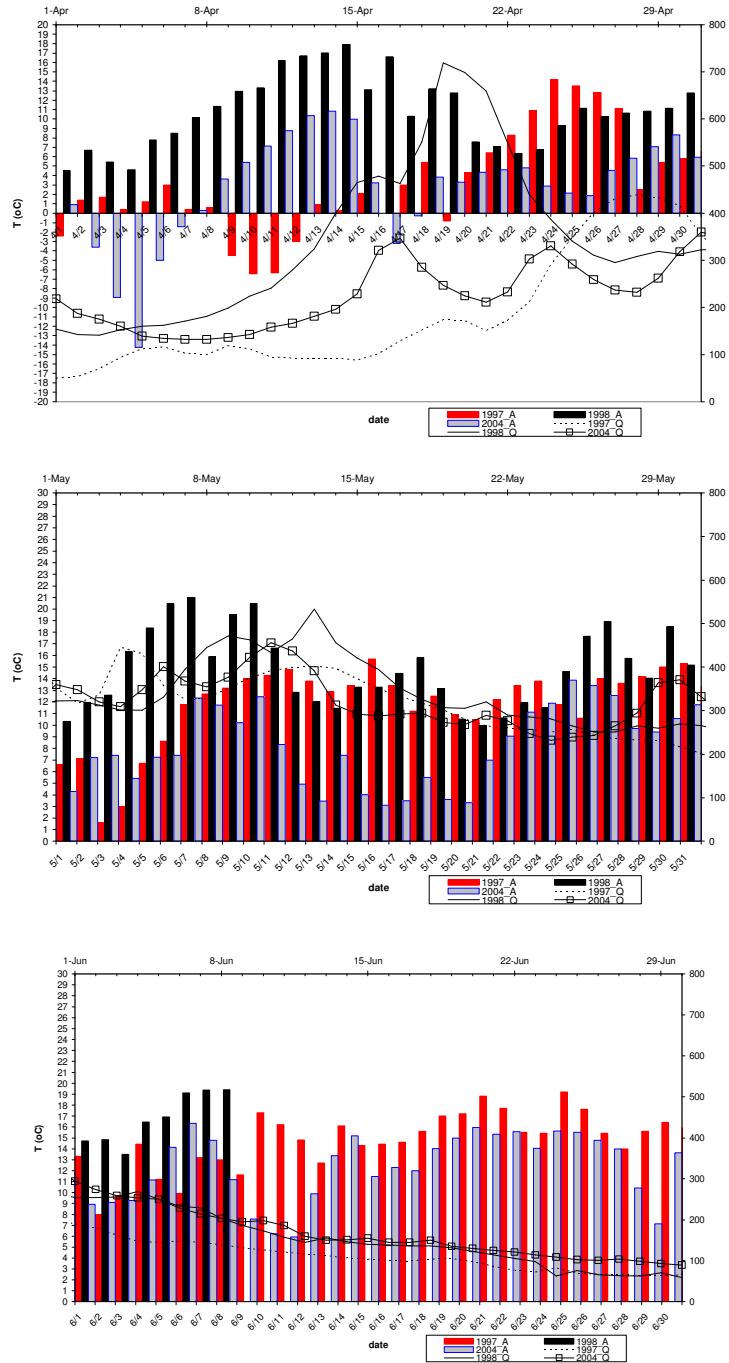


Figure A.1 Comparison of Temperature Values for Zone A

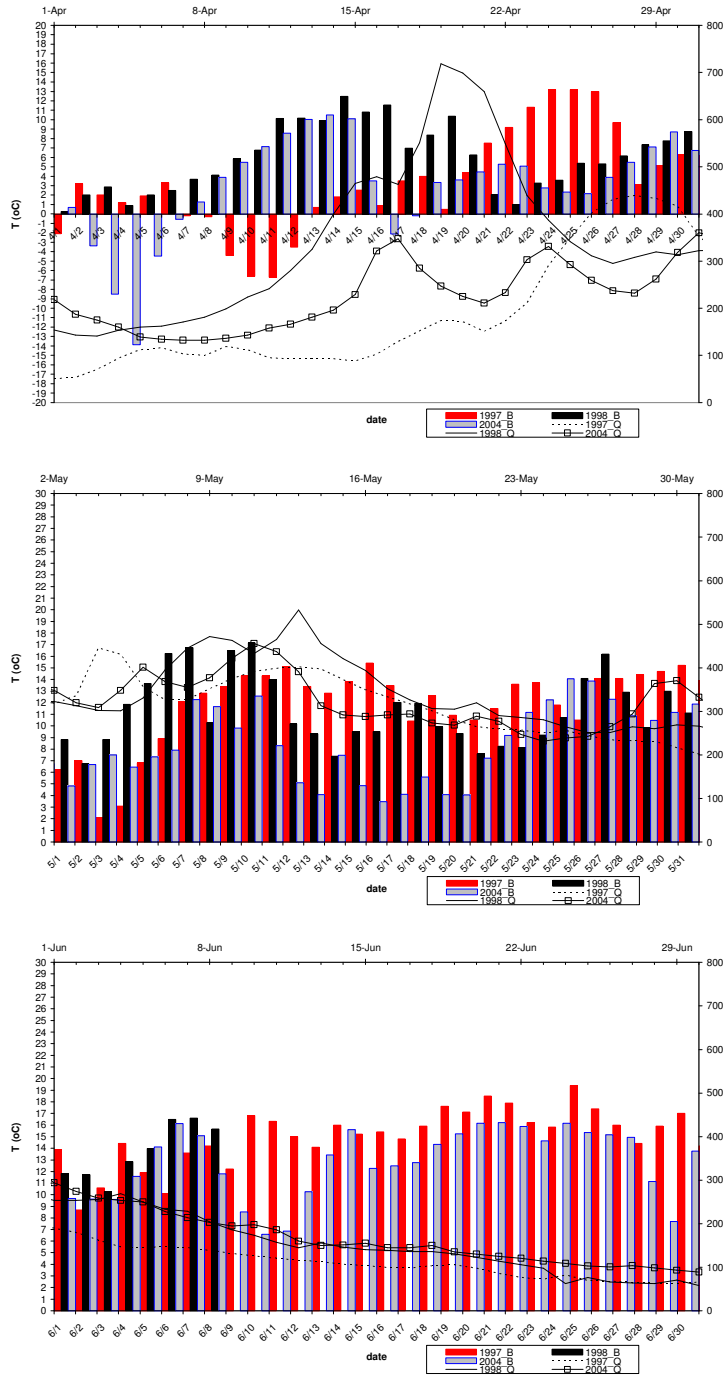


Figure A.2 Comparison of Temperature Values for Zone B

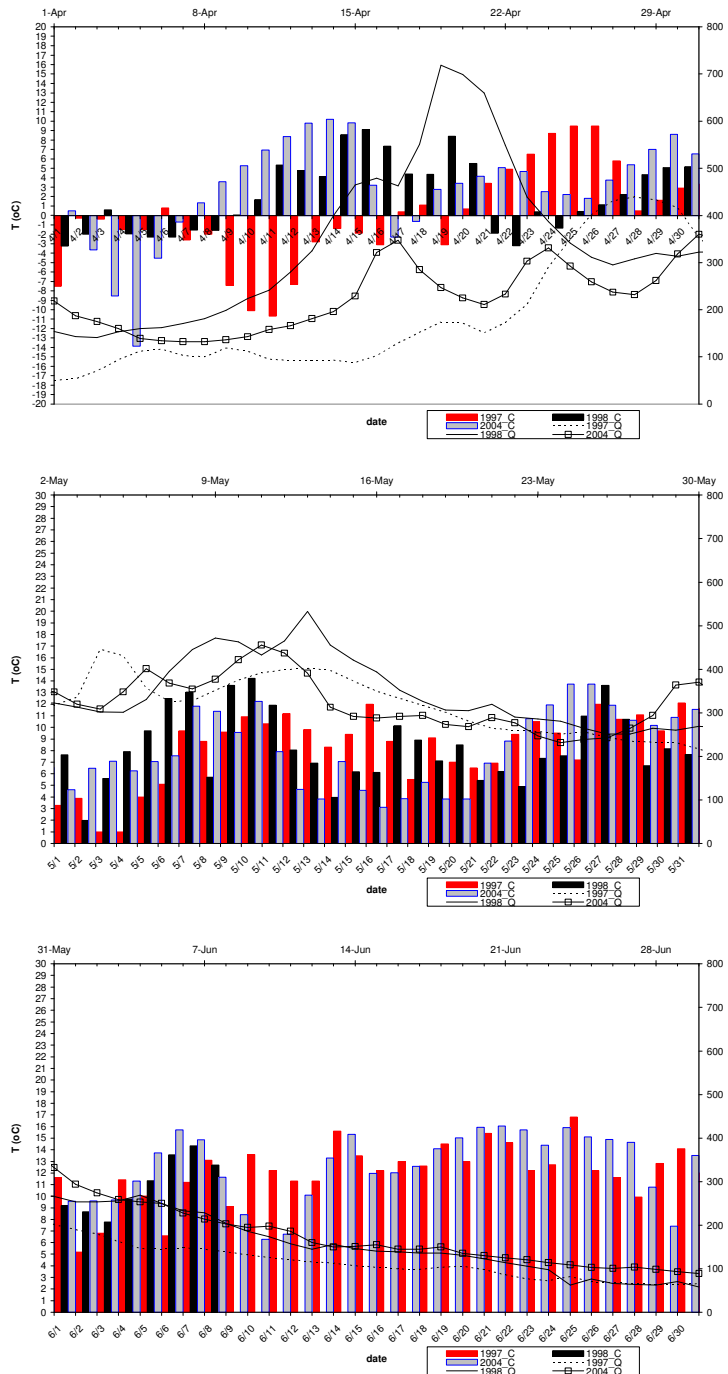


Figure A.3 Comparison of Temperature Values for Zone C

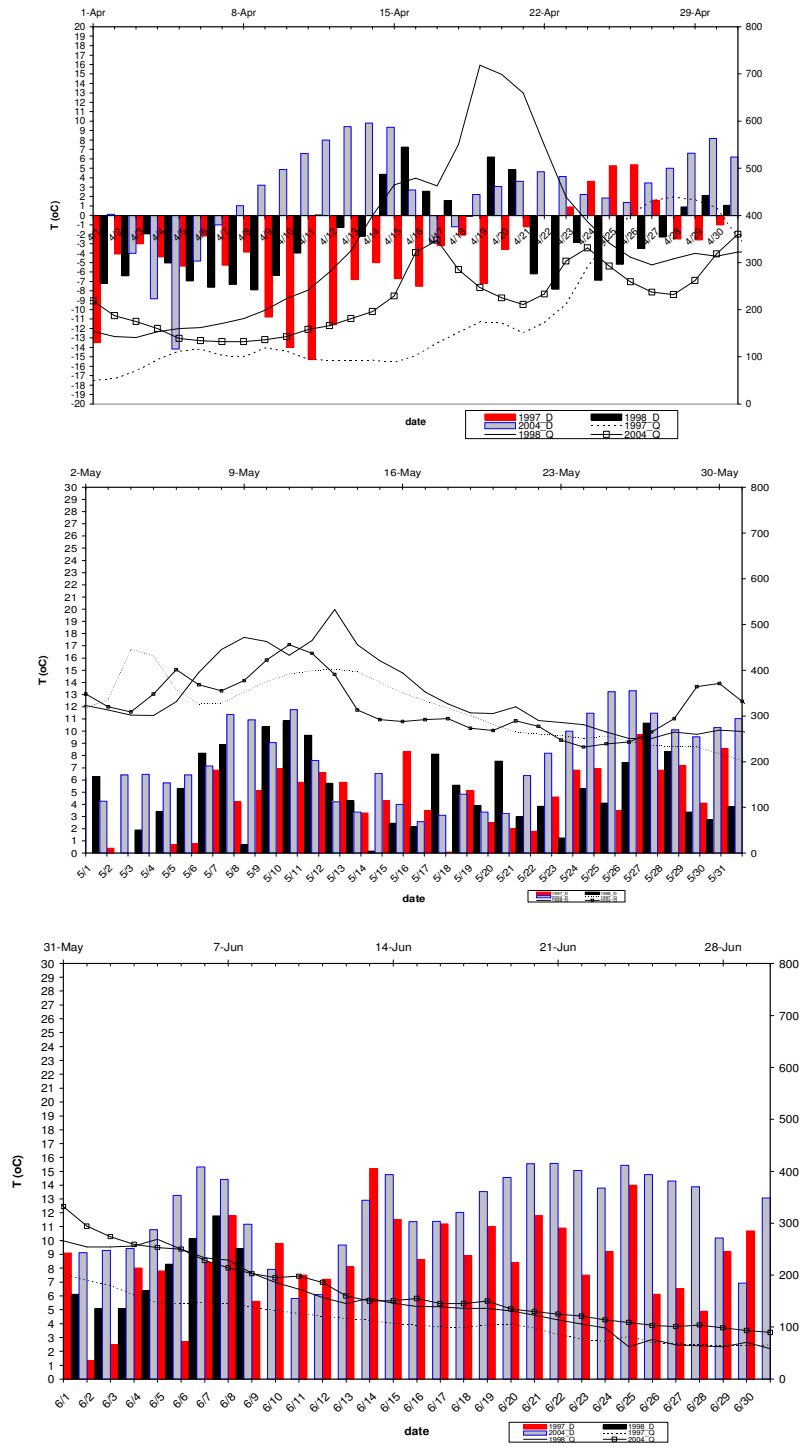


Figure A.4 Comparison of Temperature Values for Zone D

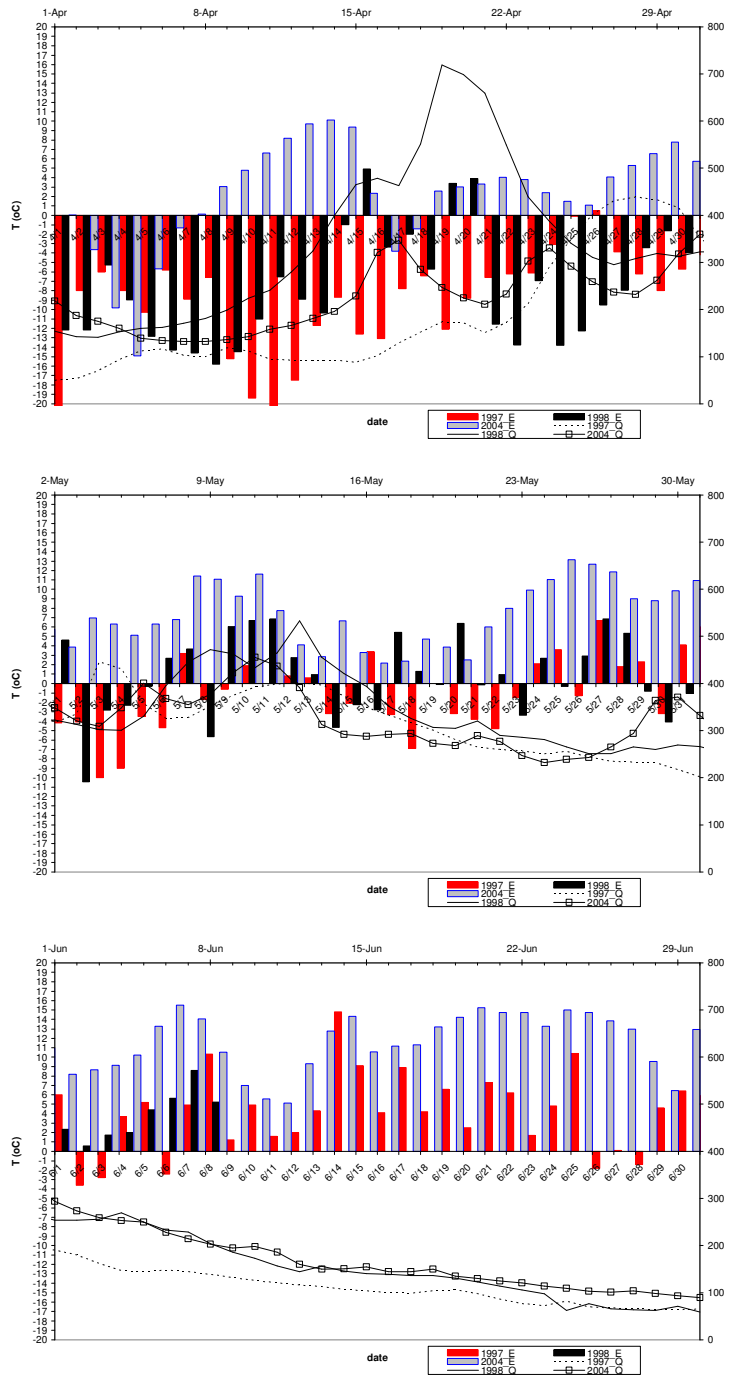


Figure A.5 Comparison of Temperature Values for Zone E

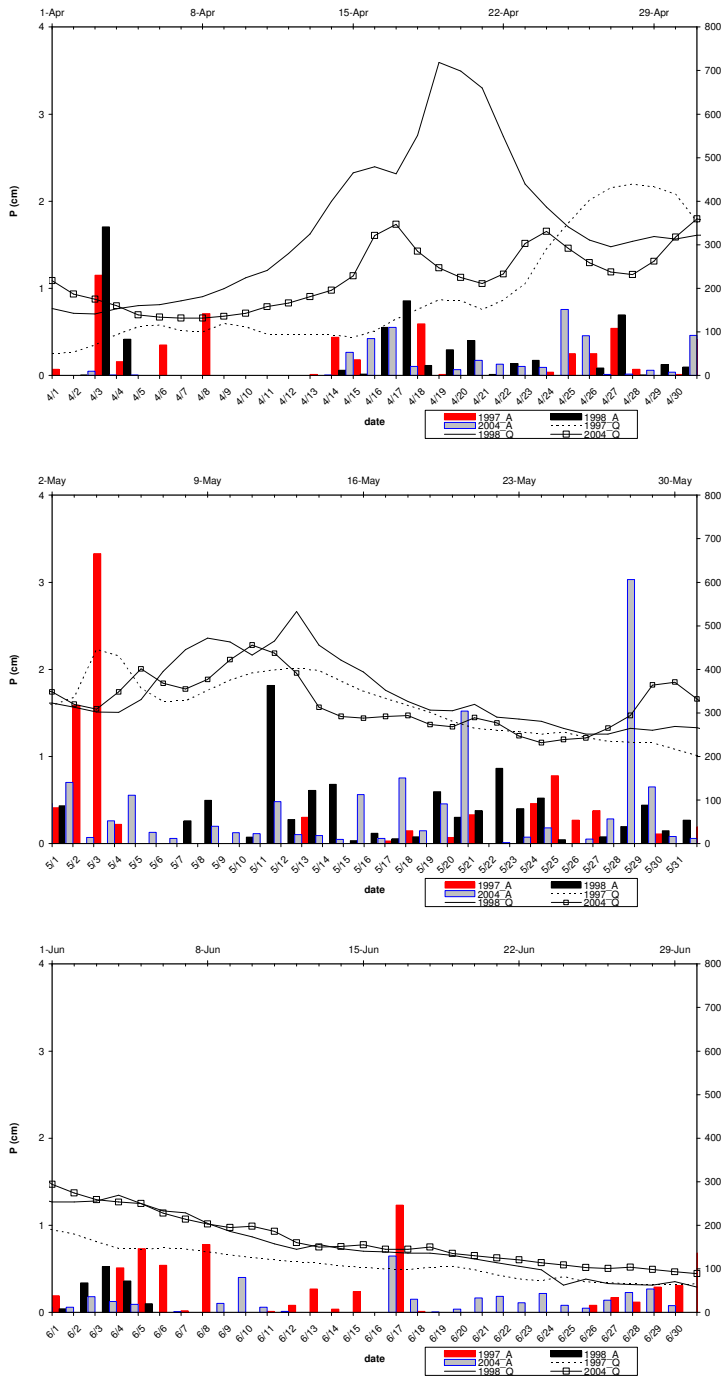


Figure A.6 Comparison of Precipitation Values for Zone A

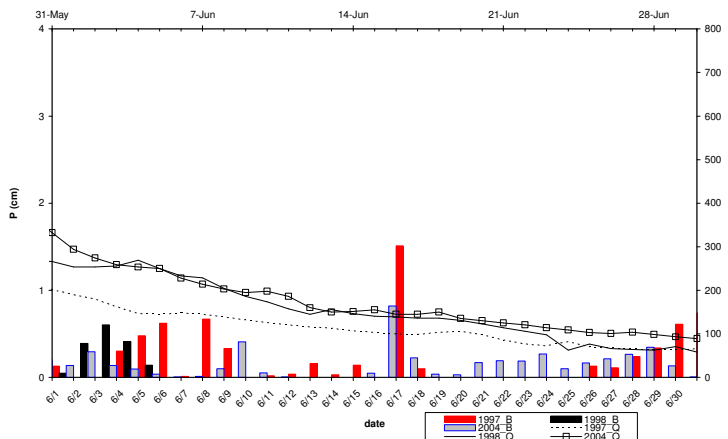
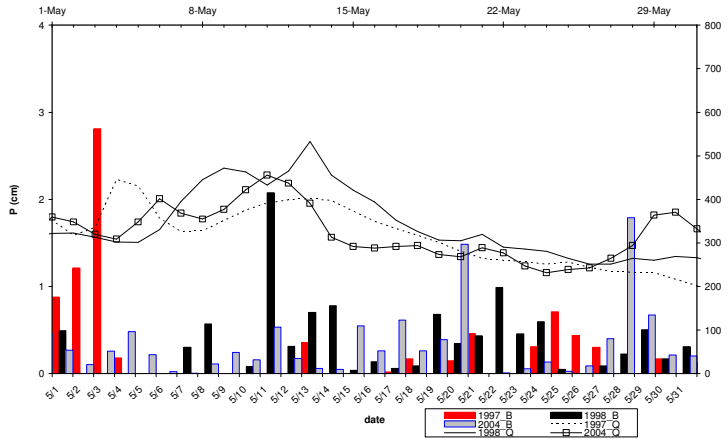
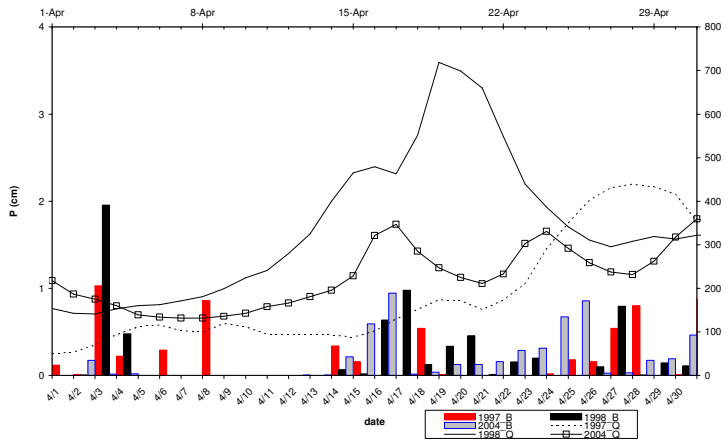


Figure A.7 Comparison of Precipitation Values for Zone B

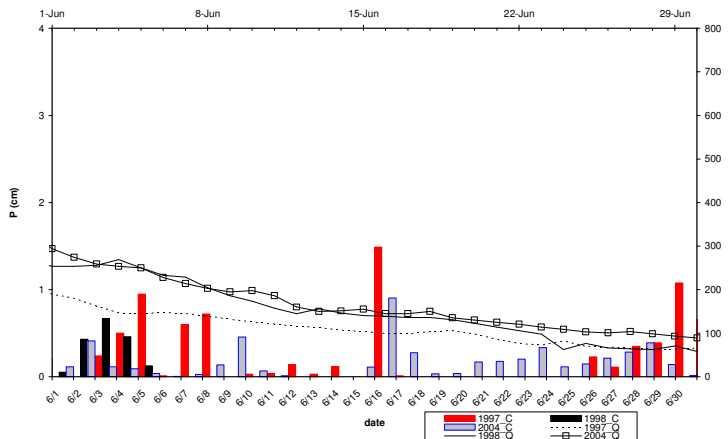
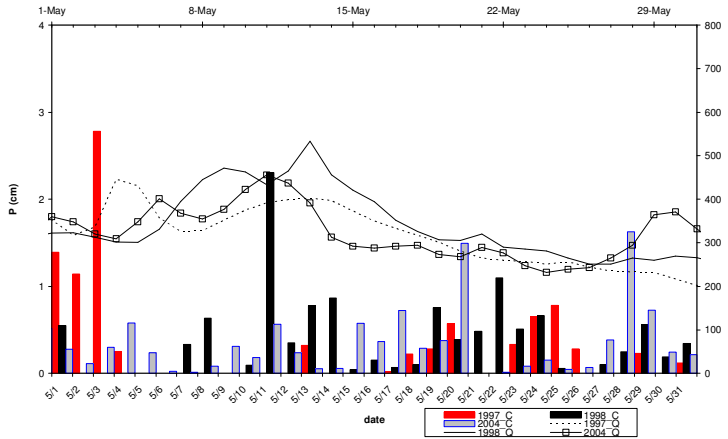
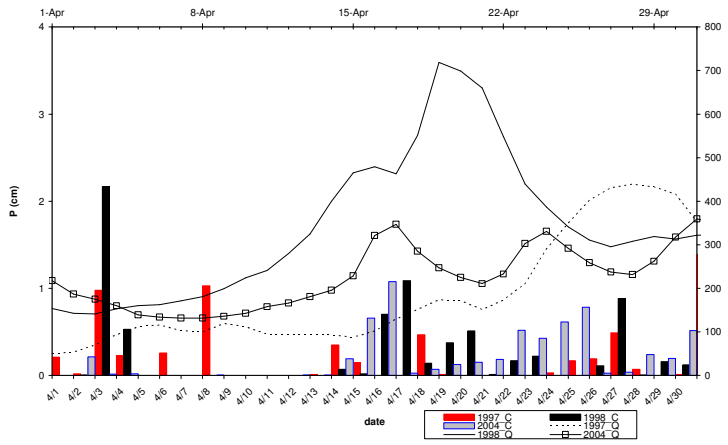


Figure A.8 Comparison of Precipitation Values for Zone C

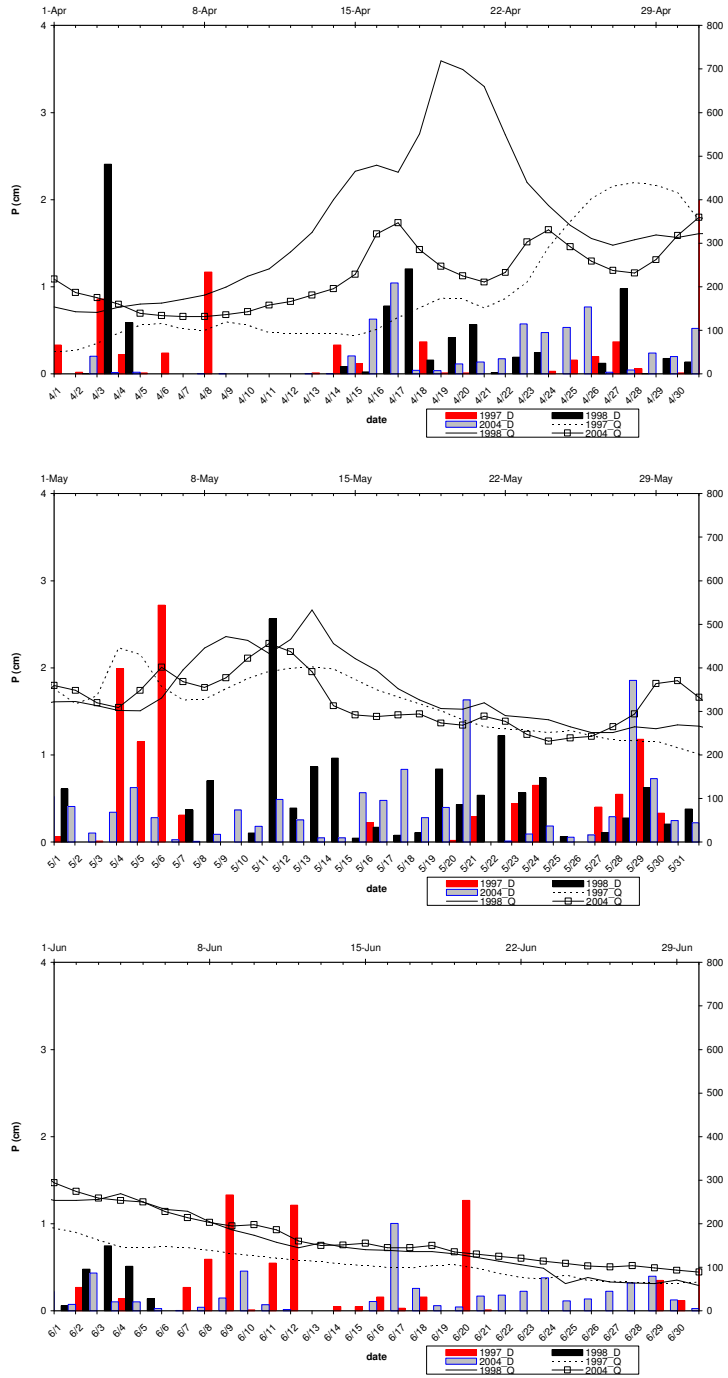


Figure A.9 Comparison of Precipitation Values for Zone D

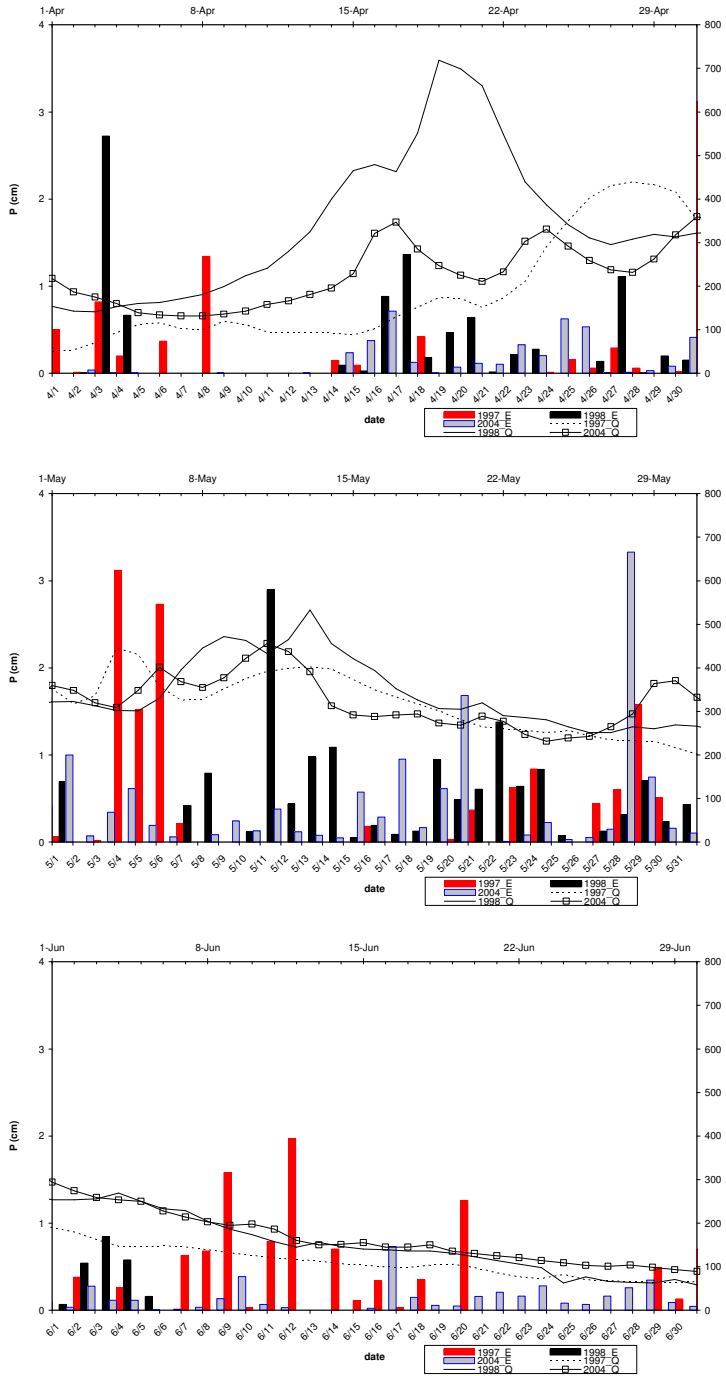


Figure A.10 Comparison of Precipitation Values for Zone E

CURRICULUM VITAE

PERSONAL INFORMATION

Surname, Name : Ahmet Emre TEKELI
Nationality : T.C.
Date and Place of Birth : 17/9/1975, Ankara
Marital Status : Single
Phone : 90-312-286 41 58
Fax :
email : emret@metu.edu.tr

EDUCATION

Degree	Institution	Year of Graduation
Ph.D.	METU Civil Engineering	2005
MS	METU Civil Engineering	2000
BS	METU Civil Engineering	1997

WORK EXPERIENCE

Year	Place	Enrollment
2005-present	State Meteorological Works	Engineer
1999-2005	METU Natural and Applied Sciences	Research Assistant
1997-1999	METU Dep. of Civil Engineering	Research Assistant

FOREIGN LANGUAGES

Advanced English

PUBLICATIONS

1. Tekeli A. E., Akyürek Z., Şensoy A., Şorman A. A., Şorman A., Modeling the temporal variation in snow covered area derived from satellite images

for simulating/forecasting of snowmelt runoff in Turkey, *Hydrological Sciences Journal*, (Accepted for press).

2. Tekeli A. E., Akyürek Z., Şorman A. A., Şensoy A., Şorman A. U, Using MODIS Snow Cover Maps in Modeling Snowmelt Runoff Processes in the Eastern Part of Turkey, *Remote Sensing of Environment*, (Accepted for press).
3. Tekeli A. E., Şorman A. A., Şensoy A., Şorman A. Ü., Bonta J., Schaefer G. (2005) Snowmelt Lysimeters for Real-Time Snowmelt Studies in Turkey, *Turkish Journal of Engineering and Environmental Sciences*, Volume 29 , No 1, pp 29-40.
4. Şensoy A., Tekeli A. E., Şorman A. A., Şorman A. Ü. (2003) Simulation of event-based snowmelt runoff hydrographs based on snow depletion curves and the degree-day method, *Canadian Journal of Remote Sensing*, Volume 29, No 6, pp 693-700.
5. Tekeli A. E. (2000) *Integration of remote sensing and geographic information systems on snow hydrology modeling*, MSc. Thesis, Department of Civil Engineering, Middle East Technical University.

HOBIES

Reading, traveling